THESE de DOCTORAT DE L'UNIVERSITE DE LYON
opérée au sein de l'Ecole centrale de Lyon

Ecole Doctorale N° 160 Electronique
Electrotechnique et Automatique (EEA)

Spécialité de doctorat : Automatique

Soutenue publiquement le 27/01/2021, par :
Federico MORELLI

Optimal identification experiment design: contributions to its robustification and to its use for dynamic network identification. Resonance Frequency Tracking.

Devant le jury composé de :

POINOT, Thierry	Professeur des Universités	LIAS	Président
ROJAS, Cristian	Professeur Associé	KTH	Rapporteur
MERCÈRE, Guillaume	Maître de Conférences (HDR)	LIAS	Rapporteur
GILSON, Marion	Professeure des Universités	CRAN	Examinatrice
BOMBOIS, Xavier	Directeur de Recherche CNRS	Ampère	Directeur de thèse
BAKO, Laurent	Maître de Conférences (HDR)	Ampère	Co-directeur de thèse

To my family.

Acknowledgements

Behind every result, every discovery, every work, there is an incredible mosaic of faces and choices who made that result possible. I hope that the words I am going to spend for thanking every person, who constitutes a piece of this mosaic, will be appreciated, since I am not really capable in this type of things. Actually, every person who collaborated with me, motivated me, or just shared its time with me in a simple and meaningful way during these years, constitutes a part of this mosaic. I hope that my memory does not betray me and I do not forgot anyone. Obviously, this is going to be really long, so, without further ado, let's start.

First of all, I want to thank BpiFrance for financing the project PSPC Next4MEMS, founding this PhD thesis. Without their financial support it would not have been possible to attend international conferences. This thesis would not just exists without it.

I want to thank the Thesis's Jury for agreeing evaluating my thesis in this singular and unique context, the valuable remarks of the reviewers, Mr Cristian ROJAS and Mr Guillaume MERCÈRE, and the interesting questions during the defence from Mrs Marion GILSON and Mr Thierry POINOT. A special thanks to my thesis' directors, Xavier BOMBOIS and Laurent BAKO. Thank you, Xavier for all the comments you gave me throughout these years, which helped greatly improving my writing and presenting skill, together with the precious help in the research activity and for what you taught me on System Identification and Optimal Experiment Design. Thank you, Laurent for all your comments and for the important insights on Recursive Identification. I want to thank also Hakan Hjalmarsson for the important contribution and help he gave for Chapter 3. I want to thank Anton KORNIIENKO for proposing me the activity in the Next4MEMS project and supervising it and for its contagious enthusiasm. I owe an important thank also to two professors of my former university, Daniele Bortoluzzi and Luca Zaccarian; without their questions I would not be here.

But these were only the firsts pieces of the mosaic. By making a step back we can observe the other pieces near to the centre: the people I met at Ampere Laboratory. During these years I worked literally side by side with Kevin COLIN: thank you for explaining me certain *nuances* of French language and the implications of minimization problems in personal relationship. In front of my desk I have had the joyful face of Fabricio SAGGIN: thank you for inventing the *word of the day* moment during my first months at Lyon, while I was still learning French. I will never forget the first word[1]. I have had the luck of seeing every day the peaceful face of Jorge AYALA, who I have to thank for having taught me how to be *Zen* also at the office. At the middle of this voyage, our office became the home also of *Maman-Provence*: Eva MARKIEWICZ. Thank

---

[1]which we cannot report here for obvious reasons. For the records, my reaction was "Do you really have a verb only for THAT action ?"

you for bringing many rays of joy and gentleness in our office[2] together with your battling and caring spirit, among one order of re-heating the water and the other one. And I want to thank you by revealing you a secret: in Italy we do not cut spaghetti because it is just a matter of logic, cooking long pasta and cutting it because it is long, it just does not make any sense. During these last months our Next5MEMS team (Kevin, Fabricio, Jorge, Eva and me) acquired a new member, Cecile PERNIN, who revamped long closed discussions on whether we put ananas on pizza and similar[3]. And I also thank you for having brought the additional dose of humor in our team. Speaking of the Next6MEMS team (Next5MEMS + Cecile), everyone has criticized me for being closed minded because I do not accept ananas on pizza. Since I am at the end at this voyage, I decided to show you that I am not so closed minded and I am putting ananas on pizza, as you can see in Figure 1. I want also to thank Priscilla, Fabricio's wife, and Anaïs, Jorge's girlfriend, for the additional dose of joy you bring to our team and for teaching Kevin how to be more environment friendly.

Figure 1: Ananas on pizza. Source www.ricette.giallozafferano.it and www.doctissimo.fr.

Thank you Gérard SCORLETTI for your precious advices during the my first year of thesis. Thank you Edith for all the help you gave me with the administration during these years, you made dealing with the french bureaucracy (almost) a joy. A special thank also to Paolo Massioni and Giacomo Casadei, your presence at Ampere made more bearable explaining to my collegues why a pizza it is not a "tarte flambée". I want to thank all the PhD students at Ampere Laboratory: Arthur, Alexandre, Ouassim, François, Hussein, Yanis. Thanks also to the professors of the Laboratory and the staff: Christian, Sebastien, Laure, Alice, Julien, Gilles, Catherine, Emanuel, Eric B, Eric V, Arnaud. I will conserve in my memory a lot of beautiful moments with you

---

[2]especially in form of cakes and incredible dishes

[3]This is sufficient to make falter my will to thank you, Cecile, but I forgive you because you're still young and you do not know what you're saying.

all, from the *Journées Vertes* of the lab, to the discovery of why you may need scotch when you have an hamster, the possibility to teach with Catherine and Emmanuel, the raclette evenings with the other PhD students and the advices I received during the first year evaluation committee (Comité suivi thèse). These precious moments are just non-countable, thank you very much.

Obviously I did not spend these years only inside the Ampere Laboratory, so there is an entire population who supported me outside the scientific field. I want then to thank Mirco and Eloisa and all the Iadarola family, for your important and familiar presence. Thanks to Jean-Jacques and Carole, you have been almost like having grand-parents in Lyon. A special thanks to Blandine, you made me re-discover my desire for helping others, in particular the ones who have an history less fortunate than mine. Thank you, Simone for being an example of how to survive a PhD. Thank you, Lucille for your contagious enthusiasm. Thank you, Teresa and Carola for the incredible boost of life you two brought to Lyon with your simplicity. Thank you, Lorenzo, Francesca and Maria for your beautiful presence. Thanks to all the movement of CL for their companionship: Edith, Patricia, Cecile, Laurent et Françoise Quenard, Yassine, Martina, Marie-thé et Thierry, Pietro.

Now it's time to thank the part of the mosaic who resides in Italy. This is probably the most emotional part. You made me feel your support and love despite of the distance. Certain of you have contributed to important choices, despite of the fact we see each other one or two times per year. Honestly, it is simply mysterious why certain of you are still in my life and it is the proof that, in the end, relations are not in our hands.

Thank you, Davide for all the times you tried to make me doing the path of Santiago de Compostela (without success), for trying teaching me the Mazurka (once again, without success), for the long phone calls, even at 7AM while going to work, for all the innumerable times you encouraged me, thank you for being there. Thank you, Greta for your explosive joy, for cheating in literally every board game, for the afternoon walks at the phone, for the unexpected video calls, for being an unmeasurable source of motivation. Thank you, Denise for all the advices you gave me in difficult moments, for the long phone calls, for having been sometimes an amplifier for my strange ideas, for having been a precious presence. Thank you, Veronica and Emanuele for all your advices and patience in listening to my various misadventures, for asking me being your best man at your marriage. Following the same line, I want to thank also Ilaria and Francesco, for being your best man, and Giacomo and Margherita. Your company has been a joy during these years. Thank you, Lorenzo for all the long discussions about politics whenever I felt the urge to criticize a political decision[4], for sharing a part of my madness all along and allowing me think about other things than the thesis.

Thanks to all my friends in Riccione, my homeland, in random order: Azzurra, Daniele D, Mattia, Angela, Emanuele, Daniele, Benedetta, Giulia B, Emiliano, Camilla

---

[4] so basically every decision made by a politician

Abstract of the thesis

Optimal identification experiment design: contributions to its robustification and to its use for dynamic network identification. Resonance Frequency Tracking.

Federico Morelli

At the roots of every engineering field there are mathematical models. They allow us to make predictions on the evolution of a process, monitor the health of a plant and design a control scheme. System Identification provides us with techniques for obtaining such a model directly from experimental data collected from the system we want to model, leading to a model which is accurate enough. In order to obtain a good model using the tools of System Identification, a user has to choose: a model structure, the experimental data and an estimation method.

The choice of the experimental data relies on designing the experiment and it has important consequences on the final quality of the model. Indeed, if we consider the identification of a model among a set of transfer functions (model structure) in the Prediction Error framework, the "larger" the power spectrum of the excitation signal, the more accurate the model. On the other hand, a "large" power spectrum for the excitation signal represents a high cost for the experiment. In this context, the least-costly experiment design framework has been proposed, where the cost is minimized while requiring a model which is just accurate enough.

In all optimal experiment design problems, the underlying optimisation problem depends on the unknown true system that we want to identify. This problem is generally circumvented by replacing the true system by an initial estimate. One important consequence of this approach is that we can underestimate the actual cost of the experiment and that the accuracy of the identified model can be lower than desired. Many efforts have been done in the literature to make this optimisation problem robust, leading to the research area of robust optimal experiment design. However, except for simple cases, all the approaches proposed so far do not completely robustify the optimisation problem. In this thesis, based on an a-priori uncertainty set for the true system, we propose a convex optimization approach that guarantees that the experiment cost will not be higher than a computed upper bound and that the accuracy of the model is at least the desired one. We do this considering that the excitation signal is a multisine signal.

In recent years we have observed in control engineering a rising interest in networks. Even if many Identification problems in the network context have been recently studied, this is not the case for the optimal experiment design. In this thesis, we consider the optimal experiment design for the identification of one module in a given network

of locally controlled systems. The identification experiment will be designed in such a way that we obtain a sufficiently accurate model of the to-be-identified module with the smallest identification cost i.e. with the least perturbation of the network.

Finally, in the second part of this thesis we consider the drive mass system of MEMS gyroscope. This drive mass system is meant to oscillate at its resonance frequency in order to have the desired performances. However, during its operation the gyroscope undergoes environmental changes, such as temperature changes, that affect the resonance frequency of the resonator. It is then important to track these changes during the operation of the gyroscope. To do so, in this thesis, we investigate two solutions: one coming from adaptive control, the extremum seeking scheme, and one coming from System Identification, the recursive least squares algorithm.

Résumée de la thèse

Optimal identification experiment design: contributions to its robustification and to its use for dynamic network identification. Resonance Frequency Tracking.

Federico Morelli

À la base de chaque domaine de l'ingénierie, il y a des modèles mathématiques. Ils nous permettent de faire des prédictions sur l'évolution d'un processus, de surveiller la santé d'un système et de concevoir une loi de contrôle. L'Identification des Systèmes nous fournit des techniques permettant d'obtenir un modèle directement à partir de données expérimentales recueillies sur le système que nous voulons modéliser et qui permet d'obtenir un modèle qui est suffisamment précis. Pour obtenir un bon modèle, en utilisant les outils de l'Identification des Systèmes, l'utilisateur doit choisir: une structure de modèle, les données expérimentales et un critère d'identification.

Le choix des données expérimentales repose sur la conception d'expérience et a des conséquences importantes sur la qualité finale du modèle. En effet, si l'on considère l'identification d'un modèle parmi un ensemble de fonctions de transfert (structure du modèle) dans le cadre de l'Erreur de Prédiction, plus le spectre du signal d'excitation est "grand", plus le modèle est précis. D'autre part, un "grand" spectre du signal d'excitation représente un coût élevé pour l'expérience. Dans ce contexte, le cadre de la conception least costly d'expérience a été proposé, où le coût est minimisé en exigeant un modèle suffisamment précis.

Dans tout problème de conception optimale d'expérience, le problème d'optimisation sous-jacent dépend du système réel inconnu qu'on veut identifier. Ce problème est généralement contourné en remplaçant le système réel par une estimation initiale. Un inconvénient important de cette approche est qu'elle pourrait sous-estimer le coût réel de l'expérience. De plus, la précision du modèle identifié peut être inférieure à celle souhaitée. De nombreux efforts ont été faits dans la littérature pour rendre robuste ce problème d'optimisation, ce qui a conduit au domaine de recherche de la conception optimale robuste d'expérience. Cependant, à l'exception de cas simples, toutes les approches proposées jusqu'à présent ne robustifient pas complètement le problème d'optimisation. Dans cette thèse, nous proposons une approche d'optimisation convexe, qui minimise le pire cout associé à un ensemble d'incertitude paramétrique donné a-priori et qui garantit que la précision du modèle soit au moins celle souhaitée. Nous faisons cela en considérant que le signal d'excitation est un signal multisinus.

Dans les dernières années, nous avons observé dans le domaine de l'Automatique un intérêt grandissant pour les réseaux. Même si plusieurs problèmes pour l'identification dans le contexte d'un réseau ont étés récemment attaquée, cela n'est pas le cas pour

la conception optimale d'expérience. Dans cette thèse, nous considérons la conception optimale d'expérience pour l'identification d'un module dans un réseau de systèmes contrôlés localement. L'expérience d'identification sera conçue de manière à obtenir un modèle suffisamment précis du module à identifier avec le coût d'identification le plus faible, c'est-à-dire avec la perturbation la plus faible du réseau.

Enfin, dans la deuxième partie de cette thèse, nous considérons le système de masse drive d'un gyroscope MEMS. Ce système de masse drive est censé osciller à sa fréquence de résonance afin d'obtenir les performances souhaitées. Cependant, pendant son fonctionnement, le gyroscope subit des changements environnementaux, comme des changements de température, qui affectent la fréquence de résonance du résonateur. Il est donc important de suivre ces changements pendant le fonctionnement du gyroscope. Pour ce faire, dans cette thèse, nous étudions deux solutions : l'une provenant du contrôle adaptatif, le schéma dit Extremum Seeking, et l'autre provenant de l'Identification des Systèmes, l'algorithme de Moindres Carrées Récursive.

Contents

Acronyms

SISO	Single-Input Single-Output
LTI	Linear Time Invariant
LPV	Linear Parameter Varying
LMI	Linear Matrix Inequality
BJ	Box-Jenkins
OE	Output Error
ARX	Auto Regressive Exogenous
ARMAX	Auto Regressive Moving-Average Exogenous
FIR	Finite Impulse Response
LFT	Linear Fractional Transformation
RBS	Random Binary Sequence
ES	Extremum Seeking
RLS	Recursive Least Squares
OED	Optimal Experiment Design
MEMS	Micro-Electro-Mechanical System
HPF	High-Pass Filter
LPF	Low-Pass Filter

Notations

Notations pertaining to matrices

The matrix

$$\begin{pmatrix} X_1 & 0 & 0 \\ 0 & \ddots & 0 \\ 0 & 0 & X_N \end{pmatrix}$$

will be denoted $diag(X_1, \ldots, X_N)$ if the elements X_i $(i = 1, \ldots, N)$ are scalar quantities while it will be denoted $bdiag(X_1, \ldots, X_N)$ if the elements X_i $(i = 1, \ldots, N)$ are matrices.

$A > 0$	The matrix A is positive definite
$A \geq 0$	The matrix A is positive semi-definite
A^T	Transpose of the matrix A
A^*	Transpose conjugate of the matrix A
I_n	Identity matrix of dimension n
$\mathbf{0}$	A vector or a matrix containing only zeros

Other notations:

$\otimes$	Kronecker product
E	Expectation operator
ω	Angular frequency rad/s
$\chi^2(k)$	χ^2 probability density function with k degrees of freedom
$\mathbf{R}$	Set of real numbers
$\mathbf{C}$	Set of complex numbers

Introduction

1.1 System Identification

Parametric dynamical models allows us to have a mathematical description of a dynamical system. Such models play a key role in many fields of science and engineering: Chemistry, Mechanics, Electronic, Biology and many others. Without them, we cannot make predictions on the evolution of an epidemic outbreak, we cannot design the control system of a resonator, monitor the health of a wind turbine in order to plan its maintenance, and the list may continue.

How do we obtain a dynamical model ? We can build a model for a dynamical system starting from first principles, the laws of physics governing its behaviour. We refer to this method as *white-box* modelling or first principle modelling. The model so obtained has an immediate physical interpretation, but it may rely on constants or parameters that are uncertain. These parameters can then be calibrated/determined using input-output data collected on the true system (grey-box modeling).

Determining mathematical models based on data is the objective of *system identification* [1]. As mentioned in the previous paragraph, the parameters that will be calibrated/identified using the data collected on the system may be physical parameters. However, these parameters can also be just the coefficients of a transfer function. In the latter case, the parameters do not have necessarily a physical meaning and we then speak of black-box modeling.

In this thesis, we will restrict attention to the modeling of linear systems using black-box models (transfer functions). We can divide a system identification procedure in the following four steps:

1. Model structure selection. In this step, we determine the set of transfer functions in which the identified model will be determined[1]. This set of transfer functions

---

[1]We in fact generally use two transfer functions: one describing the input-output relation (the plant transfer function) and one describing the stochastic noise corrupting the data.

is generally the set of all transfer functions having a certain order. These transfer functions are thus entirely determined by the coefficients of their numerator and denominator, coefficients that we regroup in a parameter vector θ. In this thesis, we will generally make the assumption that the to-be-identified system (the so-called true system) can be described by one (unknown) element of the chosen set of transfer functions i.e., there exists a true parameter vector θ_0. Under this full-order model structure assumption, the goal of system identification will therefore be to determine an accurate estimate $\hat{\theta}$ of θ_0. Determining such a full-order model structure is generally obtained in an iterative manner [1].

2. Experiment Design. The estimate $\hat{\theta}$ of θ_0 will be determined based on the input-output data collected on the system. These input-output data are obtained during an identification experiment where the system is excited using an excitation signal during a certain amount of time. When the system is operated in open loop, the excitation signal is the input signal itself. When the system is operated in closed loop, the excitation signal is an external signal that is added to the loop. It is important to note that deciding all the details of the experiment is not a merely formal step. Indeed, many of these experimental choices (such as the properties of the excitation signal and the experiment duration) have an important effect on the quality of the final model.

3. Parameter estimation. Starting from the data collected we have then to obtain an estimate $\hat{\theta} \in \mathbf{R}^k$ of θ_0. This is done by minimizing a certain criterion which aims at maximizing the capability of the model to explain data. A widely used criterion is the Prediction Error criterion [1].

4. Model Validation. In this validation step, the uncertainty of the identified model is assessed by e.g., inspecting the covariance matrix P_θ of the identified parameter vector $\hat{\theta}$. Other model validation tests verify the ability of the identified model to explain not only the data used for the identification, but also other input-output data (that have been reserved for this validation step).

This thesis will be made up of a theoretical part and an applied part. In the theoretical part, we will make new contributions to the optimal design of an identification experiment. In the second part, we will show that system identification can be used as an efficient tool to solve a problem that arises in the Next4MEMS project, the project that helped fund this PhD thesis.

1.2 Optimal identification experiment design

1.2.1 State-of-the-art

Optimal identification experiment design consists in optimally designing the excitation signal of an identification experiment to balance two contradictory objectives:

- obtaining the most accurate estimate $\hat{\theta}$ of θ_0 i.e., obtaining an estimate $\hat{\theta}$ with the smallest possible covariance matrix P_θ

- perturbing the to-be-identified system with the excitation signal as little as possible i.e., the cost of the experiment is the smallest possible.

These objectives are contradictory since the larger the spectrum Φ of the excitation signal, the smaller P_θ, but, at the same time, the larger Φ, the larger the cost of the experiment. To balance these contradictory objectives, one can e.g. maximize the accuracy of $\hat{\theta}$ given a certain bound on the cost of the experiment. This is the classical formulation of the optimal experiment design problem that dates back from the seventies (see e.g., [2]). More recently, a second (dual) formulation (the so-called *least costly* formulation) has been considered where the objective is to determine the spectrum Φ of the excitation signal in such a way that the cost of the experiment is minimized while guaranteeing a given accuracy for the identified model [3]. Mathematically speaking, the least costly experiment design problem consists in determining the spectrum Φ of the excitation signal which minimizes the cost $\mathcal{J}(\Phi)$ of the experiment while guaranteeing that $P_\theta^{-1}(\Phi) \geq R_{adm}$ where R_{adm} is a matrix reflecting the desired accuracy and where the cost $\mathcal{J}(\Phi)$ is measured by a linear combination of the power of the perturbation induced by the excitation signal onto the input and output signal of the to-be-identified system [3, 4].

The least costly formulation for optimal experiment design is closer to the requirements in robust control where the robust performance of a controller designed with the identified model can be guaranteed if the model uncertainty is smaller than a given limit (or, equivalently, if the accuracy of the identified model is larger than a certain limit). This has led to a number of contributions on *least costly experiment design for robust control*. In [3], a methodology is developed to design the excitation spectrum in such a way that, with the smallest identification cost, the identified model is guaranteed to have a sufficiently small uncertainty to enable robust control design. In [3], an H_∞ control framework is used, but other control frameworks can also be considered as shown in [4, 5]. The results in [3] and [4] are based on the technical results in [6, 7, 8]. Indeed, the papers [6, 7, 8] show that, using smart parametrizations of the to-be-determined spectrum Φ, both $\mathcal{J}(\Phi)$ and $P_\theta^{-1}(\Phi)$ can be expressed as affine functions of the (to-be-determined) spectrum coefficients. Two parametrizations of Φ are in fact considered in [6, 7, 8]: one corresponding to the spectrum of a multisine excitation signal and one corresponding to the spectrum of a filtered white noise where the filter is restricted to have a finite impulse response. Based on these technical results, the least costly experiment design problem introduced in the previous paragraph can be turned to an LMI[2] optimization problem[3] [9]. It is however important to note that this

---

[2]Linear Matrix Inequality.

[3]An LMI optimization problem is an optimization problem with a scalar objective function that is affine in the decision variables and with constraints that are also affine in the decision variables and that are under the form of matricial inequalities.

LMI optimization problem depends on the unknown true parameter vector θ_0 since both the covariance matrix P_θ and the cost $\mathcal{J}$ of the experiment not only depends on Φ, but also on θ_0 (we will therefore use the notations $\mathcal{J}(\theta_0, \Phi)$ and $P_\theta(\theta_0, \Phi)$ in the sequel). A classical (but not fully satisfactory) approach to circumvent this so-called *chicken-and-egg* issue is to replace, in the LMI optimization problem, the unknown θ_0 by an initial estimate $\hat{\theta}_{init}$ (see e.g. [8, 3]). One of the contribution of this thesis is to derive a method to deal with this chicken-and-egg issue via convex optimization.

The results in [3] and [4] pertain to experiments to identify linear time-invariant (LTI) single-input single-output (SISO) systems that can be described by ordinary differential equations and that are operated either in open loop or in closed loop. The results have been extended to multivariable systems in [10] and to systems that can be described by partial differential equations in [11, 12]. First attempts to deal with optimal experiment design for nonlinear systems can be found in [13, 14, 15, 16]. A first contribution towards optimal experiment design in another operating configuration than the open or closed loop can be found in [17] where a network configuration is considered. A second contribution of this thesis will be to extend further the results presented in [17].

1.2.2 Theoretical contributions

Robust experiment design

The least costly experiment design problem consists in determining the spectrum Φ of the excitation signal that minimizes the cost $\mathcal{J}(\theta_0, \Phi)$ of the experiment under the constraint that $P_\theta^{-1}(\theta_0, \Phi) \geq R_{adm}$. As mentioned in the previous section, this optimization problem can be expressend as an LMI optimization problem provided a solution is found to the fact that the true parameter vector θ_0 is unknown. As already mentioned, this *chicked-and-egg* issue is generally circumvented by replacing θ_0 in the optimization problem by an initial estimate $\hat{\theta}_{init}$ of θ_0 (see e.g. [8, 3]). However, this approach has the drawback that the optimal spectrum $\Phi_{opt}^{\hat{\theta}_{init}}$ obtained in this way is not guaranteed to yield the desired accuracy and that the experiment cost $\mathcal{J}(\hat{\theta}_{init}, \Phi_{opt}^{\hat{\theta}_{init}})$ computed with $\hat{\theta}_{init}$ and $\Phi_{opt}^{\hat{\theta}_{init}}$ can underestimate the actual experiment cost $\mathcal{J}(\theta_0, \Phi_{opt}^{\hat{\theta}_{init}})$. These observations are at the root of the research areas on *adaptive experiment design* [18, 19] and on *robust optimal experiment design* (see [20] for a good survey). In adaptive experiment design, both the estimate and the optimal spectrum are obtained in a recursive manner (see [18, 19] for more details).

In robust experiment design, different lines of research have been considered. In [21], a spectrum that yields good accuracy for a very broad set of systems (also of different orders) is discussed. However, in the engineering literature, the most widely used approach is the one that consists in considering an uncertainty set U containing the unknown true parameter vector θ_0 (the so-called min-max design [20, 22]). The optimal experiment design problem can then be formulated as determining the spectrum

Φ minimizing the value of a scalar γ under the constraints that $\mathcal{J}(\theta, \Phi) \leq \gamma \; \forall \theta \in U$ and that $P_\theta^{-1}(\theta, \Phi) \geq R_{adm} \; \forall \theta \in U$. If we denote by γ_{opt} and Φ_{opt} the solution of this optimization problem, we have the guarantee that $P_\theta^{-1}(\theta_0, \Phi_{opt}) \geq R_{adm}$ and that γ_{opt} is an upper bound for the actual experiment cost $\mathcal{J}(\theta_0, \Phi_{opt})$. However, finding a tractable approach to deal with such a robustified optimal experiment design problem is still an open research question. While, for very particular or simple situations, this optimization problem can be either exactly solved (see e.g. [20, 23]) or tackled via an Sum-Of-Squares approach (see [24]), the general approach when facing more complex systems is to replace the initial uncertainty set (containing an infinite number of elements) by a number n_g of grid points of this uncertainty set U (see e.g. [8, 3, 20, 25]). Consequently, the cost constraint and the accuracy constraint over the set U in the robustified optimal experiment design problem are replaced each by n_g constraints (one for each grid point). Even though it is obviously better from a robustification point-of-view than just replacing θ_0 by one grid point i.e. $\hat{\theta}_{init}$, this relaxation of the original robustified optimal experiment design problem cannot yield the guarantees linked to the original problem.

In [26, 27, 28], approaches are presented to uniquely tackle the robustified cost constraint $\mathcal{J}(\theta, \Phi) \leq \gamma \; \forall \theta \in U$ (i.e. in the accuracy constraint, θ_0 is replaced by $\hat{\theta}_{init}$). However, these approaches all entail some approximation: a first-order approximation in [27], a second-order approximation in [26] and an approximation based on the unscented transform in [28].

In this thesis, our contribution is to present an approach in order to tackle the robust optimal experiment design problem without approximation[4]. For this purpose, we observe that, except for its dependence on the to-be-determined spectrum, the robustified cost constraint and the robustified accuracy constraint are similar to constraints that are treated in robustness analysis. Based on this observation and on the separation of graph framework [29, 30, 31], we derive constraints that are linear in the decision variables of the optimal experiment design problem and that imply the original robustified cost and accuracy constraints. As we will see, the proposed approach will nevertheless not cover all possible situations. These restrictions will be detailed in Chapter 3, together with our robust experiment design approach.

Least costly experiment design for a network of locally controlled systems

Until recently, system identification has only considered systems operated in open loop or in a closed loop. Due to the increasing importance of the concept of network in control engineering, we have however recently seen major efforts to develop techniques for the identification of large-scale or interconnected systems. In many papers, the problem is seen as a multivariable identification problem and structural properties of the system are then used to simplify this complex problem (see e.g. [32]). The identifiability of the multivariable structure is studied in a prediction error context in [33]

---

[4]but with some (limited) conservatism.

while this multivariable structure is exploited in other papers to reduce the variance of a given module in the network (see [34, 35, 36]). In other contributions, conditions are derived for the consistent estimation of a given module in a dynamic network (see e.g. [37, 38, 39]).

While many different problems have thus been studied in the dynamical network context, this is not the case for optimal experiment design. In the very limited literature on this particular subject, the contribution [17] presents first steps towards optimal experiment design in a dynamical network context.

The paper [17] considers the case of a network made up of the interconnection of locally controlled systems (also called modules or nodes). In these networks, the interconnection is realized by the fact that neighbouring modules are allowed to exchange their measured output. In particular, the reference signal of each module in the network will be computed based on the measured outputs transmitted by its neighbouring modules. This type of networks is usual in the literature on multiagent systems (see e.g. [40, 41])) and can e.g. be used to ensure that all modules of the network track a given reference known only to one of these modules. For this particular type of dynamical networks, it is showed in [17] how to design the excitation signals that have to be added to each module in order to identify models of these different modules that are sufficiently accurate to enhance the network performance by a redesign of the local controllers. The accuracy of each model can be measured by the inverse of the covariance matrix of the identified parameter vector of each module. In [17], an expression for the inverse of this covariance matrix as an affine function of the excitation signal spectra is derived. It is important to note that the inverse of the covariance matrix of a given module l is obviously a function of the excitation signal applied to this particular module, but also, though in a lesser extent, a function of the excitation signals applied to all modules k having a path to l. Consequently, the excitation signal applied to such a module k contributes to the accuracy of the model of l. In other words, the propagation of the excitation signals due to the interconnection is a positive feature when we want to obtain sufficiently accurate estimates of every module with the smallest excitation power (see also [42, 43, 44]).

In Chapter 4 of this thesis, like in [17], we will consider the optimal experiment design problem for a network of locally controlled systems. However, unlike in [17], we will do that for the case where we are only interested in the accurate identification of one specific module l of the network. Like in [17], to maintain the network performance, this identification will be performed in the original network configuration via the application of an excitation signal to module l. Since the other modules do not have to be identified, the propagation of this excitation signal to the other modules due to the interconnection is a negative feature that has to be limited as much as possible[5].

---

[5]This is especially the case when the experiment is performed in a network where all modules have to track a given reference. In this case, the excitation signal introduces an undesired perturbation on the tracking performance.

For this purpose, we extend the least costly identification framework to this particular dynamic network identification problem. In particular, we design the spectrum of the excitation signal applied to l in such a way that the accuracy of the identified model (measured via the inverse of the covariance matrix) is larger than a given threshold while entailing the smallest perturbation on the network. The perturbation (i.e. the cost of the identification) will be measured by the sum of the effects of the excitation signal on the input and output of each system in the network.

With respect to the least costly framework introduced in [3] for a single closed loop, the cost of the identification experiment in the network context thus not only contains the perturbation induced by the excitation signal in the closed loop where it is applied and where the system has to be identified, but also the perturbation induced in other loops by this excitation signal. This propagation of the effect of the excitation signal is due to the fact that the output signal of the to-be-identified loop (which is perturbed by the excitation signal) is transmitted to neighbouring modules. In this thesis, in order to reduce this propagation, we propose an approach where the signal transmitted to the neighbouring modules is no longer the actual output signal, but a sanitized version of this output signal where the contribution of the excitation signal has been (partially) removed. This approach is inspired by the concept of stealth identification introduced in [45] for a single closed loop and that we here extend to the network case.

1.3 Resonance frequency tracking of a MEMS gyroscope

In the first part of this thesis, we have considered the identification of time-invariant systems. In the second part, we will consider the case of a time-varying system i.e. a system whose parameters vary with time. In this case too, system identification can be an efficient tool to derive accurate mathematical models based on input-output data. In particular, recursive identification [1] allows one to determine, at each time instant, an estimate of the time-varying parameter vector of a time-varying system.

In Chapter 5, we will use recursive identification to tackle a problem arising in the Next4MEMS project, the project that funded this PhD project. The aim of the Next4MEMS project is to improve the control system of MEMS gyroscopes to increase their reliability. In a MEMS gyroscope, one of the major control loops is the loop that pertains to the drive mass system [46]. The drive mass system is basically a mass fixed to a reference frame via micro-silicon beams and that can be actuated via a force. The transfer function between this force u_x and the position x of the drive mass is a second-order resonating system and the objective of the drive mass control system is that x follows a sinusoidal reference signal x_{ref}. Generally, this control objective is achieved via two parallel loops that respectively control the amplitude and the phase of the phasor representation of the to-be-controlled signal x [46]. This phasor approach introduces unnecessary nonlinearities (e.g., to transform the signal x into its phasor description) and an alternative control approach has been proposed in the Next4MEMS project. In this alternative (and more classical) control configuration, the force u_x is

computed as the output of a linear controller K_x that takes as input the difference between the sinusoidal reference signal x_{ref} and the signal x i.e., the position of the drive mass. Irrespectively of the control approach, it is important to note that, to reduce the energy consumption (i.e., to enforce a small actuation signal u_x), the frequency of the sinusoidal reference signal x_{ref} must be equal to (or at least close to) the resonance frequency of the drive mass system.

A MEMS gyroscope has to operate in a large range of ambient temperatures and it is well known [46] that the resonance frequency of the drive mass system changes with the temperature. In the classical control configuration (the phasor configuration), these variations were automatically taken care of via the phase loop. However, this is no longer the case in the new control configuration and a procedure has to be designed in order to adapt the frequency of the reference signal x_{ref} in such a way that this frequency is always equal (or at least close to) the actual resonance frequency of the system. In Chapter 5, we use recursive identification to follow the dynamics of the drive mass system allowing in this way to adapt the frequency of the reference signal x_{ref}. We show the potential of this approach via simulations and we compare the recursive approach with another possible approach to tackle this problem, the extremum seeking approach. This approach has indeed been already used in the context of the phasor approach to adapt the reference of the phase loop in order to deal more efficiently with the effect of temperature variations [47].

1.4   Content of the thesis

In Chapter 2, we present in more details the prediction error identification method and the design of optimal identification experiments.

In Chapter 3, we present our contribution on robust optimal experiment design. This chapter is based on the following paper:

> X. Bombois, F. Morelli, H. Hjalmarsson, L. Bako and K. Colin, "Robust optimal identification experiment design for multisine excitation", submitted to Automatica, September 2019

In Chapter 4, we present our extension of the least costly framework to the network situation. This chapter is based on the following papers:

> F. Morelli, X. Bombois, H. Hjalmarsson, L. Bako and K. Colin, "Optimal experiment design for the identification of one module in the interconnection of locally controlled systems", European Control Conference, Naples, 2019

> F. Morelli, X. Bombois, H. Hjalmarsson, L. Bako and K. Colin, "Least costly identification experiment for the identification of one module in a dynamic net-

work", submitted to Automatica, November 2019

Finally, in Chapter 5, we tackle the problem of tracking the resonance frequency of the drive mass system of a mass gyroscope.

Prediction Error Identification and Optimal Experiment Design

2.1 Introduction and description of the to-be-identified system

In this chapter, we will present in more details the concepts of prediction error identification and the concepts of optimal identification experiment design that have been touched upon in Chapter 1. We will do that for both the open-loop and the closed-loop configuration.

Let us first describe the system that we wish to identify. This system will have one input u and one output y (single-input single-output (SISO) system) and will be, in most of the thesis, linear time-invariant (the only exception will be the system considered in Chapter 5). We will furthermore use a discrete-time representation for this system: the input $u(t)$ and the output $y(t)$ are thus discrete-time signals (t is an integer representing the sample number and corresponding to an actual time $\tilde{t} = tT_s$ where T_s is the sampling time). If not specified otherwise and without loss of generality, the sampling time T_s will be supposed equal to 1 s.

The relation between $y(t)$ and $u(t)$ will be described as follows using two stable discrete-time transfer functions $G_0(z)$ and $H_0(z)$ (z represents both the forward shift operator and the Z-transform variable):

$$\mathcal{S}: \quad y(t) = G_0(z)u(t) + \underbrace{H_0(z)e(t)}_{=v(t)} \tag{2.1}$$

where $v(t) = H_0(z)e(t)$ represents both the measurement noise and the disturbance acting on the system (process noise). In (2.1), $e(t)$ is a white noise with variance σ_e^2. Besides being stable, $H_0(z)$ is also assumed to be inversely stable and monic[1].

---

[1]i.e. $H_0^{-1}(z)$ is stable and $H_0(z = \infty) = 1$.

Prediction error identification [1] allows to derive a model of this so-called *true system* $\mathcal{S} = \{G_0, \ H_0\}$ based on input-output data.

2.2   Prediction-error identification in open loop

Let us first present how we can identify a model of the system (2.1) using the prediction error framework when the system (2.1) is operated in open loop. In the prediction error framework, we need to define the black-box model structure in which the models of $G_0(z)$ and $H_0(z)$ will be identified. A model structure $\mathcal{M}$ is a set of transfer functions of fixed order parametrized by a parameter vector θ: $\mathcal{M} = \{G(z,\theta), \ H(z,\theta) \mid \theta \in \mathbf{R}^k\}$. The model structures that are typically used in prediction-error (i.e., BJ, OE, ARMAX, ARX model structures) are described in Appendix A.

In this thesis, we will generally assume that the model structure $\mathcal{M}$ has been chosen in such a way that it is rich enough to contain the true system $\mathcal{S} = \{G_0(z) \ H_0(z)\}$ (full-order model structure) and that it is identifiable:

Assumption 2.1. *Consider the to-be-identified system* (2.1). *We will assume that the chosen model structure $\mathcal{M}$ is such that there exists a so-called true parameter vector $\theta_0 \in \mathbf{R}^k$ such that $G_0(z) = G(z,\theta_0)$ and $H_0(z) = H(z,\theta_0)$ and that this parameter vector θ_0 is unique i.e. if $G_0(z) = G(z,\theta)$ and $H_0(z) = H(z,\theta)$, then $\theta = \theta_0$.*

Besides a model structure, a second crucial ingredient in the prediction error identification framework is a data set collected on the to-be-identified system: $Z^N = \{y(t), \ u(t) \mid t = 1,\ldots,N\}$. When the system is operated in open loop, the data set Z^N is obtained by applying a sequence $\{u(t) \mid t = 1,\ldots,N\}$ to (2.1) and by collecting the corresponding output $\{y(t) \mid t = 1,\ldots,N\}$. In prediction error identification, it is generally assumed that $u(t)$ is a quasi-stationary signal (see [1, p. 34]) that is uncorrelated with the noise $e(t)$ in (2.1) and that is characterized by its power spectrum Φ_u. The richness of the excitation signal u can be described by its order of excitation:

Definition 2.1. *Consider a quasi-stationary signal $x(t)$. The order of excitation of $x(t)$ is the number of frequencies at which the power spectrum $\Phi_x(\omega)$ of x is nonzero in the interval $]-\pi, \ \pi]$.*

Based on a full-order model structure $\mathcal{M} = \{G(z,\theta), \ H(z,\theta) \mid \theta \in \mathbf{R}^k\}$ and a data set Z^N, an estimate $\hat{\theta}_N$ of θ_0 can be deduced using the following criterion [1]:

$$\hat{\theta}_N = \arg \min_{\theta} \frac{1}{N} \sum_{t=1}^{N} \epsilon^2(t,\theta) \tag{2.2}$$

where $\epsilon(t,\theta)$ is the so-called prediction error:

$$\epsilon(t,\theta) = H^{-1}(z,\theta) \left(y(t) - G(z,\theta)u(t) \right) \tag{2.3}$$

For the estimate $\hat{\theta}_N$ given by (2.2) to have interesting properties (e.g., the property to be consistent), we will have to make an additional assumption on the excitation signal u that has generated the data set Z^N i.e., u must be sufficiently rich for $\epsilon(t, \theta)$ to be different at each θ (data informativity).

Assumption 2.2. *Consider a model structure $\mathcal{M}$ satisfying Assumption 2.1 and a data set Z^N generated with an excitation signal $u(t)$. Consider also the prediction error $\epsilon(t, \theta)$ defined in (2.3). We assume that the order of excitation of $u(t)$ (see Definition 2.1) ensures that the prediction error $\epsilon(t, \theta)$ has the following property for any parameter vectors θ_1 and θ_2*

$$\bar{E} \left(\epsilon(t, \theta_1) - \epsilon(t, \theta_2) \right)^2 = 0 \implies \theta_1 = \theta_2 \tag{2.4}$$

where $\bar{E}x(t) = \lim_{N \to \infty} \frac{1}{N} \sum_{t=1}^{N} Ex(t)$ (E is the expectation operator).

As shown in [48], Assumption 2.2 will hold if the order of excitation of u is larger than a given threshold that only depends on the respective parametrization and the order of the parametrized transfer functions $G(z, \theta)$ and $H(z, \theta)$ in $\mathcal{M}$.

In [1], it is shown that, under Assumptions 2.1 and 2.2, the estimate $\hat{\theta}_N$ (see (2.2)) is a consistent estimate of θ_0 i.e. it converges to θ_0 with probability one when the number N of data tends to infinity. The consistency property also entails that θ_0 is the unique minimum of the asymptotic identification criterion:

$$\theta^* = \arg \min_{\theta} \bar{E} \epsilon^2(t, \theta) \tag{2.5}$$

Moreover, the estimate $\hat{\theta}_N$ is (asymptotically) normally distributed around θ_0 with a covariance matrix P_θ given by:

$$P_\theta = \frac{\sigma_e^2}{N} \, \bar{E} \left(\psi(t, \theta_0) \psi^T(t, \theta_0) \right)^{-1} \tag{2.6}$$

where $\psi(t, \theta) = -\frac{\partial \epsilon(t, \theta)}{\partial \theta}$. Note that P_θ can be estimated using the data set Z^N and $\hat{\theta}_N$:

$$P_\theta \approx \frac{\hat{\sigma}_e^2}{N} \, \left(\frac{1}{N} \sum_{t=1}^{N} \psi \left(t, \hat{\theta}_N \right) \psi^T \left(t, \hat{\theta}_N \right) \right)^{-1} \tag{2.7}$$

where $\hat{\sigma}_e^2 = \frac{1}{N} \sum_{t=1}^{N} \epsilon^2(t, \hat{\theta}_N)$. Using the fact that $\hat{\theta}_N \sim \mathcal{N}(\theta_0, P_\theta)$, we can build, after an identification experiment, the following ellipsoid U that is a $\eta\%$-confidence region for the unknown true parameter vector θ_0:

$$U = \left\{ \theta \mid (\theta - \hat{\theta}_N)^T P_\theta^{-1} (\theta - \hat{\theta}_N) \leq \chi \right\} \tag{2.8}$$

with χ such that $Pr(\chi^2(k) \leq \chi) = \eta$ (the symbol $\chi^2(k)$ represents the χ^2-distribution with k degrees of freedom). Since $\theta_0 \in U$ (modulo the probability level η), the ellipsoid U can be considered as the uncertainty set for the identified parameter vector $\hat{\theta}_N$. From the expression of U, it is clear that the inverse P_θ^{-1} of the covariance matrix of $\hat{\theta}_N$ is a measure of the accuracy of the identified parameter vector $\hat{\theta}_N$.

2.3   Prediction-error identification in closed loop

In many applications, it is of interest of identifying a model of the system (2.1) when this system is operated in closed loop with a stabilizing controller $K(z)$. The objective of this closed-loop configuration can be the rejection of the disturbance $v(t)$ and/or the tracking of a given reference $ref(t)$. Closed-loop identification allows to obtain a model of the system (2.1) while continuing to fulfill these control objectives. Let us assume that the closed-loop configuration can be described by (2.1) and:

$$u(t) = r(t) + K(z)\left(ref(t) - y(t)\right) \tag{2.9}$$

where $ref(t)$ is the reference of the closed loop (which is assumed given and which can be equal to zero) and $r(t)$ is an excitation signal that can be chosen by the user for identification purpose ($r(t) = 0$ in normal operations). For simplicity, we will suppose that $ref(t)$ and $r(t)$ are uncorrelated quasi-stationary signals and have spectra Φ_{ref} and Φ_r. We also suppose that $ref(t)$ and $r(t)$ are uncorrelated with the white noise $e(t)$ in (2.1). In the closed-loop configuration described by (2.1) and (2.9) (see also Figure 2.1), the input and output signal of the true system (2.1) are given by:

$$u(t) = \overbrace{\frac{1}{1 + K(z)G_0(z)}r(t)}^{=u_r(t)} + \frac{K(z)}{1 + K(z)G_0(z)}\left(ref(t) - v(t)\right) \tag{2.10}$$

$$y(t) = \underbrace{\frac{G_0(z)}{1 + K(z)G_0(z)}r(t)}_{=y_r(t)} + \frac{K(z)G_0(z)}{1 + K(z)G_0(z)}ref(t) + \frac{1}{1 + K(z)G_0(z)}v(t) \tag{2.11}$$

where $u_r(t)$ and $y_r(t)$ are the perturbations induced by the excitation signal $r(t)$ on the normal operation of the closed-loop system.
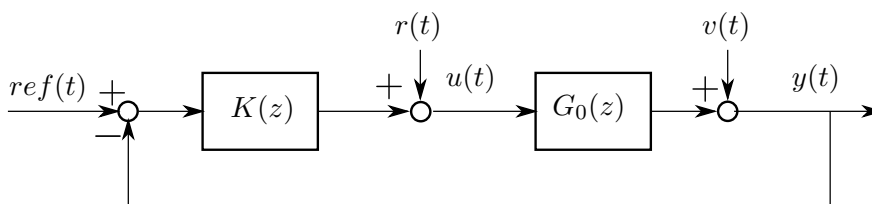
Figure 2.1: Configuration for closed-loop identification.

Let us now describe how a model of the true system (2.1) can be deduced in this closed-loop configuration. As already mentioned, we can excite the closed loop via a sequence $\{r(t) \mid t = 1, \ldots, N\}$. By collecting, during this identification experiment, the signals $u(t)$ and $y(t)$, we obtain the following data set $Z^N = \{y(t),\ u(t) \mid t = 1, \ldots, N\}$. Based on this data set Z^N and a model structure $\mathcal{M}$ satisfying Assumption 2.1, an estimate $\hat{\theta}_N$ of the true parameter vector θ_0 can be obtained using the identification

criterion (2.2). Moreover, this estimate $\hat{\theta}_N$ is a consistent estimate of θ_0 and has the same statistical properties as in the open loop case if the product $K(z)G_0(z)$ contains at least one delay and if the excitation signal $r(t)$ and the reference signal $ref(t)$ satisfies the following data informativity assumption.

Assumption 2.3. *Consider a model structure $\mathcal{M}$ satisfying Assumption 2.1 and a data set Z^N generated in the closed-loop configuration described by (2.1) and (2.9) with an excitation signal $r(t)$ and a reference signal $ref(t)$. Consider also the prediction error $\epsilon(t, \theta)$ defined in (2.3). We assume that the orders of excitation of the chosen excitation signal $r(t)$ and of the given reference signal $ref(t)$ ensure that the property (2.4) holds for the prediction error $\epsilon(t, \theta)$.*

Since $r(t)$ and $ref(t)$ are assumed uncorrelated, their order of excitation just adds up. Consequently, Assumption 2.3 will hold if the total order of excitation of $r(t)$ and $ref(t)$ is larger than a given threshold that only depends on the respective parametrization and the order of the parametrized transfer functions $G(z, \theta)$ and $H(z, \theta)$ in $\mathcal{M}$ and on the order of the controller $K(z)$ [48].

The closed-loop approach described above (called *direct closed-loop identification* in the literature) has been here presented for a single closed loop. As shown in [17], it can however be extended to the case where different closed-loop systems are interconnected in a network and where the reference signal $ref(t)$ of a given loop is computed based on (some of) the measured outputs of the other closed-loop systems in the network (see Section 1.2.2). For this particular case of networks, the direct closed-loop identification presented above can be applied without any modification. As we will see in further details in Chapter 4, the excitation signal r can be applied to a particular loop in the network in order to identify the system present in this particular loop. However, as shown in [17], an excitation signal can also be applied simultaneously to all the loops in the network in order to be able to identify all systems in the network. In both cases, similarly as in direct closed-loop identification, the system present in a given loop can be identified using the identification criterion (2.2) where the prediction error is computed using the input-output data of the to-be-identified system.

2.4   Optimal experiment design: least costly experiment design

2.4.1   Optimal experiment design for open-loop identification

As mentioned in the introduction, optimal experiment design consists in determining the experimental conditions of an identification experiment in an optimal manner. Let us first analyze the case of open-loop identification. The experimental conditions are characterized by the spectrum Φ_u of the excitation signal $u(t)$ (we will indeed suppose that the data length N is given). In the *least costly identification* framework for optimal experiment design, the spectrum Φ_u of the excitation signal u will be determined in such a way that the cost of the experiment is minimized while guaranteeing

that the accuracy of the estimate $\hat{\theta}_N$ identified with such excitation signal is larger than a given threshold [3].

The cost of the identification experiment is generally defined based on the perturbation induced by the excitation signal u on the true system (2.1) and will be here measured by a linear combination of the power of u and of the power of $\breve{y}(t) = G_0(z)u(t) = G(z, \theta_0)u(t)$:

$$\mathcal{J}(\theta_0, \Phi_u) = \frac{1}{2\pi} \int_{-\pi}^{\pi} \left(1 + \beta \, |G(e^{j\omega}, \theta_0)|^2 \right) \, \Phi_u(\omega) \, d\omega \qquad (2.12)$$

where $\beta \geq 0$ is an user-chosen constant that weighs the two terms in $\mathcal{J}$. We use the notation $\mathcal{J}(\theta_0, \Phi_u)$ for the cost of an (open-loop) experiment to stress that this cost both depends on the power spectrum Φ_u of the excitation signal u and on the true parameter vector θ_0 describing the true system (2.1).

As mentioned in Section 2.2, the accuracy of the identified parameter vector $\hat{\theta}_N$ can be measured by the inverse of the covariance matrix P_θ of $\hat{\theta}_N$. Consequently, as also mentioned in Chapter 1, a simple way to formulate the accuracy constraint in the least costly experiment design problem is as follows:

$$P_\theta^{-1}(\theta_0, \Phi_u) \geq R_{adm} \qquad (2.13)$$

where R_{adm} is a given positive-definite matrix that reflects the desired level of accuracy [4, 49]. As indicated in (2.13), the covariance matrix P_θ of $\hat{\theta}_N$ (and its inverse) depends both on the true parameter vector θ_0 and on the spectrum Φ_u of the excitation signal. Indeed, from (2.6), we can derive the following expression for the inverse of P_θ (see e.g., [8])):

$$P_\theta^{-1} = \frac{N}{2\pi\sigma_e^2} \int_{-\pi}^{\pi} F_u(e^{j\omega}, \theta_0)F_u^*(e^{j\omega}, \theta_0)\Phi_u(\omega) + F_e(e^{j\omega}, \theta_0)F_e^*(e^{j\omega}, \theta_0)\sigma_e^2 \, dw \qquad (2.14)$$

where $F_u(z, \theta) = H^{-1}(z, \theta)\frac{\partial G(z,\theta)}{\partial \theta}$ and $F_e(z, \theta) = H^{-1}(z, \theta)\frac{\partial H(z,\theta)}{\partial \theta}$.

Based on the above expressions, we can now formulate the optimal experiment design problem in open loop as the following optimization problem:

$$\min_{\Phi_u} \mathcal{J}(\theta_0, \Phi_u) \qquad (2.15)$$

$$\text{such that } P_\theta^{-1}(\theta_0, \Phi_u) \geq R_{adm} \qquad (2.16)$$

Like all other optimal experiment design problems, the above optimization problem unfortunately depends on the unknown true parameter vector via $\mathcal{J}(\theta_0, \Phi_u)$ and $P_\theta^{-1}(\theta_0, \Phi_u)$. The classical approach to deal with this so-called *chicken-and-egg* problem is to replace the unknown true parameter vector θ_0 by an initial estimate $\hat{\theta}_{init}$ of θ_0. Even though this approach is far from optimal in practice (Chapter 3 will present a methodology

to deal more effectively with the chicken-and-egg issue by considering not only the initial estimate $\hat{\theta}_{init}$, but also its uncertainty), we will for the moment suppose that θ_0 is indeed replaced by $\hat{\theta}_{init}$ in the above optimization problem. Then, as shown in [8, 3], the optimization problem (2.15)-(2.16) is a convex optimization problem since both $\mathcal{J}(\theta_0, \Phi_u)$ and $P_\theta^{-1}(\theta_0, \Phi_u)$ are affine in the decision variable Φ_u.

The remaining issue is that the decision variable Φ_u has an infinite dimension (Φ_u has indeed to be defined at each frequency ω). This issue is generally circumvented by choosing a finite parametrization of the power spectrum. Two parametrizations are generally chosen in practice [8, 3]. The first parametrization corresponds to the spectrum of an excitation signal that can be generated by filtering a white noise by an arbitrary FIR filter of degree L:

$$\Phi_u(\omega) = c_0 + \sum_{m=1}^{L} c_m \left(e^{-j\omega} + e^{j\omega} \right) \geq 0 \quad \forall \omega \tag{2.17}$$

where c_m $(m = 0, \ldots, L)$ are the spectrum coefficients that are to be determined by the optimization problem (2.15)-(2.16). The second parametrization corresponds to the spectrum of a multisine excitation signal at fixed frequencies ω_m $(m = 1, \ldots, L)$ but with arbitrary amplitudes

$$\Phi_u(\omega) = \pi \sum_{m=1}^{L} c_m \left(\delta(\omega - \omega_m) + \delta(\omega + \omega_m) \right) \tag{2.18}$$

where $c_m \geq 0$ $(m = 1, \ldots, L)$ are the spectrum coefficients that are to be determined by the optimization problem (2.15)-(2.16) and the L frequencies ω_m $(m = 1, \ldots, L)$ are chosen to cover the interval $[0, \pi]$. For given c_m $(m = 1, \ldots, L)$, (2.18) can be realized by a multisine $u(t) = \sum_{m=1}^{L} \sqrt{2c_m} \sin(\omega_m t + \phi_m)$ with arbitrary phase shifts ϕ_m $(m = 1, \ldots, L)$. Since, in both parametrizations, the spectrum Φ_u is linear in the to-be-determined coefficients c_m, the optimization problem (2.15)-(2.16) remains a convex optimization problem in these new decision variables.

Remark 2.1. The solution $\Phi_{u,opt}$ of the optimal experiment design problem (2.15)-(2.16) will always lead to an excitation signal u that respects Assumption 2.2. Indeed, the constraint (2.16) and the fact that $R_{adm} > 0$ implies that $P_\theta^{-1}(\theta_0, \Phi_{u,opt}) > 0$. The latter is a sufficient condition for an excitation signal of spectrum $\Phi_{u,opt}$ to yield an informative data set Z^N.

Remark 2.2. We have here for simplicity presented an accuracy constraint (see (2.13)) that puts constraints on the accuracy of all parameters in the parameter vector θ. However, we are generally only interested to obtain a sufficiently accurate model for the plant transfer function G_0. Consequently, in many cases, the matrix R_{adm} will mainly put constraints on the parameters that appear in the transfer function $G(z, \theta)$. In Chapter 3, we will by the way have to restrict attention to accuracy constraints that only pertain to those parameters in $G(z, \theta)$ (see Chapter 3 for more details).

Remark 2.3. We have here presented the so-called *least costly identification* framework for optimal experiment design [3, 4]. Optimal experiment design can also be formulated in a dual fashion. For example, let us consider the classical *E*-optimality framework:

$$\max_{\Phi_u,\ \varepsilon} \ \varepsilon \qquad (2.19)$$

$$\text{such that } \mathcal{J}(\theta_0, \Phi_u) \leq \gamma \qquad (2.20)$$

$$\text{and } P_\theta^{-1}(\theta_0, \Phi_u) \geq \varepsilon I_k \qquad (2.21)$$

where ε is a scalar decision variable and γ is a given bound on the cost of the identification. It is clear that the above optimization problem can be treated similarly as the *least costly* optimization problem (2.15)-(2.16).

2.4.2 Optimal experiment design for closed-loop identification

For direct closed-loop identification, the experimental conditions are characterized by the spectrum Φ_r of the excitation signal $r(t)$ (we will here also suppose that the data length N is given). Like in the open-loop case, the spectrum Φ_r of the excitation signal r will be determined in such a way that the cost of the experiment is minimized while guaranteeing that the accuracy of the estimate $\hat{\theta}_N$ identified with such excitation signal is larger than a given threshold [3].

The cost of a closed-loop identification experiment will be defined based on the perturbation induced by the excitation signal r on the normal operations of the closed-loop system described by equations (2.1) and (2.9). More precisely, we will use the following linear combination of the power of the contribution u_r of r in the input signal u and of the power of the contribution y_r of r in the output signal y (see (2.10)-(2.11)):

$$\mathcal{J}_{cl}(\theta_0, \Phi_r) = \frac{1}{2\pi} \int_{-\pi}^{\pi} \left(|S(e^{j\omega}, \theta_0)|^2 + \beta \, |G(e^{j\omega}, \theta_0)S(e^{j\omega}, \theta_0)|^2 \right) \, \Phi_r(\omega) \, d\omega \qquad (2.22)$$

where $\beta \geq 0$ is here also an user-chosen constant that weights the two terms in $\mathcal{J}_{cl}$ and $S(z, \theta_0) = (1 + K(z)G(z, \theta_0))^{-1} = (1 + K(z)G_0(z))^{-1}$. We observe that, for a closed-loop experiment, the cost $\mathcal{J}_{cl}(\theta_0, \Phi_r)$ depends both on the power spectrum Φ_r of r and on the true parameter vector θ_0 describing the true system (2.1).

Like in the open-loop case, we can also rewrite in the closed-loop case the inverse of the covariance matrix of the identified parameter vector $\hat{\theta}_N$ as an affine function of the excitation spectrum Φ_r:

$$P_\theta^{-1}(\theta_0, \Phi_r) = \dots$$
$$\frac{N}{2\pi\sigma_e^2} \int_{-\pi}^{\pi} F_u(e^{j\omega}, \theta_0)F_u^*(e^{j\omega}, \theta_0) \left(|S(e^{j\omega}, \theta_0)|^2\Phi_r(\omega) + |K(e^{j\omega})S(e^{j\omega}, \theta_0)|^2\Phi_{ref}(\omega) \right) d\omega +$$
$$\dots + \frac{N}{2\pi} \int_{-\pi}^{\pi} F_v(e^{j\omega}, \theta_0)F_v^*(e^{j\omega}, \theta_0)d\omega \qquad (2.23)$$

where $F_v(z,\theta) = H^{-1}(z,\theta)\frac{\partial H(z,\theta)}{\partial \theta} - \frac{K(z)}{1+K(z)G(z,\theta)}\frac{\partial G(z,\theta)}{\partial \theta}$ and $F_u(z,\theta)$ is defined below (2.14).

Based on these expressions, we can formulate the following optimal experiment design problem for the closed-loop identification case:

$$\min_{\Phi_r} \mathcal{J}_{cl}(\theta_0, \Phi_r) \tag{2.24}$$

$$\text{such that } P_\theta^{-1}(\theta_0, \Phi_r) \geq R_{adm} \tag{2.25}$$

Since both $\mathcal{J}_{cl}(\theta_0, \Phi_r)$ and $P_\theta^{-1}(\theta_0, \Phi_r)$ are affine in the decision variable Φ_r, the above optimization problem can be treated in a similar way as the one for the open-loop identification case.

In Chapter 4, we will extend the least costly formulation presented in this section to the case of closed-loop systems that are interconnected.

Robust Optimal Identification Experiment Design for Multisine Excitation

3.1 Introduction

The optimal experiment design formulations presented in the previous chapter (see e.g., (2.15)-(2.16)) all depend on the unknown true parameter vector θ_0. A classical approach to deal with this issue is to replace the unknown θ_0 by an initial estimate $\hat{\theta}_{init}$ of θ_0. However, this approach has the drawback that the optimal spectrum is not guaranteed to yield the desired accuracy and that the experiment cost computed with $\hat{\theta}_{init}$ can underestimate the actual experiment cost. These observations are at the root of the research area on *robust optimal experiment design* (see [20] for a good survey).

As mentioned in Chapter 1, in the engineering literature, the most widely used approach for robust optimal experiment design is the one that consists in considering an uncertainty set U containing the unknown true parameter vector θ_0 (the so-called min-max design [20, 22]). The optimal experiment design problem can then be formulated as determining the spectrum Φ of the excitation signal (i.e., Φ_u in the open-loop case and Φ_r in the closed-loop case) minimizing the value of a scalar γ under the constraints that $\mathcal{J}(\theta, \Phi) \leq \gamma \ \forall \theta \in U$ and that $P^{-1}(\theta, \Phi) \geq R_{adm} \ \forall \theta \in U$. If we denote by γ_{opt} and Φ_{opt} the solution of this optimization problem, we have the guarantee that $P^{-1}(\theta_0, \Phi_{opt}) \geq R_{adm}$ and that γ_{opt} is an upper bound for the actual experiment cost $\mathcal{J}(\theta_0, \Phi_{opt})$. However, as also stressed in Chapter 1, finding a tractable approach to deal with such a robustified optimal experiment design problem is still an open research question. While this optimization problem can be exactly solved in very particular and simple situations (see e.g. [20, 23]), the general approach when facing more complex systems is to replace the initial uncertainty set (containing an infinite number of elements) by a number n_g of grid points of this uncertainty set U (see e.g. [8, 3, 20]). Consequently, the cost constraint and the accuracy constraint over the set U in the ro-

bustified optimal experiment design problem are replaced each by n_g constraints (one for each grid point). Even though it is obviously better from a robustification point-of-view than just replacing θ_0 by one grid point i.e. $\hat{\theta}_{init}$, this relaxation of the original robustified optimal experiment design problem cannot yield the guarantees linked to the original problem.

The main contribution of this chapter is to present an approach in order to tackle the robust optimal experiment design problem without approximation. For this purpose, we observe that, except for its dependence on the to-be-determined spectrum, the robustified cost constraint and the robustified accuracy constraint are similar to constraints that are treated in robustness analysis. Based on this observation and on the separation of graph framework [29, 30, 31], we derive constraints that are linear in the decision variables of the optimal experiment design problem and that imply the original robustified cost and accuracy constraints. As we will see in the sequel, to derive these linear constraints, it will be required to parametrize the to-be-determined spectrum using the parametrization (2.18) i.e., the one corresponding to a multisine excitation signal. We will also see that we will have to restrict attention to open-loop identification with a Box-Jenkins (BJ) model structure (see Appendix A) and to accuracy constraints that uniquely pertain to the parameters in the plant transfer function G. We will nevertheless propose possible (suboptimal) extensions towards closed-loop identification and other model structures.

3.2 Open-loop identification in a BJ model structure

As mentioned in the previous section, we assume that the true system (2.1) is operated in open loop and that we will identify this true system in a (full-order) BJ model structure i.e. a BJ model structure satisfying Assumption 2.1. Let us for further reference give more details on the parametrization of the BJ model structure (see also Appendix A):

$$\mathcal{M} = \{G(z,\theta) = G(z,\rho), \ H(z,\theta) = H(z,\zeta) \mid \theta = (\rho^T, \zeta^T)^T \in \mathbf{R}^k\} \qquad (3.1)$$

$$G(z,\theta) = \frac{z^{-n_k}\left(b_0 + b_1 z^{-1} + \cdots + b_{n_b} z^{-n_b}\right)}{1 + f_1 z^{-1} + \cdots + f_{n_f} z^{-n_f}}$$

$$H(z,\theta) = \frac{1 + c_1 z^{-1} + \cdots + c_{n_c} z^{-n_c}}{1 + d_1 z^{-1} + \cdots + d_{n_d} z^{-n_d}}$$

with $\theta = (\rho^T, \zeta^T)^T \in \mathbf{R}^k$ with $\rho = (b_0, \ldots, b_{n_b}, f_1, \ldots, f_{n_f})^T$ and $\zeta = (c_1, \ldots, c_{n_c}, d_1, \ldots, d_{n_d})^T$. We will denote by k_G (resp. k_H) the dimension of ρ (resp. ζ) and we have thus $k_G = n_b + n_f + 1$, $k_H = n_c + n_d$ and $k = k_G + k_H$. The orders n_b, n_f, n_c and n_d as well as the delay n_k can be freely chosen by the user. To satisfy Assumption 2.1, the orders of $G(z,\theta)$ and $H(z,\theta)$ are thus chosen in such a way that there exists an unique parameter vector $\theta_0 = (\rho_0^T, \zeta_0^T)^T$ such that $G_0(z) = G(z,\theta_0) = G(z,\rho_0)$ and $H_0(z) = H(z,\theta_0) = H(z,\zeta_0)$. Note that the BJ model structure is the most flexible model structure in practice and that a BJ model structure satisfying Assumption 2.1

can be found for all LTI systems of the type (2.1).

If we apply a sequence $\{u(t) \mid t = 1, \ldots, N\}$ of spectrum Φ_u to (2.1) and collect the corresponding output $\{y(t) \mid t = 1, \ldots, N\}$, an estimate $\hat{\theta}_N = (\hat{\rho}_N^T, \hat{\zeta}_N^T)^T$ of $\theta_0 = (\rho_0^T, \zeta_0^T)^T$ can be obtained using the prediction-error criterion (2.2). As shown in Chapter 2, if u satisfies Assumption 2.2, this estimate $\hat{\theta}_N$ is (asymptotically) normally distributed around θ_0 with a covariance matrix $P_\theta(\theta_0, \Phi_u)$ whose expression is given in (2.6) (see also (2.14)). In the case of an open-loop identification in a BJ model structure, this expression presents a block-diagonal structure [8, 50]:

$$P_\theta = \begin{pmatrix} P_\rho & \mathbf{0} \\ \mathbf{0} & P_\zeta \end{pmatrix} \tag{3.2}$$

and the inverse of the diagonal blocks are given by:

$$P_\rho^{-1}(\theta_0, \Phi_u) = \frac{N}{\sigma_e^2} \frac{1}{2\pi} \int_{-\pi}^{\pi} F_{u,\rho}(e^{j\omega}, \theta_0) F_{u,\rho}^*(e^{j\omega}, \theta_0) \Phi_u(\omega) \, d\omega \tag{3.3}$$

$$P_\zeta^{-1}(\theta_0) = N \frac{1}{2\pi} \int_{-\pi}^{\pi} F_{e,\zeta}(e^{j\omega}, \theta_0) F_{e,\zeta}^*(e^{j\omega}, \theta_0) \, d\omega \tag{3.4}$$

with

$$F_{u,\rho}(z, \theta) = H^{-1}(z, \zeta) \frac{\partial G(z, \rho)}{\partial \rho} \quad \text{and} \quad F_{e,\zeta}(z, \theta) = H^{-1}(z, \zeta) \frac{\partial H(z, \zeta)}{\partial \zeta} \tag{3.5}$$

Note that the notations $P_\rho(\theta_0, \Phi_u)$ and $P_\zeta(\theta_0)$ are used to stress that the covariance matrix of $\hat{\rho}_N$ is a function of both θ_0 and Φ_u and the one of $\hat{\zeta}_N$ is a function of just θ_0. We will also use the notation $P_\theta(\theta_0, \Phi_u)$ for the whole covariance matrix (3.2).

As mentioned in Chapter 2, $P_\theta^{-1}(\theta_0, \Phi_u)$ is a measure of the accuracy of $\hat{\theta}_N = (\hat{\rho}_N^T, \hat{\zeta}_N^T)^T$ [8]. In general, we are mainly interested in the accuracy of the part $\hat{\rho}_N$ of the vector $\hat{\theta}_N$ (the part that defines the model $G(z, \hat{\rho}_N)$ of $G(z, \rho_0)$). Due to (3.2), the accuracy of $\hat{\rho}_N$ can thus be measured by $P_\rho^{-1}(\theta_0, \Phi_u)$ (see (3.3)).

In the sequel, we will suppose that an initial identification experiment has delivered an initial estimate $\hat{\theta}_{init} = (\hat{\rho}_{init}^T, \hat{\zeta}_{init}^T)^T$ with covariance matrix $P_{\theta,init}$. Consequently, the following ellipsoid U_{init} is a $\eta\%$-confidence region for the unknown true parameter vector θ_0:

$$U_{init} = \left\{ \theta \mid (\theta - \hat{\theta}_{init})^T P_{\theta,init}^{-1} (\theta - \hat{\theta}_{init}) \leq \chi \right\} \tag{3.6}$$

with χ such that $Pr(\chi^2(k) \leq \chi) = \eta$ (say 95 %). As mentioned in Chapter 2, the ellipsoid U_{init} can be used as a description of the uncertainty of the initial estimate $\hat{\theta}_{init}$ and, from now on, we will assume that θ_0 indeed belongs to the ellipsoid U_{init} constructed based on the initial estimate $\hat{\theta}_{init}$ and its covariance matrix $P_{\theta,init}$.

We will suppose that the accuracy $P_{\rho,init}^{-1}$ of $\hat{\rho}_{init}$ is not sufficient for the purpose of the identified model ($P_{\rho,init} = (I_{k_G} \; \mathbf{0}) P_{\theta,init} (I_{k_G} \; \mathbf{0})^T$). Similarly as was done for

the full vector θ in Chapter 2 (see (2.13)), we will deem an estimate of ρ_0 sufficiently accurate when the inverse of its covariance matrix satisfies $P_\rho^{-1} \geq R_{adm,\rho}$ for a given positive-definite matrix $R_{adm,\rho} \in \mathbf{R}^{k_G \times k_G}$.

In order to obtain such a sufficiently accurate estimate, we need to perform a second experiment that yields a new estimate $\hat{\theta}_N = (\hat{\rho}_N^T, \hat{\zeta}_N^T)^T$ of θ_0 having a covariance matrix P_θ. We can then combine the information on θ_0 contained in the estimates $\hat{\theta}_N$ and $\hat{\theta}_{init}$ using the following estimator[1]:

$$\hat{\theta}_{final} = (P_\theta^{-1} + P_{\theta,init}^{-1})^{-1} \left(P_\theta^{-1}\hat{\theta}_N + P_{\theta,init}^{-1}\hat{\theta}_{init} \right)$$

whose covariance matrix is given by $(P_\theta^{-1} + P_{\theta,init}^{-1})^{-1}$ [1, page 464]. The estimate $\hat{\theta}_{final}$ can be split into $\hat{\theta}_{final} = (\hat{\rho}_{final}^T, \hat{\zeta}_{final}^T)^T$ and the inverse of the covariance matrix $P_{\rho,final}$ of $\hat{\rho}_{final}$ has thus the following expression:

$$P_{\rho,final}^{-1} = P_\rho^{-1}(\theta_0, \Phi_u) + P_{\rho,init}^{-1}$$

with Φ_u the spectrum of the input signal used during the second experiment. Consequently, the input spectrum Φ_u of the second experiment must be designed to guarantee that $P_{\rho,final}^{-1} = P_\rho^{-1}(\theta_0, \Phi_u) + P_{\rho,init}^{-1} \geq R_{adm,\rho}$.

For the sequel, it will be important to make the following observation and the following assumption:

Observation 3.1. *In the BJ model structure (3.1), $G(z, \theta)$ and $H(z, \theta)$ are rational functions of the parameter vector θ. Consequently, they can be expressed as:*

$$G(z, \theta) = \frac{Z_N(z)\theta}{1 + Z_D(z)\theta} \tag{3.7}$$

$$H(z, \theta) = \frac{1 + Z_{N,H}(z)\theta}{1 + Z_{D,H}(z)\theta} \tag{3.8}$$

where $Z_N(z)$, $Z_D(z)$, $Z_{N,H}(z)$ and $Z_{D,H}(z)$ are row vectors of transfer functions (see Appendix B.1 for an example). ∎

Assumption 3.1. *The uncertainty U_{init} defined in (3.6) is small enough to guarantee that, like $G(z, \theta_0)$ and $H^{-1}(z, \theta_0)$, $G(z, \theta)$ and $H^{-1}(z, \theta)$ are stable transfer functions for all $\theta \in U_{init}$. Due to (3.5), this also implies that $F_{u,\rho}(z, \theta)$ is a vector of stable transfer functions for all $\theta \in U_{init}$.* ∎

Note that we can easily verify whether a given U_{init} satisfies the property mentioned in Assumption 3.1 using the results in [51].

---

[1]In this estimator, we use the estimated covariance matrix P_θ that can be deduced with $\hat{\theta}_N$ and Z^N (see (2.7)).

3.3 Robust optimal experiment design

Similarly as was proposed in Section 2.4.1, the spectrum Φ_u of the second experiment described above will be the one that leads to the smallest identification cost $\mathcal{J}(\theta_0, \Phi_u)$ (see (2.12)) while guaranteeing that $P_\rho^{-1}(\theta_0, \Phi_u) + P_{\rho,init}^{-1} \geq R_{adm}$. Like all other optimal experiment design problems, the above optimization problem unfortunately depends on the unknown true parameter vector via $\mathcal{J}(\theta_0, \Phi_u)$ and $P_\rho^{-1}(\theta_0, \Phi_u)$. As mentioned in the introduction, the classical approach to deal with this so-called *chicken-and-egg* problem is to replace the unknown true parameter vector θ_0 by its initial estimate $\hat{\theta}_{init}$. This yields to the following optimization problem:

$$\min_{\Phi_u^{\hat{\theta}_{init}}} \mathcal{J}(\hat{\theta}_{init}, \Phi_u^{\hat{\theta}_{init}}) \tag{3.9}$$

$$\text{such that } P_\rho^{-1}(\hat{\theta}_{init}, \Phi_u^{\hat{\theta}_{init}}) + P_{\rho,init}^{-1} \geq R_{adm,\rho} \tag{3.10}$$

This classical approach has two main disadvantages. If we denote by $\Phi_{u,opt}^{\hat{\theta}_{init}}$ the solution of (3.9)-(3.10), the actual cost $\mathcal{J}(\theta_0, \Phi_{u,opt}^{\hat{\theta}_{init}})$ of the identification can be underestimated by $\mathcal{J}(\hat{\theta}_{init}, \Phi_{u,opt}^{\hat{\theta}_{init}})$. Moreover, $\Phi_{u,opt}^{\hat{\theta}_{init}}$ can lead to a covariance matrix $P_\rho^{-1}(\theta_0, \Phi_{u,opt}^{\hat{\theta}_{init}})$ for which $P_\rho^{-1}(\theta_0, \Phi_{u,opt}^{\hat{\theta}_{init}}) + P_{\rho,init}^{-1} \geq R_{adm}$ is not respected.

The robust approach for optimal experiment design has been introduced to increase the guarantees of the experiment design by taking not only the initial estimate $\hat{\theta}_{init}$ of θ_0 into account, but also the uncertainty set U_{init} [20, 22]. The robustified optimal experiment design problem is defined as:

$$\min_{\Phi_u, \gamma} \gamma \tag{3.11}$$

$$\text{such that } \mathcal{J}(\theta, \Phi_u) \leq \gamma \quad \forall \theta \in U_{init} \tag{3.12}$$

$$\text{and } P_\rho^{-1}(\theta, \Phi_u) + P_{\rho,init}^{-1} \geq R_{adm,\rho} \quad \forall \theta \in U_{init} \tag{3.13}$$

If we denote by $\Phi_{u,opt}^{orig}$ and γ_{opt}^{orig} the solution of this optimization problem, we have that $\gamma_{opt}^{orig} = \sup_{\theta \in U_{init}} \mathcal{J}(\theta, \Phi_{u,opt}^{orig})$. Moreover, the spectrum $\Phi_{u,opt}^{orig}$ is, by construction, the spectrum Φ_u leading to the smallest value of $\sup_{\theta \in U_{init}} \mathcal{J}(\theta, \Phi_u)$ while guaranteeing the robustified accuracy constraint (3.13). Since we assume that $\theta_0 \in U_{init}$, this robustified formulation ensures that:

- the a-priori unknown cost $\mathcal{J}(\theta_0, \Phi_{u,opt}^{orig})$ is smaller than γ_{opt}^{orig}

- $P_\rho(\theta_0, \Phi_{u,opt}^{orig})$ is guaranteed to satisfy $P_\rho^{-1}(\theta_0, \Phi_{u,opt}^{orig}) + P_{\rho,init}^{-1} \geq R_{adm,\rho}$.

As already mentioned in Chapter 1, the optimization problem (3.11)-(3.13) has been until now tackled using a gridding approach (see e.g. [8, 3, 20]):

$$\min_{\Phi_u^g, \gamma_g} \gamma_g \tag{3.14}$$

$$\text{such that } \mathcal{J}(\theta_i, \Phi_u^g) \leq \gamma_g \quad \forall \, \theta_i \in \Theta_{n_g} \tag{3.15}$$

$$\text{and } P_\rho^{-1}(\theta_i, \Phi_u^g) + P_{\rho,init}^{-1} \geq R_{adm} \quad \forall \, \theta_i \in \Theta_{n_g} \tag{3.16}$$

where Θ_{n_g} is a set containing n_g grid points θ_i ($i = 1, \ldots, n_g$) such that $\theta_i \in U_{init}$. Since Θ_{n_g} is always a strict subset of U_{init}, the solution $\gamma_{g,opt}$ of (3.14)-(3.16) is a lower bound of the solution γ_{opt}^{orig} of (3.11)-(3.13). For the same reason, this gridding approach cannot yield the guarantees linked to the original problem (3.11)-(3.13). The main contribution of this chapter is to derive, based on robustness analysis tools, a convex optimization problem having the same guarantees as the original problem (3.11)-(3.13).

The original robust optimization problem (3.11)-(3.13) can be relaxed into a convex optimization problem if (3.12) and (3.13) can be transformed into two constraints that are linear in the decision variables Φ_u and γ.

In the sequel, we will show that, as very often in robustness analysis theory, we cannot find tractable linear constraints that are equivalent to (3.12) and (3.13), but we can find one that implies (3.12) and another one that implies (3.13). This entails a certain conservatism. However, if we solve the optimization problem with these alternative constraints and if we denote its solution by γ_{opt} and $\Phi_{u,opt}$, we still have the guarantee that:

1. $P_\rho^{-1}(\theta, \Phi_{u,opt}) + P_{\rho,init}^{-1} \geq R_{adm,\rho} \quad \forall \, \theta \in U_{init}$ and thus $P_\rho^{-1}(\theta_0, \Phi_{u,opt}) + P_{\rho,init}^{-1} \geq R_{adm,\rho}$

2. $\mathcal{J}(\theta_0, \Phi_{u,opt}) \leq \sup_{\theta \in U_{init}} \mathcal{J}(\theta, \Phi_{u,opt}) \leq \gamma_{opt}$.

In addition, we have also that γ_{opt} is an upper bound for γ_{opt}^{orig}, the solution of the original optimization problem (3.11)-(3.13).

We will derive the tractable alternative constraints discussed in the previous paragraph in the case where the spectrum Φ_u will be parametrized as in (2.18) i.e. Φ_u corresponds to the spectrum of a multisine with fixed frequencies ω_m ($m = 1, \ldots, L$), but with aribtrary amplitudes. Using this particular parametrization of Φ_u, the constraint (3.12) can be rewritten as follows:

$$\sum_{m=1}^{L} c_m \left(1 + \beta \, |G(e^{j\omega_m}, \theta)|^2 \right) \leq \gamma \quad \forall \, \theta \in U_{init} \tag{3.17}$$

Collecting the terms $G(e^{j\omega_m}, \theta)$ ($m = 1, \ldots, L$) in $\mathcal{G}(\theta) = (G(e^{j\omega_1}, \theta), G(e^{j\omega_2}, \theta), \ldots, G(e^{j\omega_L}, \theta))^T$, we can rewrite (3.17) as:

$$\left(\sum_{m=1}^{L} c_m \right) + \beta \, \mathcal{G}^*(\theta) \, \bar{C} \, \mathcal{G}(\theta) \leq \gamma \quad \forall \, \theta \in U_{init} \tag{3.18}$$

with $\bar{C} = diag(c_1, c_2, \ldots, c_L)$.

Using (3.3) and (2.18), the term $P_\rho^{-1}(\theta, \Phi_u)$ in (3.13) can also be rewritten as follows:

$$P_\rho^{-1}(\theta, \Phi_u) = \frac{N}{2\,\sigma_e^2} \sum_{m=1}^{L} c_m \left(F_{u,\rho}(e^{j\omega_m}, \theta) F_{u,\rho}^*(e^{j\omega_m}, \theta) + F_{u,\rho}(e^{-j\omega_m}, \theta) F_{u,\rho}^*(e^{-j\omega_m}, \theta) \right)$$

If we denote by $F_{u,\rho,i}(z, \theta)$ the ith entry of the vector $F_{u,\rho}(z, \theta)$ and we collect the terms $F_{u,\rho,i}(e^{j\omega_m}, \theta)$ $(m = 1, \ldots, L)$ in complex vectors $\mathcal{F}_i(\theta)$ $(i = 1, \ldots, k_G)$, of dimension $L \times 1$, defined as:

$$\mathcal{F}_i(\theta) = (F_{u,\rho,i}(e^{j\omega_1}, \theta), F_{u,\rho,i}(e^{j\omega_2}, \theta), \ldots, F_{u,\rho,i}(e^{j\omega_L}, \theta))^T \tag{3.19}$$

we can then rewrite $P_\rho^{-1}(\theta, \Phi_u)$ as:

$$P_\rho^{-1}(\theta, \Phi_u) = \frac{N}{2\,\sigma_e^2} \sum_{i=1}^{k_G} \sum_{j=1}^{k_G} (m_i \otimes \mathcal{F}_i(\theta))^* \bar{C} (m_j \otimes \mathcal{F}_j(\theta)) + (m_i \otimes \mathcal{F}_j(\theta))^* \bar{C} (m_j \otimes \mathcal{F}_i(\theta))$$

$$\tag{3.20}$$

where m_i $(i = 1, \ldots, k_G)$ is a unit vector of dimension $1 \times k_G$ whose entries are all zero except the ith entry which is equal to 1 and where $\otimes$ represents the Kronecker product.

Remark 3.1. The particular structure (3.20) will be instrumental in developing a convex relaxation for the robust accuracy constraint (3.13). Since the inverse $P_\zeta^{-1}(\theta_0)$ of the covariance matrix of $\hat{\zeta}_N$ (see (3.4)) cannot be rewritten in a similar way, the same robustness analysis tools cannot be used to robustify an accuracy constraint based on this part of the covariance matrix.

Remark 3.2. In (3.20), the actual value of the variance σ_e^2 of the white noise e (see (2.1)) is generally unknown. However, we can also robustify the optimal experiment design problem against this uncertainty. For this purpose, we can replace σ_e^2 in (3.20) by $\sigma_{e,max}^2$, where $\sigma_{e,max}^2$ is the maximal value of the $\eta\%$-confidence interval $[\sigma_{e,min}^2, \sigma_{e,max}^2]$ for σ_e^2 that can be constructed using the initial identification experiment (the one yielding $\hat{\theta}_{init}$) [1].

Let us now derive the tractable alternatives for the constraints (3.12) and (3.13).

3.4 Tackling the robustified cost constraint using robustness analysis tools

We will start by deriving a tractable alternative for the robustified cost constraint (3.12) using the fact that this constraint is equivalent to (3.17)-(3.18) when the parametrization (2.18) is used for Φ_u. An important step towards the developments of this result is to rewrite $\mathcal{G}(\theta)$ in the Linear Fractional Transformation (LFT) framework [52].

3.4.1 Linear Fractional Transformation

Let us first observe that, due to Observation 3.1, $\breve{y}(t) = G(z, \theta)u(t)$ can be written as the following LFT in θ involving the internal scalar signal $q(t)$ and the internal vector of signals $p(t)$:

$$p(t) = \theta \; q(t) \;\; \text{and} \;\; \left(\begin{array}{c} q(t) \\ \breve{y}(t) \end{array} \right) = \underbrace{\left(\begin{array}{cc} -Z_D(z) & 1 \\ Z_N(z) & 0 \end{array} \right)}_{M_G(z)} \left(\begin{array}{c} p(t) \\ u(t) \end{array} \right) \qquad (3.21)$$

Let us denote by $x(e^{j\omega})$ the Fourier transform of a signal (or vector of signals) $x(t)$ and let us recall that the Fourier transform $\breve{y}(e^{j\omega})$ of $\breve{y}(t) = G(z, \theta)u(t)$ is equal to $G(e^{j\omega}, \theta)$ when $u(t)$ is equal to a pulse signal $\delta(t)$ (i.e. $u(e^{j\omega}) = 1$). Consequently, the frequency response $G(e^{j\omega}, \theta)$ of $G(z, \theta)$ at one given frequency ω can also be deduced by solving for $\breve{y}(e^{j\omega})$ in the following system of equations:

$$p(e^{j\omega}) = \theta \; q(e^{j\omega}) \;\; \text{and} \;\; \left(\begin{array}{c} q(e^{j\omega}) \\ \breve{y}(e^{j\omega}) \end{array} \right) = M_G(e^{j\omega}) \left(\begin{array}{c} p(e^{j\omega}) \\ 1 \end{array} \right) \qquad (3.22)$$

Note that, in this system of equations, all Fourier transforms are well defined for all $\theta \in U_{init}$ due to Assumption 3.1.

Using the same reasoning, the vector $\mathcal{G}(\theta)$, containing the frequency response of $G(z, \theta)$ at the frequencies present in the spectrum (2.18), can be determined by solving for $\bar{y}$ in the system of equations (3.23) derived using (3.22):

$$\bar{p} = (I_L \otimes \theta) \; \bar{q} \qquad \text{and}$$
$$\left(\begin{array}{c} \bar{q} \\ \bar{y} \end{array} \right) = \underbrace{\left(\begin{array}{cc} \bar{M}_{11,\mathcal{G}} & \bar{M}_{12,\mathcal{G}} \\ \bar{M}_{21,\mathcal{G}} & \bar{M}_{22,\mathcal{G}} \end{array} \right)}_{\bar{M}_\mathcal{G}} \left(\begin{array}{c} \bar{p} \\ 1 \end{array} \right) \qquad (3.23)$$

with $\bar{p} = (p^T(e^{j\omega_1}), \dots, p^T(e^{j\omega_L}))^T$, $\bar{q} = (q(e^{j\omega_1}), \dots, q(e^{j\omega_L}))^T$ and

$$\bar{M}_{11,\mathcal{G}} = -bdiag(Z_D(e^{j\omega_1}), \dots, Z_D(e^{j\omega_L}))$$
$$\bar{M}_{12,\mathcal{G}} = (1, \dots, 1)^T$$
$$\bar{M}_{21,\mathcal{G}} = bdiag(Z_N(e^{j\omega_1}), \dots, Z_N(e^{j\omega_L}))$$
$$\bar{M}_{22,\mathcal{G}} = \mathbf{0}$$

3.4.2 Set of multipliers related to the uncertainty set U_{init}

Since we consider here (3.18), the parameter vector θ in the LFT for $\mathcal{G}(\theta)$ is restricted to be in the uncertainty set U_{init} (see (3.6)). In our approach, a necessary ingredient to find a tractable alternative for (3.18) is to associate, with the set U_{init}, a so-called set of multipliers. In a nutshell, the set of multipliers $\mathcal{A}_n$ that we will consider here is an explicit and affine parametrization of the quadratic constraints satisfied by

the graphs of the signals q_n and p_n when $p_n(t) = (I_n \otimes \theta)q_n(t)$ with $\theta \in U_{init}$ (n is an arbitrary integer such that $n \geq 1$) [29, 30, 31].

Definition 3.1. *Consider the set U_{init} defined in (3.6) satisfying Assumption 3.1. Consider also an integer $n \geq 1$. We define the set of multipliers $\mathcal{A}_n$ as a set of affinely parametrized Hermitian matrices A_n (of dimension $n(k+1) \times n(k+1)$) that all have the following property:*

$$\begin{pmatrix} I_n \\ I_n \otimes \theta \end{pmatrix}^T A_n \begin{pmatrix} I_n \\ I_n \otimes \theta \end{pmatrix} \geq 0 \quad \forall \theta \in U_{init} \tag{3.24}$$

In other words, $A_n \in \mathcal{A}_n \implies$ (3.24).

It is important to stress that the more extensive the parametrization of the set of multipliers, the smaller the conservatism discussed in Section 3.3 will be [29, 30, 31]. An extensive parametrization of the set of multipliers corresponding to U_{init} can be easily derived from [10] and is given in the following proposition:

Proposition 3.1. *Consider Definition 3.1 and the set U_{init} defined in (3.6). The matrices $A_n = \begin{pmatrix} A_{n,11} & A_{n,12} \\ A_{n,12}^* & A_{n,22} \end{pmatrix}$ belonging to the set $\mathcal{A}_n$ corresponding to U_{init} are parametrized as follows ($j = \sqrt{-1}$):*

$$A_{n,11} = A_0 \left(\chi - \hat{\theta}_{init}^T P_{\theta,init}^{-1} \hat{\theta}_{init} \right) \qquad A_{n,22} = -A_0 \otimes P_{\theta,init}^{-1} + j\tilde{A} - \tilde{B} \tag{3.25}$$

$$A_{n,12} = A_0 \otimes (P_{\theta,init}^{-1} \hat{\theta}_{init})^T + \begin{pmatrix} j\hat{v}_{11}^T & j\hat{v}_{12}^T & \cdots & j\hat{v}_{1n}^T \\ j\hat{v}_{12}^T & j\hat{v}_{22}^T & \cdots & j\hat{v}_{2n}^T \\ \vdots & \vdots & \ddots & \vdots \\ j\hat{v}_{1n}^T & j\hat{v}_{2n}^T & \cdots & j\hat{v}_{nn}^T \end{pmatrix} + \ldots$$

$$\ldots + \begin{pmatrix} 0 & \tilde{v}_{12}^T & \cdots & \tilde{v}_{1n}^T \\ -\tilde{v}_{12}^T & 0 & \ddots & \vdots \\ \vdots & \ddots & \ddots & \tilde{v}_{(n-1)n}^T \\ -\tilde{v}_{1n}^T & \cdots & -\tilde{v}_{(n-1)n}^T & 0 \end{pmatrix}$$

where $A_0 \in \mathbf{C}^{n \times n}$ can take any value as long as A_0 is a positive definite Hermitian matrix, where $\hat{v}_{lr} \in \mathbf{R}^k$ and $\tilde{v}_{lr} \in \mathbf{R}^k$ are column vectors that can take any value ($l = 1, \ldots, n$ and $r = 1, \ldots, n$) and finally where $\tilde{A}$ and $\tilde{B}$ are square matrices of

dimension nk that can take any values as long as:

$$\tilde{A} = \begin{pmatrix} L_{11} & L_{12} & \dots & L_{1n} \\ L_{12} & L_{22} & \dots & L_{2n} \\ \vdots & \vdots & \ddots & \vdots \\ L_{1n} & L_{2n} & \dots & L_{nn} \end{pmatrix} \quad with \quad L_{ij} = -L_{ij}^T \in \mathbf{R}^{k \times k}$$

$$\tilde{B} = \begin{pmatrix} 0 & K_{12} & \dots & K_{1n} \\ -K_{12} & 0 & \ddots & \vdots \\ \vdots & \ddots & \ddots & K_{(n-1)n} \\ -K_{1n} & \dots & -K_{(n-1)n} & 0 \end{pmatrix} \quad with \quad K_{ij} = -K_{ij}^T \in \mathbf{R}^{k \times k}$$

The set of multipliers $\mathcal{A}_n$ consists thus in the set of all matrices A_n that can be parametrized with the free variables A_0, $\tilde{A}$, $\tilde{B}$, $\hat{v}_{lr}$ and $\tilde{v}_{lr}$ ($l = 1, \dots, n$ and $r = 1, \dots, n$) satisfying the above constraints.

Proof. See Appendix B.2. ■

In the optimization problem that we will introduce in the sequel to tackle the robust optimal experiment design problem, two of the decision variables will be matrices A_n as introduced in the previous proposition. Consequently, as mentioned at the end of the statement of the proposition, one will have to determine, in both cases, the free parameters/variables in the parametrization of A_n i.e. A_0, $\tilde{A}$, $\tilde{B}$, $\hat{v}_{lr}$ and $\tilde{v}_{lr}$ ($l = 1, \dots, n$ and $r = 1, \dots, n$). The number of real scalar values[2] in these free variables is given by $n^2 \left(\frac{k^2+k}{2} + 1 \right)$. This number is thus the number of scalar decision variables if the matrix A_n is a matricial decision variable in an optimization problem. For the sequel, it is important to note that this number can be become large if n and/or k are large.

3.4.3   Robustified cost contraint

Based on the sets of multipliers $\mathcal{A}_n$ when $n = L$ and the LFT representation (3.23) of $\mathcal{G}(\theta)$, we have now all the ingredients to derive a tractable alternative constraint for (3.18).

Proposition 3.2. *Consider an initial uncertainty set U_{init} (see (3.6)) satisfying Assumption 3.1 and the robust cost constraint (3.18) obtained when the spectrum Φ_u is parametrized as in (2.18). Consider the LFT representation (3.23) for $\mathcal{G}(\theta)$ as well as the set of multipliers $\mathcal{A}_L$ associated with U_{init} (see Definition 3.1 and Proposition 3.1 with $n = L$). Then, the constraint (3.18) holds for a given γ if we can find a matrix*

---

[2]Each complex scalar entry in A_n counts as two real scalar variables.

$A_L \in \mathcal{A}_L$ *such that*

$$\mathcal{V}^* \, A_L \, \mathcal{V} + \mathcal{L}^* \, \bar{C} \, \mathcal{L} \leq \begin{pmatrix} \mathbf{0} & \mathbf{0} \\ \mathbf{0} & \frac{\gamma - \left(\sum_{m=1}^{L} c_m\right)}{\beta} \end{pmatrix} \tag{3.26}$$

where $\mathcal{L} = \begin{pmatrix} \bar{M}_{21,\mathcal{G}} & \bar{M}_{22,\mathcal{G}} \end{pmatrix}$ *and*

$$\mathcal{V} = \begin{pmatrix} \bar{M}_{11,\mathcal{G}} & \bar{M}_{12,\mathcal{G}} \\ I_{kL} & \mathbf{0} \end{pmatrix}$$

We observe that the matrix inequality (3.26) *is linear in* γ, A_L *and in the coefficients* c_m *$(m = 1, \ldots, L)$ present in* $\bar{C}$.

Proof. Let us consider (3.23) for a given $\theta \in U_{init}$ and let us consider the corresponding signals $\bar{p}$, $\bar{q}$ and $\bar{y} = \mathcal{G}(\theta)$. Let us then pre- and post-multiply the LMI constraint (3.26) with $(\bar{p}^*, 1)$ and $(\bar{p}^T, 1)^T$, respectively. Using (3.23) and $\bar{y} = \mathcal{G}(\theta)$, this yields:

$$\begin{pmatrix} \bar{q} \\ \bar{p} \end{pmatrix}^* A_L \begin{pmatrix} \bar{q} \\ \bar{p} \end{pmatrix} + \mathcal{G}^*(\theta)\bar{C}\mathcal{G}(\theta) \leq \frac{\gamma - \sum_{m=1}^{L} c_m}{\beta} \tag{3.27}$$

Since $\bar{p} = (I_L \otimes \theta)\bar{q}$, we can rewrite (3.27) as follows:

$$\bar{q}^* \begin{pmatrix} I_L \\ I_L \otimes \theta \end{pmatrix}^T A_L \begin{pmatrix} I_L \\ I_L \otimes \theta \end{pmatrix} \bar{q} + \mathcal{G}^*(\theta)\bar{C}\mathcal{G}(\theta) \leq \frac{\gamma - \sum_{m=1}^{L} c_m}{\beta} \tag{3.28}$$

The above reasoning can be done for any value of $\theta \in U_{init}$. In other words, for the matrix $A_L \in \mathcal{A}_L$ found by the optimization problem, (3.28) holds true for all $\theta \in U_{init}$. Consequently, using Definition 3.1 with $n = L$, we have therefore also that $\mathcal{G}^*(\theta)\bar{C}\mathcal{G}(\theta) \leq \frac{\gamma - \sum_{m=1}^{L} c_m}{\beta}$ for each $\theta \in U_{init}$; which is the desired result. ∎

As already mentioned, in Proposition 3.2, when we speak of finding a matrix $A_L \in \mathcal{A}_L$, we more precisely mean finding the free parameters in the affine structure of the matrix A_L (i.e. A_0, $\tilde{A}$, $\tilde{B}$, $\hat{v}_{lr}$ and $\tilde{v}_{lr}$ $(l = 1, \ldots, L$ and $r = 1, \ldots, L))$.

3.5 Tackling the robustified accuracy constraint

Taking inspiration from what has been done for the robustified cost constraint, we will now derive a tractable alternative for the accuracy constraint (3.13) when the parametrization (2.18) is used for Φ_u. For this purpose, recall the expression (3.20) for $P_\rho^{-1}(\theta, \Phi_u)$ and let us observe that $F_{u,\rho}(z, \theta)$ (see (3.5)) is a rational function of θ due to Observation 3.1. Consequently, we can find signals p_F and q_F such that $s(t) = F_{u,\rho}(z, \theta)u(t)$ can be expressed as:

$$p_F = (I_f \otimes \theta) \, q_F \qquad \text{and}$$

$$\begin{pmatrix} q_F \\ s \end{pmatrix} = \underbrace{\begin{pmatrix} M_{11,F} & M_{12,F} \\ M_{21,F} & M_{22,F} \end{pmatrix}}_{M_F(z)} \begin{pmatrix} p_F \\ u \end{pmatrix} \tag{3.29}$$

where $f = 3$ as shown in Appendix B.3. Note that $f = 2$ in the case where $H(z, \theta) = 1$ (OE model structure).

Using a similar reasoning as in Section 3.4.1, we can derive from (3.29) an LFT expression for $\bar{s}_i = \mathcal{F}_i(\theta)$ $(i = 1, \ldots, k_G)$ defined in (3.19). Moreover, if we denote $\bar{s} = (\bar{s}_1^T, \bar{s}_2^T, \ldots, \bar{s}_{k_G}^T)^T$:

$$
\bar{p}_F = (I_{fL} \otimes \theta) \ \bar{q}_F \qquad \text{and}
$$

$$
\left(\begin{array}{c} \bar{q}_F \\ \bar{s} \end{array} \right) = \underbrace{\left(\begin{array}{cc} \bar{M}_{11,F} & \bar{M}_{12,F} \\ \bar{M}_{21,F} & \bar{M}_{22,F} \end{array} \right)}_{\bar{M}_F(z)} \left(\begin{array}{c} \bar{p}_F \\ 1 \end{array} \right) \tag{3.30}
$$

$$
\bar{M}_{11,F} = bdiag(M_{11,F}(e^{j\omega_1}), \ldots, M_{11,F}(e^{j\omega_L}))
$$
$$
\bar{M}_{12,F} = (M_{12,F}(e^{j\omega_1}), \ldots, M_{12,F}(e^{j\omega_L}))^T
$$
$$
\bar{M}_{21,F} = (\mathcal{H}_1^T, \ldots, \mathcal{H}_{k_G}^T)^T \quad \bar{M}_{22,F} = (\mathcal{K}_1^T, \ldots, \mathcal{K}_{k_G}^T)^T
$$
$$
\mathcal{H}_i = bdiag(M_{21,F}^{i:}(e^{j\omega_1}), \ldots, M_{21,F}^{i:}(e^{j\omega_L})) \quad (i = 1, \ldots, k_G)
$$
$$
\mathcal{K}_i = (M_{22,F}^i(e^{j\omega_1}), \ldots, M_{22,F}^i(e^{j\omega_L}))^T \quad (i = 1, \ldots, k_G)
$$

where $M_{21,F}^{i:}$ (resp. $M_{22,F}^i$) denotes the ith line of $M_{21,F}$ (resp. the ith entry of $M_{22,F}$). Note that, in this system of equations, all elements are well defined for all $\theta \in U_{init}$ due to Assumption 3.1.

We have then the following result that gives a tractable alternative for the robustified accuracy constraint (3.13).

Proposition 3.3. *Consider an initial uncertainty set U_{init} (see (3.6)) satisfying Assumption 3.1 and the robustified accuracy constraint (3.13) when the spectrum Φ_u is parametrized as in (2.18) and where, for this reason, $P_\rho^{-1}(\theta, \Phi_u)$ has the expression given in (3.20). Consider the LFT (3.30) in $I_{fL} \otimes \theta$ which is the LFT representation for $\bar{s} = (\mathcal{F}_1(\theta)^T, \mathcal{F}_2(\theta)^T, \ldots, \mathcal{F}_{k_G}(\theta)^T)^T$ and consider the set of multipliers $\mathcal{A}_{k_G fL}$ associated with U_{init} (see Definition 3.1 with $n = k_G fL$). Then, the constraint (3.13) holds for a given $R_{adm,\rho}$ and a given $P_{\rho,init}$ if we can find a matrix $A_{k_G fL} \in \mathcal{A}_{k_G fL}$ such that[3]*

$$
\frac{N}{2\,\sigma_e^2} \sum_{i=1}^{k_G} \sum_{j=1}^{k_G} \left((m_i \otimes \mathcal{X}_i)^* \bar{C} (m_j \otimes \mathcal{X}_j) + (m_i \otimes \mathcal{X}_j)^* \bar{C} (m_j \otimes \mathcal{X}_i) \right) + \ldots
$$

$$
\cdots + \left((P_{\rho,init}^{-1} - R_{adm,\rho}) \otimes \left(\begin{array}{cc} \mathbf{0} & \mathbf{0} \\ \mathbf{0} & 1 \end{array} \right) \right) - \mathcal{M}^* \, A_{k_G fL} \, \mathcal{M} \geq 0 \tag{3.31}
$$

where $\mathcal{X}_i = \left(\begin{array}{cc} \mathcal{H}_i & \mathcal{K}_i \end{array} \right)$ $(i = 1, \ldots, k_G)$ and

$$
\mathcal{M} = \left(\begin{array}{c} I_{k_G} \otimes \left(\begin{array}{cc} \bar{M}_{11,F} & \bar{M}_{12,F} \end{array} \right) \\ I_{k_G} \otimes \left(\begin{array}{cc} I_{kfL} & \mathbf{0} \end{array} \right) \end{array} \right)
$$

---

[3] The matrix made of zeros and a one in the second line of (3.31) has dimension $(fLk+1) \times (fLk+1)$.

We observe that the matrix inequality (3.31) is linear in $A_{k_G f L}$ and in the coefficients c_m $(m = 1, \ldots, L)$ present in $\bar{C}$.

Proof. Let us consider (3.30) for a given $\theta \in U_{init}$ and let us consider the corresponding signals $\bar{p}_F$, $\bar{q}_F$ and $\bar{s} = (\mathcal{F}_1(\theta)^T, \mathcal{F}_2(\theta)^T, \ldots, \mathcal{F}_{k_G}(\theta)^T)^T$. Let us then pre- and post-multiply the LMI constraint (3.31) with $(I_{k_G} \otimes (\bar{p}_F^T, 1)^T)^*$ and $I_{k_G} \otimes (\bar{p}_F^T, 1)^T$, respectively. Using (3.30), (3.20) and the lemma in Appendix B.4 , this yields:

$$P_\rho^{-1}(\theta, \Phi_u) + P_{\rho,init}^{-1} - R_{adm,\rho} - X(\theta) \geq 0 \tag{3.32}$$

where $P_\rho^{-1}(\theta, \Phi_u)$ is given by (3.20) and $X(\theta)$ is a matrix given by

$$X(\theta) = \left(\begin{array}{c} I_{k_G} \otimes \bar{q}_F \\ I_{k_G} \otimes \bar{p}_F \end{array} \right)^* A_{k_G f L} \left(\begin{array}{c} I_{k_G} \otimes \bar{q}_F \\ I_{k_G} \otimes \bar{p}_F \end{array} \right)$$

Since $\bar{p}_F = (I_{fL} \otimes \theta) \; \bar{q}_F$, $X(\theta)$ can be rewritten as:

$$X(\theta) = (I_{k_G} \otimes \bar{q}_F)^* \; Y(\theta) \; (I_{k_G} \otimes \bar{q}_F)$$

$$Y(\theta) = \left(\begin{array}{c} I_{k_G f L} \\ I_{k_G f L} \otimes \theta \end{array} \right)^T A_{k_G f L} \left(\begin{array}{c} I_{k_G f L} \\ I_{k_G f L} \otimes \theta \end{array} \right)$$

The above reasoning can be done for any value of $\theta \in U_{init}$. In other words, for the matrix $A_{k_G f L} \in \mathcal{A}_{k_G f L}$ found by the optimization problem, (3.32) holds true for all $\theta \in U_{init}$. Using Definition 3.1 with $n = k_G f L$ and the Lemma in Appendix B.4, note also that:

$$X(\theta) \geq 0 \quad \forall \theta \in U_{init}$$

Consequently, we have that $P_\rho^{-1}(\theta, \Phi_u) + P_{\rho,init}^{-1} \geq R_{adm,\rho}$ for each $\theta \in U_{init}$; which is the desired result. ∎

3.6 Convex formulation of the optimal experiment design problem

Using Propositions 3.2 and 3.3, we can now straightforwardly derive a convex formulation for the optimal experiment design problem (3.11)-(3.13). Before formulating it, let us recall the different ingredients that are required to fully define this convex optimization problem. We suppose that an initial identification experiment has delivered an initial estimate $\hat{\theta}_{init}$ of the true parameter vector θ_0 and an estimate of its covariance matrix $P_{\theta,init}$. For a user-chosen confidence level η, we can then define the value of χ that defines the uncertainty set U_{init}. As a user, we can also choose the matrix $R_{adm,\rho}$ describing the desired accuracy, the scalar β defining the cost (2.12) of the experiment and the frequencies ω_m $(m = 1, \ldots, L)$ that will be considered in the parametrization (2.18) of the to-be-designed spectrum Φ_u. Once the frequencies ω_m $(m = 1, \ldots, L)$ have been chosen, the spectrum Φ_u is entirely defined by the coefficients

c_m ($m = 1, \ldots, L$). Using these ingredients, we can now solve the following LMI optimization problem [9] which is a convex formulation for the robust optimal experiment design problem (3.11)-(3.13):

LMI formulation *Consider the parametrization (2.18) for the to-be-designed spectrum Φ_u. The LMI optimization problem has as decision variables a scalar $\gamma > 0$, coefficients $c_m \geq 0$ ($m = 1, \ldots, L$), a matrix $A_L \in \mathcal{A}_L$ and a matrix $A_{k_G fL} \in \mathcal{A}_{k_G fL}$ (see Definition 3.1) and consists in determining the smallest value of γ for which the LMI constraints (3.26) and (3.31) hold.*

As mentioned in Section 3.3, if we denote the solution of the above LMI optimization problem by γ_{opt} and $\Phi_{u,opt}$, γ_{opt} is an upper bound for the solution γ_{opt}^{orig} of the original robustified optimization problem (3.11)-(3.13) i.e. the minimal value of the cost that is required to guarantee the robust accuracy constraint (3.13). Moreover, γ_{opt} is an upper bound for $\sup_{\theta \in U_{init}} \mathcal{J}(\theta, \Phi_{u,opt})$ and, since we assume that $\theta_0 \in U_{init}$, we have the guarantees that:

1. $P_\rho^{-1}(\theta_0, \Phi_{u,opt}) + P_{\rho,init}^{-1} \geq R_{adm,\rho}$

2. $\mathcal{J}(\theta_0, \Phi_{u,opt}) \leq \gamma_{opt}$.

3.7   Possible extensions of the framework

In this chapter, we have robustified an optimal experiment design problem expressed in the *least costly identification* framework. However, the results in this chapter can also be used to robustify other optimal experiment design problems such as e.g., the E-optimal problem introduced at the end of Section 2.4.1. When robustified, this problem is given by:

$$\max_{\Phi_u, \, \varepsilon} \ \varepsilon$$

$$\text{such that } \mathcal{J}(\theta, \Phi_u) \leq \gamma \quad \forall \theta \in U_{init} \tag{3.33}$$

$$\text{and } P_\rho^{-1}(\theta, \Phi_u) + P_{\rho,init}^{-1} \geq \varepsilon I_{k_G} \quad \forall \theta \in U_{init} \tag{3.34}$$

where ε is a scalar decision variable and γ is a given bound on the cost of the identification experiment. It is clear that (3.33) and (3.34) can be tackled with the tools of Sections 3.4 and 3.5. Note that, here, $R_{adm,\rho} = \varepsilon I_{k_G}$ is not fixed, but a decision variable. This however does not pose a problem since the constraint (3.31) is also linear in $R_{adm,\rho}$.

Our results can also be extended to identification in closed loop with the direct approach (BJ/OE model structures). Indeed, in this case, $P_\rho^{-1}(\theta, \Phi_u)$ will be the sum of a term which is linear in the to-be-designed spectrum (such as (3.3)) and a term which reflects the contribution of the noise (see e.g., [50]). Since the latter term is

positive-definite, one can neglect it and just consider the former term which can be tackled using the tools presented in this chapter (the only consequence will be that the cost will be larger than strictly necessary). The same approach consisting in neglecting the contribution of the noise to the accuracy can be considered to tackle, using the tools presented in this chapter, the robust optimal experiment design problem for open-loop experiments in the case of ARX and ARMAX model structures.

3.8 Dealing with the numerical complexity

In the LMI optimization problem presented in Section 3.6, the decision variables A_L and $A_{k_G f L}$ are square matrices with the structure described in Proposition 3.1. Consequently, the total number of decision variables in this LMI optimization problem is given by:

$$\#var = L^2(1 + (k_G f)^2)\left(\frac{k^2 + k}{2} + 1\right) + L + 1 \tag{3.35}$$

From (3.35) it is clear that the numerical complexity of the LMI approach presented in Section 3.6 increases with the dimension k of the true parameter vector θ_0 and the number L of frequencies in the to-be-determined spectrum (2.18). In other words, the LMI approach of Section 3.6 can become computationally intensive if both k and L are large. We propose in this section an approach to reduce the numerical complexity of our approach. For this purpose, let us observe the following. Even though the to-be-designed spectrum (2.18) contain frequencies covering the whole frequency range $[0, \pi]$, the optimal spectrum will generally only contain contributions at a limited number of frequencies. We will call these frequencies the optimal frequencies. Based on this observation, we can reduce the number of frequencies that have to be considered in (2.18) by determining these optimal frequencies in advance. To determine these optimal frequencies, we can e.g., use the gridding approach for robust experiment design i.e. the optimization problem (3.14)-(3.16). If n_g is not too large, (3.14)-(3.16) is less computationally intensive than the optimization problem of Section 3.6. Consequently, we can solve (3.14)-(3.16) with a spectrum (2.18) characterized by a large number of frequencies covering the whole interval $[0 \ \pi]$. The optimal frequencies are then chosen as the L_{opt} frequencies where $\Phi_{u,opt}^g(\omega) \neq 0$ ($\Phi_{u,opt}^g$ is the optimal solution of (3.14)-(3.16)). The LMI optimization problem of Section 3.6 can subsequently be solved using a parametrization (2.18) of the spectrum restricting attention to these L_{opt} frequencies.

3.9 Numerical illustrations

3.9.1 First numerical illustration

The considered system in this first example is $y(t) = G_0(z)u(t) + e(t)$ with $G_0(z) = \frac{1 \ z^{-1}}{1-0.7 \ z^{-1}}$ and $e(t)$ a white noise having variance $\sigma_e^2 = 1$. The true parameter vector θ_0 is thus $\theta_0 = \rho_0 = (1, -0.7)^T$. The cost of an identification experiment on this system

is defined by (2.12) with $\beta = 1$ and the desired accuracy is described by a matrix $R_{adm,\rho}$ defined as the inverse of the following diagonal matrix $diag((0.02)^2, (0.014)^2)$. We perform an initial identification experiment of duration $N = 1000$ on this true system with an input excitation u having a spectrum $\Phi_u^{init}(\omega) = 0.1 \ \forall \omega$. This initial identification experiment (whose cost $\mathcal{J}(\theta_0, \Phi_u^{init})$ is equal to 0.3) yields an initial estimate $\hat{\theta}_{init} = (0.904, -0.7161)^T$ of θ_0 and its covariance matrix $P_{\theta,init}$. Fixing η to 95%, we determine the size $\chi = 5.99$ of the uncertainty region U_{init} for θ_0 (see (3.6)). This set U_{init} effectively contains θ_0 and satisfies Assumption 3.1. However, the covariance matrix $P_{\theta,init} = P_{\rho,init}$ of the initial estimate $\hat{\theta}_{init}$ does not satisfy $P_{\rho,init}^{-1} \geq R_{adm,\rho}$.

We use the LMI formulation of Section 3.6 to determine the spectrum Φ_u of a second identification experiment of duration $N = 1000$ that will minimize a robustified version of the cost (3.12) under the robust accuracy constraint (3.13). Note that we here choose $\beta = 1$ in the expression of the cost (2.12). The to-be-determined spectrum will be parametrized as in (2.18) with the $L = 9$ frequencies ω_m $(m = 1, \ldots, 9)$ given in Table 3.1. With these settings, the LMI optimization problem of Section 3.6 yields $\gamma_{opt} = 5.4948$ and an optimal multisine of spectrum $\Phi_{u,opt}$ for which all the amplitudes are negligible except the ones at $\omega = 0.5$ and $\omega = 1$ (see Table 3.1). By construction, we know that, if an excitation signal of spectrum $\Phi_{u,opt}$ is used in the second identification experiment, the obtained accuracy will be satisfactory (i.e. $P_\rho^{-1}(\theta_0, \Phi_{u,opt}) + P_{\rho,init}^{-1} \geq R_{adm,\rho}$) and the cost $\mathcal{J}(\theta_0, \Phi_{u,opt})$ of this second identification experiment will be such that $\mathcal{J}(\theta_0, \Phi_{u,opt}) \leq \gamma_{opt} = 5.4948$. The value γ_{opt} is indeed an upper bound for $\sup_{\theta \in U_{init}} \mathcal{J}(\theta, \Phi_{u,opt})$ as discussed in Section 3.3 and thus also an upper bound for the a-priori unknown cost $\mathcal{J}(\theta_0, \Phi_{u,opt})$ which is here equal to 4.7.

In order to check the conservatism linked to the proposed LMI formulation, we will compare the above result with the one that is obtained using the gridding approach for robust optimal experiment design (3.14)-(3.16). We have solved this optimization problem for $n_g = 25$ using the same spectrum parametrization as above (same number L of frequencies and same frequencies ω_m) and we have obtained $\gamma_{g,opt} = 5.4866$ and a spectrum $\Phi_{u,opt}^g$ which has also only contributions at the two frequencies $\omega = 0.5$ and $\omega = 1$, but with (slightly) different amplitudes (see Table 3.1).

ω_m	0.1	0.2	0.3	0.5	1	1.6	2	2.5	3
c_m of $\Phi_{u,opt}$	≈ 0	≈ 0	≈ 0	0.9934	1.9324	≈ 0	≈ 0	≈ 0	≈ 0
c_m of $\Phi_{u,opt}^g$	≈ 0	≈ 0	≈ 0	1.0093	1.8939	≈ 0	≈ 0	≈ 0	≈ 0

Table 3.1: Coefficients c_m, $m = 1, \ldots, 9$ for $\Phi_{u,opt}$ and $\Phi_{u,n_g,opt}$

As mentioned in Sections 3.3 and 3.6, γ_{opt} (obtained with the LMI approach proposed in Section 3.6) is an upper bound for the solution γ_{opt}^{orig} of the original robustified optimization problem (3.11)-(3.13). It is also clear that the value $\gamma_{g,opt}$ obtained with the gridding approach is a lower bound for the same quantity. We thus observe that,

in this example, the upper bound $\gamma_{opt} = 5.4948$ is almost equal to the lower bound $\gamma_{g,opt} = 5.4866$. The conservatism is thus very limited in this example. It is also important to note that, unlike the gridding approach, the approach of Section 3.6 gives the guarantee that, with $\Phi_{u,opt}$, the robustified accuracy constraint (3.13) will be respected and also gives a guaranteed upper bound (i.e., γ_{opt}) on both $\sup_{\theta \in U_{init}} \mathcal{J}(\theta, \Phi_{u,opt})$ and the actual cost $\mathcal{J}(\theta_0, \Phi_{u,opt})$ of the second experiment.

To verify this property, we have generated 1000 grid points θ_i in U_{init} and we have computed $\mathcal{J}(\theta_i, \Phi_{u,opt})$ and $P_\rho^{-1}(\theta_i, \Phi_{u,opt})$ for these 1000 grid points. For all these grid points, we have indeed observed that $P_\rho^{-1}(\theta_i, \Phi_{u,opt}) + P_{\rho,init}^{-1} \geq R_{adm,\rho}$. We have also observed that the smallest eigenvalue of $P_\rho^{-1}(\theta_i, \Phi_{u,opt}) + P_{\rho,init}^{-1} - R_{adm,\rho}$ is, for one of these grid points θ_i, equal to 0.0004 (and thus very close to zero) and that the cost $\mathcal{J}(\theta_i, \Phi_{u,opt})$ is equal to 5.4948 for one of these grid points. This once again confirms that the conservatism of our approach is very limited in this example. Let us now compute, for these 1000 grid points, $P_\rho^{-1}(\theta_i, \Phi_{u,opt}^g)$ with the spectrum $\Phi_{u,opt}^g$ obtained with the gridding approach. Here, 82 of the θ_i led to a matrix $P_\rho^{-1}(\theta_i, \Phi_{u,opt}^g)$ for which $P_\rho^{-1}(\theta_i, \Phi_{u,opt}^g) + P_{\rho,init}^{-1} \geq R_{adm,\rho}$ is not satisfied. This shows the clear advantage of the approach of this chapter upon the gridding approach.

In this example, we have directly applied the LMI procedure of Section 3.6 to determine the optimal spectrum using the parametrization (2.18) with $L = 9$. The computation time required to compute this optimal spectrum is 8 hours on a standard laptop. To reduce the computation time, we can also consider the approach proposed in Section 3.8. As shown in Table 3.1, the gridding approach with $n_g = 25$ selects the two optimal frequencies $\omega = 1$ and $\omega = 5$ and the LMI approach of Section 3.6 can then be applied with a parametrization (2.18) restricting attention to these two optimal frequencies. These two steps are performed in a few seconds on a standard laptop.

3.9.2 Second numerical illustration

We now consider a second order system with a resonance at the frequency 0.5. This system is in the OE form:

$$y(t) = G_0(z)u(t) + e(t) \;\; \text{with} \;\; G_0(z) = \frac{0.5 \; z^{-1}}{1 - 1.6674 \; z^{-1} + 0.9025 \; z^{-2}}$$

where $e(t)$ is a white noise of variance $\sigma_e^2 = 1$. The true parameter vector θ_0 is thus $\theta_0 = \rho_0 = (0.5, -1.6674, 0.9025)^T$. The cost of an identification experiment on this system is defined by (2.12) with $\beta = 1$ and the desired accuracy is described by a matrix $R_{adm,\rho}$ defined as the inverse of the following diagonal matrix $diag((0.01)^2, (0.0067)^2, (0.0036)^2)$. We perform an initial identification experiment of duration $N = 1000$ on this true system with an input excitation u having a spectrum $\Phi_u^{init}(\omega) = 0.1 \; \forall \omega$. This initial identification experiment (whose cost $\mathcal{J}(\theta_0, \Phi_u^{init})$ is equal to 0.68) yields an initial estimate $\hat{\theta}_{init} = (0.4671, -1.6808, 0.9110)^T$ of θ_0 and its covariance matrix $P_{\theta,init}$. Fixing η to 98%, we determine the size $\chi = 9.84$ of the

uncertainty region U_{init} for θ_0 (see (3.6)). This set U_{init} effectively contains θ_0 and satisfies Assumption 3.1. However, the covariance matrix $P_{\theta,init} = P_{\rho,init}$ of the initial estimate $\hat{\theta}_{init}$ does not satisfy $P_{\rho,init}^{-1} \geq R_{adm,\rho}$.

To obtain an estimate of θ_0 with the desired accuracy, we want to design the second experiment of duration $N = 1000$ with the minimal cost. We decide to parametrize the spectrum Φ_u as in (2.18) with the frequencies ω_m ($m = 1, \ldots, L = 50$) representing a fine grid of the frequency range $[0, \pi]$. Since L is large, let us use the two-step procedure of Section 3.8 to tackle the LMI optimization problem of Section 3.6. We thus first solve the optimization problem (3.14)-(3.16) with $n_g = 25$ and with the spectrum parametrization with $L = 50$. This leads to an optimal spectrum $\Phi_{u,opt}^g$ that has negligible contributions except at the frequencies 0.39 and 0.58 ($L_{opt} = 2$). Consequently, to solve the LMI optimization problem of Section 3.6, we choose a parametrization (2.18) for Φ_u with $L = L_{opt} = 2$ and with ω_m ($m = 1, 2$) equal to 0.39 and 0.58. With these settings, the LMI optimization problem of Section 6 yields $\gamma_{opt} = 6.6997$ and an optimal spectrum $\Phi_{u,opt}$ described by $c_{1,opt} = 0.0768$ and $c_{2,opt} = 0.1232$. The computation time required to perform this two-step procedure is equal to three minutes on a standard laptop.

By construction, we know that, if an excitation signal of spectrum $\Phi_{u,opt}$ is used in the second identification experiment, the obtained accuracy will be satisfactory (i.e. $P_\rho^{-1}(\theta_0, \Phi_{u,opt}) + P_{\rho,init}^{-1} \geq R_{adm}$) and the cost $\mathcal{J}(\theta_0, \Phi_{u,opt})$ of this second identification experiment will be such that $\mathcal{J}(\theta_0, \Phi_{u,opt}) \leq \gamma_{opt} = 6.6997$. The value γ_{opt} is indeed guaranteed to be an upper bound for the a-priori unknown cost $\mathcal{J}(\theta_0, \Phi_{u,opt})$ which is here equal to 5.7097.

Let us now evaluate the conservatism of the two-step approach of Section 3.8 yielding $\gamma_{opt} = 6.6997$ with respect to the solution γ_{opt}^{orig} of the original robust optimal experiment design problem (3.11)-(3.13) when the spectrum Φ_u is parametrized with $L = 50$. We know that $\gamma_{opt}^{orig} \leq \gamma_{opt} = 6.6997$. To evaluate the conservatism of this upper bound, let us evaluate a (hopefully tight) lower bound of γ_{opt}^{orig} using the gridding approach (3.14)-(3.16) with a large n_g (say $n_g = 250$) and with the parametrization of Φ_u with $L = 50$ frequencies. For one realization of the 250 points in U_{init}, we observe that $\gamma_{g,opt} = 6.6825$. We have thus that $\gamma_{g,opt} = 6.6825 \leq \gamma_{opt}^{orig} \leq \gamma_{opt} = 6.6997$. We can thus conclude that, in this example also, the difference between γ_{opt} and γ_{opt}^{orig} is negligible (it is indeed smaller than 0.3%).

3.10   Summary

In this chapter, we have presented a convex relaxation that allows to robustify the least costly optimal experiment design problem using an initial uncertainty set for the unknown true parameter vector θ_0. This robustification is obtained using tools from robustness analysis, while restricting our attention to multisine excitation signal. This

approach is able to ensure that the new experiment will lead to an estimate having the desired accuracy. Moreover, using our approach the solution of the optimization problem returns an optimal cost, which is ensured to be an upper bound for the true experiment cost. Our approach presents some issues related to the dimension of the minimization problem involved, but we proposed a procedure to properly choose the frequencies of the multisine signal thus allowing us to avoid the curse of dimensionality.

Least Costly Identification Experiment for the Identification of One Module in a Dynamic Network

4.1 Introduction

As shown in Chapter 2, the least costly optimal experiment design concept has been originally formulated for identification experiments in the open-loop configuration and in the closed-loop configuration. In this chapter, we extend this concept to the case of a typical network situation. We indeed consider the case of a network made up of the interconnection of locally controlled systems (also called modules or nodes). In these networks, the interconnection is realized by the fact that neighbouring modules are allowed to exchange their measured output. In particular, the reference signal of each module in the network will be computed based on the measured outputs transmitted by its neighbouring modules. This type of networks is usual in the literature on multi-agent systems (see e.g. [40, 41])) and can e.g. be used to ensure that all modules of the network track a given reference known only to one of these modules.

In this chapter, we propose a method in order to design, for such a network, an identification experiment in the least costly manner when we are interested in the accurate identification of one specific module l of the network. To maintain the network performance, this identification will be performed in the original network configuration via the application of an excitation signal to module l. In particular, we propose a method to design the spectrum of this excitation signal in such a way that the accuracy of the identified model (measured here also via the covariance matrix of the identified parameter vector) is larger than a given threshold while entailing the smallest perturbation on the network. The perturbation (i.e. the cost of the identification) will be measured by the sum of the effects of the excitation signal on the input and output of each system in the network.

41

With respect to the least costly framework introduced in Section 2.4.2 for a single closed loop, the cost of the identification experiment in the network context thus not only contains the perturbation induced by the excitation signal in the closed loop where the system has to be identified, but also the perturbation induced in other loops by this excitation signal. This propagation of the effect of the excitation signal is due to the fact that the output signal of the to-be-identified loop (which is perturbed by the excitation signal) is transmitted to neighbouring modules. In order to reduce this propagation as much as possible, we propose an approach where the signal transmitted to the neighbouring modules is no longer the actual output signal, but a sanitized version of this output signal where the contribution of the excitation signal has been (partially) removed. Indeed, using an initial estimate of the to-be-identified system, we derive an estimate of this contribution and we subtract this estimate from the measured output signal before the transmission to the neighbouring modules.

This new configuration is inspired by the concept of stealth identification introduced in [45] for a single closed loop and that we here extend to the network case. The use of the stealth identification in this chapter is also a new application of this concept since, in [45], it was introduced as a tool to enable classical optimal experiment design in a loop where the controller is not linear time-invariant (LTI). With respect to [45], we also analyze which accuracy condition the initial estimate used to compute the sanitized version of the output signal must respect for the stealth configuration to be effective (i.e., to yield a smaller identification cost). Moreover, another contribution of this chapter is to robustify the stealth approach by considering the uncertainty of this initial estimate and its influence on the cost of the identification. For this purpose, as we will see in the sequel, we will need to consider an optimal experiment design where the cost constraint is robustified with respect to the uncertainty of the initial estimate. In Chapter 3, we have proposed an approach to tackle such a robustified cost constraint. However, given the possible high dimension of the network, the approach of Chapter 3 can lead to an excessive computational complexity (see the discussion in Section 3.8). To avoid this problem, we propose an alternative approach which is more appropriate to the network situation (and its possible high dimension) and which, while being (slightly) more conservative, has the same property as the one in Chapter 3 i.e., it is not based on any approximation. Note that, like in Chapter 3, the robustification of the cost constraint in the optimal experiment design problem requires to restrict attention to multisine excitation signals.

4.2 Description of the network configuration

We consider a network made up of N_{mod} SISO systems $\mathcal{S}_i$ $(i = 1, \ldots, N_{mod})$ operated in closed loop with a SISO decentralized controller K_i $(i = 1, \ldots, N_{mod})$:

$$\mathcal{S}_i : \ y_i(t) = G_{0,i}(z)u_i(t) + v_i(t) \tag{4.1}$$

$$u_i(t) = K_i(z)(y_{ref,i}(t) - y_i(t)) \tag{4.2}$$

where the signal u_i is the input applied to the system $\mathcal{S}_i$ and y_i is the measured output. This output is made up of a contribution of the input u_i and of a disturbance term $v_i(t) = H_{0,i}(z)e_i(t)$ that represents both process and measurement noises. The different systems $\mathcal{S}_i$ $(i = 1, \ldots, N_{mod})$ are thus described by two stable transfer functions $G_{0,i}(z)$ and $H_{0,i}(z)$, the later being also minimum-phase and monic. For the sequel, it will be important to suppose that these transfer functions are parametrized by an unknown true parameter vector $\theta_{0,i} \in \mathbf{R}^{n_{\theta_i}}$ in a known model structure: $G_{0,i}(z) = G_i(z, \theta_{0,i})$ and $H_{0,i}(z) = H_i(z, \theta_{0,i})$. For each i $(i = 1, \ldots, N_{mod})$, the signal e_i $(i = 1, \ldots, N_{mod})$ defining v_i is a zero mean white noise signal of variance $\sigma_{e_i}^2$ and these white noise signals e_i are for simplicity supposed to be mutually independent. Note that the closed-loop systems (4.1)-(4.2) are very similar to the one introduced in Section 2.3. The main difference is that, in (4.2), $y_{ref,i}$ is a reference signal that will be computed based on the measured outputs of neighbouring modules (see later). We can rewrite the above equations as follows:

$$\bar{y}(t) = \bar{G}(z, \theta_0)\bar{u}(t) + \bar{H}(z, \theta_0)\bar{e}(t) \tag{4.3}$$

$$\bar{u}(t) = \bar{K}(z)(\bar{y}_{ref}(t) - \bar{y}(t)) \tag{4.4}$$

where $\bar{y} = (y_1, \ldots, y_{N_{mod}})^T$ and $\bar{u}$, $\bar{e}$, $\bar{y}_{ref}$ are defined in a similar way and where[1] $\theta_0 = (\theta_{0,1}^T, \ldots, \theta_{0,N_{mod}}^T)^T \in \mathbf{R}^{n_\theta}$ concatenates the true parameter vectors $\theta_{0,i}$ $(i = 1, \ldots, N_{mod})$. In these equations, we also use the notation $\bar{G} = diag(G_1, \ldots, G_{N_{mod}})$ ($\bar{H}$ and $\bar{K}$ are defined in a similar way).

The closed-loop systems described in (4.3)-(4.4) are interconnected via the following equation:

$$\bar{y}_{ref}(t) = \mathcal{A}\ \bar{y}(t)\ +\ \mathcal{B}\ ref_{ext}(t) \tag{4.5}$$

where the matrix $\mathcal{A}$ and the vector $\mathcal{B}$ represent the flow of information in the network and ref_{ext} is a (scalar) external reference signal that should be followed by all outputs y_i and that is generally only available at one node of the network. This type of interconnections is typical in formation control or multi-agent systems (see e.g. [40, 41]).

To illustrate (4.5), let us consider the network represented in Figure 4.1. In this network, we have $N_{mod} = 6$ systems/modules, all of the form (4.1) and all operated as in (4.2) with a decentralized controller K_i (see Figure 4.2). These local closed loops are represented by a circle/node in Figure 4.1. The objective of this network is that the outputs y_i of all modules follow the external reference ref_{ext} even though this reference is only available at Node 1. For this purpose, a number of nodes are allowed to exchange information (i.e. their measured output) with some other neighbouring nodes. The arrows between the nodes in Figure 4.1 indicate the flow of information.

For example, Node 5 receives the output of two nodes (i.e. Nodes 3 and 4) and sends its output (i.e. y_5) to three nodes (Nodes 3, 4, and 6). The reference signal

---

[1]In this chapter, we will use the notation n_θ for the dimension of the vector θ_0 and n_{θ_i} for the dimension of $\theta_{0,i}$ $(i = 1, \ldots, N_{mod})$.
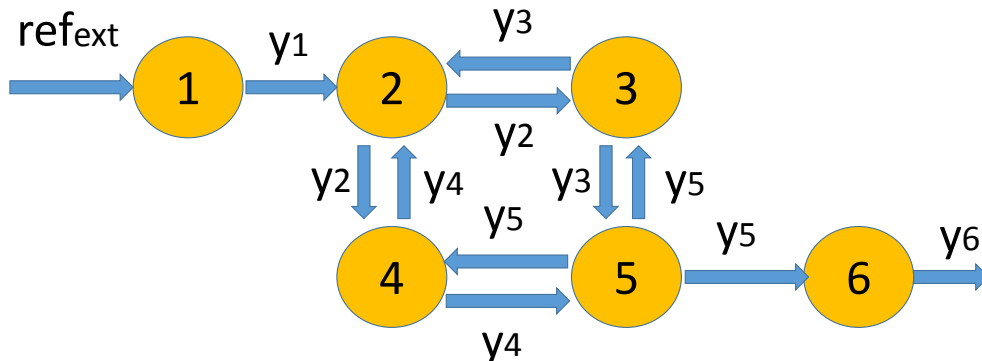
Figure 4.1: Example of graph representation of the network, each circle represents a
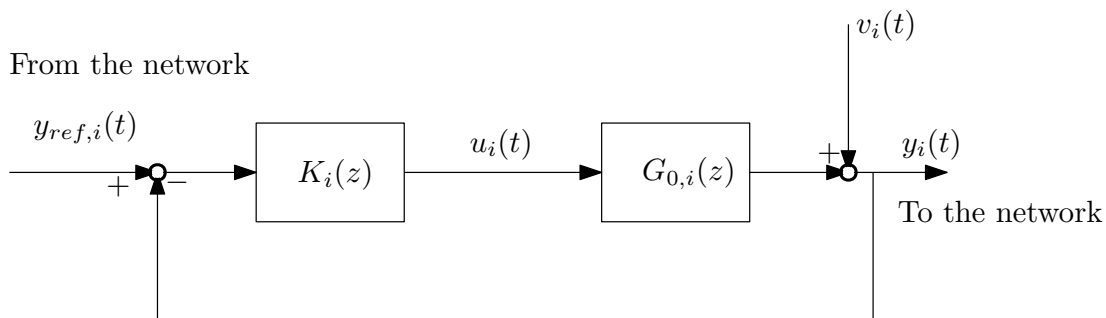node i and the edges represent the communication link between the nodes

Figure 4.2: Representation of a single module/node i

$y_{ref,i}$ of Node i will be computed as a linear combination of the received information
at Node i. For Node 5, $y_{ref,5}$ will thus be a linear combination of y_3 and y_4. More
precisely, for all outputs y_i to be able to follow the external reference ref_{ext}, $\mathcal{A}$ and $\mathcal{B}$
in (4.5) are generally chosen as [40, 41]:

$$
\mathcal{A} = \begin{pmatrix}
0 & 0 & 0 & 0 & 0 & 0 \\
1/3 & 0 & 1/3 & 1/3 & 0 & 0 \\
0 & 0.5 & 0 & 0 & 0.5 & 0 \\
0 & 0.5 & 0 & 0 & 0.5 & 0 \\
0 & 0 & 0.5 & 0.5 & 0 & 0 \\
0 & 0 & 0 & 0 & 1 & 0
\end{pmatrix}
\qquad
\mathcal{B} = \begin{pmatrix}
1 \\ 0 \\ 0 \\ 0 \\ 0 \\ 0
\end{pmatrix}.
$$

The matrix $\mathcal{A}$ is called the normalized adjacency matrix in the literature [40]. Us-
ing (4.5), we, e.g., see that the tracking error signals $y_{ref,1} - y_1$ and $y_{ref,2} - y_2$ of Nodes

1 and 2 are respectively given by $ref_{ext} - y_1$ and $1/3\left((y_1 - y_2) + (y_3 - y_2) + (y_4 - y_2)\right)$. Similar relations can be found for all the other nodes. If the different loops $[K_i \; G_i]$ are designed to make the tracking error $y_{ref,i} - y_i$ as small as possible, it can be proven that such an interconnection allows good tracking of ref_{ext} at all nodes [41, 40]. A normalized adjacency matrix can be defined for any information flow using the following rules. Row i of $\mathcal{A}$ is zero if no output is sent to Node i. If y_i is sent to Node j, entry (j,i) of $\mathcal{A}$ will be nonzero. Finally, all nonzero entries in a row are equal and sum up to one.

We also need to introduce the notion of *(directed) path* between two nodes. There exists a path from Node i to Node j if $\mathcal{A}_{ji} \neq 0$ or we can find a set of ζ intermediary nodes described by the indexes $\{n_1, \ldots, n_\zeta\}$ such that $\mathcal{A}_{n_1 i} \neq 0$, $\mathcal{A}_{n_2 n_1} \neq 0$, $\ldots$, $\mathcal{A}_{jn_\zeta} \neq 0$. Using this notion of path, Definition 4.1 introduces two sets of indexes for each node of the network:

Definition 4.1. *Consider an arbitrary node of a network containing N_{mod} nodes, say Node j ($j = 1, \ldots, N_{mod}$). For this node, we define the set $\mathcal{P}_j$ as a set of indexes of nodes. A certain index $i \neq j$ belongs to $\mathcal{P}_j$ if there exists a path from Node j to Node i. Similarly, for the same Node j, we also define the set $\mathcal{L}_j$. A certain index $i \neq j$ belongs to $\mathcal{L}_j$ if there exists a path from Node i to Node j.*

As an example, $\mathcal{P}_5 = \{2, 3, 4, 6\}$ and $\mathcal{L}_5 = \{1, 2, 3, 4\}$ for the network of Figure 4.1. For the sequel, it is important to note the following facts. If an external signal (e.g., the disturbance v_i or an excitation signal r) is added to Node j, this external signal will also influence all nodes i with $i \in \mathcal{P}_j$. Conversely, Node j will be influenced by all external signals added in nodes i with $i \in \mathcal{L}_j$.

In the sequel, we will suppose that a prediction error identification procedure has delivered initial estimates $\hat{\theta}_{init,i}$ of $\theta_{0,i}$ ($i = 1, \ldots, N_{mod}$) and that, consequently, all these estimates are (asymptotically) normally distributed around $\theta_{0,i}$ with a covariance matrix $P_{init,i}$ [1, 17]. These initial estimates can e.g. be obtained using an open-loop experiment on each system $\mathcal{S}_i$ disconnected from the network (see Section 2.2) Alternatively, these initial estimates can also be obtained in the network configuration using the procedure introduced in [17] and described at the end of Section 2.3. In both cases, we have then that the concatenated vector $\hat{\theta}_{init} = (\hat{\theta}_{init,1}^T, \ldots, \hat{\theta}_{init,N_{mod}}^T)^T$ is normally distributed around $\theta_0 = (\theta_{0,1}^T, \ldots, \theta_{0,N_{mod}}^T)^T$ with a covariance matrix $P_{init} = bdiag(P_{init,1}, \ldots, P_{init,N_{mod}})$. Based on this statistical property, the following ellipsoid U_{init} is a $\eta\%$-confidence region for the unknown parameter vector θ_0:

$$U_{init} := \left\{ \theta \in \mathbf{R}^{n_\theta} \mid (\theta - \hat{\theta}_{init})^T P_{init}^{-1} (\theta - \hat{\theta}_{init}) < \chi \right\} \tag{4.6}$$

where $\theta = (\theta_1^T, \ldots, \theta_{N_{mod}}^T)^T$ and $Pr(\chi^2(n_\theta) < \chi) = \eta$. This ellipsoid U_{init} can be considered as an uncertainty set for the unknown true parameter vector θ_0. From now onwards, we will therefore assume that $\theta_0 \in U_{init}$.

In the sequel, we will suppose that the model accuracy obtained after this initial experiment is satisfactory for all, but one node, say Node l ($l = 1, \ldots, N_{mod}$). We will therefore have to perform a new identification experiment to obtain a better estimate of the parameter vector $\theta_{0,l}$ describing this node. This experiment is described in the next section.

4.3 Identification of one module in the network and cost of the experiment

4.3.1 Cost of an experiment in the stealth and non-stealth configurations

We thus wish to obtain a better estimate of the parameter vector $\theta_{0,l}$ describing Node l. In line with the least costly philosophy (see e.g., Section 2.4.2), this estimate will be obtained by performing an identification experiment in the original network configuration while limiting as much as possible the perturbations induced by this experiment on the normal operations of the network. The experiment is performed in the original network configuration since we wish to maintain the tracking performance during the identification experiment i.e., to maintain the transfer functions between ref_{ext} and the outputs y_i ($i = 1, \ldots, N_{mod}$) and the transfer functions between ref_{ext} and the outputs u_i ($i = 1, \ldots, N_{mod}$).
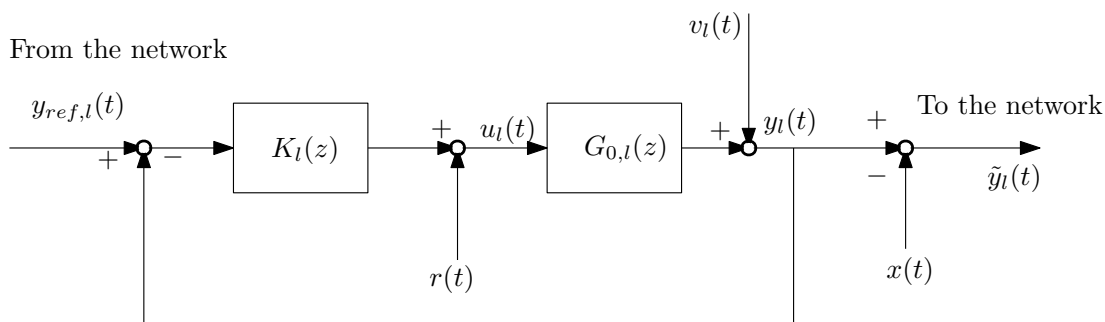

Figure 4.3: To-be-identified node (i.e. Node l) during the identification experiment. In the stealth setting, $x(t)$ is given by (4.7). In the non-stealth setting, $x(t) = 0$.

During the identification experiment, similarly as was done in Section 2.3, we use an excitation signal $r(t)$ of spectrum Φ_r and we apply a sequence $\{r(t) \mid t = 1, \ldots, N\}$ of this signal at the ouput of the controller K_l (see Figure 4.3). This allows to collect the data set $Z_l^N = \{y_l(t), u_l(t) \mid t = 1, \ldots, N\}$ that will be used for the identification (see Section 4.3.2). In Figure 4.3, we also observe the signal $x(t)$. Here we will consider two choices for $x(t)$ corresponding to two configurations/settings: the stealth and the non-stealth configurations. In the non-stealth setting, the signal $x(t)$ will be chosen equal to zero. This choice corresponds to the classical setting for an identification experiment in a closed-loop/network context (see Section 2.3 and e.g., [17]). In the

stealth setting, $x(t)$ will be chosen as the following estimate of the contribution of r in y_l:

$$x(t) = \underbrace{\frac{G_l(z, \hat{\theta}_{init,l})}{1 + K_l(z)G_l(z, \hat{\theta}_{init,l})}}_{=T_{init,l}(z)} r(t) \quad (t = 1, \ldots, N) \tag{4.7}$$

where $\hat{\theta}_{init,l}$ is the subvector of $\hat{\theta}_{init}$ corresponding to $\mathcal{S}_l$. Note that (4.7) can be easily computed since both r and $T_{init,l}(z)$ are known.

As shown in Figure 4.3, the signal $x(t)$ is subtracted from the measured output $y_l(t)$ to give $\tilde{y}_l(t) = y_l(t) - x(t)$ which will be the signal that will be transmitted to compute $\bar{y}_{ref}$. Consequently, during the identification experiment, the equations (4.4)-(4.5) become:

$$\bar{u}(t) = \bar{m}_l \ r(t) + \bar{K}(z) \ (\bar{y}_{ref}(t) - \bar{y}(t)) \tag{4.8}$$

$$\bar{y}_{ref}(t) = \mathcal{A} \ (\bar{y}(t) - \bar{m}_l x(t)) + \mathcal{B} \ ref_{ext}(t) \tag{4.9}$$

where $\bar{m}_i \ (i = 1, \ldots, N_{mod})$ denotes a unit (column) vector of dimension N_{mod} for which the ith entry is equal to 1 and the other entries are equal to zero.

We will show, in the sequel, the advantage of the stealth setting in order to reduce the cost of the identification experiment. For this purpose, we need to define this cost in the network context. Let us first consider the stealth setting. In this case, the output vector $\bar{y}$ and the input vector $\bar{u}$ in the network configuration (4.3)-(4.8)-(4.9) can be rewritten as follows as a function of the external signals r, ref_{ext} and $\bar{e}$:

$$\bar{y}(t) = R^y(z, \theta_0) \ r(t) + R^y_{ext}(z, \theta_0) \ ref_{ext}(t) + S^y(z, \theta_0) \ \bar{e}(t) \tag{4.10}$$

$$\bar{u}(t) = R^u(z, \theta_0) \ r(t) + R^u_{ext}(z, \theta_0) \ ref_{ext}(t) + S^u(z, \theta_0) \ \bar{e}(t) \tag{4.11}$$

for some vectors of transfer functions R^y_{ext}, R^u_{ext}, some matrices of transfer functions S^y, S^u and

$$R^u(z, \theta_0) = \bar{m}_l \ S_{0,l}(z) + \bar{\mathcal{N}}(z, \theta_0) \ (T_{0,l}(z) - T_{init,l}(z)) \tag{4.12}$$

$$R^y(z, \theta_0) = \bar{G}(z, \theta_0) \ R^u(z, \theta_0) \tag{4.13}$$

where $S_{0,l}(z) = 1/(1 + K_l(z)G_l(z, \theta_{0,l}))$ and $T_{0,l}(z) = G_l(z, \theta_{0,l})/(1 + K_l(z)G_l(z, \theta_{0,l}))$ are scalar transfer functions and $\bar{\mathcal{N}}(z, \theta_0)$ is a vector of transfer functions:

$$\bar{\mathcal{N}}(z, \theta_0) = \bar{K}(z)\bar{S}(z, \theta_0) \left(I_{N_{mod}} - \mathcal{A}\bar{S}(z, \theta_0)\bar{G}(z, \theta_0)\bar{K}(z)\right)^{-1} \mathcal{A} \ \bar{m}_l$$

$$\bar{S}(z, \theta_0) = \left(I_{N_{mod}} + \bar{G}(z, \theta_0)\bar{K}(z)\right)^{-1} \tag{4.14}$$

The derivations leading to (4.12)-(4.14) are given in Appendix C.1. For the sequel, it is important to note that $T_{init,l}(z)$ (see (4.7)) is the initial model of $T_{0,l}(z)$ that corresponds to the parameter $\hat{\theta}_{init,l}$. Consequently, in (4.12), $T_{0,l}(z) - T_{init,l}(z)$ is the modeling error of this initial model $T_{init,l}(z)$.

With respect to the normal operations (4.3)-(4.4)-(4.5), $\bar{y}$ and $\bar{u}$ are thus perturbed during the identification experiment by $R^y(z)r(t)$ and $R^u(z)r(t)$, respectively. Consequently, in line with the philosophy of Section 2.4.2, it makes sense to define the cost of the identification experiment as the following function of the spectrum Φ_r of the excitation signal r :

$$\mathcal{J}(\theta_0, \Phi_r) = \frac{1}{2\pi} \int_{-\pi}^{\pi} \left(\beta \left(R^y(e^{j\omega}, \theta_0) \right)^* R^y(e^{j\omega}, \theta_0) + \left(R^u(e^{j\omega}, \theta_0) \right)^* R^u(e^{j\omega}, \theta_0) \right) \Phi_r(\omega) \, d\omega$$

$$\mathcal{J}(\theta_0, \Phi_r) = \frac{1}{2\pi} \int_{-\pi}^{\pi} \mathcal{R}^*(e^{j\omega}, \theta_0) \mathcal{R}(e^{j\omega}, \theta_0) \, \Phi_r(\omega) \, d\omega \tag{4.15}$$

where $\beta \geq 0$ is a user chosen weighting factor and $\mathcal{R}(z, \theta_0)$ is the following vector of transfer functions of dimension $2N_{mod}$:

$$\mathcal{R}(z, \theta_0) = \begin{pmatrix} \sqrt{\beta} \, R^y(z, \theta_0) \\ R^u(z, \theta_0) \end{pmatrix} \tag{4.16}$$

The cost $\mathcal{J}(\theta_0, \Phi_r)$ can be rewritten as the sum of the individual costs $\mathcal{J}_i(\theta_0, \Phi_r)$ ($i = 1, \ldots, N_{mod}$) in each module:

$$\mathcal{J}(\theta_0, \Phi_r) = \sum_{i=1}^{N_{mod}} \mathcal{J}_i(\theta_0, \Phi_r) \quad \text{with} \tag{4.17}$$

$$\mathcal{J}_i(\theta_0, \Phi_r) = \frac{1}{2\pi} \int_{-\pi}^{\pi} \mathcal{R}_i^*(e^{j\omega}, \theta_0) \mathcal{R}_i(e^{j\omega}, \theta_0) \Phi_r(\omega) \, d\omega \tag{4.18}$$

$$\mathcal{R}_i(z, \theta) = \begin{pmatrix} \sqrt{\beta} \, R_i^y(z, \theta) \\ R_i^u(z, \theta) \end{pmatrix}$$

where R_i^y (resp. R_i^u) is the ith entry of R_y (resp. R^u). Due to (4.13), we can also rewrite (4.18) as follows:

$$\mathcal{J}_i(\theta_0, \Phi_r) = \frac{1}{2\pi} \int_{-\pi}^{\pi} \left(1 + \beta |G_i(e^{j\omega}, \theta_{0,i})|^2 \right) |R_i^u(e^{j\omega}, \theta_0)|^2 \Phi_r(\omega) \, d\omega \tag{4.19}$$

In the non-stealth setting, the cost $\mathcal{J}(\theta_0, \Phi_r)$ of an identification experiment and the individual costs $\mathcal{J}_i(\theta_0, \Phi_r)$ can be defined in a very similar way. However, the expressions for R^y and R^u that are used in (4.15) and (4.18) have a different expression:

$$R^{u,NS}(z, \theta_0) = \bar{m}_l \, S_{0,l}(z) + \bar{\mathcal{N}}(z, \theta_0) \, T_{0,l}(z) \tag{4.20}$$

$$R^{y,NS}(z, \theta_0) = \bar{G}(z, \theta_0) \, R^{u,NS}(z, \theta_0) \tag{4.21}$$

By comparing (4.20) and (4.12), we observe that the modeling error $T_{0,l}(z) - T_{init,l}(z)$ is replaced by $T_{0,l}(z)$ in the expression of $R^{u,NS}$.

For both the stealth and non-stealth settings, using the definition of $\mathcal{P}_l$ (see Definition 4.1), the individual costs $\mathcal{J}_i(\theta_0, \Phi_r)$ for $i \notin \mathcal{P}_l$ will be equal to zero. However, for $i \in \mathcal{P}_l$, these costs $\mathcal{J}_i(\theta_0, \Phi_r)$ will be nonzero. Consequently, the excitation signal r will not have an influence only on Node l (where it is applied and where it is necessary for the identification of $\mathcal{S}_l$), but also on all nodes i with $i \in \mathcal{P}_l$. For the network in Figure 4.1, if the excitation signal r is applied in Node 5, besides $\mathcal{J}_5(\theta_0, \Phi_r)$, the individual costs $\mathcal{J}_i(\theta_0, \Phi_r)$ for $i = 2, 3, 4,$ and 6 will also be non-zero. This result is equivalent to the fact that $\mathcal{N}_i(z, \theta_0)$ (i.e. the ith entry of $\bar{\mathcal{N}}(z, \theta_0)$) is a nonzero transfer function for all $i \in \mathcal{P}_l$ and is equal to zero for all $i \neq l$, $i \notin \mathcal{P}_l$.

The role of the stealth compensation $x(t)$ is to reduce as much as possible this propagation of the influence of the excitation r (applied in Node l) towards the nodes $i \in \mathcal{P}_l$. Before explaining this in more details, let us make the following assumptions on Node l and the considered network:

Assumption 4.1. *Consider the set $\mathcal{P}_l$ (see Definition 4.1) corresponding to the to-be-identified Node l. We assume that $\mathcal{P}_l$ is a non-empty set.*

Assumption 4.2. *Consider the set $\mathcal{P}_l$ (see Definition 4.1) corresponding to the to-be-identified Node l and the vector of transfer functions $\mathcal{N}(z, \theta_0)$ (see (4.14)). We will assume that, for all $i \in \mathcal{P}_l$, the ith entry $\mathcal{N}_i(z, \theta_0)$ of $\mathcal{N}(z, \theta_0)$ is such that $\mathcal{N}_i(e^{j\omega}, \theta_0) \neq 0$ for (almost) all frequencies.*

If $\mathcal{P}_l$ would be empty, there is of course no need for the stealth setting since the signal r will not be propagated to other nodes. Assumption 4.2 will in fact always hold, except in pathological cases that we here want to formally exclude.

We can now explain the role of the stealth compensation in reducing the propagation of the influence of the excitation r towards the nodes $i \in \mathcal{P}_l$. Let us first consider the ideal case i.e. when $T_{init,l} = T_{0,l}$. This choice does not change the situation in the non-stealth setting i.e. $\mathcal{J}_i(\theta_0, \Phi_r)$ remains nonzero for all $i \in \mathcal{P}_l$ since $R_i^{u,NS}$ and $R_i^{y,NS}$ remain the same nonzero transfer functions for all these i (they are not function of $T_{init,l}$). However, in the stealth setting, for all $i \neq l$, the transfer functions R_i^u and R_i^y are identically zero when $T_{init,l} = T_{0,l}$. Consequently, in this ideal case, the effect of the excitation $r(t)$ will only be felt in the to-be-identified module i.e. $\mathcal{J}_i(\theta_0, \Phi_r) = 0$ for all $i \neq l$.

In practice, $T_{init,l}$ will of course always be different from $T_{0,l}$, but, as shown in the following proposition, the stealth configuration will remain beneficial if $T_{init,l}$ satisfies a certain accuracy constraint that will hold in the vast majority of the cases.

Proposition 4.1. *Consider that, following the procedure described in this section, an excitation signal $r(t)$ of spectrum Φ_r is applied to Node l of a network like the*

one described in Section 4.2 and satisfying Assumptions 4.1 and 4.2. Let us for this spectrum Φ_r compute the individual costs $\mathcal{J}_i(\theta_0, \Phi_r)$ $(i = 1, \ldots, N_{mod})$ in the stealth setting and in the non-stealth setting using the respective expression for these costs in the two settings (see Section 4.3.1). Suppose finally that the initial model $T_{init,l}(z)$ of $T_{0,l}(z)$ satisfies the following accuracy constraint at the frequencies ω where $\Phi_r(\omega) \neq 0$:

$$\frac{|T_{0,l}(e^{j\omega}) - T_{init,l}(e^{j\omega})|}{|T_{0,l}(e^{j\omega})|} < 1. \tag{4.22}$$

Then, for all $i \in \mathcal{P}_l$ (see Definition 4.1), the individual cost $\mathcal{J}_i(\theta_0, \Phi_r)$ in the stealth configuration is strictly smaller than the one in the non-stealth configuration. Recall also that, for the nodes i with $i \neq l$ and $i \notin \mathcal{P}_l$, $\mathcal{J}_i(\theta_0, \Phi_r) = 0$ in both configurations.

Proof. See Appendix C.2. ∎

The property (4.22) is equivalent to say that, at ω, $T_{init,l}$ is a better model of $T_{0,l}$ than the zero transfer function (i.e. $|T_{0,l}(e^{j\omega}) - T_{init,l}(e^{j\omega})| < |T_{0,l}(e^{j\omega}) - 0|$). As already mentioned, this property will generally be met in practice. The advantage of the stealth configuration will be further discussed in the next section.

4.3.2 Identification of one given module

In Section 4.2, we assumed that we have obtained an initial estimate $\hat{\theta}_{init} = (\hat{\theta}_{init,1}^T, \ldots, \hat{\theta}_{init,N_{mod}}^T)^T$ of the true parameter vector $\theta_0 = (\theta_{0,1}^T, \ldots, \theta_{0,N_{mod}}^T)^T$. As already mentioned at the end of Section 4.2, we will suppose that we want to increase the accuracy of the estimate[2] $\hat{\theta}_{init,l}$ of the true parameter vector $\theta_{0,l}$ corresponding to Node l. The accuracy of $\hat{\theta}_{init,l}$ can be measured with $P_{init,l}^{-1}$ where $P_{init,l}$ is the covariance matrix of $\hat{\theta}_{init,l}$. The accuracy of $\hat{\theta}_{init,l}$ can be improved by combining it with a new estimate of $\theta_{0,l}$ obtained using a data set $Z_l^N = \{y_l(t), u_l(t) | t = 1, \ldots, N\}$ collected as shown in Figure 4.3 in the stealth or the non-stealth setting.

We consider for this purpose a model structure $\mathcal{M} = \{G_l(z, \theta_l), H_l(z, \theta_l) \mid \theta_l \in \mathbf{R}^{n_{\theta_l}}\}$ for $\mathcal{S}_l$. We suppose that this model structure satisfies Assumption 2.1. In other words, there exists a unique parameter vector $\theta_{0,l}$ for which $G(z, \theta_{0,l}) = G_{0,l}(z)$ and $H(z, \theta_{0,l}) = H_{0,l}(z)$ ($\mathcal{M}$ is full-order and identifiable). We will also suppose that the excitation signal $r(t)$ (see Figure 4.3) and the white noise vector $\bar{e}$ (see (4.3)) are uncorrelated and that $ref_{ext}(t)$ is a stationary signal uncorrelated with $r(t)$ and $\bar{e}(t)$. Then, using the model structure $\mathcal{M}$ and the data set $Z_l^N = \{y_l(t), u_l(t) | t = 1, \ldots, N\}$, an estimate $\hat{\theta}_{N,l}$ of $\theta_{0,l}$ can be obtained via prediction error identification [1]:

---

[2]This estimate $\hat{\theta}_{init,l}$ is also the one with which the transfer function $T_{init,l}$, used for the stealth compensation, is constructed.

$$\hat{\theta}_{N,l} \quad = \quad \arg\min_{\theta_l} \frac{1}{N} \sum_{t=1}^{N} \epsilon^2(t, \theta_l) \quad \text{with:} \tag{4.23}$$

$$\epsilon(t, \theta_l) \quad = \quad H_l^{-1}(z, \theta_l)\left(y_l(t) - G_l(z, \theta_l)u_l(t)\right)$$

We will show in the following proposition that the estimate (4.23) is a consistent estimate of $\theta_{0,l}$ under mild conditions on the excitation signal $r(t)$. Let us for this purpose make a similar assumption as Assumption 4.2 to exclude pathological cases for the matrix S^u in (4.11).

Assumption 4.3. *Consider the set $\mathcal{L}_l$ (see Definition 4.1) corresponding to the to-be-identified Node l and the matrix of transfer functions $S^u(z, \theta_0)$ (see (4.11)). We will assume that, for all $i \in \mathcal{L}_l$, the (l, i) entry $S_{li}^u(z, \theta_0)$ of $S^u(z, \theta_0)$ is such that $S_{li}^u(e^{j\omega}, \theta_0) \neq 0$ for (almost) all frequencies ω.*

Proposition 4.2. *Consider the network setup described in Section 4.2 and the identification procedure described above yielding the estimate $\hat{\theta}_{N,l}$ of $\theta_{0,l}$ using data collected as shown in Figure 4.3 (using the stealth or the non-stealth settings). Consider also the set $\mathcal{L}_l$ corresponding to Node l (see Definition 4.1) and suppose that Assumption 4.3 holds. Then, the estimate $\hat{\theta}_{N,l}$ is a consistent estimate of $\theta_{0,l}$ if the product $K_l(z)G_l(z, \theta_{0,l})$ contains (at least) one delay and if one of the following two conditions is satisfied*

- *the set $\mathcal{L}_l$ is non-empty. In this case, $\hat{\theta}_{N,l}$ is consistent even if the external excitation $r(t)$ and the external reference signal ref_{ext} are equal to zero.*

- *The order of excitation of r (see Definition 2.1) and the order of excitation of the external reference signal ref_{ext} are sufficient for (4.23) to be consistent when the data set $Z_l^N = \{y_l(t), u_l(t) | t = 1, \ldots, N\}$ is collected in the following simple closed-loop system:*

$$y_l(t) = G_l(z, \theta_{0,l})u_l(t) + H_l(z, \theta_{0,l})e_l(t) \tag{4.24}$$

$$u_l(t) = r(t) + K_l(z)(ref_{ext}(t) - y_l(t)) \tag{4.25}$$

Proof. See Appendix C.3.1. ∎

Let us interpret this proposition for the example of the network of Figure 4.1. In this network, $\mathcal{L}_l$ is non-empty for all nodes $l \neq 1$. For all these nodes, as shown in the proof of Proposition 4.2, the perturbations $v_i(t) = H_i(z, \theta_{i,0})e_i(t)$ for $i \in \mathcal{L}_l$ will be sufficient to yield and informative data set $Z_l^N = \{y_l(t), u_l(t) | t = 1, \ldots, N\}$ and thus a consistent $\hat{\theta}_{N,l}$ (even if $r(t) = ref_{ext}(t) = 0$). It is however to be noted that, unless we have the luxury of performing an arbitrary long experiment, a nonzero excitation $r(t)$ will generally be required to obtain the desired accuracy for $\hat{\theta}_{N,l}$ (see later). As far as Node 1 is concerned, we see that this node can indeed be described as in (4.24)-(4.25). Consequently, for this node, the consistency of (4.23) will be guaranteed under the same condition on $r(t)$ and $ref_{ext}(t)$ as in direct closed-loop identification i.e. under

Assumption 2.3 (see the discussion on this matter in Section 2.3).

We will from now on suppose that the estimate $\hat{\theta}_{N,l}$ is consistent. As shown in Appendix C.3.2, the estimate $\hat{\theta}_{N,l}$ is then also (asymptotically) normally distributed around $\theta_{0,l}$ with a covariance matrix P_{θ_l} that can be estimated from the data and whose inverse has the following expression:

$$
P_{\theta_l}^{-1}(\theta_0, \Phi_r) = M_{\bar{e}}(\theta_0) +
$$
$$
\frac{N}{2\pi\sigma_l^2} \int_{-\pi}^{\pi} F_l(e^{j\omega}, \theta_{0,l}) F_l^*(e^{j\omega}, \theta_{0,l}) \left(|R_l^u(e^{j\omega}, \theta_0)|^2 \Phi_r(\omega) + |R_{ext,l}^u(e^{j\omega}, \theta_0)|^2 \Phi_{ref_{ext}}(\omega) \right) \, d\omega
$$
$$
(4.26)
$$

with R_l^u and $R_{ext,l}^u$ the lth entry of R^u and of R_{ext}^u, respectively, and with $\Phi_{ref_{ext}}$ the power spectrum of ref_{ext}, $F_l(z, \theta_l) = H_l^{-1}(z, \theta_l)\frac{\partial G_l(z,\theta_l)}{\partial \theta_l}$ and $M_{\bar{e}}(\theta_0)$ the contribution of $\bar{e}$ to the accuracy of the estimate (see Appendix C.3.2 for more details). We observe that $P_{\theta_l}^{-1}(\theta_0, \Phi_r)$ is an affine function of the power spectrum Φ_r of the excitation signal r and of the power spectrum $\Phi_{ref_{ext}}$ of the external reference ref_{ext} (and a more complex function of θ_0). Equation (4.26) pertains to the stealth configuration. In the non-stealth configuration, we can use the same expression for $P_{\theta_l}(\theta_0, \Phi_r)$, but we have to replace R_l^u by $R_l^{u,NS}$ (see (4.20)).

Similarly to what we have done in Chapter 3, we can combine the information on $\theta_{0,l}$ contained in the estimates $\hat{\theta}_{N,l}$ and $\hat{\theta}_{init,l}$ using the following estimator $\hat{\theta}_{final,l} = (P_{\theta_l}^{-1} + P_{init,l}^{-1})^{-1} \left(P_{\theta_l}^{-1}\hat{\theta}_{N,l} + P_{init,l}^{-1}\hat{\theta}_{init,l} \right)$ whose covariance matrix is given by $(P_{\theta_l}^{-1} + P_{init,l}^{-1})^{-1}$ [1, page 464].

The accuracy of the estimate $\hat{\theta}_{final,l}$ can thus be measured with $P_{\theta_l}^{-1}(\theta_0, \Phi_r) + P_{init,l}^{-1}$. Similarly to Chapters 2 and 3, we will then suppose that this accuracy will be deemed satisfactory if the following accuracy constraint $P_{\theta_l}^{-1}(\theta_0, \Phi_r) + P_{init,l}^{-1} > R_{adm}$ is satisfied. The matrix R_{adm} is a given strictly positive-definite and symmetric matrix that reflects the desired accuracy [49, 53].

4.4 Optimal experiment design problem

In line with the least costly philosophy, we will design the spectrum Φ_r of the excitation signal r of the identification experiment described in the previous section in such a way that the accuracy constraint $P_{\theta_l}^{-1}(\theta_0, \Phi_r) + P_{init,l}^{-1} > R_{adm}$ is satisfied with the smallest cost $\mathcal{J}(\theta_0, \Phi_r)$ (see (4.15)). This optimization problem can thus be formulated as follows:

$$\min_{\Phi_r} \mathcal{J}(\theta_0, \Phi_r) \qquad (4.27)$$

$$\text{such that } P_{\theta_l}^{-1}(\theta_0, \Phi_r) + P_{init,l}^{-1} \geq R_{adm} \qquad (4.28)$$

This optimization problem can be considered both in the stealth and in the non-stealth setting by using the respective expressions for $\mathcal{J}(\theta_0, \Phi_r)$ and for $P_{\theta_l}^{-1}(\theta_0, \Phi_r)$ in both cases. Before discussing how this optimization problem can be solved in practice, let us formulate the following result that illustrates the advantage of the stealth configuration. For this purpose, let us here also exclude some pathological cases:

Assumption 4.4. *Consider the notations introduced in Section 4.3.1 for the identification of Node l and in particular the lth entries $R_l^u(z, \theta_0)$ and $R_l^{u,NS}(z, \theta_0)$ of the vectors of transfer functions $R^u(z, \theta_0)$ and $R^{u,NS}(z, \theta_0)$ defined in (4.12) and in (4.20), respectively. We assume that $R_l^u(e^{j\omega}, \theta_0)$ and $R_l^{u,NS}(e^{j\omega}, \theta_0)$ are equal to zero only at those frequencies ω where the frequency response $K_l(e^{j\omega})$ of the controller present in Node l is infinite[3] (due to an integrator or a resonator).*

Proposition 4.3. *Consider an identification experiment in Node l of a network satisfying Assumptions 4.1, 4.2, and 4.4. Consider, for this identification experiment, the optimal experiment design problem (4.27)-(4.28) in the stealth and in the non-stealth setting (i.e. using the respective expressions for $\mathcal{J}(\theta_0, \Phi_r)$ and for $P_{\theta_l}^{-1}(\theta_0, \Phi_r)$ in both cases) and let us denote by $\Phi_{r,opt}^S$ and $\Phi_{r,opt}^{NS}$ the optimal spectra obtained in these two settings. Then, we have that the optimal cost $\mathcal{J}(\theta_0, \Phi_{r,opt}^S)$ in the stealth setting is strictly smaller than the cost $\mathcal{J}(\theta_0, \Phi_{r,opt}^{NS})$ in the non-stealth setting if the model $T_{init,l}$ of $T_{0,l}$ used in the stealth compensation (4.7) has the following property for all ω where $\Phi_{r,opt}^{NS}(\omega) \neq 0$:*

$$\frac{|T_{0,l}(e^{j\omega}) - T_{init,l}(e^{j\omega})|}{|T_{0,l}(e^{j\omega})|} < \frac{|R_l^u(e^{j\omega}, \theta_0)|}{|R_l^{u,NS}(e^{j\omega}, \theta_0)|} \qquad (4.29)$$

where R_l^u (resp. $R_l^{u,NS}$) is the lth entry of R^u (resp. $R^{u,NS}$) defined in (4.12) (resp. (4.20)).

Proof. See Appendix C.4. ∎

As shown in Proposition 4.3, we thus see that the stealth configuration, which can be very easily implemented in a network of locally controlled systems (such as the one considered in this chapter), will be, in many cases, advantageous[4] to obtain the required accuracy for the model of $\mathcal{S}_l$ with the smallest possible identification cost.

Let us now turn to the problem of solving the optimal experiment design problem (4.27)-(4.28). We observe that, like many optimal experiment design problems,

---

[3]At those frequencies ω where $K_l(e^{j\omega})$ is infinite, we have indeed that $S_{0,l}(e^{j\omega}) = T_{0,l}(e^{j\omega}) = T_{init,l}(e^{j\omega}) = 0$.

[4]The condition (4.29) on $T_{init,l}$ is more complex than (4.22). However, (4.29) will be respected if $T_{init,l}$ is not a too poor estimate of $T_{0,l}$.

this optimization problem is dependent on the unknown vector $\theta_0 = (\theta_{0,1}^T, \ldots, \theta_{0,N_{mod}}^T)^T$. Since θ_0 is unknown, the optimization problem (4.27)-(4.28) cannot be tackled as such. As already mentioned in Chapters 2 and 3, a commonly used approach to circumvent this problem is to replace θ_0 by an initial estimate. If we use the initial estimate $\hat{\theta}_{init}$ for this purpose (see Section 4.2), this would yield an optimization problem consisting in minimizing $\mathcal{J}(\hat{\theta}_{init}, \Phi_r)$ under the constraint $P_{\theta_l}^{-1}(\hat{\theta}_{init}, \Phi_r) + P_{init,l}^{-1} \geq R_{adm}$. Besides the typical shortcomings of this approach (see Chapter 3), this classical approach presents, in the stealth configuration, an even more important disadvantage. Recall indeed that $T_{init,l}$ in (4.7) is also computed based on $\hat{\theta}_{init}$. The latter has as consequence that $\mathcal{J}(\hat{\theta}_{init}, \Phi_r) = \mathcal{J}_l(\hat{\theta}_{init}, \Phi_r)$ (because $\mathcal{J}_i(\hat{\theta}_{init}, \Phi_r) = 0$ for all $i \neq l$). In other words, the propagation of the signal $r(t)$ towards the nodes i with $i \in \mathcal{P}_l$ will not be taken into account in the optimal experiment design problem if we replace θ_0 by $\hat{\theta}_{init}$. We will therefore instead consider the following formulation where the cost constraint has been robustified using the initial uncertainty region U_{init} (see (4.6)):

$$\min_{\Phi_r, \gamma} \gamma \tag{4.30}$$

$$\text{such that } \mathcal{J}(\theta, \Phi_r) \leq \gamma \quad \forall \theta \in U_{init} \tag{4.31}$$

$$\text{and } P_{\theta_l}^{-1}(\hat{\theta}_{init}, \Phi_r) + P_{init,l}^{-1} \geq R_{adm} \tag{4.32}$$

Note that, for simplicity, we do not robustify the accuracy constraint in the above optimization problem. The optimization problem (4.30)-(4.32) can be considered both in the stealth and in the non-stealth settings by using the respective expressions for $\mathcal{J}(\Phi_r, \theta)$ and for $P_{\theta_l}^{-1}(\Phi_r, \hat{\theta}_{init})$ in both cases.

As opposed to the case where θ_0 is replaced by $\hat{\theta}_{init}$, the above formulation will also take into account the propagation of the excitation signal in the stealth setting. In this setting, we will also observe a *robustification* of the stealth compensation. Indeed, the robustified formulation will favour spectra Φ_r yielding, for all $\theta \in U_{init}$, small perturbations $R_i^u(z, \theta) r(t)$ and $R_i^y(z, \theta) r(t)$ for $i = l$ and for $i \in \mathcal{P}_l$ (see (4.11)-(4.10)). For nodes $i \in \mathcal{P}_l$, this e.g. means that the power of the following signal has to be made small for all $\theta \in U_{init}$:

$$R_i^u(z, \theta) r(t) = \bar{\mathcal{N}}_i(z, \theta) \left(\frac{G_l(z, \theta)}{1 + K_l(z) G_l(z, \theta)} - T_{init,l}(z) \right) r(t)$$

Consequently, the robustified optimal experiment design problem will generally and among other considerations favour spectra $\Phi_r(\omega)$ with more contributions in the frequency ranges where the stealth compensation will be more effective due to a small uncertainty of $T_{init,l}(z)$ (thereby *robustifying* the stealth configuration).

In both the stealth and non-stealth settings, the robustified optimal experiment design problem (4.30)-(4.32), has also the following properties (see also Chapter 3). If we denote by $\Phi_{r,opt}$ and γ_{opt} the solution of this optimization problem, we have that $\gamma_{opt} = \sup_{\theta \in U_{init}} \mathcal{J}(\theta, \Phi_{r,opt})$. Since we assume that $\theta_0 \in U_{init}$, this robustified

formulation ensures that the a-priori unknown cost $\mathcal{J}(\theta_0, \Phi_{r,opt})$ is guaranteed to be smaller than γ_{opt}. This would not have been the case if, instead of the robustified constraint (4.31), we would have used the non-robustified constraint $\mathcal{J}(\hat{\theta}_{init}, \Phi_r) \leq \gamma$.

Since the optimization problem (4.30)-(4.32) can be considered for the stealth and the non-stealth configurations, the solution of the optimization problem in both settings can be compared to verify whether the stealth configuration indeed yields a smaller cost. Note that this will generally be the case since, as explained above, the robust formulation will imply a robustification of the stealth compensation. However, in the case of (4.30)-(4.32), we do not have a condition such as (4.29) to guarantee this property.

4.5 Tackling the robust cost constraint in a convex way

Since (4.32) is affine in the decision variable Φ_r, the optimization problem (4.30)-(4.32) will be convex if (4.31) can be transformed into a constraint linear in the decision variables Φ_r and γ. As already mentioned in Chapter 3, it is impossible to find a linear tractable constraint that is equivalent to (4.31), but we can find one that implies (4.31). Consequently, if we solve the optimization problem with this alternative constraint, its solution γ_{opt} will be an upper bound for $\sup_{\theta \in U_{init}} \mathcal{J}(\theta, \Phi_{r,opt})$. This entails a certain conservatism, but this γ_{opt} remains an upper bound for the (unknown) cost $\mathcal{J}(\theta_0, \Phi_{r,opt})$ of an identification experiment with spectrum $\Phi_{r,opt}$.

In order to derive a tractable constraint implying (4.31), we have to take into account that we are in the network context and thus that the vector θ can be of high dimension. Therefore, using the results of Chapter 3 to derive this tractable constraint may lead to a problem that is too complex from a computational point-of-view (see Section 3.8). Consequently, instead of working directly on the uncertain vector θ as in Chapter 3, it is preferable to consider the so-called hierarchical approach. The hierarchical approach has indeed been introduced in [54] to analyze the robustness of large-scale (interconnected) systems. Consequently, our objective here will be to determine a tractable constraint implying (4.31) and that can be used in the context of the hierarchical approach.

To derive such a tractable linear constraint implying (4.31), we will assume, as in Chapter 3, that the to-be-designed excitation signal r is a multisine i.e., $r(t) = \sum_{m=1}^{L} A_m \sin(\omega_m t)$ where the frequencies ω_m $(m = 1, \ldots, L)$ are fixed by the user (as e.g. a fine grid of the frequency range $[0, \ \pi]$) and where the amplitudes A_m $(m = 1, \ldots, L)$ will be optimally determined[5]. Such parametrization of the excitation signal corresponds to the following spectrum (see also (2.18)):

$$\Phi_r(\omega) = \pi \sum_{m=1}^{L} c_m \ (\delta(\omega - \omega_m) + \delta(\omega + \omega_m)) \geq 0 \quad \forall \omega \tag{4.33}$$

---

[5]Arbitrary phase shifts can also be added to each sinusoid.

where the positive scalars $c_m = \frac{A_m^2}{2}$ $(m = 1, \ldots, L)$ will be the decision variables of the optimization problem.

Using (4.33) and (4.15), the robust cost constraint (4.31) can be rewritten as follows:

$$\sum_{m=1}^{L} c_m \left(\mathcal{R}^*(e^{j\omega_m}, \theta) \mathcal{R}(e^{j\omega_m}, \theta) \right) \leq \gamma \qquad \forall \theta \in U_{init} \tag{4.34}$$

In the next section, we will show that the hierarchical approach can be used to deduce, for each ω, an accurate upper bound $\alpha(\omega)$ for

$$\mathcal{R}_{wc}(\omega) = \sup_{\theta \in U_{init}} \left(\mathcal{R}^*(e^{j\omega}, \theta) \mathcal{R}(e^{j\omega}, \theta) \right) \tag{4.35}$$

i.e. $\mathcal{R}_{wc}(\omega) \leq \alpha(\omega)$. This computable upper bound $\alpha(\omega)$ for $\mathcal{R}_{wc}(\omega)$ is important since it is a necessary ingredient to derive a tractable linear constraint implying the robust cost constraint (4.34) as shown in the following proposition.

Proposition 4.4. *Consider the robust cost constraint* (4.34) *corresponding to a spectrum of the type* (4.33)*. Then, the constraint* (4.34) *holds for a given γ if the following inequality linear in the decision variables c_m $(m = 1, \ldots, L)$ holds:*

$$\sum_{m=1}^{L} c_m \, \alpha(\omega_m) \leq \gamma \tag{4.36}$$

where $\alpha(\omega)$ $(m = 1, \ldots, L)$ is an upper bound for $\mathcal{R}_{wc}(\omega)$ (see(4.35)*)*

Proof. For any frequency ω_m, we have that:

$$\left(\mathcal{R}^*(e^{j\omega_m}, \theta) \mathcal{R}(e^{j\omega_m}, \theta) \right) \leq \alpha(\omega_m) \quad \forall \theta \in U_{init}$$

The latter relation confirms that (4.34) holds if (4.36) holds. ∎

Let us observe that (4.36) is an inequality constraint linear in the coefficients c_m $(m = 1, \ldots, L)$. Moreover, since Φ_r is affine in c_m $(m = 1, \ldots, L)$, the accuracy constraint (4.32) is also linear in these coefficients. Consequently, the following Linear Matrix Inequality (LMI) optimization problem is a convex formulation for the original robust optimal experiment design problem (4.30)-(4.32).

LMI formulation. *Consider the parametrization* (4.33) *for the to-be-designed spectrum Φ_r. For this parametrization, the LMI optimization problem has as decision variables a scalar $\gamma > 0$ and coefficients $c_m \geq 0$ $(m = 1, \ldots, L)$ and consists in determining the smallest value of γ for which both the LMI constraint* (4.32) *and the constraint* (4.36) *hold for some $c_m \geq 0$ $(m = 1, \ldots, L)$.*

Let us denote by $c_{m,opt}$ $(m = 1, \ldots, L)$ and by γ_{opt} the solution of this LMI optimization problem and let us also denote by $\Phi_{r,opt}$ the spectrum corresponding to the coefficients $c_{m,opt}$. Then, due to Proposition 4.4, we have that γ_{opt} is an upper bound of $\sup_{\theta \in U_{init}} \mathcal{J}(\theta, \Phi_{r,opt})$ and thus of $\mathcal{J}(\theta_0, \Phi_{r,opt})$. Moreover, by construction, the spectrum $\Phi_{r,opt}$ is also the one yielding the smallest value of (the upper bound of) $\sup_{\theta \in U_{init}} \mathcal{J}(\theta, \Phi_{r,opt})$ for which the accuracy constraint (4.32) is met.

Remark 4.1. The solution $\gamma_{opt} = \sum_{m=1}^{L} c_{m,opt} \, \alpha(\omega_m)$ of the optimization problem gives an upper bound $\mathcal{J}^{ub}$ for the total cost $\mathcal{J}(\theta_0, \Phi_{r,opt})$. We can also compute an upper bound $\mathcal{J}_i^{ub}$ for the individual costs $\mathcal{J}_i(\theta_0, \Phi_{r,opt})$ defined in (4.18). This upper bound $\mathcal{J}_i^{ub}$ $(i = 1, \ldots, N_{mod})$ is given by:

$$\mathcal{J}_i^{ub} = \sum_{m=1}^{L} c_{m,opt} \, \alpha_i(\omega_m) \tag{4.37}$$

where, for any frequency ω, $\alpha_i(\omega)$ $(i = 1, \ldots, N_{mod})$ is an upper bound for

$$\mathcal{R}_{wc,i}(\omega) = \sup_{\theta \in U_{init}} \left(\mathcal{R}_i^*(e^{j\omega}, \theta) \mathcal{R}_i(e^{j\omega}, \theta) \right) \tag{4.38}$$

Such an upper bound can also be computed using the tools that will be presented in the next section.

Remark 4.2. The approach that we propose in this chapter to robustify the cost constraint is not based on any approximation. However, as already mentioned, it comes with a dose of conservatism. There are two sources of conservatism when we replace the original constraint (4.34) by the constraint (4.36). The first source consists in going from (4.34) to $\sum_{m=1}^{L} c_m \mathcal{R}_{wc}(\omega_m) \leq \gamma$ and the second one in going from $\sum_{m=1}^{L} c_m \mathcal{R}_{wc}(\omega_m) \leq \gamma$ to (4.36). Let us explain these sources of conservatism in more details. In the first source of conservatism, we consider the optimization problem (4.35) leading to $\mathcal{R}_{wc}(\omega_m)$ independently at each ω_m $(m = 1, \ldots, L)$. Consequently, the parameter θ at which the supremum $\mathcal{R}_{wc}(\omega_m)$ is obtained can be different at each frequency ω_m (unlike in the original constraint (4.34)). In the second source of conservatism, we replace the quantity $\mathcal{R}_{wc}(\omega_m)$ by an upper bound $\alpha(\omega_m)$ computed via the hierarchical approach (presented in the next section).

Remark 4.3. As already mentioned in Section 4.4, we have not robustified the accuracy constraint (4.32). If, from a theoretical point-of-view, we could consider extending the relaxations of Section 3.6 to the network case in order to derive a tractable constraint for this robust accuracy constraint, the numerical complexity is bound to become excessive for networks of high dimension. Moreover, we have not found a way to tackle a robustified accuracy constraint using the hierarchical approach. Consequently, if the user wishes to robustify (4.32), a reasonable solution would be to use the gridding approach for robust optimal experiment design presented in Section 3.3.

4.6 Computation of $\alpha(\omega)$ using the hierarchical approach

4.6.1 LFT representation of $\mathcal{R}(z, \theta)$

To be able to use the LMI formulation of the optimal experiment design problem (4.30)-(4.32) given in the previous section, it is necessary to determine a way to compute an (accurate) upper bound $\alpha(\omega)$ for $\mathcal{R}_{wc}(\omega)$ at a given[6] frequency ω. As mentioned before, the hierarchical approach will be used here for this purpose. In order to use the hierarchical approach for the problem at stake (see e.g. [17]), we first need to rewrite $\bar{s}(t) = \mathcal{R}(z, \theta)r(t)$ in a Linear Fractional Transformation (LFT) representation having a special form i.e., we have to determine vectors of signals $\bar{p}$ and $\bar{q}$ such that:

$$\bar{p}(t) = \bar{T}(z, \theta)\bar{q}(t) \quad \text{and} \quad \begin{pmatrix} \bar{q}(t) \\ \bar{s}(t) \end{pmatrix} = M(z) \begin{pmatrix} \bar{p}(t) \\ r(t) \end{pmatrix} \tag{4.39}$$

where $M(z)$ is not a function of θ and where $\bar{T}(z, \theta)$ is a diagonal matrix of dimension $N_{mod} \times N_{mod}$ for which the (i, i) entry is a closed-loop transfer function related to an isolated[7] loop made up of the controller K_i and a model $G_i(z, \theta_i)$ of $G_i(z, \theta_{i,0})$. In our case, $\bar{T}(z, \theta)$ will be chosen as:

$$\bar{T}(z, \theta) = diag(T_1(z, \theta_1), \ldots, T_{N_{mod}}(z, \theta_{N_{mod}})) \tag{4.40}$$

where $T_i(z, \theta_i) = G_i(z, \theta_i)/(1 + K_i(z)G_i(z, \theta_i))$. Note that, in the sequel, we will often use the shorthand notation $\mathcal{R}(z, \theta) = \mathcal{F}(M(z), \bar{T}(z, \theta))$ for the LFT (4.39).

We will determine this LFT both in the stealth setting and in the non-stealth setting. Let us start with the stealth setting and let us pose $\bar{e} = 0$ and $ref_{ext} = 0$ in (4.3)-(4.8)-(4.9). If we express these equations for an arbitrary θ, we obtain

$$\bar{y}(t) = \bar{G}(z, \theta)\bar{u}(t) \tag{4.41}$$

$$\bar{u}(t) = \bar{m}_l r(t) + \bar{K}(z) (\bar{y}_{ref}(t) - \bar{y}(t)) \tag{4.42}$$

$$\bar{y}_{ref}(t) = \mathcal{A} \left(\bar{y}(t) - \bar{m}_l \underbrace{T_{init,l}(z)r(t)}_{=x(t)} \right) \tag{4.43}$$

Inserting (4.42) in (4.41) yields:

$$\bar{y}(t) = \bar{T}(z, \theta) \left(\bar{K}(z)\bar{y}_{ref}(t) + \bar{m}_l r(t) \right) \tag{4.44}$$

with the definition of $\bar{T}(z, \theta)$ given in (4.40). Let us now define $\bar{p}(t) := \bar{y}(t)$ and $\bar{q}(t) := \bar{K}\bar{y}_{ref}(t) + \bar{m}_l r(t)$ and let us notice that, using (4.43), $\bar{q}(t)$ is equal to:

---

[6]We will indeed need to determine $\alpha(\omega)$ at the L frequencies present in (4.33).

[7]By isolated, we mean that the considered loop is not connected to other loops via a network connection.

$$\bar{q}(t) = \bar{K}(z)\mathcal{A}\left(\underbrace{\bar{y}(t)}_{\bar{p}(t)} - \bar{m}_l T_{init,l}(z)r(t)\right) + \bar{m}_l r(t)$$

Using (4.10) and (4.11), let us also notice that $\bar{s}(t) = (\bar{s}_y^T(t),\ \bar{s}_u^T(t))^T$ with $\bar{s}_y(t) = \sqrt{\beta}R^y(z,\theta)r(t) = \sqrt{\beta}\bar{y}(t) = \sqrt{\beta}\bar{p}(t)$ and $\bar{s}_u(t) = R^u(z,\theta)r(t) = \bar{u}(t)$ (when $\bar{e} = 0$ and $ref_{ext} = 0$). Inserting (4.43) in (4.42) and using the fact that $\bar{y}(t) = \bar{p}(t)$, we obtain:

$$\bar{u}(t) = \bar{K}(z)\left(\mathcal{A} - I_{N_{mod}}\right)\bar{p}(t) + \left(\bar{m}_l - \bar{K}(z)\mathcal{A}\bar{m}_l T_{init,l}(z)\right)r(t)$$

This therefore yields the following expression for $M(z)$:

$$M(z) = \left(\begin{array}{c|c} \begin{array}{c} \bar{K}(z)\mathcal{A} \\ \hline \sqrt{\beta}\ I_{N_{mod}} \end{array} & \begin{array}{c} \bar{m}_l - \bar{K}(z)\mathcal{A}\bar{m}_l T_{init,l}(z) \\ \hline 0 \end{array} \\ \hline \bar{K}(z)\left(\mathcal{A} - I_{N_{mod}}\right) & \left(\bar{m}_l - \bar{K}(z)\mathcal{A}\bar{m}_l T_{init,l}(z)\right) \end{array}\right) \quad (4.45)$$

Let us now consider the non-stealth configuration. In this configuration, R^y and R^u (see (4.12)-(4.13)) are replaced by $R^{y,NS}$ and $R^{u,NS}$ (see (4.20)-(4.21)) in the above reasoning. By doing this, $\mathcal{R}(z,\theta)$ can also be written as an LFT $\mathcal{F}(M(z),\bar{T}(z,\theta))$ with

$$M(z) = \left(\begin{array}{c|c} \begin{array}{c} \bar{K}(z)\mathcal{A} \\ \hline \sqrt{\beta}\ I_{N_{mod}} \end{array} & \begin{array}{c} \bar{m}_l \\ \hline 0 \end{array} \\ \hline \bar{K}(z)\left(\mathcal{A} - I_{N_{mod}}\right) & \bar{m}_l \end{array}\right)$$

4.6.2 Hierarchical approach

Based on the LFT representation $\mathcal{R}(z,\theta) = \mathcal{F}(M(z),\bar{T}(z,\theta))$ deduced in the previous subsection (for both the stealth and non-stealth settings), we have now all the elements to derive the hierarchical approach to determine an upper bound $\alpha(\omega)$ for $\mathcal{R}_{wc}(\omega)$ (see (4.35)). This approach is an adaptation of the procedure proposed in Section 3 of [17]. The main difference with [17] is that $\mathcal{R}(z,\theta)$ is here a vector of transfer functions while, in [17], $\mathcal{R}(z,\theta)$ was a scalar transfer function.

Let us first notice that, at each frequency ω, the frequency response $\bar{T}(e^{j\omega},\theta)$ of every transfer matrix $\bar{T}(z,\theta)$ with $\theta \in U_{init}$ lies in the following multiplicative uncertainty region [52]:

$$\mathcal{T}(\omega) = \{\bar{T}(e^{j\omega}) \mid \bar{T}(e^{j\omega}) = (1 + \Delta(e^{j\omega}))\ \bar{T}(e^{j\omega},\hat{\theta}_{init}) \text{ with } \Delta(e^{j\omega}) \in \boldsymbol{\Delta}(\omega)\} \quad (4.46)$$

$$\boldsymbol{\Delta}(\omega) = \{\Delta(e^{j\omega}) = diag(\Delta_1(e^{j\omega}),\ldots,\Delta_{N_{mod}}(e^{j\omega})) \mid |\Delta_i(e^{j\omega}) - \tilde{c}_i(\omega)| < \rho_i(\omega)\ i = 1,\ldots,N_{mod}\} \quad (4.47)$$

where, for each $i = 1,\ldots,N_{mod}$, $\tilde{c}_i(\omega)$ is a complex scalar and $\rho_i(\omega)$ is a real scalar determined as follows:

$$\min_{\rho_i(\omega),\ \tilde{c}_i(\omega)} \rho_i(\omega)$$

$$\text{s.t. } |\tilde{T}_i(e^{j\omega},\theta_i) - \tilde{c}_i(\omega)| < \rho_i(\omega) \quad \forall \theta_i \in U_{init,i} \quad (4.48)$$

with $\tilde{T}_i(e^{j\omega}, \theta_i) = \frac{T_i(e^{j\omega}, \theta_i) - T_i(e^{j\omega}, \hat{\theta}_{init,i})}{T_i(e^{j\omega}, \hat{\theta}_{init,i})}$ and

$$U_{init,i} = \{\theta_i \mid \theta \in U_{init}\} = \left\{\theta_i \mid (\theta_i - \hat{\theta}_{init,i})^T P_{init,i}^{-1}(\theta - \hat{\theta}_{init,i}) \le \chi\right\}$$

By virtue of (4.48), $\mathcal{T}(\omega)$ is in fact the smallest multiplicative uncertainty region that contains $T(e^{j\omega}, \theta)$ for all $\theta \in U_{init}$. As shown in Appendix C.5, the quantities $\tilde{c}_i(\omega)$ and $\rho_i(\omega)$ can be exactly computed for each i and for each ω. Consequently, $\mathcal{T}(\omega)$ can thus be entirely defined.

Using the LFT $\mathcal{R}(z, \theta) = \mathcal{F}(M(z), \bar{T}(z, \theta))$, the quantity $\mathcal{R}_{wc}(\omega)$ at a given ω can be rewritten as:

$$\mathcal{R}_{wc}(\omega) = \sup_{\theta \in U_{init}} \left(\mathcal{F}^*\left(M(e^{j\omega}), \bar{T}(e^{j\omega}, \theta)\right) \ \mathcal{F}\left(M(e^{j\omega}), \bar{T}(e^{j\omega}, \theta)\right)\right) \tag{4.49}$$

Using the multiplicative uncertainty region $\mathcal{T}(\omega)$ defined above, we have the following property:

$$\mathcal{R}_{wc}(\omega) \le \underbrace{\sup_{\bar{T}(e^{j\omega}) \in \mathcal{T}(\omega)} \left(\mathcal{F}^*\left(M(e^{j\omega}), \bar{T}(e^{j\omega})\right) \ \mathcal{F}\left(M(e^{j\omega}), \bar{T}(e^{j\omega})\right)\right)}_{=\tilde{\alpha}(\omega)} \tag{4.50}$$

Using the fact that:

$$\bar{T}(e^{j\omega}) = \mathcal{F}\left(\begin{pmatrix} 0 & \bar{T}(e^{j\omega}, \hat{\theta}_{init}) \\ I_{N_{mod}} & \bar{T}(e^{j\omega}, \hat{\theta}_{init}) \end{pmatrix}, \Delta(e^{j\omega})\right),$$

we can determine, using simple transformations, the matrix $M_\Delta(e^{j\omega})$ such that $\mathcal{F}\left(M(e^{j\omega}), \bar{T}(e^{j\omega})\right) = \mathcal{F}\left(M_\Delta(e^{j\omega}), \Delta(e^{j\omega})\right)$. Using this new LFT description in $\Delta(e^{j\omega})$, $\tilde{\alpha}(\omega)$ in (4.50) can be rewritten equivalently as:

$$\tilde{\alpha}(\omega) = \sup_{\Delta(e^{j\omega}) \in \boldsymbol{\Delta}(\omega)} \left(\mathcal{F}^*\left(M_\Delta(e^{j\omega}), \Delta(e^{j\omega})\right) \ \mathcal{F}\left(M_\Delta(e^{j\omega}), \Delta(e^{j\omega})\right)\right) \tag{4.51}$$

An accurate upper bound for this quantity $\tilde{\alpha}(\omega)$ can be determined using the LMI optimization problem given in the following proposition. This computable upper bound for $\tilde{\alpha}(\omega)$ is thus also an upper bound for $\mathcal{R}_{wc}(\omega)$ and will therefore be chosen as the quantity $\alpha(\omega)$ that is used in the LMI formulation of Section 4.5.

Proposition 4.5. *Consider a given frequency ω and the quantities $\rho_i(\omega)$ and $\tilde{c}_i(\omega)$ ($i = 1, \ldots, N_{mod}$) defining the set $\mathcal{T}(\omega)$ (see (4.46)). Define R_ω (resp. C_ω) as a diagonal matrix of dimension N_{mod} whose elements are $\rho_i^2(\omega)$ (resp. $\tilde{c}_i(\omega)$) ($i = 1, \ldots, N_{mod}$). Then, an upper bound for $\tilde{\alpha}(\omega)$ (see (4.51)) is given by $\tilde{\gamma}_{opt}(\omega)$ where $\tilde{\gamma}_{opt}(\omega)$ is the solution of the following LMI optimization problem. This LMI optimization problem has as decision variables a real scalar $\tilde{\gamma}(\omega) > 0$ and a strictly positive definite diagonal matrix $T_\omega \in \boldsymbol{R}^{N_{mod} \times N_{mod}}$.*

$$\min_{\tilde{\gamma}(\omega), \ T_\omega} \quad \tilde{\gamma}(\omega)$$

$$subject\ to\ \left(\begin{array}{c} M_\Delta(e^{j\omega}) \\ I \end{array} \right)^* \mathcal{N}(\tilde{\gamma}(\omega)) \left(\begin{array}{c} M_\Delta(e^{j\omega}) \\ I \end{array} \right) < 0 \tag{4.52}$$

$$with\ \mathcal{N}(\tilde{\gamma}(\omega)) \triangleq \left(\begin{array}{c|c} \left(\begin{array}{c|c} T_\omega(R_\omega - C_\omega^* C_\omega) & 0 \\ \hline 0 & I_{2N_{mod}} \end{array} \right) & \left(\begin{array}{c|c} T_\omega C_\omega^* & 0 \\ \hline 0 & 0 \end{array} \right) \\ \hline \left(\begin{array}{c|c} T_\omega C_\omega & 0 \\ \hline 0 & 0 \end{array} \right) & \left(\begin{array}{c|c} -T_\omega & 0 \\ \hline 0 & -\tilde{\gamma}(\omega) \end{array} \right) \end{array} \right) \tag{4.53}$$

Proof. See Appendix C.6. ∎

Remark 4.4. From a computational point-of-view, the hierarchical approach is advantageous for large networks. Indeed, due to the embedding in a multiplicative uncertainty, the complexity of the multiplier T_ω in the above proposition remains very limited (i.e., N_{mod} elements in T_ω). Moreover, the quantities $\rho_i(\omega)$ and $\tilde{c}_i(\omega)$ are computed locally in each node. In other words, the complexity of the network does not play a role in the computation of $\rho_i(\omega)$ and $\tilde{c}_i(\omega)$.

Remark 4.5. The quantity $\alpha_i(\omega)$ $(i = 1, \ldots, N_{mod})$ that can be used to determine the upper bound $\mathcal{J}_i^{ub}$ on the individual cost $\mathcal{J}_i$ (see (4.37)) can also be determined using the hierarchical approach presented above. For this purpose, we just have to replace, in the above reasoning, the LFT representation for $\mathcal{R}(z, \theta)$ by an LFT representation for $\mathcal{R}_i(z, \theta)$ (this LFT representation can be easily deduced from the one of $\mathcal{R}(z, \theta)$).

4.7 Numerical illustrations

4.7.1 First numerical illustration

In this first numerical illustration, we consider the network of Figure 4.1 made up of $N_{mod} = 6$ homogenous nodes. In other words, the true systems $\mathcal{S}_i$ $(i = 1, \ldots, 6)$ are all identical and given by the following ARX system [55] with two resonance peaks:

$$y_i(t) = \frac{z^{-3}B_0(z)}{A_0(z)} u_i(t) + \frac{1}{A_0(z)} e_i(t)$$

with

$$B_0(z) = 0.10276 + 0.18123 z^{-1}$$

$$A_0(z) = 1 - 1.99185 z^{-1} + 2.20265 z^{-2} - 1.84083 z^{-3} + 0.89413 z^{-4}$$

The variances of the white noises $e_i(t)$ are all equal to 0.5. We further suppose that these true systems are all controlled by the same local controller $K(z) = \frac{K_B(z)}{K_A(z)}$ with $K_B(z) = 0.03742 - 0.06719 z^{-1} + 0.06995 z^{-2} - 0.03814 z^{-3} - 0.02546 z^{-4} + 0.06323 z^{-5} - 0.04707 z^{-6} + 0.03222 z^{-7}$ and $K_A(z) = 1 - 3.348 z^{-1} + 5.953 z^{-2} - 7.163 z^{-3} + 6.143 z^{-4} - 3.705 z^{-5} + 1.368 z^{-6} - 0.2482 z^{-7}$.

For simplicity, the initial estimate $\hat{\theta}_{init}$ and its covariance matrix P_{init} are determined from a single open-loop experiment on the ARX system (disconnected from the

network) with a white input signal of variance 19 and of duration $N = 1000$. This open-loop experiment yields the following identified polynomials $B_{id} = 0.09535 + 0.1769z^{-1}$ and $A_{id} = 1 - 1.989z^{-1} + 2.187z^{-2} - 1.822z^{-3} + 0.887z^{-4}$ corresponding to the identified parameter vector $\theta_{module,ol}$ of dimension 6 with covariance matrix $P_{module,ol}$. Based on this open-loop experiment, the initial estimates $\hat{\theta}_{init,i}$ of $\theta_{0,i}$ $(i = 1, \ldots, 6)$ can all be chosen equal to $\theta_{module,ol}$ i.e. $\hat{\theta}_{init} = (\theta_{module,ol}^T, \theta_{module,ol}^T, \ldots, \theta_{module,ol}^T)^T$ and P_{init} is chosen equal to $I_{N_{mod}} \otimes P_{module,ol}$. Using these quantities, we can define the uncertainty region U_{init} corresponding to a confidence level η of 95% ($\chi = 50.9985$).

Our objective will be to design the spectrum $\Phi_r(\omega)$ of the excitation signal r that has to be added to Node 5 (i.e. $l = 5$) during an identification experiment of duration $N = 1000$ to improve the accuracy of the model of $\mathcal{S}_5$ in such a way that the following accuracy constraint is satisfied $P_{\theta_5}^{-1}(\theta_0, \Phi_r) + P_{init,5}^{-1} > R_{adm}$ where R_{adm} is chosen as the inverse of the diagonal matrix $diag((0.019)^2, (0.022)^2, (0.018)^2, (0.009)^2, (0.005)^2, (0.009)^2)$. We will furthermore suppose that $ref_{ext}(t) = 0$ during the identification experiment.

To determine the spectrum $\Phi_r(\omega)$ satisfying this accuracy constraint with the smallest identification cost, we consider the optimization problem (4.30)-(4.32). We will consider this optimization problem both in the stealth setting and in the non-stealth setting. For both settings, we define the cost of the identification experiment as in (4.15) with $\beta = 1$ and we parametrize $\Phi_r(\omega)$ as in (4.33) with $L = 20$ frequencies distributed in the frequency range $[10^{-2}, \pi]$. In the stealth setting, the stealth compensation is implemented using (4.7) with the transfer function $T_{init,5}$ that can be constructed based on $\hat{\theta}_{init,5} = \theta_{module,ol}$.

To solve the optimization problem (4.30)-(4.32) in both settings, we compute, for each setting, the corresponding quantity $\alpha(\omega)$ for each frequencies ω_m $(m = 1, \ldots, L)$ present in $\Phi_r(\omega)$ (see Section 4.6). The optimal spectrum $\Phi_{r,opt}$ and the optimal value γ_{opt} can then be deduced[8] using the LMI optimization problem given at the end of Section 4.5.

Let us first consider the stealth setting. In this case, the optimal spectrum $\Phi_{r,opt}$ corresponds to a multisine for which all the amplitudes are negligible except at two frequencies $\omega = 1.35$ and $\omega = 1.65$ and γ_{opt} is equal to 34.9466. This value is an upper bound $\mathcal{J}^{ub}$ for $\sup_{\theta \in U_{init}} \mathcal{J}(\theta, \Phi_{r,opt})$ as discussed in Section 4.4 and thus also an upper bound for the a-priori unknown cost $\mathcal{J}(\theta_0, \Phi_{r,opt})$. As mentioned in the beginning of Section 4.3, our LMI approach entails a certain conservatism. Let us thus check the extent of this conservatism in this example. For this purpose, we compute a lower bound $\mathcal{J}^{lb}$ for $\sup_{\theta \in U_{init}} \mathcal{J}(\theta, \Phi_{r,opt})$ by considering the maximal value of $\mathcal{J}(\theta_i, \Phi_{r,opt})$ over a set of 1000 grid points $\theta_i \in U_{init}$. This procedure yields $\mathcal{J}^{lb} = 33.92$. Consequently, the conservatism of our procedure remains limited in this example since there is only 3% of difference between $\mathcal{J}^{lb}$ and $\mathcal{J}^{ub}$. In this simulation example, we can also

---

[8]Note that the whole procedure yielding $\Phi_{r,opt}$ and γ_{opt} takes 11 seconds using Matlab on a standard laptop with the *Intel Core i7 vPro* processor.

compute $\mathcal{J}(\theta_0, \Phi_{r,opt})$ i.e. $\mathcal{J}(\theta_0, \Phi_{r,opt}) = 31.39$. Consequently, γ_{opt} is indeed an upper bound for $\mathcal{J}(\theta_0, \Phi_{r,opt})$. Note also that, as opposed to this, $\mathcal{J}(\hat{\theta}_{init}, \Phi_{r,opt}) = 30.79$ would underestimate the actual cost of the experiment.

In order to have a better idea of how this cost is distributed in each of the six modules, let us consider the upper bound $\mathcal{J}_i^{ub}$ (see (4.37)) of the individual costs $\mathcal{J}_i(\theta_0, \Phi_{r,opt})$ for $i = 5$ and for all $i \in \mathcal{P}_5 = \{2, 3, 4, 6\}$. These upper bounds are given in Table 4.1. We observe that J_5^{ub} is almost equal to the total cost (for $i \neq 5$, $\mathcal{J}_i^{ub} \leq 3.5 \ 10^{-4}$).

Let us now compare these results with the ones obtained in the non-stealth setting. The optimal multisine in this setting is very similar to the one in the stealth setting and $\gamma_{opt} = 34.9557$. We observe that this value is (slightly) larger than in the stealth case where $\gamma_{opt} = 34.9466$. Moreover, as shown in Table 4.1, the costs $\mathcal{J}_i^{ub}$ for $i \in \mathcal{P}_5$ are all at least 16 times larger than when the stealth configuration is implemented. This shows the advantage of the stealth configuration. The maximum of these individual costs for $i \neq 5$ (i.e. $J_6^{ub} = 6 \ 10^{-3}$) remains though small with respect to $J_5^{ub} = 34.9470$. This is due to the large attenuation of this particular network. In other networks, this attenuation could be much smaller and would even more justify the use of the stealth configuration. This will be illustrated in the second numerical illustration.

Table 4.1: Upper bounds $\mathcal{J}_i^{ub}$ for the individual costs $\mathcal{J}_i$ ($i = 2, \ldots, 6$) obtained using the optimal spectrum in the stealth and non-stealth settings (first illustration)

	$\mathcal{J}_2^{ub}$	$\mathcal{J}_3^{ub}$	$\mathcal{J}_4^{ub}$	$\mathcal{J}_5^{ub}$	$\mathcal{J}_6^{ub}$
STEALTH	$7 \ 10^{-9}$	$8.8 \ 10^{-5}$	$8.8 \ 10^{-5}$	34.9461	$3.5 \ 10^{-4}$
NON-STEALTH	$1.2 \ 10^{-7}$	$1.5 \ 10^{-3}$	$1.5 \ 10^{-3}$	34.9470	$6 \ 10^{-3}$

4.7.2 Second numerical illustration

In this second numerical illustration, we consider the network of Figure 4.4 made up of $N_{mod} = 2$ nodes in cascade for which we wish to identify the first node. In this network, the matrices $\mathcal{A}$ and $\mathcal{B}$ in the interconnection (4.9) are given by

$$\mathcal{A} = \begin{pmatrix} 0 & 0 \\ 1 & 0 \end{pmatrix} \quad \mathcal{B} = \begin{pmatrix} 1 \\ 0 \end{pmatrix}$$

The true system $\mathcal{S}_1$ is equal to the ARX system used in the previous subsection while the true system $\mathcal{S}_2$ is given by the following first-order ARX system:

$$y_2(t) = \frac{3.6 \ z^{-1}}{1 - 0.7 \ z^{-1}} u_2(t) + \frac{1}{1 - 0.7 \ z^{-1}} e_2(t)$$
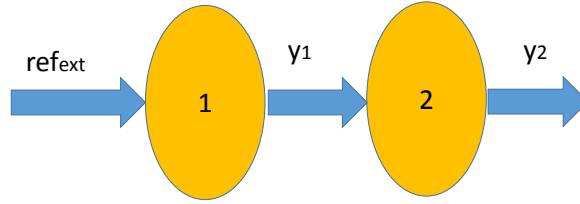
Figure 4.4: Graph representation of the network used in the second numerical illustration

(i.e. $\theta_{0,2} = (-0.7 \; 3.6)^T$). The controller K_1 is also the same as the one in the previous subsection while $K_2(z) = 10$. The variance of the white noises $e_1(t)$ and $e_2(t)$ are here also both equal to 0.5. Note that the controller K_2 ensures a large closed-loop bandwidth. Consequently, in the non-stealth configuration, any perturbation due to $r(t)$ in $y_{ref,2}(t) = y_1(t)$ will have a strong influence on $u_2(t)$ and $y_2(t)$. A stealth configuration may thus have a large impact in this example.

For simplicity, the initial estimate $\hat{\theta}_{init,1}$ and its covariance matrix $P_{init,1}$ will be chosen as in the previous section (i.e. the estimate obtained with an open-loop experiment with input variance of 19). The initial estimate $\hat{\theta}_{init,2}$ and its covariance matrix $P_{init,2}$ are determined in a similar way (open-loop experiment with input variance of 19). This yields $\hat{\theta}_{init,2} = (-0.69 \; 3.57)^T$ and a covariance matrix $P_{init,2}$. Based on this, the initial estimate $\hat{\theta}_{init}$ of θ_0 is chosen as $(\hat{\theta}_{init,1}^T, \hat{\theta}_{init,2}^T)^T$ and P_{init} is chosen equal to $bdiag(P_{init,1}, P_{init,2})$. Using these quantities, we can define the uncertainty region U_{init} corresponding to a confidence level η of 95% ($\chi = 15.5$).

Our objective will be to design the spectrum $\Phi_r(\omega)$ of the excitation signal r that has to be added to Node 1 ($l = 1$) during an identification experiment of duration $N = 1000$ to improve the accuracy of the model of $\mathcal{S}_1$ in such a way that the following accuracy constraint is satisfied $P_{\theta_1}^{-1}(\theta_0, \Phi_r) + P_{init,1}^{-1} > R_{adm}$ where R_{adm} is chosen as in the previous subsection. We will here also suppose that $ref_{ext}(t) = 0$ during the identification experiment.

To determine the spectrum $\Phi_r(\omega)$ satisfying this accuracy constraint with the smallest identification cost, we consider the optimization problem (4.30)-(4.32). We will consider this optimization problem here also both in the stealth setting and in the non-stealth setting. For both settings, we here also define the cost of the identification experiment as in (4.15) with $\beta = 1$ and we parametrize $\Phi_r(\omega)$ as in (4.33) with the same $L = 20$ frequencies as in the previous subsection. In the stealth setting, the stealth compensation is implemented using (4.7) with the transfer function $T_{init,1}$ that can be

constructed based on $\hat{\theta}_{init,1}$ ($T_{init,1}$ is here equal to the transfer function $T_{init,5}$ in the previous subsection).

Let us compare the value γ_{opt} obtained when solving (4.30)-(4.32) in the stealth and in the non-stealth settings. Like in the previous subsection, the optimal cost γ_{opt} in the stealth setting is smaller than in the non-stealth setting: the obtained γ_{opt} are respectively 33.87 and 42.38. Note that the advantage of the stealth configuration is here very clear since the stealth configuration allows to reduce the predicted cost by 25 %.

In order to have a better idea of how this cost is distributed in each of the two modules in both settings, we can consider Table 4.2 giving the upper bound $\mathcal{J}_i^{ub}$ of the individual costs $\mathcal{J}_i(\theta_0, \Phi_{r,opt})$ ($i = 1, 2$). By comparing $\mathcal{J}_2^{ub} = 0.17$ (in the stealth setting) and $\mathcal{J}_2^{ub} = 8.61$ (in the non-stealth setting), we observe that the stealth configuration plays its role entirely by reducing, by a factor of 50, the propagation of the excitation signal to Node 2. This strong reduction is also observed for the actual individual cost $\mathcal{J}_2(\theta_0, \Phi_{r,opt})$ which is equal to 0.03 in the stealth setting and to 7.04 in the non-stealth setting.

Table 4.2: Upper bounds $\mathcal{J}_i^{ub}$ for the individual costs $\mathcal{J}_i$ ($i = 1, 2$) obtained using the optimal spectrum in the stealth and non-stealth settings in the second numerical illustration

	$\mathcal{J}_1^{ub}$	$\mathcal{J}_2^{ub}$
STEALTH	33.70	0.17
NON-STEALTH	33.77	8.61

4.7.3 Case of a larger U_{init}

To show the effectiveness of the stealth configuration even in the case of a larger uncertainty U_{init} (and thus a worse model $T_{init,l}$), we repeat the above comparisons when $\hat{\theta}_{init}$ is identified with an input signal with a variance 10 times smaller than previously. In the first numerical illustration, this larger U_{init} yields a value of $\gamma_{opt} = 131.66$ in the stealth setting and a value of $\gamma_{opt} = 131.71$ in the non-stealth one. In the second numerical illustration, we obtain $\gamma_{opt} = 119$ in the stealth setting and $\gamma_{opt} = 157.84$ in the non-stealth setting. Consequently, with this larger U_{init} and this worse model $T_{init,l}$, the stealth configuration also yields a smaller identification cost than the non-stealth configuration. Even though the obtained reduction is smaller due to the worse model $T_{init,l}$, the effectiveness of the stealth setting in reducing the propagation of the influence of the excitation signal remains confirmed when looking at Tables 4.3 and 4.4 giving, for this larger U_{init} and this worse $T_{init,l}$, the upper bounds $\mathcal{J}_i^{ub}$ of the individual costs $\mathcal{J}_i(\theta_0, \Phi_{r,opt})$ for the first and second numerical illustrations, respectively. In

Table 4.3, we observe that $\mathcal{J}_i^{ub}$ for $i \in \mathcal{P}_5$ remains 4.5 times smaller (instead of 16 times smaller in Table 4.1) when the stealth configuration is implemented. In Table 4.4, J_2^{ub} remains 7 times smaller (instead of 50 times smaller in Table 4.2) when the stealth configuration is implemented.

Table 4.3: Upper bounds $\mathcal{J}_i^{ub}$ for the individual costs $\mathcal{J}_i$ ($i = 2, \ldots, 6$) obtained using the optimal spectrum in the stealth and non-stealth settings for a larger U_{init} (first numerical illustration)

	$\mathcal{J}_2^{ub}$	$\mathcal{J}_3^{ub}$	$\mathcal{J}_4^{ub}$	$\mathcal{J}_5^{ub}$	$\mathcal{J}_6^{ub}$
STEALTH	3 10^{-7}	2.1 10^{-3}	2.1 10^{-3}	131.649	8.3 10^{-3}
NON-STEALTH	1.3 10^{-6}	9.4 10^{-3}	9.5 10^{-3}	131.656	3.8 10^{-2}

Table 4.4: Upper bounds $\mathcal{J}_i^{ub}$ for the individual costs $\mathcal{J}_i$ ($i = 1, 2$) obtained using the optimal spectrum in the stealth and non-stealth settings for a larger U_{init} (second numerical illustration)

	$\mathcal{J}_1^{ub}$	$\mathcal{J}_2^{ub}$
STEALTH	113.57	5.43
NON-STEALTH	118.12	39.72

It is to be noted that, for both numerical illustrations, the condition (4.29) is verified at all frequencies even with the worse model $T_{init,l}$ considered in this section. Consequently, by virtue of Proposition 4.3, the result presented above could have been expected. However, note that this condition (4.29) cannot be verified in practice since it requires the knowledge of the unknown true system and that Proposition 4.3 only pertains to the ideal optimal experiment design problem (4.27)-(4.28) and not to (4.30)-(4.32).

4.8 Summary

In this chapter we extend the least costly identification experiment design framework to the case of the identification of one module in a network of locally controlled systems. The cost of the identification experiment (that is minimized under a certain accuracy constraint) is here defined as a function of the perturbations induced by the excitation signal on the input and output signals of each module. The propagation of the influence of the excitation signal is further reduced by an extension of the stealth identification paradigm. Note that the results here presented can easily be extended to network situations where the cost of the experiment is not related to the perturbation

induced by the excitation signal on the output of each module, but is more related to the perturbation induced by the excitation signal on the differences between the outputs of neighbouring modules. This situation can occur when the different agents in the network must remain as much as possible in a given formation configuration [56].

Resonance Frequency Tracking of a MEMS Gyroscope

5.1 Introduction

In this chapter, we will tackle a problem pertaining to the Next4MEMS project that funded this PhD thesis. The aim of the Next4MEMS project is to improve the control system of MEMS gyroscopes to increase their reliability. In a MEMS gyroscope, one of the major control loops is the loop that pertains to the drive mass system [46]. The drive mass system is basically a mass fixed to a reference frame via microsilicon beams and that can be actuated via a force. The transfer function between this force u_x and the position x of the drive mass is a second-order resonating system and the objective of the drive mass control system is that x follows a sinusoidal reference signal x_{ref}. Generally, this control objective is achieved via two parallel loops that respectively control the amplitude and the phase of the phasor representation of the to-be-controlled signal x. This phasor approach introduces unnecessary nonlinearities (e.g., to transform the signal x into its phasor description) and an alternative control approach has been proposed in the Next4MEMS project. In this alternative (and more classical) control configuration, the force u_x is computed as the output of a linear controller K_x that takes as input the difference between the sinusoidal reference signal and the signal x i.e., the position of the drive mass. Irrespectively of the control approach, it is important to note that, to reduce the energy consumption (i.e., to enforce a small actuation signal u_x), the frequency of the sinusoidal reference signal x_{ref} must be equal to (or at least close to) the resonance frequency of the drive mass system.

A MEMS gyroscope has to operate in a large range of ambient temperatures and it is well known [46] that the resonance frequency of the drive mass system changes with the temperature. In the classical control configuration (the phasor configuration), these variations were automatically taken care of via the phase loop. However, this is no longer the case in the new control configuration and a procedure has to be designed in order to adapt the frequency of the reference signal x_{ref} in such a way that this frequency is always equal (or at least close to) the actual resonance frequency of the

system. In this chapter, we compare two approaches to realize this objective. The first approach uses recursive identification, a particular identification technique that can tackle time-varying systems [1], to follow the time-varying dynamics of the drive mass system, allowing in this way to adapt the frequency of the reference signal x_{ref}. In the second approach, we observe that the to-be-determined resonance frequency is a (local) extremum of the modulus of the frequency response of the transfer function between x_{ref} and u_x and we use an adaptive control algorithm, the extremum seeking algorithm [57], to seek this local extremum. This second approach is inspired from [47] where the extremum seeking approach is used to adapt the reference of the phase loop (one of the parallel loops in the classical drive mass control scheme) in order to deal more efficiently with the effect of temperature variations.

5.2   The drive mass closed-loop system

5.2.1   Description of the drive mass system

As mentioned in the previous section, the transfer function between the force u_x and the position x of the drive mass is a second-order resonating system. Such a system can be described using the following continuous-time transfer function $\tilde{G}(s)$:

$$\tilde{G}(s) = \frac{k}{\frac{s^2}{\omega_{n,x}^2} + \frac{2\xi}{\omega_{n,x}}s + 1} \tag{5.1}$$

where s is the Laplace variable, $\xi < 1/\sqrt{2}$ the damping ratio, $\omega_{n,x}$ the natural frequency and k the static gain. The resonance frequency of $\tilde{G}$ is defined as the frequency $\omega_{r,x}$ at which the modulus $|\tilde{G}(j\omega)|$ of the frequency response of $\tilde{G}$ is the largest. Using the notations introduced in (5.1), this resonance frequency is given by $\omega_{r,x} = \omega_{n,x}\sqrt{1 - 2\xi^2}$.

As mentioned in the previous section, the dynamics of the drive mass system (5.1) varies with the temperature. More precisely, we will suppose that the only parameter that varies with the temperature is the natural frequency $\omega_{n,x}$ (k and ξ remaining constant). The variation of the natural frequency of course also implies a variation of the resonance frequency $\omega_{r,x}$.

Before describing in more details the temperature dependence, let us analyze the drive mass system considered in the Next4MEMS project at the nominal temperature $T_{nom} = 30$ degrees. At this nominal temperature, the drive mass system is described by (5.1) with $k = 6.12 \ 10^{-6}$, $\xi = 9.4 \ 10^{-6}$ and $\omega_{n,x} = 73821.22474 \ rad/s$. These parameters corresponds to a nominal resonance frequency $\omega_{r,x}^{nom} = 73821.22473 \ rad/s$.

Since the considered MEMS gyroscope is operated with an electronic card, we will here prefer a discrete-time representation of the system. At the nominal temperature,

we have the following discrete-time description[1] for the transfer function between u_x and x when the sampling time T_s is equal to $1.6 \ 10^{-5} \ s$.

$$G_x(z) = \frac{b_{0,0}z^{-1} + b_{0,1}z^{-2}}{1 + f_{0,1}z^{-1} + f_{0,2}z^{-2}} \tag{5.2}$$

with

$$\begin{pmatrix} b_{0,0} \\ b_{0,1} \\ f_{0,1} \\ f_{0,2} \end{pmatrix} = \begin{pmatrix} 4.562 \ 10^{-6} \\ -1.216 \ 10^{-5} \\ -0.7597 \\ 1 \end{pmatrix}$$

The description of the drive mass system at the nominal frequency can be completed with a description of the process and measurement noise $v_x(t)$ acting on the output $x(t)$:

$$x(t) = \underbrace{G_x(z)u_x(t)}_{\breve{x}(t)} + \underbrace{H_x(t)e_x(t)}_{v_x(t)} \tag{5.3}$$

where e_x is a Gaussian white noise of variance $\sigma_e^2 = 7.2 \ 10^{-7}$ and H_x is the following discrete-time transfer function of order 5:

$$H_x(z) = \frac{1 + \sum_{i=1}^{5} c_{0,i}z^{-i}}{1 + \sum_{i=1}^{5} d_{0,i}z^{-i}} \tag{5.4}$$

with

$$\begin{pmatrix} c_{0,1} \\ c_{0,2} \\ c_{0,3} \\ c_{0,4} \\ c_{0,5} \end{pmatrix} = \begin{pmatrix} 1.265 \\ -0.08948 \\ -1.339 \\ -0.7302 \\ -0.02449 \end{pmatrix} \quad , \quad \begin{pmatrix} d_{0,1} \\ d_{0,2} \\ d_{0,3} \\ d_{0,4} \\ d_{0,5} \end{pmatrix} = \begin{pmatrix} 0.2669 \\ -0.6584 \\ -0.8586 \\ +0.262 \\ -0.0002082 \end{pmatrix}$$

In Figures 5.1 and 5.2 we report the modulus of the frequency responses of G_x and H_x at the nominal temperature. We observe that the modulus $|G_x(e^{j\omega T_s})|$ of the frequency response of the plant transfer function G_x is negligible at all frequencies except at the resonance frequency $\omega_{r,x}^{nom} = 73821.22473 \ rad/s$ where we observe a sharp resonance peak. The modulus $|H_x(e^{j\omega T_s})|$ of the frequency response of the noise transfer function H_x presents a more classical shape. Observe nevertheless the resonance peak at a frequency which is slightly higher than $\omega_{r,x}^{nom}$ (see in particular Figure 5.2b).

5.2.2 Closed-loop system and nominal performance

As mentioned in Section 5.1, the drive mass system is operated in closed loop to generate a sinusoidal oscillation of the mass. The control configuration proposed in Next4MEMS is as follows (see also Figure 5.3):

---

[1]The values given in (5.2) (and (5.4)) are obtained via an open-loop identification experiment on the MEMS gyroscope. Note that the continuous-time equivalent of (5.2) contains a zero whose influence is negligible with respect to the main dynamics (i.e. the one given in (5.1)).

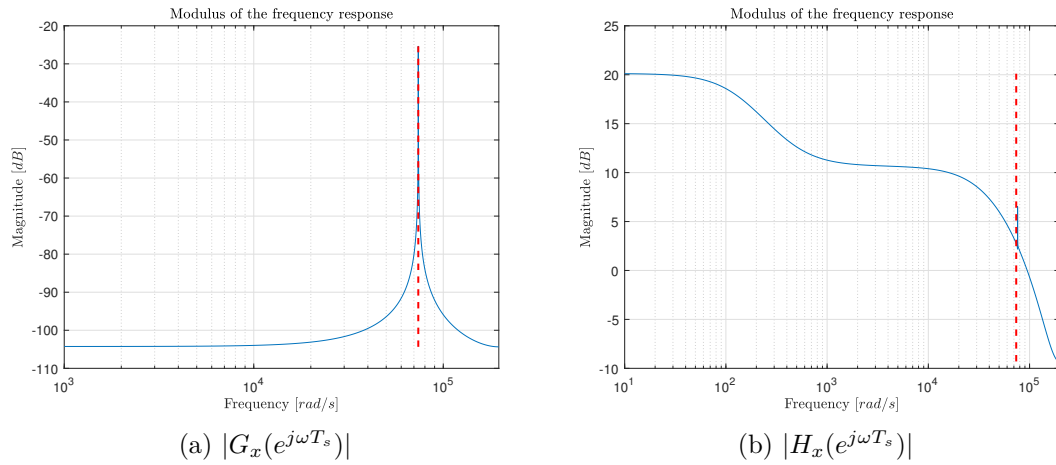(a) $|G_x(e^{j\omega T_s})|$ (b) $|H_x(e^{j\omega T_s})|$

Figure 5.1: Modulus of the frequency responses of G_x (blue line in plot (a)) and of H_x (blue line in plot (b)). The vertical line in red dashed is placed in both plots at $\omega = \omega_{r,x}^{nom}$
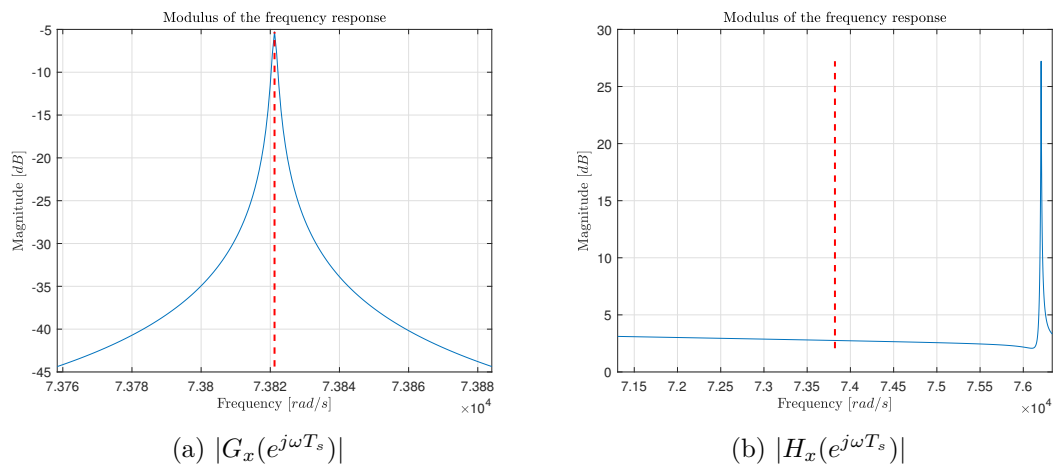

(a) $|G_x(e^{j\omega T_s})|$ (b) $|H_x(e^{j\omega T_s})|$

Figure 5.2: Zoom of Figure 5.1 around $\omega = \omega_{r,x}^{nom}$.

$$\begin{cases} x(t) = G_x(z)u_x(t) + v_x(t) \\ u_x(t) = K_x(z)\epsilon_x(t) \\ \epsilon_x(t) = x_{ref}(t) - x(t) \end{cases} \tag{5.5}$$

where the reference signal $x_{ref}(t)$ is chosen as

$$x_{ref}(t) = A_x \sin\left(\omega_{ref}tT_s\right) \tag{5.6}$$

with A_x the desired amplitude of the oscillation ($A_x = 0.1$ in our case) and ω_{ref} the desired frequency of the oscillation which will have to be chosen equal to the resonance frequency of G_x. The controller K_x will be designed in such a way that the tracking of x_{ref} is as accurate as possible while limiting the control action u_x. Another objective of K_x will be to reject the noise v_x as much possible. However, this objective will only be achievable for the component of v_x around the resonance frequency since the module of the frequency response of the plant G_x is significant only around this resonance frequency (see Figure 5.1a).
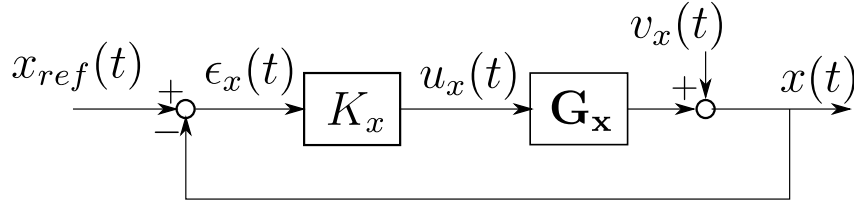
Figure 5.3: Schematic of the control strategy of the drive mass system.

As shown in [58], these objectives can be formulated in the H_∞ control framework and the controller obtained via this method for the model (5.2)-(5.3)-(5.4) of the drive mass system at the nominal temperature is given by:

$$K_x(z) = \frac{1.65 - 1.249z^{-1} - 1.659z^{-2} + 2.519z^{-3} - 1.659z^{-4} - 1.251z^{-5} + 1.649z^{-6}}{1 - 1.973z^{-1} + 3.452z^{-2} - 2.979z^{-3} + 2.186z^{-4} - 0.7527z^{-5} + 0.1971z^{-6}} \tag{5.7}$$

Let us analyze the nominal performance of this controller K_x i.e., its performance when G_x is given by (5.2)-(5.3)-(5.4) and when $x_{ref}(t) = A_x \sin(\omega_{r,x}^{nom}tT_s)$. For this purpose, let us consider the two following closed-loop transfer functions:

$$S(z) = \frac{1}{1 + G_x(z)K_x(z)} \quad , \quad F(z) = \frac{K_x(z)}{1 + G_x(z)K_x(z)} \tag{5.8}$$

These transfer functions (whose frequency responses are represented in Figures 5.4 and 5.5) relate the external signals x_{ref} and v_x to the tracking error $\epsilon_x = x_{ref} - x$ and the actuation signal u_x:

$$\epsilon_x(t) = S(z)x_{ref}(t) - S(z)v_x(t) \quad \text{and} \quad u_x(t) = F(z)x_{ref}(t) - F(z)v_x(t) \tag{5.9}$$

73

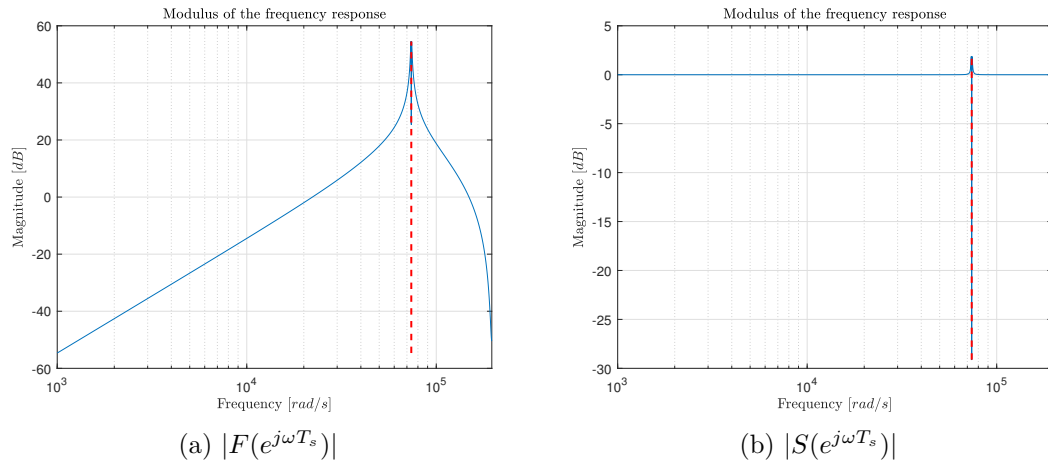(a) $|F(e^{j\omega T_s})|$

(b) $|S(e^{j\omega T_s})|$

Figure 5.4: Modulus of the frequency responses of $F(z)$ (blue line in plot (a)) and of $S(z)$ (blue line in plot (b)). The vertical line in red dashed is placed in both plots at $\omega = \omega_{r,x}^{nom}$

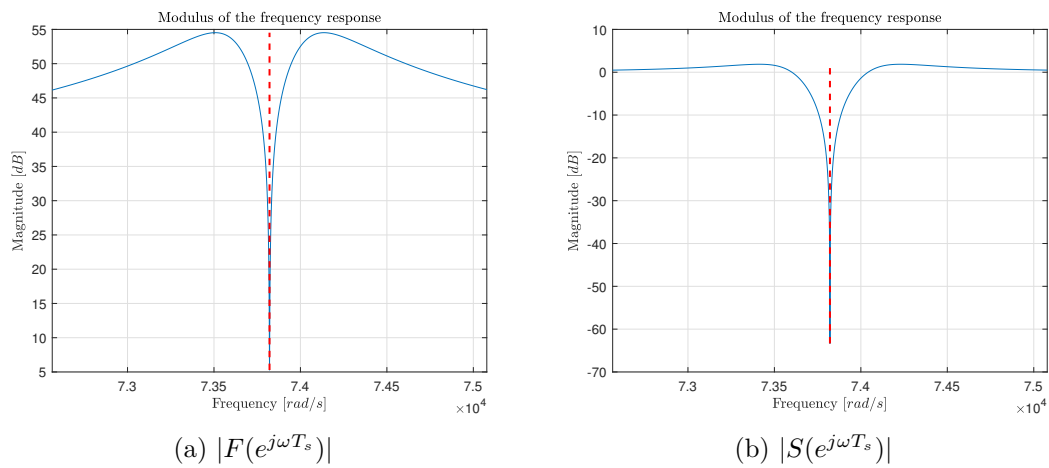

(a) $|F(e^{j\omega T_s})|$

(b) $|S(e^{j\omega T_s})|$

Figure 5.5: Zoom of Figure 5.4 around $\omega = \omega_{r,x}^{nom}$.

We observe that the modulus of the frequency response of the sensitivity function S is very low ($-63dB$) at $\omega = \omega_{r,x}^{nom}$. This will allow an accurate tracking of x_{ref} and the rejection of the component of the noise v_x around the resonance frequency. We also observe that the transfer function F has a local minimum at $\omega = \omega_{r,x}^{nom}$ ($|F(e^{j\omega_{r,x}^{nom}T_s})| = 5dB$). Consequently, the tracking of x_{ref} and the rejection of the component of the noise v_x around the resonance frequency will be achieved with low control efforts.

Let us give more details on the performance of this nominal loop using (5.9). The signal ϵ_x will be made up of a sinusoidal term of amplitude $A_x|S(e^{j\omega_{r,x}^{nom}T_s})| = A_x/1415 = 7\,10^{-5}$ and a Gaussian noise contribution of standard deviation $||H_xS||_2\sigma_e = 0.0014$ (the 2-norm $||H_xS||_2$ of H_xS is indeed equal to 1.69). This Gaussian noise contribution will therefore be the dominant part of ϵ_x.

As far as u_x is concerned, we observe that $||H_xF||_2 = 65.7$. Consequently, u_x is made up of a sinusoidal part of amplitude $A_x|F(e^{j\omega_{r,x}^{nom}T_s})| = 1.78A_x = 0.178$ and a Gaussian noise contribution of standard deviation $||H_xF||_2\sigma_e = 0.055$. These observations are confirmed by the following simulation.

The loop in 5.3 is simulated with the nominal system (5.2)-(5.3)-(5.4), with K_x as in (5.7) and with $x_{ref}(t) = 0.1\sin(\omega_{r,x}^{nom}tT_s)$. In Figure 5.6, we give the obtained ϵ_x and u_x for a simulation of 507 seconds[2].
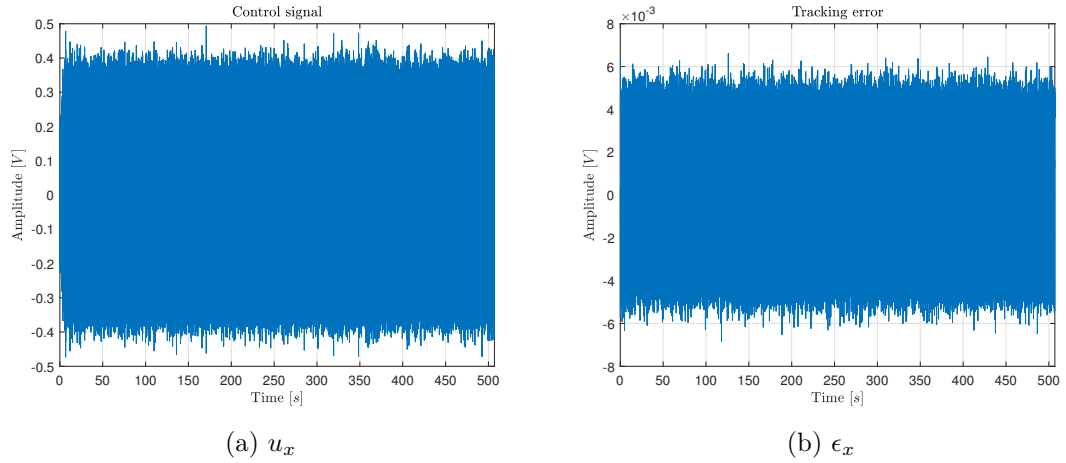

(a) u_x (b) ϵ_x

Figure 5.6: Results of the simulation described in Section 5.2.2.

---

[2]In this simulation, during the first seven seconds, the amplitude A_x of x_{ref} is progressively increased from zero to 0.1. This is done in order to limit the transient behaviour [58].

5.2.3   Temperature dependence of the resonator and performance of the control configuration for $T \neq T_{nom}$

As already mentioned, the value of the natural frequency $\omega_{n,x}$ of the continuous-time transfer function $\tilde{G}$ representing the drive mass system (see (5.1)) is dependent on the ambient temperature T (while k and ξ are assumed to be independent of T). Consequently, the resonance frequency $\omega_{r,x}$ of (5.1) will also be dependent on T (recall indeed that $\omega_{r,x} = \omega_{n,x}\sqrt{1 - 2\xi^2}$). We will suppose that, in the temperature range $\Xi = [T_{min} = -10\ ^oC \quad T_{max} = 70\ ^oC]$, the resonance frequency $\omega_{r,x}(T)$ will vary as given in Figure 5.7. As shown in this figure, $\omega_{r,x}$ varies linearly within $\Omega = [\omega_{min} \quad \omega_{max}]$ with $\omega_{min} = \omega_{r,x}^{nom} - 20\pi$ and $\omega_{max} = \omega_{r,x}^{nom} + 20\pi$.
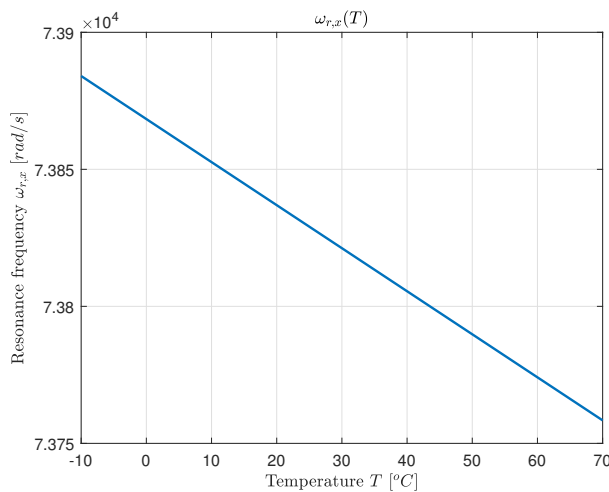

Figure 5.7: Relation between the resonance frequency $\omega_{r,x}$ and the temperature T.

From the reasoning above, when the temperature is different from the nominal temperature (i.e. $T_{nom} = 30\ ^oC$), the transfer function of the resonator will be different than the one represented in Figure 5.1. More specifically, the continuous-time transfer function of the drive mass system, when the temperature is constant and equal to T, is given by:

$$\tilde{\mathbf{G}}(s, \omega_{r,x}(T)) = \frac{k}{\frac{1-2\xi^2}{\omega_{r,x}^2(T)}s^2 + \frac{2\xi\sqrt{1-2\xi^2}}{\omega_{r,x}(T)}s + 1} \tag{5.10}$$

The discrete-time version of (5.10) is given by:

$$\mathbf{G_x}(z, \omega_{r,x}) = \frac{b_{0,0}(\omega_{r,x})z^{-1} + b_{0,1}(\omega_{r,x})z^{-2}}{1 + f_{0,1}(\omega_{r,x})z^{-1} + f_{0,2}(\omega_{r,x})z^{-2}} \tag{5.11}$$

where we observe that the coefficients of the discrete-time transfer function depend on the value of the resonance frequency at the current temperature T (we have omitted the dependence on T in (5.11) to simplify the notations). The modulus $|\mathbf{G_x}(e^{j\omega T_s}, \omega_{r,x})|$ of

the frequency response of $\mathbf{G_x}(z, \omega_{r,x})$ is represented in Figure 5.8 for different values of $\omega_{r,x}$ in the interval Ω. As opposed to G_x, the noise transfer function H_x is assumed independent of the temperature.
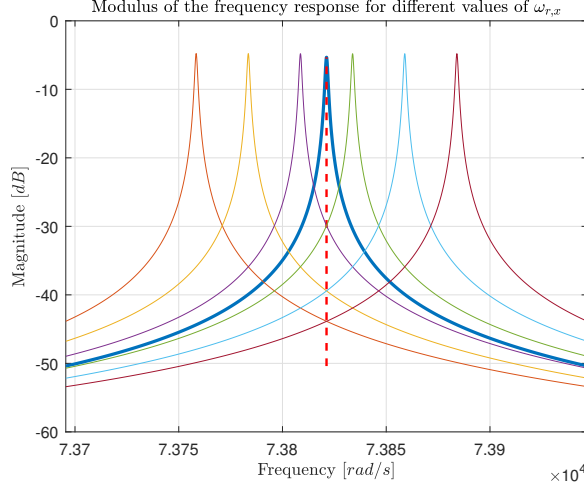

Figure 5.8: $|\mathbf{G_x}(e^{j\omega T_s}, \omega_{r,x})|$ for different values of $\omega_{r,x} \in \Omega$. The tick blue line represents this modulus for $\omega_{r,x} = \omega_{r,x}^{nom}$. The vertical line in red dashed is placed at $\omega = \omega_{r,x}^{nom}$.

Let us now see how we can achieve the control objectives described in Section 5.2.2 when the ambient temperature is different from the nominal temperature T_{nom}. This will be done using the closed-loop configuration presented in Figure 5.3 with the controller K_x given in (5.7), but with a sinusoidal reference x_{ref} whose frequency ω_{ref} is equal[3] to $\omega_{r,x}(T)$. To analyze the performance of this particular configuration for different values of the tempertaure T (and thus different values of $\omega_{r,x}(T)$), we can define:

$$S_{\omega_{r,x}}(z) = \frac{1}{1 + \mathbf{G_x}(z, \omega_{r,x})K_x(z)} \quad , \quad F_{\omega_{r,x}}(z) = \frac{K_x(z)}{1 + \mathbf{G_x}(z, \omega_{r,x})K_x(z)} \qquad (5.12)$$

The modulus of the frequency responses of these two transfer functions are represented in Figure 5.9 for different values of $\omega_{r,x} \in \Omega$.

Since the reference will be sinusoidal at a frequency equal to $\omega_{r,x}$, let us analyse the modulus of the frequency response of $S_{\omega_{r,x}}$ and $F_{\omega_{r,x}}$ at $\omega_{r,x}$. We observe that $|F_{\omega_{r,x}}(e^{j\omega_{r,x}T_s})| = 5$ dB for all $\omega_{r,x} \in \Omega$. The modulus of the frequency response $|S_{\omega_{r,x}}(e^{j\omega_{r,x}T_s})|$ of S at $\omega_{r,x}$ is equal to -50 dB for $\omega_{r,x} \neq \omega_{r,x}^{nom}$ which is a bit larger than the original -63 dB. Moreover, $||H_x F_{\omega_{r,x}}||_2$ and $||H_x S_{\omega_{r,x}}||_2$ remain (approximatively) equal to 65.7 and 1.69, respectively, as we can see in Figure 5.10. Consequently,

---

[3]Note that this is of course an ideal situation. In practice, $\omega_{r,x}(T)$ is unknown and ω_{ref} will be chosen as an estimate of this resonance (see Sections 5.3 and 5.4).

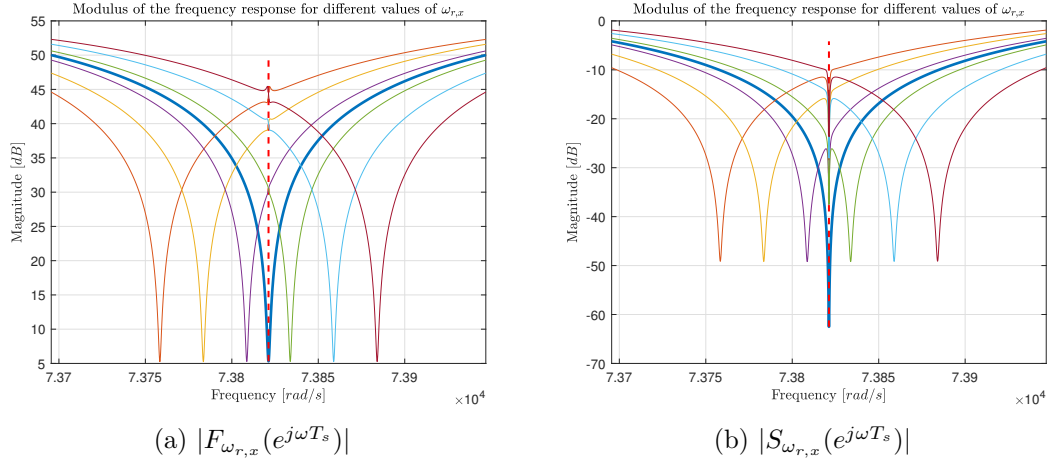(a) $|F_{\omega_{r,x}}(e^{j\omega T_s})|$ (b) $|S_{\omega_{r,x}}(e^{j\omega T_s})|$

Figure 5.9: Modulus of the frequency responses of the two transfer functions in (5.12) for different values of $\omega_{r,x} \in \Omega$. The tick blue line in both plots represents the modulus for $\omega_{r,x} = \omega_{r,x}^{nom}$. The vertical line in red dashed is placed in both plots at $\omega = \omega_{r,x}^{nom}$.

the chosen configuration seems acceptable for all the temperatures within Ξ, at least as long as the temperature is assumed constant and equal to a value within Ξ. Let us now verify whether this configuration also yields acceptable results when the temperature varies during the operation of the controller K_x.
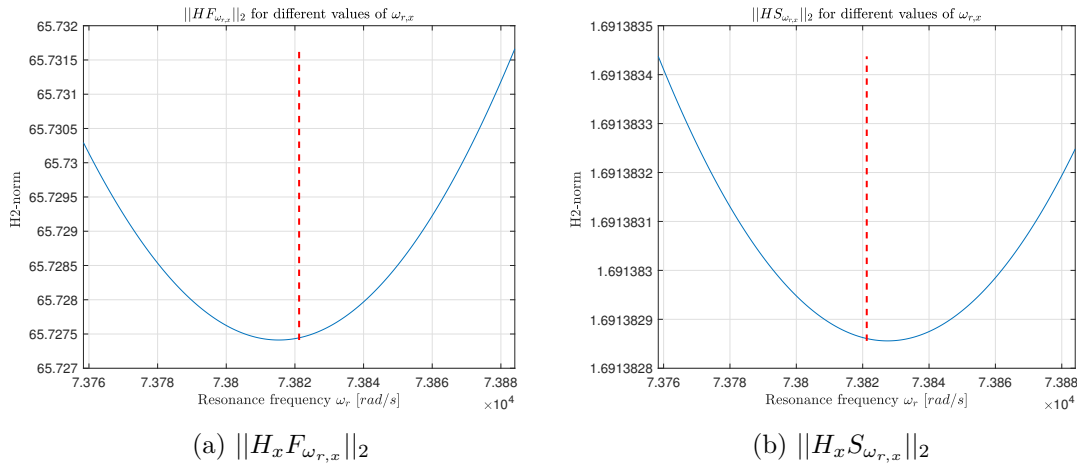

(a) $||H_x F_{\omega_{r,x}}||_2$ (b) $||H_x S_{\omega_{r,x}}||_2$

Figure 5.10: $||H_x F_{\omega_{r,x}}||_2$ and $||H_x S_{\omega_{r,x}}||_2$ as a function of $\omega_{r,x}$ for $\omega_{r,x} \in \Omega$ (blue lines). The vertical line in red dashed is placed in both plots at $\omega_{r,x} = \omega_{r,x}^{nom}$.

5.2.4 Performance of the control configuration when the temperature varies

Let us thus suppose that the temperature $T(t)$ varies with the time within Ξ. We will assume that the resonance frequency corresponding to this temperature variation will be given by $\omega_{r,x}(T(t))$. As already mentioned, we also assume that the frequency content of the noise v_x is temperature-independent. Based on these assumptions, when, due to the variation $T(t)$, the resonance frequency varies as $\omega_{r,x}(t) = \omega_{r,x}(T(t))$, the input-output system (5.3) becomes the following Linear Parameter Varying operator :

$$
\begin{cases}
\mathbf{G_x}(\omega_{r,x}(t)) \ : \ \breve{x}(t) = b_{0,0}(\omega_{r,x}(t))u_x(t-1) + b_{0,1}(\omega_{r,x}(t))u_x(t-2) + \ldots \\
\qquad\qquad \cdots - f_{0,1}(\omega_{r,x}(t))\breve{x}(t-1) - f_{0,2}(\omega_{r,x}(t))\breve{x}(t-2) \\
x(t) = \breve{x}(t) + v_x(t)
\end{cases}
\tag{5.13}
$$

Note that $\omega_{r,x}(t)$ is the so-called scheduling variable of the LPV operator (5.13) and note also that $\mathbf{G_x}(\omega_{r,x}(t)) = \mathbf{G_x}(z,\omega_{r,x})$ when $\omega_{r,x}(t) = \omega_{r,x} \ \forall t$.

Like in the previous subsection, the LPV operator (5.13) will be controlled with the controller K_x given in (5.7) and with a sinusoidal reference that follows as closely as possible the resonance frequency. For this purpose we will choose a reference of the form:

$$
x_{ref}(t) = A_x \sin\left(\sum_{\tau=1}^{t} \omega_{ref}(\tau)T_s\right)
\tag{5.14}
$$

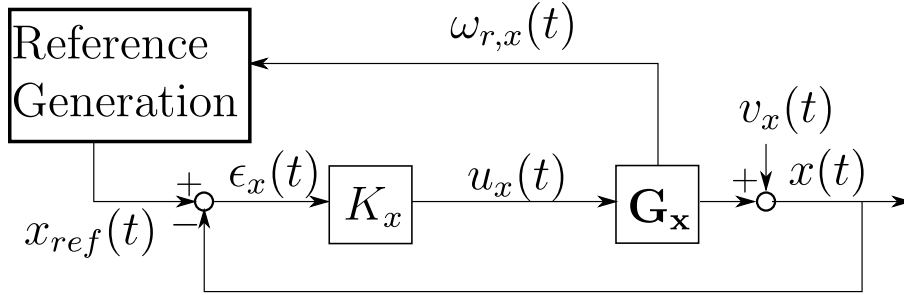with $\omega_{ref}(t) = \omega_{r,x}(t)$ (see Figure 5.11).

Figure 5.11: Control of the drive mass system for time varying resonance frequency $\omega_{r,x}(t)$. In this figure, $\mathbf{G_x}$ is the LPV operator (5.13).

We will simulate the loop represented in Figure 5.11 in the case where $\omega_{r,x}(t)$ is given by:

$$
\omega_{r,x}(t) =
\begin{cases}
\omega_{r,x}^{nom} & tT_s \le 507 \\
\omega_{r,x}^{nom} + \alpha_\omega(tT_s - 507) & 507 < tT_s \le 1007 \\
\omega_{r,x}^{nom} + 500\alpha_\omega & 1007 < tT_s \le 1507
\end{cases}
\tag{5.15}
$$

As we can see, the resonance frequency is first kept constant to its nominal value $\omega_{r,x}^{nom}$ during 507 seconds[4] and then linearly increased (or decreased) with a constant rate α_ω during 500 seconds and, finally, kept constant at the attained value during the last 500 seconds.

In the sequel we will suppose that $|\alpha_\omega| \leq 0.1257$. When $\alpha_\omega = 0.1257$ (resp. $\alpha_\omega = -0.1257$), the resonance frequency goes from $\omega_{r,x}^{nom}$ to ω_{max} (resp. ω_{min}) in 500 seconds (as shown in Figure 5.12).

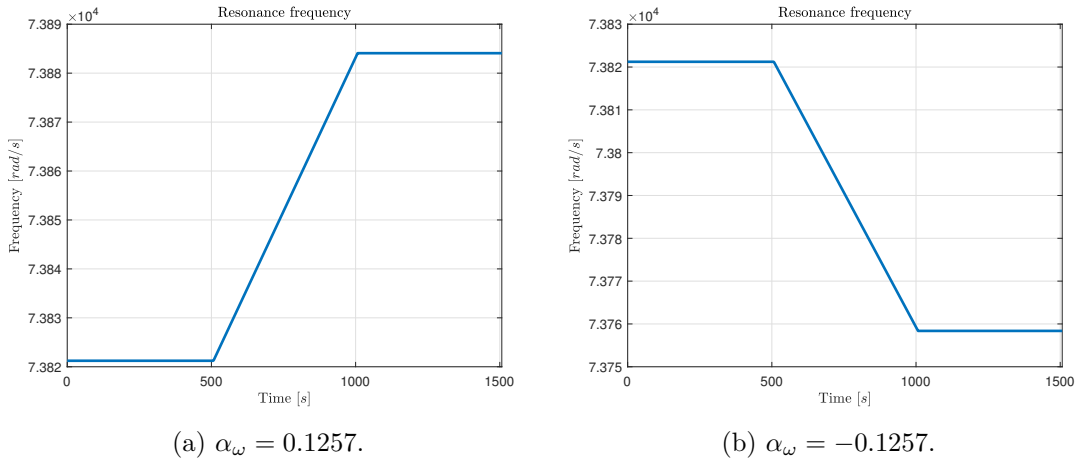(a) $\alpha_\omega = 0.1257$. (b) $\alpha_\omega = -0.1257$.

Figure 5.12: Varying resonance frequency $\omega_{r,x}(t)$ as given by (5.15) with $\alpha_\omega = 0.1257$ (plot (a)) and with $\alpha_\omega = -0.1257$ (plot (b)).

When simulating the closed-loop in Figure 5.11 with an LPV operator $\mathbf{G_x}$ (see (5.13)) with a scheduling variable $\omega_{r,x}(t)$ given by (5.15) with $\alpha_\omega = \pm 0.1257$, we obtain the signals ϵ_x and u_x given in red in Figures 5.13 and 5.14, respectively. Note that the 507 first seconds in Figures 5.13 and 5.14 are obtained in the nominal setting i.e. the setting presented in Figure 5.6 (i.e., $\omega_{r,x}(t) = \omega_{r,x}^{nom}$ and $\omega_{ref}(t) = \omega_{r,x}^{nom}$). It is therefore clear from Figures 5.13 and 5.14 that the configuration proposed in Figure 5.11 to deal with the varying resonance frequency yields acceptable results since we cannot observe any clear difference between the 507 first seconds and the rest of the simulations.

It is also important to note that choosing $\omega_{ref}(t) = \omega_{r,x}(t)$ in (5.14) is crucial to obtain these results. Indeed, if we would choose $\omega_{ref}(t) = \omega_{r,x}^{nom} \ \forall t$ in (5.14) (i.e. $x_{ref}(t) = A_x \sin(\omega_{r,x}^{nom} t T_s)$), the signal ϵ_x and u_x would be given by the blue curve in Figures 5.13 and 5.14. It is clear that the control performance is strongly altered from $tT_s = 507 \ s$, i.e. the moment where $\omega_{r,x}(t) \neq \omega_{r,x}^{nom}$.

For further reference, let us analyse further the red curves in Figures 5.13 and 5.14. For this purpose, let us compute the energy of $\epsilon_x(t)$ and $u_x(t)$ in three time intervals

---

[4]Note that, here also, the amplitude A_x of x_{ref} is increased from 0 to 0.1 in 7 seconds
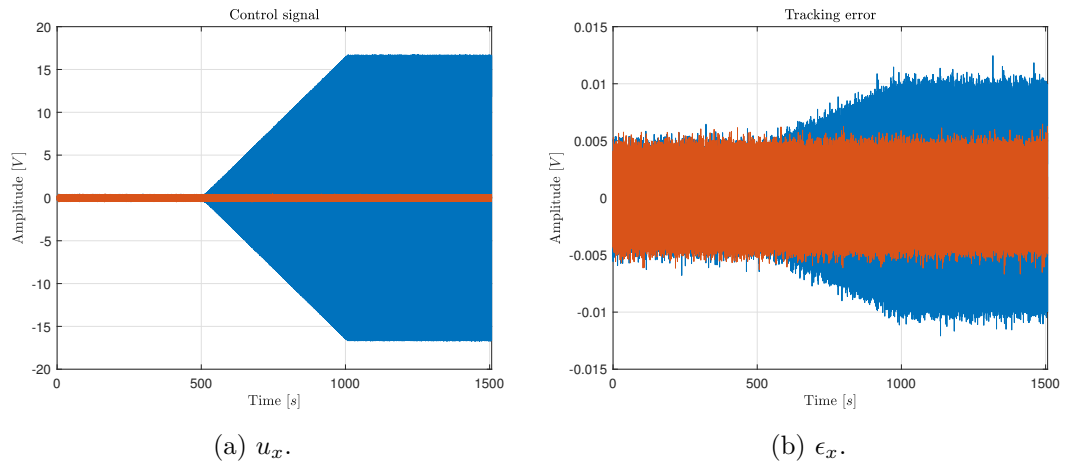
(a) u_x.

(b) ϵ_x.

Figure 5.13: Results of the simulations described in Section 5.2.4 with $\alpha_\omega = 0.1257$. The red curve corresponds to the case where x_{ref} is given by (5.14) with $\omega_{ref}(t) = \omega_{r,x}(t)$ and the blue curve corresponds to the case where x_{ref} is given by (5.14) with $\omega_{ref}(t) = \omega_{r,x}^{nom}$.
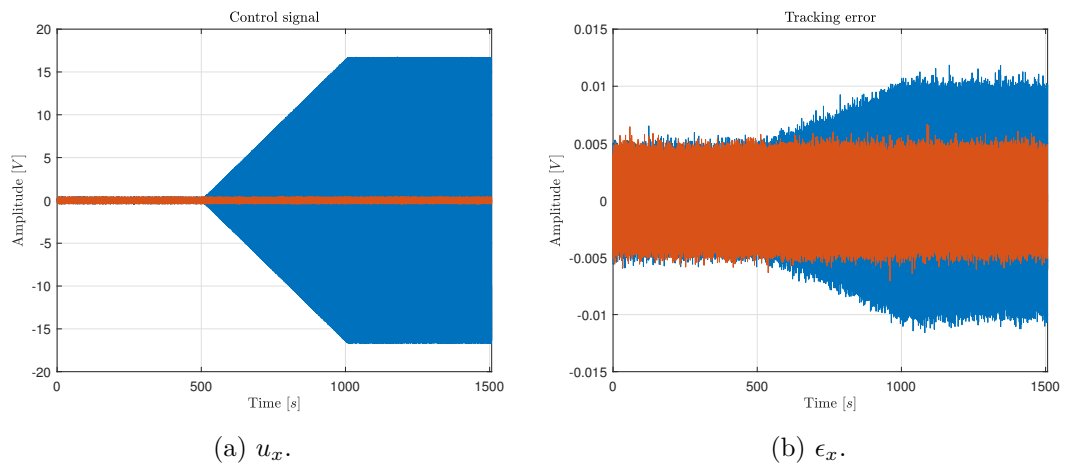

(a) u_x.

(b) ϵ_x.

Figure 5.14: Results of the simulations described in Section 5.2.4 with $\alpha_\omega = -0.1257$. The red curve corresponds to the case where x_{ref} is given by (5.14) with $\omega_{ref}(t) = \omega_{r,x}(t)$ and the blue curve corresponds to the case where x_{ref} is given by (5.14) with $\omega_{ref}(t) = \omega_{r,x}^{nom}$.

i.e. $\Delta t_1 = \{t \mid 7 < tT_s \le 507\}$ (nominal case), $\Delta t_2 = \{t \mid 507 < tT_s \le 1007\}$ (varying resonance frequencies) and $\Delta t_3 = \{t \mid 1007 < tT_s \le 1507\}$ ($\omega_{r,x} = \omega_{max}$ or $= \omega_{min}$). The energy of a signal $\psi(t)$ in an interval Δt is defined as:

$$\mathcal{E}(\psi, \Delta t) = \sum_{t \in \Delta t} |\psi(t)|^2 \tag{5.16}$$

The results are given in Table 5.1. In this table, we observe that the energy of u_x is the same in the three intervals. The energy of ϵ_x is slightly larger in Δt_2 and Δt_3 than in the nominal case Δt_1. We will consider these (small) increases acceptable for the sequel.

Table 5.1: $\mathcal{E}(u_x, .)$ and $\mathcal{E}(\epsilon_x, .)$ for the two simulations with $\omega_{ref}(t) = \omega_{r,x}(t)$

		$\mathcal{E}(u_x, .)$			$\mathcal{E}(\epsilon_x, .)$		
		Δt_1	Δt_2	Δt_3	Δt_1	Δt_2	Δt_3
α_ω	0.1257	$6.4\ 10^5$	$6.4\ 10^5$	$6.4\ 10^5$	48.7	50.5	50.6
	-0.1257	$6.4\ 10^5$	$6.4\ 10^5$	$6.4\ 10^5$	48.7	50.6	50.6

Let us now sum up the results up to now. The proposed control configuration (see Figure 5.11) consisting of the nominal controller K_x and a reference signal (5.14) with $\omega_{ref}(t) = \omega_{r,x}(t)$ yields satisfactory results both for constant resonance frequency $\omega_{r,x}$ and for a varying resonance frequency (Figure 5.12 is indeed assumed to represent the highest rate of variation of $\omega_{r,x}$ that can be encountered in practice).

As already mentioned in footnote 3, in practice, we will not be able to choose $\omega_{ref}(t)$ equal to $\omega_{r,x}(t)$ since this variation is unknown. However, in the sequel, we will show that we can obtain very similar results if $\omega_{ref}(t)$ is chosen equal to an estimate of $\omega_{r,x}(t)$. The control configuration will be then given by Figure 5.15.
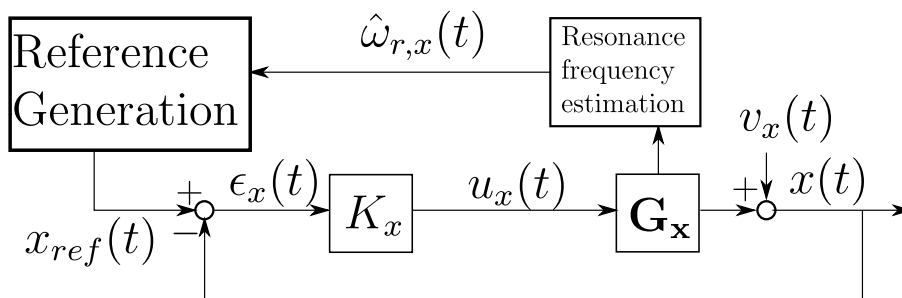

Figure 5.15: Control of the drive mass system with the estimated resonance frequency $\hat{\omega}_{r,x}$.

5.3 Recursive Identification

Recursive identification is an identification technique that allows to derive models of time-varying systems such as the one given in (5.13) via the determination at each time instant of an estimate of its time-varying parameter vector. We will here use this technique to obtain a time-varying model $\hat{G}(t)$ of the true LPV system (5.13) and, from this time-varying model $\hat{G}(t)$, we will be able to derive an estimate $\hat{\omega}_{r,x}(t)$ of the resonance frequency $\omega_{r,x}(t)$ which is the scheduling variable of the LPV system (5.13). At each time instant t, this estimate $\hat{\omega}_{r,x}(t)$ will be given by the resonance frequency of the transfer function that can be obtained if we freeze the coefficients of the time-varying operator $\hat{G}(t)$ at their value at time t.

This estimate $\hat{\omega}_{r,x}(t)$ can then be used in the control configuration of Figure 5.15 to generate x_{ref}. However, to obtain an accurate estimate of $\omega_{r,x}(t)$ and as in all identification methods, we will need to excite the system with an external signal $r(t)$. This external signal will be added at the output of the controller K_x :

$$u_x(t) = K_x(z)\left(x_{ref}(t) - x(t)\right) + r(t) \qquad (5.17)$$

where $r(t)$ is chosen equal to a RBS (Random Binary Sequence) signal of amplitude 0.01 (which is small with respect to the amplitude of the signal u_x observed in Figures 5.6, 5.13 and 5.14). Figure 5.15 is thus modified in Figure 5.16.
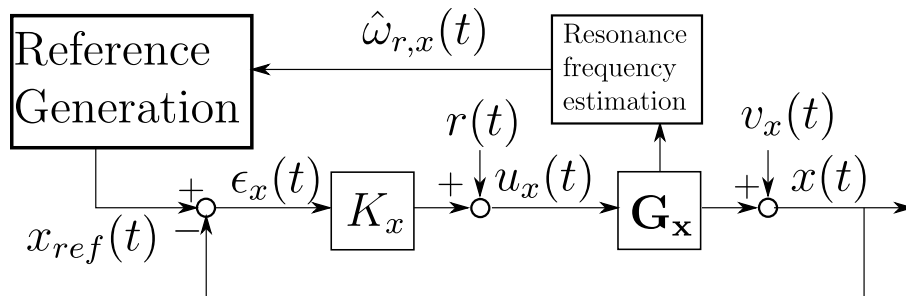

Figure 5.16: Control of the drive mass system with the estimated resonance frequency $\hat{\omega}_{r,x}$ and with the excitation signal added for identification purpose.

The system (5.13) is a Box-Jenkins system. Recursive identification for Box-Jenkins systems can be cumbersome in practice [1, pp. 371]. Consequently, we will instead identify an ARX model for the system (5.13). In other words, we will suppose that (5.13) can be sufficiently accurately described by the following input-output relation:

$$x(t) = \varphi(t)^T \theta_0(t) + e(t), \quad \varphi(t) = \begin{pmatrix} -x(t-1) \\ \vdots \\ -x(t-n_a) \\ u_x(t-n_k) \\ \vdots \\ u_x(t-n_k-n_b) \end{pmatrix} \tag{5.18}$$

where $e(t)$ is a white noise signal and $\theta_0(t)$ is a time-varying parameter that we will estimate at each time t. It is well known that, in the LTI case, any Box-Jenkins system can be accurately represented by a high-order ARX system. Here, using a trial-and-error aproach, we have observed that, if we choose $n_a = 9$, $n_b = 4$ and $n_k = 1$, (5.18) allows to sufficiently represent (5.13).

We thus wish to determine, using recursive identification, an estimate of $\theta_0(t)$ based on data $u_x(t)$ and $x(t)$ collected in the loop represented in Figure 5.16. We will use for this purpose a technique called Recursive Least Squares (RLS) in the literature [1]. RLS determines the estimate $\hat{\theta}(t)$ of $\theta_0(t)$ based on the estimate $\hat{\theta}(t-1)$ at time $t-1$ as follows:

$$\hat{\theta}(t) = \hat{\theta}(t-1) + R^{-1}(t)\varphi(t)(x(t) - \varphi^T(t)\hat{\theta}(t-1)) \tag{5.19}$$

$$R(t) = \lambda R(t-1) + \varphi(t)\varphi^T(t) \tag{5.20}$$

We observe that, to obtain $\hat{\theta}(t)$ from $\hat{\theta}(t-1)$, we only require the regressor φ at time t and the output x at time t. Besides the initialization values $\hat{\theta}(t=0)$ and $R(t=0)$, the only other coefficient that the user has to choose in (5.19)-(5.20) is the so-called forgetting factor λ ($0 < \lambda < 1$). To explain the role of λ, let us recall that $\hat{\theta}(t)$ (see (5.19)-(5.20)) is equal to the solution of the following weighted least square problem with a regularisation term [1]:

$$\hat{\theta}(t) = \arg\min_{\theta} \left(\sum_{k=1}^{t} \left(\lambda^{t-k}(x(k) - \varphi^T(k)\theta)^2 \right) + \lambda^t(\theta - \hat{\theta}(t=0))^T R(t=0)(\theta - \hat{\theta}(t=0)) \right) \tag{5.21}$$

Let us first note that, since λ^t decreases exponentially with t, the effect of the initialization disappears after a while. When this has happened, since λ^{t-k} decreases exponentially when $t-k$ increases, the estimate $\hat{\theta}(t)$ will be mostly determined based on the prediction error $x(k) - \varphi^T(k)\theta$ for values of k close to t (i.e., the estimate at time t is mostly determined with the most recent data). Moreover, we have also that the smaller λ, the fewer data are taken into account to determine $\hat{\theta}(t)$. Based on this reasoning, it is clear that, to obtain a satisfactory bias-variance trade-off, λ must be chosen based on the *assumed* rate of variation of $\theta_0(t)$ i.e., the faster $\theta_0(t)$ varies, the smaller λ has to be chosen. Here, using a trial-and-error approach with variation of the resonance frequency such as in (5.15) with different α_ω between -0.1257 and 0.1257,

we have determined that $\lambda = 1 - 10^{-6}$ is a reasonable value. Moreover, to initialize the algorithm (5.19)-(5.20), we choose the matrix $R(t = 0)$ as $I_{n_a+n_b+1}\ 10^2$ (see [59, pp. 299-302] for more details on this choice). To determine a good value for $\hat{\theta}(t = 0)$, we perform an open-loop identification of the BJ system (5.2)-(5.3)-(5.4) using an ARX model structure with $n_a = 9$, $n_b = 4$ and $n_k = 1$ (see Section 5.2) and we choose the identified parameter vector as $\hat{\theta}(t = 0)$ i.e.,

$$\hat{\theta}(t = 0) = (-1.06, 0.92, -0.45, 0.22, -0.42, 0.14,\ 0.13, -4.5\ 10^{-5}, -1.5\ 10^{-4}, \ldots$$
$$\ldots, -4.5\ 10^{-5}, 4.7\ 10^{-5}, 5\ 10^{-5}, 7.4\ 10^{-6}, -5.2\ 10^{-6}\Big)$$

It is to be noted that the algorithm (5.19)-(5.20) requires a matrix inversion at each time step. However, as shown in [1], this algorithm can also be implemented as in (5.22) where no matrix inversion is involved:

$$\begin{cases} \hat{\theta}(t) = \hat{\theta}(t-1) + L(t)(x(t) - \varphi^T(t)\hat{\theta}(t-1)) \\ L(t) = \frac{P(t-1)\varphi(t)}{\lambda + \varphi^T(t)P(t-1)\varphi(t)} \\ P(t) = \frac{1}{\lambda}\left[P(t-1) - \frac{P(t-1)\varphi(t)\varphi^T(t)P(t-1)}{\lambda + \varphi^T(t)P(t-1)\varphi(t)}\right] \end{cases} \tag{5.22}$$

Note that, in (5.22), $P(t) = R^{-1}(t)$.

Let us now show how we can derive $\hat{\omega}_{r,x}(t)$ from $\hat{\theta}(t)$. If we freeze the value of $\hat{\theta}(t)$ at its value at time t and we denote the coefficients of this frozen vector as $(a_1, a_2, \ldots, a_9, b_0, \ldots, b_4)$, the transfer function corresponding to $\hat{\theta}(t)$ is given by (see (5.18)):

$$\hat{G} = \frac{z^{-1}\left(b_0 + \sum_{l=1}^{4} b_l z^{-l}\right)}{1 + \sum_{l=1}^{9} a_l z^{-l}} \tag{5.23}$$

As opposed to (5.2), this transfer function will be charaterized by 9 poles. However, one of these poles will be (relatively) close to the pole p_{nom} of (5.2). Consequently, the pole p^* of $\hat{G}$ close to p_{nom} can be determined using a Newton-Raphson scheme, see [60], initialized at p_{nom}. From that pole p^*, we can then use the following expression to determine (approximately) the resonance frequency[5] $\hat{\omega}_{r,x}$ of $\hat{G}$:

$$\hat{\omega}_{r,x}(t) = \frac{1}{T_s} \arg(p^*(t)) \tag{5.24}$$

where $\arg(p)$ denotes the argument of the complex number p.

The above procedure is repeated at each time instant yielding the estimate $\hat{\omega}_{r,x}(t)$ of $\omega_{r,x}(t)$ in (5.13). The control configuration with the RLS estimate of the resonance frequency is summarized in Figure 5.17 where x_{ref} is given by (5.14) with $\omega_{ref}(t) = \hat{\omega}_{r,x}(t)$.

---

[5]This approximation is very accurate when the damping is very small as in the case considered in this chapter.
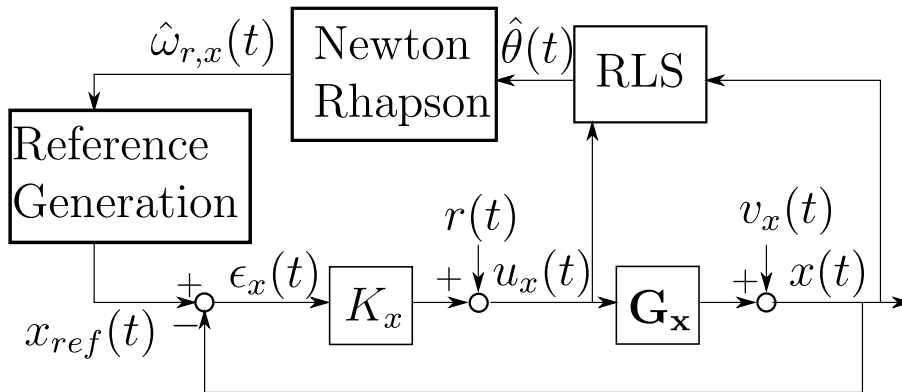
Figure 5.17: Control of the drive mass system with the estimate $\hat{\omega}_{r,x}$ of the resonance frequency $\omega_{r,x}$ obtained with the Recursive Least Squares algorithm.

As we will see in Section 5.5, the configuration given in Figure 5.17 will yield very similar results as the ideal configuration given in Figure 5.11. However, before showing these results, we will analyze another method to derive an estimate of $\omega_{r,x}(t)$. This method is called *extremum seeking*.

5.4   Extremum Seeking

The Extremum Seeking was introduced in 1922 as an adaptive control scheme [57]. In its original form, its aim was to adapt the input of a plant in order to minimize the values of its output. In this section, we will use the extremum seeking philosophy to obtain, at each instant, an estimate of the resonance frequency of the drive mass system. We will for this purpose take advantage of the fact that the amplitude of the control signal u_x is minimal when the reference signal x_{ref} is a sinusoidal signal at this resonance frequency. Before presenting its utilisation for our problem, we briefly present the extremum seeking algorithm for a *non linear* continuous time system. It is indeed the way this algorithm is generally presented in the literature.

5.4.1   General aspects

Let us consider a plant dynamics, with input w and output q, described as follows:

$$
\begin{cases}
\dot{\zeta}(\tilde{t}) = f(\zeta, w, \tilde{t}) & (5.25) \\
q_p(\tilde{t}) = h(\zeta, \tilde{t}) & (5.26) \\
q(\tilde{t}) = q_p(\tilde{t}) + v(\tilde{t}) & (5.27)
\end{cases}
$$

where $\tilde{t}$ represents the (continuous) time variable, ζ the state vector of the system and v the measurement noise. Moreover, the functions f and h are assumed to be differen-

tiable in their arguments. When we apply a constant input $w(\tilde{t}) = w_c$ at time $\tilde{t}_0$ we assume that $\exists g : \mathbf{R} \to \mathbf{R}$ a function three times differentiable, s.t.: $\lim_{\tilde{t} \to \infty} q_p(\tilde{t}) = g(w_c)$. We will call this function g the steady-state characteristic of the system (5.25)-(5.26) and we will use the shorthand notation $q_p = g(w)$ for $\lim_{\tilde{t} \to \infty} q_p(\tilde{t}) = g(w_c)$. Let us also define the characteristic time τ of the system (5.25)-(5.26) as the real scalar τ such that $|q_p(\tilde{t}) - g(w_c)| < 0.05 g(w_c) \ \forall \tilde{t} > \tau + \tilde{t}_0$.

Moreover, we will also assume that there exists a (local) minimum (w^*, q_p^*) of g: $\frac{dg}{dw}(w^*) = 0$ and $\frac{d^2 g}{dw^2}(w^*) > 0$. The Extremum Seeking strategy aims at adapting w in order to reach (w^*, q_p^*) using, as we will see in the sequel, a gradient-descent method based on an estimate of the gradient of the function g.
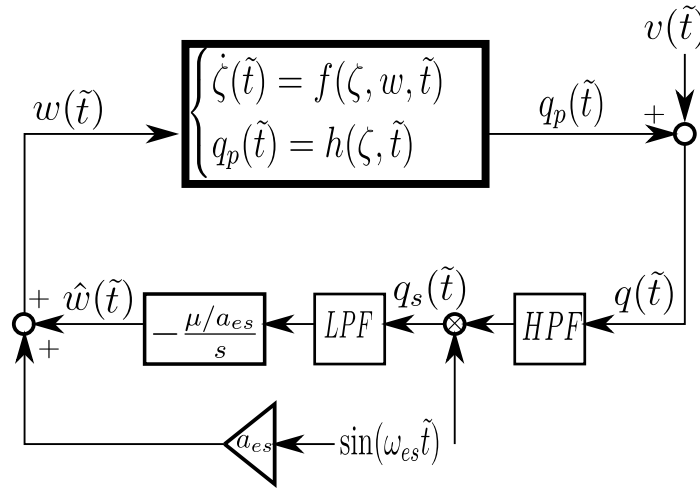

Figure 5.18: Schematic of the Extremum Seeking strategy.

Figure 5.18 depicts in more details the Extremum Seeking strategy. The perturbation signal $\sin(\omega_{es}\tilde{t})$ that we can see in this figure is used to modulate the output of the plant $q(\tilde{t})$. The filters HPF and LPF are high-pass and low-pass filters, respectively, having cut-off frequencies ω_h and ω_l. The modulated output passes through the integrator with gain $-\frac{\mu}{a_{es}}$ in order to compute the adapted input signal $\hat{w}(\tilde{t})$. The parameter μ is usually interpreted as the *learning rate* of the scheme. Indeed, as we will see in the sequel, the smaller μ, the slower the evolution of $\hat{w}(\tilde{t})$ will be. In other words, μ regulates the dynamics of $\hat{w}(\tilde{t})$. As seen in Figure 5.18, the input signal $w(\tilde{t})$ of the plant is given by:

$$w(\tilde{t}) = \hat{w}(\tilde{t}) + a_{es}\sin(\omega_{es}\tilde{t}) \tag{5.28}$$

with a_{es} a small constant. The convergence of w and q to a neighbourhood of (w^*, q_p^*) has been proved in the literature [57] under certain conditions on the noise $v(\tilde{t})$ and with an appropriate choice of the parameters involved in the Extremum Seeking strategy. More precisely: (i) $\frac{1}{\tau} \gg \omega_{es}$ i.e. the transient response of the plant must be fast w.r.t. the excitation injected by the ES strategy. (ii) $\mu \ll \omega_{es}$ i.e. the dynamic of

the adapted term $\hat{w}(\tilde{t})$ must be slow w.r.t. the excitation injected. (*iii*) $\omega_l \ll \omega_{es}$, $\omega_h \ll \omega_{es}$ i.e. the excitation injected must be well-inside the pass band of the HP filter and well outside the pass band of the LP filter.

In order to illustrate the working principle of the ES scheme, let us consider the plant operated as in Figure 5.18, but without noise. Moreover, we consider that the parameters of the ES scheme have been set as stated above. Let us recall that the input signal $w(\tilde{t})$ of the plant is given by the adapted input $\hat{w}$ plus a small perturbation $a_{es}\sin(\omega_{es}\tilde{t})$ (see (5.28)). This input signal will be a slowly varying signal w.r.t. the transient response of the plant (recall that $\mu \ll \omega_{es} \ll \frac{1}{\tau}$). Consequently, we can neglect the transient response and consider the output of the plant to be:

$$q_p(\tilde{t}) \approx g(\hat{w}(\tilde{t}) + a_{es}\sin(\omega_{es}\tilde{t})) \tag{5.29}$$

Moreover, since a_{es} is small, we can (accurately) approximate $q_p(\tilde{t})$ with a Taylor expansion truncated at the first term, centred in $\hat{w}(\tilde{t})$:

$$q_p(\tilde{t}) \approx g\left(\hat{w}(\tilde{t})\right) + a_{es}\frac{\partial g}{\partial w}\left(\hat{w}(\tilde{t})\right)\sin(\omega_{es}\tilde{t}) \tag{5.30}$$

Then the output $q_p(\tilde{t})$ passes through the HP filter, assumed here to be ideal, whoose cut-off frequency has been chosen s.t. $\omega_h \ll \omega_{es}$. Consequently, only the much slower term $g(\hat{w}(\tilde{t}))$ will be filtered out by the HP filter. Afterwards, the multiplication by $\sin(\omega_{es}\tilde{t})$ gives:

$$q_s(\tilde{t}) = \frac{a_{es}}{2}\frac{\partial g}{\partial w}\left(\hat{w}(\tilde{t})\right) - \frac{a_{es}}{2}\frac{\partial g}{\partial w}\left(\hat{w}(\tilde{t})\right)\cos(2\omega_{es}\tilde{t}) \tag{5.31}$$

We assume the LPF to be ideal and to have $\omega_l \ll \omega_{es}$. Therefore, it filters out the time-varying part of $q_s(\tilde{t})$. Finally, $\hat{w}(\tilde{t})$ is updated thanks to the integral block:

$$\dot{\hat{w}}(\tilde{t}) = -\frac{\mu}{2}\frac{\partial g}{\partial w}(\hat{w}(\tilde{t})) \tag{5.32}$$

The dynamic of $\hat{w}$ is then governed by $\frac{\partial g}{\partial w}(\hat{w})$, which is a nonlinear function in $\hat{w}$, and by the user-chosen parameter μ. We know that w^* is an equilibrium point of (5.32) due to the fact that $\frac{\partial g}{\partial w}(w^*) = 0$. In addition, we have that the derivative of the r.h.s. of (5.32) is negative at w^*, since we assumed $\frac{d^2 g}{dw^2}(w^*) > 0$. Consequently, by [61, pp. 72], w^* is a locally exponentially stable equilibrium point i.e., there exists a ball $B \subset \mathbf{R}$ around w^* such that every solution $\hat{w}(\tilde{t})$ to (5.32) which starts inside B converges exponentially to w^*. Therefore, the Extremum Seeking scheme converges to (w^*, q_p^*) if we start sufficiently close to (w^*, q_p^*). To conclude, the appropriate choice of parameters ensures that the Extremum Seeking is able to steer the input signal $w(\tilde{t})$ in order to reach a neighbourhood of the stationary point (w^*, q_p^*). Furthermore, from (5.32) we can legitimately interpret the Extremum Seeking scheme as a gradient-descent method, since it converges to a minimum of g using its gradient. In other words, the Extremum Seeking scheme is an optimization method with an embedded gradient estimation block
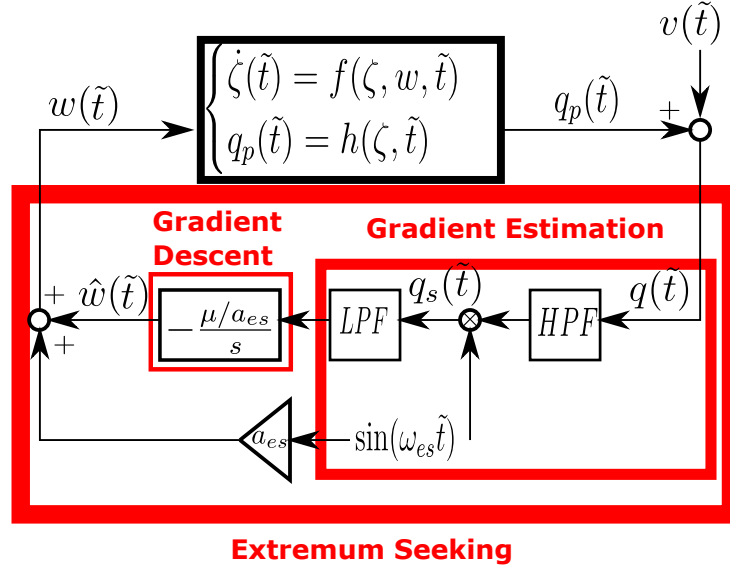
Figure 5.19: Interpretation of the Extremum Seeking strategy.

(see Figure 5.19).

Remark 5.1. The Extremum Seeking scheme can be used also for steering w to a maximum (w^*, q_p^*) of g. In this case, the gain of the integral would be $\frac{\mu}{a_{es}}$, then making w^* a locally exponentially stable equilibrium point if $\frac{d^2 g}{dw^2}(w^*) < 0$, i.e. (w^*, q_p^*) is a maximum of g.

5.4.2 Application to the estimation of the resonance frequency

Let us first consider the case where the temperature is constant i.e. the resonator is given by $\mathbf{G_x}(z, \omega_{r,x})$ with $\omega_{r,x} = \omega_{r,x}(T)$ (see Section 5.2.3). In this case, the transfer function $F_{\omega_{r,x}}(z) = \frac{K_x(z)}{1+K_x(z)\mathbf{G_x}(z,\omega_{r,x})}$, from the external reference $x_{ref}(t)$ to the input signal $u_x(t)$, is such that the modulus of its frequency response has a local minimum at $\omega = \omega_{r,x}$ (see Figures 5.4a and 5.9a). If we consider a reference signal $x_{ref}(t) = A_x \sin(\omega_{ref}tT_s)$ with a constant ω_{ref}, the input signal $u_x(t)$ will just be given by $A_u \sin(\omega_{ref}tT_s + \phi_u)$, where $A_u = A_x|F_{\omega_{r,x}}(e^{j\omega_{ref}T_s})|$ and $\phi_u = \arg(F_{\omega_{r,x}}(e^{j\omega_{ref}T_s}))$. We can thus consider $A_x|F_{\omega_{r,x}}(e^{j\omega_{ref}T_s})|$ as a steady-state characteristic between the frequency ω_{ref} of x_{ref} and the amplitude A_u of the control signal u_x. Therefore, if we are able to retrieve the amplitude A_u of u_x (using e.g. synchronous demodulation [58]), we can use the Extremum Seeking strategy in order to determine the frequency ω_{ref} of the reference x_{ref} that will yield the smallest A_u (and, in this way, determine an estimate of the resonance frequency).

The ES is implemented as in the red frame of Figure 5.19 with the excitation $a_{es} \sin(\omega_{es}tT_s)$ and the HF and LP filters. The input $q(t)$ of this red frame is here the

amplitude of the control signal $u_x(t)$ (obtained by synchronous demodulation) while the ouput $w(t)$ of the red frame will be here denoted by $\omega_{ref}(t)$. This signal $\omega_{ref}(t)$ is given by:

$$\omega_{ref}(t) = \hat{\omega}_{r,x}(t) + a_{es}\sin(\omega_{es}tT_s) \tag{5.33}$$

where $a_{es}\sin(\omega_{es}tT_s)$ is the small perturbation signal introduced by the extremum seeking algorithm and $\hat{\omega}_{r,x}(t)$ is the output of the integrator block ($\hat{\omega}_{r,x}(t)$ can be considered as an estimate of the resonance frequency). This signal $\omega_{ref}(t)$ is then used to generate the reference signal x_{ref} using (5.14). This is summarized in Figure 5.20.
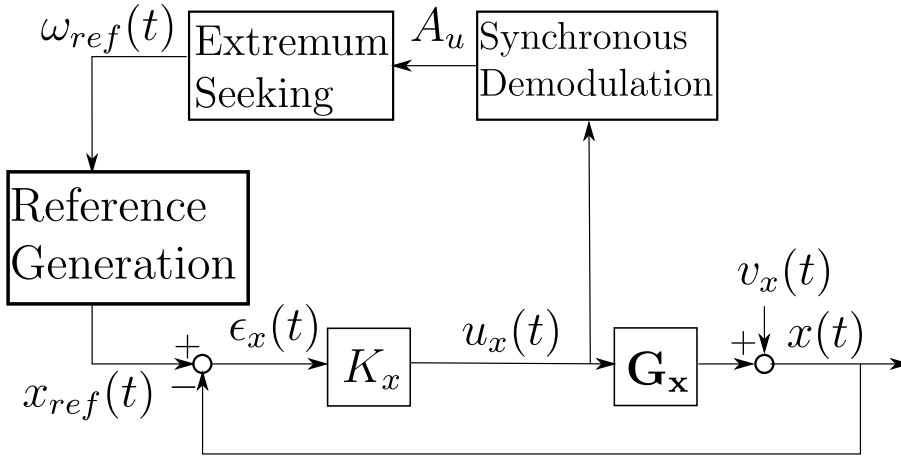

Figure 5.20: Control of the drive mass system with the estimate $\hat{\omega}_{r,x}$ of the resonance frequency $\omega_{r,x}$ obtained with the Extremum Seeking scheme.

The above reasoning pertains to the case where $\omega_{r,x}$ remains constant. However, if the rate of variation of $\omega_{r,x}(t)$ is slow with respect to the learning rate of the ES algorithm (which is governed by the parameter μ), the above scheme can also be used to obtain an estimate $\hat{\omega}_{r,x}(t)$ of a time-varying resonance frequency $\omega_{r,x}(t)$.

5.4.3 Parameter tuning

In this section, we show how we can choose the parameters μ, ω_{es}, ω_l, ω_h and a_{es} that are used in the extremum seeking algorithm of Figure 5.20. For this purpose, a first step is to determine the characteristic time τ for the system considered by the extremum seeking algorithm of Figure 5.20. In this particular case, we can determine τ by applying a step variation to the frequency ω_{ref} of the reference signal x_{ref} and we determine τ as the time needed for the amplitude of u_x to reach a steady-state value. For this purpose, we simulate the closed loop (5.5), with K_x given in (5.7) and $x_{ref}(t)$ as in (5.14) with:

$$\omega_{ref}(t) = \begin{cases} \omega_{r,x}^{nom} & tT_s < 3\ s \\ \omega_{r,x}^{nom} + \Delta_\omega & tT_s \geq 3\ s \end{cases} \tag{5.34}$$

where $\Delta_\omega = \pi \; rad/s$. In Figure 5.21, we represent the corresponding amplitude A_u of u_x (obtained via synchronous demodulation). We observe that A_u presents a small overshoot before settling to a fixed value with some noise. From Figure 5.21, we can say that the time characteristic τ is here given by $\tau = 0.2 \; s$. Using the rule $\mu \ll \omega_{es} \ll \frac{1}{\tau}$, we choose $\omega_{es} = 0.5 \; rad/s$ and $\mu = 0.05$. Using the rule $\omega_h \ll \omega_{es}$ and $\omega_l \ll \omega_{es}$, let us choose the cut-off frequencies of the HP and LP filters as $\omega_h = \omega_l = 0.05 \; rad/s$. Finally, it just remains to determine the amplitude a_{es} of the perturbation signal injected by the ES strategy. We have already said that a_{es} should be a small constant. Let us go a bit further considering (5.14) and (5.33). Since $\mu \ll \omega_{es}$, we can consider $\hat{\omega}_{r,x}(t)$ constant over a period of the perturbation signal $a_{es} \sin(\omega_{es} t T_s)$. Consequently, using (5.33), the signal $\omega_{ref}(t)$ will vary in the interval $[\hat{\omega}_{r,x} - a_{es} \; \hat{\omega}_{r,x} + a_{es}]$. Since the reference signal will be generated as in (5.14) with that $\omega_{ref}(t)$, it is important that the steady-state characteristic $A_x |F_{\omega_{r,x}}(e^{j\omega T_s})|$ considered in this application of the extremum seeking algorithm remains almost constant for all ω in this interval $[\hat{\omega}_{r,x} - a_{es} \; \hat{\omega}_{r,x} + a_{es}]$. Using Figure 5.9a, we choose $a_{es} = 0.06$.
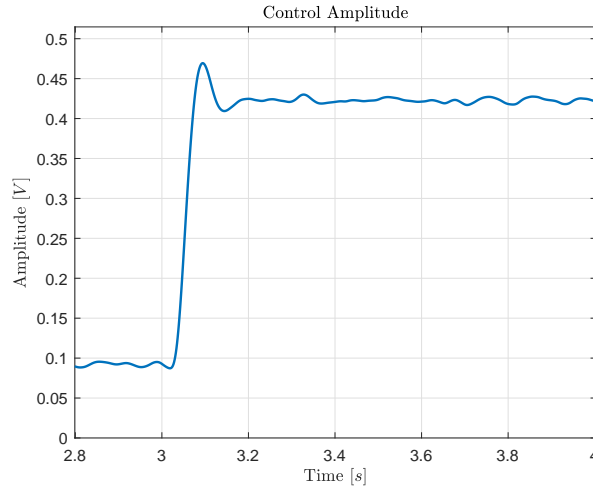

Figure 5.21: Amplitude A_u corresponding to the test described in Section 5.4.3.

5.5 Comparison of the RLS and the ES algorithms: Tracking of $\omega_{r,x}(t)$

We will now perform similar simulations as in Section 5.2.4. Indeed, we will simulate the closed-loop made up of K_x (see (5.7)) and of the LPV system (5.13) with the scheduling variable $\omega_{r,x}(t)$ given by (5.15) ($\alpha_\omega = 0.1257$). The only difference is that the signal $\omega_{ref}(t)$ defining the reference signal $x_{ref}(t)$ (see (5.14)) will no longer be equal to the exact value of $\omega_{r,x}(t)$, but either equal to the estimate $\hat{\omega}_{r,x}(t)$ of $\omega_{r,x}(t)$ obtained with the RLS algorithm of Section 5.3 or equal to the signal $\omega_{ref}(t)$ given in (5.33) and obtained via the ES algorithm of Section 5.4. Let us start with the case

where the RLS algorithm is used. The signals ϵ_x and u_x are represented in red in Figure 5.22. When comparing these signals with those obtained in Figure 5.13, we see no differences. This is also confirmed by the computed energies in Table 5.2.
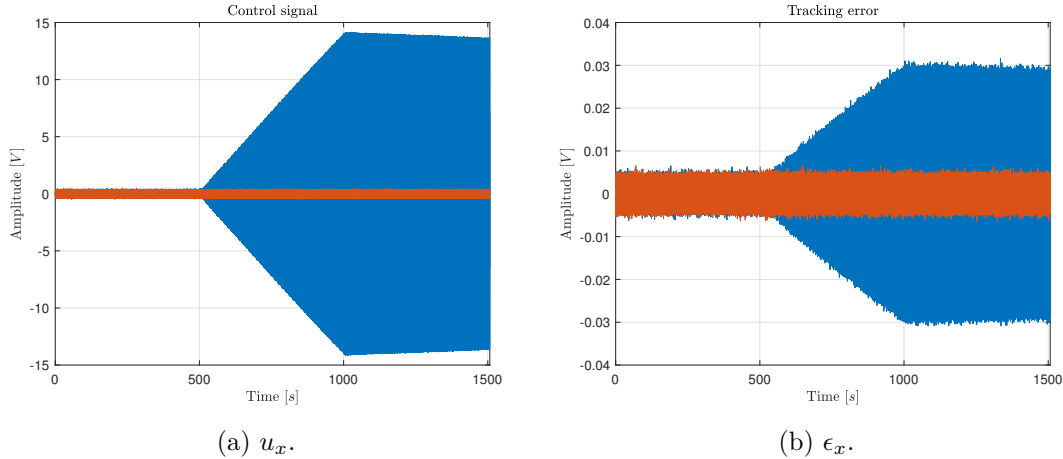

(a) u_x.

(b) ϵ_x.

Figure 5.22: Results of the simulation described in Section 5.5. The red curve corresponds to the RLS algorithm and the blue curve corresponds to the ES algorithm with the tuning given in Section 5.4.3.

Table 5.2: $\mathcal{E}(u_x, .)$ and $\mathcal{E}(\epsilon_x, .)$ obtained for the simulation described in Section 5.5 with the RLS method and with the ES algorithm (tuning of Section 5.4.3).

		$\mathcal{E}(u_x, .)$			$\mathcal{E}(\epsilon_x, .)$		
		Δt_1	Δt_2	Δt_3	Δt_1	Δt_2	Δt_3
Method	RLS	$6.46\ 10^5$	$6.48\ 10^5$	$6.46\ 10^5$	48.8	50.6	50.6
	ES	$6.45\ 10^5$	$1.05\ 10^9$	$2.93\ 10^9$	48.8	$3.7\ 10^3$	$1.05\ 10^4$

Indeed, even though an excitation signal has been added to the loop and the resonance frequency is now estimated, these energies are only slightly larger than the one obtained in the ideal case considered in Section 5.2.4 (see Table 5.1). We have obtained the above result for a varying resonance frequency with the highest rate of variation (recall that we assume $|\alpha_\omega| \le 0.1257$ in (5.15)). As expected, similar results are also observed for smaller values of $|\alpha_\omega|$. The RLS algorithm seems thus an efficient solution to tackle the problem considered in this chapter. The same cannot be said when the ES algorithm is used with the parameters given in Section 5.4.3 (see the blue curve in Figure 5.22 and Table 5.2). In fact, the ES algorithm is not able to follow the high rate of variation of $\omega_{r,x}(t)$ as shown in Figure 5.23, where we see that $\hat{\omega}_{r,x}(t)$ (see (5.33)) is a poor estimate of $\omega_{r,x}(t)$. As opposed to this, the RLS algorithm[6] yields an estimate

---

[6]As mentioned in Section 5.3, the forgetting factor λ of the RLS algorithm is here chosen equal to

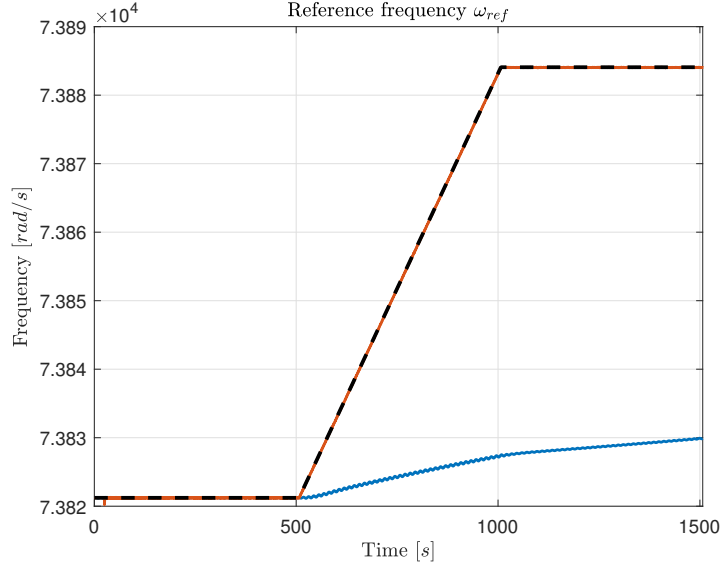$\hat{\omega}_{r,x}(t)$ that almost perfectly follows $\omega_{r,x}(t)$.

Figure 5.23: Resonance frequency estimated with the RLS algorithm (red line) and with the ES algorithm using the tuning of Section 5.4.3 (blue line) compared to the true resonance frequency (black dashed line).

When we follow the rules presented in Section 5.4.1 to tune the parameters of the ES algorithm, the ES algorithm is thus too slow to follow the variations of the resonance frequency when α_w is equal to 0.1257 (better results are obtained for smaller values of α_w).

Let us relax these rules a little and choose $\omega_{es} = 20$ and $\mu = 2$ to increase the learning rate (the other parameters keep the values given in Section 5.4.3). With these new tuning parameters, the signal u_x and ϵ_x are the ones presented in Figure 5.24 and Table 5.3 presents the computed energies. The results are now closer to the results obtained with the RLS algorithm (see also Table 5.2). The improved results with the new tuning of the ES algorithm can be explained by the fact that the signal $\hat{\omega}_{r,x}(t)$ given in (5.33) is now able to follow $\omega_{r,x}(t)$ as shown in Figure 5.25. It is nevertheless to be noted that, as shown in Table 5.2 and in Figure 5.24, the RLS algorithm still yields a smaller u_x and a smaller ϵ_x in Δt_2.

It is also to be noted that the new tuning is based on a relaxation of the tuning rules of the ES algorithm and such a relaxation must be handled with care. Indeed, since the rules of Section 5.4.1 are no longer respected, we cannot guarantee the convergence

---

$1 - 10^{-6}$. In Appendix D, we show that this value has to be chosen with care since other values of this forgetting factor yields results that can be far from satisfactory.
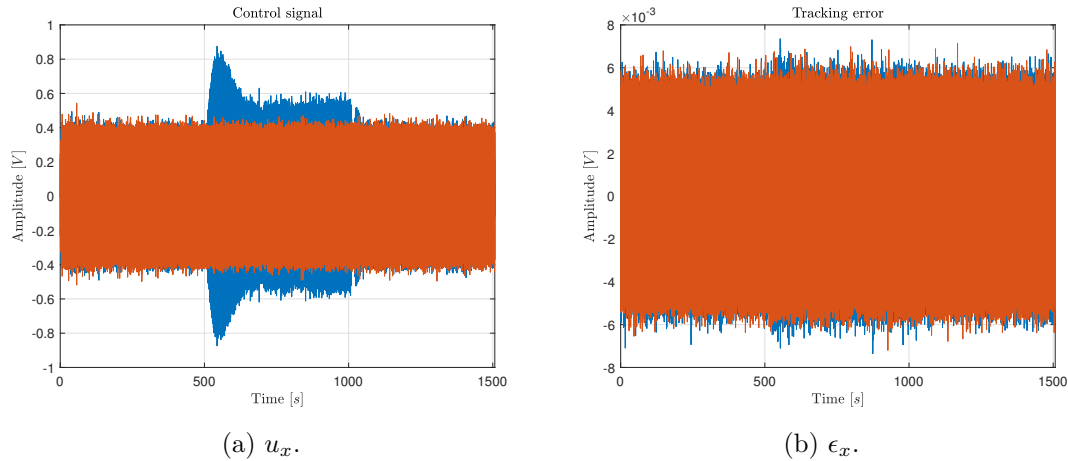
(a) u_x.

(b) ϵ_x.

Figure 5.24: Results of the simulation described in Section 5.5. The red curve corresponds to the RLS algorithm and the blue curve corresponds to the ES algorithm with the new tuning given in Section 5.5.

Table 5.3: $\mathcal{E}(u_x,.)$ and $\mathcal{E}(\epsilon_x,.)$ obtained for the simulation described in Section 5.5 with the RLS method and with the ES algorithm (new tuning of Section 5.5).

		$\mathcal{E}(u_x,.)$			$\mathcal{E}(\epsilon_x,.)$		
		Δt_1	Δt_2	Δt_3	Δt_1	Δt_2	Δt_3
Method	RLS	$6.46\ 10^5$	$6.48\ 10^5$	$6.46\ 10^5$	48.8	50.6	50.6
	ES	$6.45\ 10^5$	$2.25\ 10^6$	$6.82\ 10^5$	48.75	55.98	50.78

of the algorithm.

5.6   Summary

In this chapter, we have shown, via simulations, that an RLS approach seems a valid solution to deal with the variations of the resonance frequency of the drive mass system in the new control configuration of the Next4MEMS project. The RLS algorithm is moreover easily tunable. We have compared the RLS approach with an extremum seeking approach, an approach that had been proposed in the past to improve the classical control configuration for the drive mass system in order to deal more efficiently with the effect of the resonance frequency variations. We have found this ES algorithm more difficult to tune in the new control configuration and acceptable results could only be obtained if the classical rules for the tuning of the algorithm are not (fully) respected.
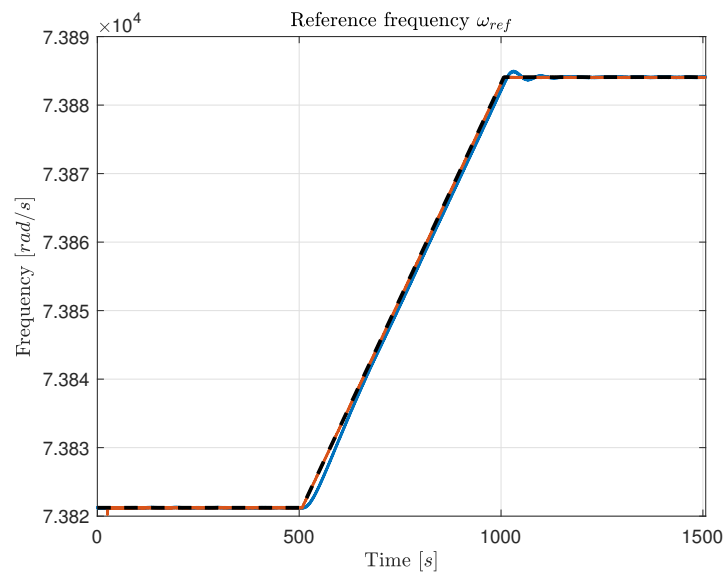
Figure 5.25: Resonance frequency estimated with the RLS algorithm (red line) and with the ES algorithm using the new tuning of Section 5.5 (blue line) compared to the true resonance frequency (black dashed line)

Conclusion

We are at the end of this manuscript. Before discussing the lines of future research, it is advisable to briefly outline the problems tackled in this work and the contributions.

6.1 Summary

In Chapter 2, we presented the general aspects of Prediction Error identification and of optimal experiment design. These concepts were instrumental for the discussions of Chapters 3 and 4, where we presented our contributions in robust experiment design and in the least costly framework for networks.

6.1.1 Robust experiment design

We restricted our attention to a SISO system G_0 operated in open loop which can be described by models without terms in common between the process and the noise model, i.e. Box-Jenkins and Output Error. For such a system, we considered to already have an initial parametric model coming from a previous identification experiment. Together with the identified parameters, we also have a confidence region for these parameters, which is unfortunately too "large" for the intended application. We consider then the problem of optimally designing the experiment that leads to an identified model with a prescribed accuracy level with the lowest experiment cost. In particular, we restricted our attention to an experiment performed by exciting the system with a multisine excitation signal. Moreover, we focused only on the accuracy of the plant model.

We tackled the *chicken-and-egg* problem of our optimal experiment design problem in the robust experiment design framework, which, on the other hand, leads to an optimization problem whose constraints are not tractable as such. Efforts have been made in the literature to make these constraints tractable, but the proposed solutions do not fully ensure the guarantees associated to the original constraints. Our contribution

in Chapter 3 was to develop tractable alternative constraints to the original ones. When used in place of the original constraints, they ensure that the obtained solution will have the desired guarantees associated to the original constraints. These alternative constraints are developed by taking inspiration from some methods from robust control theory. In order to develop these constraints, we exploited the model structure in order to rewrite the constraints in a form coherent with robust control, the LFT form. Successively, we introduced the so called set of multipliers for an uncertainty set coming from a previous identification experiment. Using these two ingredients, the multipliers and the LFT form of the constraints, we proposed the tractable alternative constraints for the original robust experiment design problem. They ensure us that the so-obtained optimal spectrum will be s.t. the experiment cost will be lower than the optimal one and that the to-be-obtained estimate will have the desired accuracy. However, these guarantees come at the cost of large computation times when the system is of high dimension. On the other hand, we showed that we can circumvent this issue by properly selecting in advance the frequencies which parametrize the to-be-designed multisine excitation signal.

6.1.2   Optimal experiment design for networks

In Chapter 4, we extended the least costly experiment design framework to the identification of one module in the interconnection of locally controlled systems. We defined the experiment cost as a measure of the perturbation induced by the experiment on the whole network, and we proposed the utilisation of the stealth configuration in order to reduce the propagation of the effects of the experiment to the other modules. In Chapter 4 we provided the conditions for obtaining a consistent estimate for the to-be-identified module. These conditions concern both the cases where the stealth configuration is used or not. In addition, we provided also the conditions that the initial model, used in the stealth configuration, should have in order to ensure that the propagation is reduced. Moreover, for the least costly experiment design problem, we gave the conditions that allow us to know whether it is more advantageous to consider the problem in the stealth setting or not.

When formulating the least costly experiment design problem, the utilisation of an initial estimate for circumventing the *chicken-and-egg* problem has an important drawback when using the stealth configuration: we neglect the propagation through the other modules. Therefore, we need to robustify the cost constraint. This has also the effect of *robustifying* the stealth configuration, since the obtained optimization problem would generally favour spectra having important contributions in the frequency range where the stealth compensation is more effective, due to a small uncertainty of the model used for the stealth configuration. The robustified cost constraint is not tractable as such, but we can use the tools of Chapter 3 to tackle this problem. However, this would entail a high computation time due to the dimension of the network. Thus, in Chapter 4 we proposed also a robustification approach which entails a certain conservatism, but allows us to solve the problem efficiently. Finally, the nu-

merical illustrations show the advantage of the stealth configuration for what concern the propagation of the perturbation through the network.

6.1.3   Resonance frequency tracking

In Chapter 5 we dealt with the problem of tracking the resonance frequency of the drive mass system of a MEMS gyroscope. This work started within the scope of the Next4MEMS project, where the MEMS gyroscope presents a resonance frequency which changes due to temperature changes. We have shown, by means of simulations, that tracking the resonance frequency in order to make the resonator oscillate at its resonance frequency allows to have good performances despite the temperature changes. Afterwards we presented two methods to track the resonance frequency: recursive identification and extremum seeking. The former is well-known in the literature and easy to implement and tune. The latter is also known in the literature and has already been used in the project, but for a different control strategy and its tuning is not trivial. For both methods, we proposed an effective implementation adapted to the control strategy used in the Next4MEMS project. Finally, we compared the two methods by means of simulations where we observed that the recursive identification outperforms the extremum seeking. We have also observed that certain tunings of the extremum seeking present a good tracking capability, at the cost of losing any guaranty of stability and/or convergence, since they do not respect the classical criteria reported in Section 5.4.1. Consequently, the recursive identification seems to be a better solution for tracking the resonance frequency, due to its easiness of tuning and its tracking capability.

6.2   Suggestions for future works

6.2.1   Robust experiment design

The results we presented in Chapter 3 allow us to obtain a solution to the robust experiment design problem, which actually ensures the original constraint. However, for the robustification of the accuracy constraint we can develop a tractable alternative only for the part of the covariance matrix P_θ given by the spectrum of the excitation signal Φ_u. In model structures such as ARX and ARMAX, where the plant and noise model have terms in common, the noise also contributes to the identification of the plant model. As already mentioned in Section 3.7, we can neglect the contribution of the noise in the robust experiment design problem. However, this would lead to a cost typically higher than necessary, since the contribution of the noise typically helps in reducing the experiment cost for these model structures. Therefore, a first important line of research is to extend the results of Chapter 3 also to the noise contribution in P_θ. This result will then allow also the extension to experiments performed in closed loop, where the noise always plays a role in the identification of the plant model.

In the future, we will investigate whether the least costly optimal experiment design problem can also be robustified when the to-be-determined excitation spectrum is the

one of a filtered white noise. This spectrum parametrization is indeed also a commonly used parametrization in optimal experiment design (see Section 2.4.1). We will also investigate how the presented results can be extended to tackle the robustification of more complex accuracy constraints (such as the ones presented in [3]).

6.2.2   Optimal experiment design for networks

As already mentioned in Chapter 4, the utilisation of the tools we developed in Chapter 3 for obtaining a tractable formulation of the cost constraint would lead to excessively high computation times in a network context. For this reason we used a different approach for the robustification of the cost, whose higher conservatism was counterbalanced by its far lower computation time. Unfortunately, we do not have similar results for the robustification of the accuracy constraint. This implies that the user should rely on a gridding approach, which does not completely ensure that the accuracy requirement will be met in practice. Alternatively, the user can rely on our results presented in Chapter 3, then eventually requiring long computation time in a network context. It is then interesting to tackle the accuracy constraint in a way similar to what we have done in Section 4.5 for the cost, in order to develop an alternative constraint which ensures the robust accuracy constraint at the cost of an higher conservatism, but with a lower numerical complexity.

Another important line of research would be the extension of the robustification approach of Chapter 4 also to another widely used type of excitation signal: filtered white noise. To this aim, the robustification of the OED problem should be done using tools similar to the ones used in Chapter 4, in order to efficiently solve the problem despite the, possibly, high dimension of the network, while admitting a certain conservatism.

Finally, in this thesis we restricted our attention to a network made up of the interconnection of locally controlled systems. Obviously, this is not the only type of network existing. Just to give an idea of how various can be the network configurations, only for a formation control task there exists many types of network configuration, see [62] for a survey. Therefore, another line of research would be the extension of the results of Chapter 4 also to other types of network.

6.2.3   Resonance frequency tracking

The study presented in Chapter 5 has been done by means of simulations. The first extension is obviously to test these two algorithms on the MEMS gyroscope of the Next4MEMS project. This implies performing tests in an chamber which allows us to impose a certain profile of temperature, and therefore of the resonance frequency. First tests for the Extremum Seeking have already been performed at room temperature and showed a response slightly faster than what we observed in Section 5.5, but many

tunings which were stable in simulations turned out to be unstable when implemented on the actual gyroscope.

The MEMS resonator in Chapter 5 is an LPV system, whose scheduling parameter is the resonance frequency. This frequency varies with the temperature following a known relation. In the Next4MEMS project the control strategy of the resonator have just been changed to use an LPV controller, having as scheduling parameter the resonance frequency. Therefore, the discussion we made in Chapter 5 should be extended to the case where the estimate of the resonance frequency is used not only for generating the reference signal, but also as scheduling variable for the controller. In this line, we can use the results presented in [53] to asses whether the estimated resonance frequency yields satisfactory performances when used in the LPV controller.

Besides these extensions, another one would be to include in the comparison also other techniques such as Kalman Filtering and Adaptive Notch Filtering.

Bibliography

[1] L. Ljung, *System Identification-Theory for the User 2nd edition, Prentice-Hall.* Upper Saddle River, USA, 1999.

[2] M. Zarrop, *Design for Dynamic System Identification.* Lecture Notes in Control and Inform. Sci. 21, Springer Verlag, Berlin, New-York, 1979.

[3] X. Bombois, G. Scorletti, M. Gevers, P. M. Van den Hof, and R. Hildebrand, "Least costly identification experiment for control," *Automatica*, vol. 42, no. 10, pp. 1651–1662, 2006.

[4] H. Hjalmarsson, "System identification of complex and structured systems," *European Journal of Control*, vol. 15, no. 3-4, pp. 275–310, 2009.

[5] C. Larsson, C. Rojas, X. Bombois, and H. Hjalmarsson, "Experimental evaluation of model predictive control with excitation (mpc-x) on an industrial depropanizer," *Journal of Process Control*, vol. 31, pp. 1–16, 2015.

[6] K. Lindqvist and H. Hjalmarsson, "Optimal input design using Linear Matrix Inequalities," in *Proc. IFAC Symposium on System Identification, Santa-Barbara*, 2000.

[7] K. Lindqvist, "On experiment design in identification of smooth linear systems," Licentiate Thesis, Royal Institute of Technology, Stockholm, Sweden, 2001.

[8] H. Jansson and H. Hjalmarsson, "Input design via LMIs admitting frequency-wise model specifications in confidence regions," *IEEE Transactions on Automatic Control*, vol. 50, no. 10, pp. 1534–1549, Oct. 2005.

[9] S. Boyd, L. El Ghaoui, E. Feron, and V. Balakrishnan, *Linear Matrix Inequalities in Systems and Control Theory*, ser. Studies in Appl. Math. Philadelphia: SIAM, Jun. 1994, vol. 15.

[10] M. Barenthin, X. Bombois, H. Hjalmarsson, and G. Scorletti, "Identification for control of multivariable systems: Controller validation and experiment design via LMIs," *Automatica*, vol. 44, no. 12, pp. 3070–3078, 2008.

[11] M. Potters, X. Bombois, M. Mansoori, and P. M. Van den Hof, "Estimating parameters with pre-specified accuracies in distributed parameter systems using optimal experiment design," *International Journal of Control*, vol. 89, no. 8, pp. 1533–1553, 2016.

[12] M. Potters, M. Mansoori, X. Bombois, J. Jansen, and P. M. Van den Hof, "Optimal input experiment design and parameter estimation in core-scale pressure oscillation experiments," *Journal of Hydrology*, vol. 534, pp. 534–552, 2016.

[13] H. Hjalmarsson and J. Martensson, "Optimal input design for identification of non-linear systems: Learning from the linear case," in *American Control Conference*, 2007, pp. 1572–1576.

[14] M. Forgione, X. Bombois, P. M. Van den Hof, and H. Hjalmarsson, "Experiment design for parameter estimation in nonlinear systems based on multilevel excitation," in *European Control Conference (ECC)*, 2014, pp. 25–30.

[15] A. D. Cock, M. Gevers, and J. Schoukens, "D-optimal input design for nonlinear fir-type systems: A dispersion-based approach," *Automatica*, vol. 73, pp. 88–100, 2016.

[16] A. D. Cock, "D-optimal input design for the identification of structured nonlinear systems," PhD thesis, VUB, Brussels, Belgium, 2017.

[17] X. Bombois, A. Korniienko, H. Hjalmarsson, and G. Scorletti, "Optimal identification experiment design for the interconnection of locally controlled systems," *Automatica*, vol. 89, pp. 169–179, 2018.

[18] L. Gerencsér and H. Hjalmarsson, "Adaptive input design in system identification," in *Proceedings of the 44th IEEE Conference on Decision and Control*, IEEE, 2005, pp. 4988–4993.

[19] L. Gerencsér, H. Hjalmarsson, and L. Huang, "Adaptive input design for lti systems," *IEEE Transactions on Automatic Control*, vol. 62, no. 5, pp. 2390–2405, 2016.

[20] C. Rojas, J. Welsh, G. Goodwin, and A. Feuer, "Robust optimal experiment design for system identification," *Automatica*, vol. 43, pp. 993–1008, 2007.

[21] C. Rojas, J. Agüero, J. Welsh, G. Goodwin, and A. Feuer, "Robustness in experiment design," *IEEE Transactions on Automatic Control*, vol. 57, no. 4, pp. 860–874, 2012.

[22] L. Pronzato and E. Walter, "Robust experiment design via maximin optimization," *Mathematical Biosciences*, vol. 89, no. 2, pp. 161–176, 1988.

[23] S. Abrashov, R. Malti, M. Moze, X. Moreau, F. Aioun, and F. Guillemard, "Simple and Robust Experiment Design for System Identification Using Fractional Models," *IEEE Transactions on Automatic Control*, vol. 62, no. 6, pp. 2648–2658, June, 2017.

[24] J. Mårtensson and H. Hjalmarsson, "Robust input design using sum of squares constraints," *IFAC Proceedings Volumes*, vol. 39, no. 1, pp. 1352–1357, 2006.

[25] J. S. Welsh and C. R. Rojas, "A scenario based approach to robust experiment design," *IFAC Proceedings Volumes*, vol. 42, no. 10, pp. 186–191, 2009.

[26] A. Kumar and S. Narasimhan, "Robust plant friendly optimal input design," *IFAC Proceedings Volumes*, vol. 46, no. 32, pp. 553–558, 2013.

[27] M. Forgione, X. Bombois, and P. M. Van den Hof, "Data-driven model improvement for model-based control," *Automatica*, vol. 52, pp. 118–124, 2015.

[28] A. Kumar, "Optimal input signal design for plant friendly identification of process systems," PhD thesis, Department of Chemical Engineering, Indian Institute of Technology, Madras, 2016.

[29] M. G. Safonov, *Stability and Robustness of Multivariable Feedback Systems*. Cambridge: MIT Press, 1980.

[30] K. Goh and M. Safonov, "Robust analysis, sectors and quadratic functionals," IEEE, Ed., New Orleans, Louisiana, 1995.

[31] A. Megretski and A. Rantzer, "System analysis via integral quadratic constraints," pp. 819–830, Jun. 1997.

[32] A. Haber and M. Verhaegen, "Moving horizon estimation for large-scale interconnected systems," *IEEE Transactions on Automatic Control*, vol. 58, no. 11, pp. 2834–2847, 2013.

[33] H. Weerts, A. Dankers, and P. M. Van den Hof, "Identifiability in dynamic network identification," in *Proc. IFAC Symposium on System Identification*, Beijing, China, 2015, pp. 1409–1414.

[34] P. Hägg and B. Wahlberg, "On identification of parallel cascade serial systems," in *Proc. IFAC World Congress*, Cape Town, South Africa, 2014, pp. 9978–9983.

[35] B. Gunes, A. Dankers, and P. M. Van den Hof, "A variance reduction technique for identification in dynamic networks," in *Proc. IFAC World Congress*, Cape Town, South Africa, 2014, pp. 2842–2847.

[36] N. Everitt, G. Bottegal, C. Rojas, and H. Hjalmarsson, "On the variance analysis of identified linear MIMO models," in *Proc. 54th IEEE Conference on Decision and Control*, Osaka, Japan, 2015, pp. 1447–1452.

[37] A. Dankers, P. M. Van den Hof, X. Bombois, and P. Heuberger, "Identification of dynamic models in complex networks with prediction error methods - predictor input selection," *IEEE Transactions on Automatic Control*, vol. 61, no. 4, pp. 937–952, 2016.

[38] M. Gevers and A. Bazanella, "Identification in dynamic networks: Identifiability and experiment design issues," in *Proc. 54th IEEE Conference on Decision and Control*, Osaka, Japan, 2015, pp. 4005–4010.

[39] J. Hendrickx, M. Gevers, and A. Bazanella, "Identifiability of dynamical networks with partial node measurements," to appear in IEEE Transactions on Automatic Control, June 2019, [Online]. Available: `https://arxiv.org/pdf/1803.05885`.

[40] J. Fax and R. Murray, "Information flow and cooperative control of vehicle formations," *IEEE Transactions on Automatic Control*, vol. 49, no. 9, pp. 1465–1476, 2004.

[41] A. Korniienko, G. Scorletti, E. Colinet, and E. Blanco, "Performance control for interconnection of identical systems: Application to pll network design," *International Journal of Robust and Nonlinear Control*, 2014.

[42] B. Wahlberg, H. Hjalmarsson, and J. Mårtensson, "Variance results for identification of cascade systems," *Automatica*, vol. 45, no. 6, pp. 1443–1448, 2009.

[43] N. Everitt, H. Hjalmarsson, and C. Rojas, "A geometric approach to variance analysis of cascaded systems," in *Proceedings 52st IEEE Conference on Decision and Control*, Florence, Italy, 2013.

[44] N. Everitt, C. R. Rojas, and H. Hjalmarsson, "Variance results for parallel cascade serial systems," in *The 19th IFAC World Congress*, Cape Town, South Africa, 2014.

[45] M. Potters, X. Bombois, M. Forgione, P. Modén, M. Lundh, H. Hjalmarsson, and P. Van den Hof, "Optimal experiment design in closed loop with unknown, nonlinear and implicit controllers using stealth identification," in *Proceedings of the European Control Conference (ECC)*, IEEE, Strasbourg, France, 2014, pp. 726–731.

[46] M. Saukoski, "System and circuit design for a capacitive mems gyroscope," PhD thesis, Helsinki University of Technology, Faculty of Electronics, Communications and Automation, 2008.

[47] T. Dehaeze, "Modélisation et contrôle robuste d'un micro-gyroscope basé sur la plateforme électronique développée à asygn," Master's thesis, Laboratoire Ampère, Ecole Centrale Lyon, Ecully, 2017.

[48] M. Gevers, A. S. Bazanella, and L. Miskovic, "Informative data: How to get just sufficiently rich?" In *Proc. 47th IEEE Conference on Decision and Control*, Cancun, Mexico, 2008, pp. 1962–1967.

[49] M. G. Potters, "Experiment design for identification of structured linear systems," PhD thesis, Delft University of Technology, 2016.

[50] X. Bombois, B. Anderson, and G. Scorletti, "Open-loop vs. closed-loop identification of box-jenkins systems in a least costly context," in *Proc. European Control Conference*, Kos, 2007.

[51] X. Bombois, M. Gevers, G. Scorletti, and B. Anderson, "Robustness analysis tools for an uncertainty set obtained by prediction error identification," *Automatica*, vol. 37, no. 10, pp. 1629–1636, 2001.

[52] K. Zhou and J. Doyle, *Essentials of Robust Control*. Prentice Hall, Upper Saddle River, New Jersey, 1998.

[53] D. Ghosh, X. Bombois, J. Huillery, G. Scorletti, and G. Mercere, "Optimal identification experiment design for LPV systems using the local approach," *Automatica*, vol. 87, pp. 258–266, 2018.

[54] M. G. Safonov, "Propagation of conic model uncertainty in hierarchical systems," *IEEE Transactions on Circuits and Systems*, pp. 388–396, Jun. 1983.

[55] I. Landau, D. Rey, A. Karimi, A. Voda, and A. Franco, "A flexible transmission system as a benchmark for robust digital control," *European Journal of Control*, vol. 1, no. 2, pp. 77–96, 1995.

[56] P. Seiler, A. Pant, and K. Hedrick, "Disturbance propagation in vehicle strings," *IEEE Transactions on automatic control*, vol. 49, no. 10, pp. 1835–1842, 2004.

[57] Y. Tan, W. H. Moase, C. Manzie, D. Nešić, and I. Mareels, "Extremum seeking from 1922 to 2010," in *Proceedings of the 29th Chinese Control Conference*, IEEE, 2010, pp. 14–26.

[58] Fabricio Saggin, Xavier Bombois, Gerard Scorletti, Anton Korniienko, "Robust control for mems inertial sensors," Technical report, Laboratoire Ampère, 2018.

[59] L. Ljung and T. Söderström, *Theory and practice of recursive identification*. MIT press, 1983.

[60] M. Bramanti, C. D. Pagani, and S. Salsa, *Analisi matematica 1*. Zanichelli, 2008.

[61] J. P. Hespanha, *Linear systems theory*. Princeton university press, 2009.

[62] K.-K. Oh, M.-C. Park, and H.-S. Ahn, "A survey of multi-agent formation control," *Automatica*, vol. 53, pp. 424–440, 2015.

Appendix for Chapter 2

We present in this appendix the (black-box) model structures that are typically used in prediction-error identification. The general parametrization[1] for the models $G(z,\theta)$ and $H(z,\theta)$ is:

$$G(z,\theta) = \frac{z^{-n_k}B(z,\theta)}{F(z,\theta)A(z,\theta)} \qquad \text{and} \qquad H(z,\theta) = \frac{C(z,\theta)}{D(z,\theta)A(z,\theta)} \tag{A.1}$$

where $A(z,\theta)$, $B(z,\theta)$, $C(z,\theta)$, $D(z,\theta)$ and $F(z,\theta)$ are polynomials given by:

$$A(z,\theta) = 1 + a_1 z^{-1} + \cdots + a_{n_a} z^{-n_a}$$
$$B(z,\theta) = b_0 + b_1 z^{-1} + \cdots + b_{n_b} z^{-n_b}$$
$$C(z,\theta) = 1 + c_1 z^{-1} + \cdots + c_{n_c} z^{-n_c}$$
$$D(z,\theta) = 1 + d_1 z^{-1} + \cdots + d_{n_d} z^{-n_d}$$
$$F(z,\theta) = 1 + f_1 z^{-1} + \cdots + f_{n_f} z^{-n_f}$$
$$\theta^T = \left(a_1, \ldots, a_{n_a}, b_0, \ldots, b_{n_b}, c_1, \ldots, c_{n_c}, d_1, \ldots, d_{n_d}, f_1, \ldots, f_{n_f} \right)$$

The parameter vector[2] θ has dimension k with $k = n_a + n_b + 1 + n_c + n_d + n_f$.

The parametrization given in (A.1) is too general in practice and the model structures that are used in practice are special cases of this general parametrization. We can distinguish two main families: the first family is characterized by transfer function $G(z,\theta)$ and $H(z,\theta)$ that are independently parametrized (BJ and OE model structures). In this first family n_a is chosen equal to zero ($A(z,\theta) = 1$). The second family supposes that $G(z,\theta)$ and $H(z,\theta)$ shares the same denominator. In this second family, n_f and n_d are chosen equal to zero ($F(z,\theta) = D(z,\theta) = 1$). Let us describe these two families in more details.

---

[1]also used in the Matlab System Identification Toolbox.
[2]The coefficients of the polynomials can also be concatenated in θ in a different way (see Chapter 3).

The first family contains the Box-Jenkins (BJ) and the Output-Error (OE) model structures. In the BJ model structure, the transfer functions $G(z, \theta)$ and $H(z, \theta)$ are described as follows:

$$G(z, \theta) = \frac{z^{-n_k} B(z, \theta)}{F(z, \theta)} \qquad \text{and} \qquad H(z, \theta) = \frac{C(z, \theta)}{D(z, \theta)}$$

The OE model structure is a BJ model structure where $C(z, \theta) = D(z, \theta) = 1$:

$$G(z, \theta) = \frac{z^{-n_k} B(z, \theta)}{F(z, \theta)} \qquad \text{and} \qquad H(z, \theta) = 1$$

The second family contains the ARMAX and ARX model structures. In the ARMAX model structure, the transfer functions $G(z, \theta)$ and $H(z, \theta)$ are described as follows:

$$G(z, \theta) = \frac{z^{-n_k} B(z, \theta)}{A(z, \theta)} \qquad \text{and} \qquad H(z, \theta) = \frac{C(z, \theta)}{A(z, \theta)}$$

The ARX model structure is an ARMAX model structure where $C(z, \theta) = 1$:

$$G(z, \theta) = \frac{z^{-n_k} B(z, \theta)}{A(z, \theta)} \qquad \text{and} \qquad H(z, \theta) = \frac{1}{A(z, \theta)}$$

Appendices for Chapter 3

B.1 Example for Observation 3.1

Consider the BJ model structure (3.1) with $n_k = n_f = n_c = n_d = 1$ and $n_b = 0$ i.e.

$$G(z, \theta) = \frac{b_0 \ z^{-1}}{1 + f_1 z^{-1}}$$

$$H(z, \theta) = \frac{1 + c_1 z^{-1}}{1 + d_1 z^{-1}}$$

where $\theta = (\rho^T, \zeta^T)^T \in \mathbf{R}^k$ with $\rho = (b_0, f_1)^T$ and $\zeta = (c_1, d_1)^T$ ($k_G = 2$, $k_H = 2$, $k = k_G + k_H = 4$). This parametrization satisfies Observation 3.1 with $Z_N(z) = (z^{-1} \ 0 \ 0 \ 0)$, $Z_D(z) = (0 \ z^{-1} \ 0 \ 0)$, $Z_{N,H}(z) = (0 \ 0 \ z^{-1} \ 0)$ and $Z_{D,H}(z) = (0 \ 0 \ 0 \ z^{-1})$.

B.2 Proof of Proposition 3.1

This proposition is similar to Proposition 2 in [10]. The only difference is that the set U_{init} is here not centered at 0 as it was the case in [10], but at $\hat{\theta}_{init}$. The expression of the matrices A_n are thus slightly different[1].

In order to prove this proposition, we have to show that (3.24) holds when A_n is parametrized as in the proposition. Let us first observe that, since θ is a real vector, we have the following identities for all $\tilde{A}$ and $\tilde{B}$ which are parametrized as in the proposition:

$$\begin{aligned} (I_n \otimes \theta)^T \ j \ \tilde{A} \ (I_n \otimes \theta) &= 0 \\ (I_n \otimes \theta)^T \ \tilde{B} \ (I_n \otimes \theta) &= 0 \end{aligned} \tag{B.1}$$

Moreover, for all $A_{n,12}$ parametrized as in the proposition we have:

---

[1]The original set of multipliers (the one given in [10]) can also be considered if, as shown in [10], LFT's in θ (such as (3.23)) are transformed into LFT's in $\theta - \hat{\theta}_{init}$.

$$A_{n,12} (I_n \otimes \theta) + (I_n \otimes \theta)^T A_{n,12}^* = \left(A_0 \otimes (P_{\theta,init}^{-1} \hat{\theta}_{init})^T\right)(I_n \otimes \theta) + \dots$$
$$\dots + (I_n \otimes \theta)^T \left(A_0^* \otimes (P_{\theta,init}^{-1}\hat{\theta}_{init})\right)$$
$$= A_0(\hat{\theta}_{init}^T P_{\theta,init}^{-1}\theta + \theta^T P_{\theta,init}^{-1}\hat{\theta}_{init}) \qquad \text{(B.2)}$$

where the last equality comes from the fact that $A_0 = A_0^*$. Using (B.1) and (B.2), we have then that:

$$\begin{pmatrix} I_n \\ I_n \otimes \theta \end{pmatrix}^T A_n \begin{pmatrix} I_n \\ I_n \otimes \theta \end{pmatrix} = \left(\chi - \hat{\theta}_{init}^T P_{\theta,init}^{-1}\hat{\theta}_{init} + \dots \right.$$
$$\left. \dots + \hat{\theta}_{init}^T P_{\theta,init}^{-1}\theta + \theta^T P_{\theta,init}^{-1}\hat{\theta}_{init} - \theta^T P_{\theta,init}^{-1}\theta\right) A_0$$
$$\text{(B.3)}$$

Finally, recollecting the terms on the right-hand-side we get:

$$\begin{pmatrix} I_n \\ I_n \otimes \theta \end{pmatrix}^T A_n \begin{pmatrix} I_n \\ I_n \otimes \theta \end{pmatrix} = \left(\chi - (\theta - \hat{\theta}_{init})^T P_{\theta,init}^{-1}(\theta - \hat{\theta}_{init})\right) A_0 \qquad \text{(B.4)}$$

Recalling the expression (3.6) of U_{init} and the fact that A_0 can take any values as long as it is positive definite, we see that the above expression is indeed positive semi-definite for all $\theta \in U_{init}$.
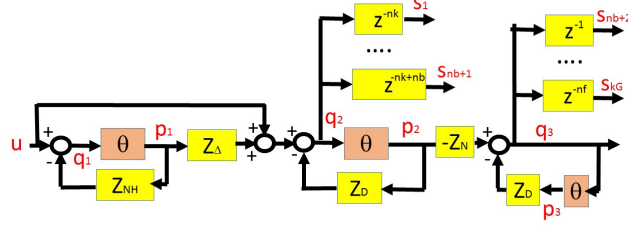
B.3 LFT representation of $F_{u,\rho}(z,\theta)$

Using Observation 3.1 and the expression of the BJ model structure and of $F_{u,\rho}(z,\theta)$, we have that $s(t) = F_{u,\rho}(z,\theta)u(t)$ is given by:

$$s(t) = \begin{pmatrix} s_1(t) \\ \vdots \\ s_{n_b+1} \\ s_{n_b+2} \\ \vdots \\ s_{k_G}(t) \end{pmatrix} = \begin{pmatrix} \frac{z^{-n_k}}{1+Z_D(z)\theta} \\ \vdots \\ \frac{z^{-(n_k+n_b)}}{1+Z_D(z)\theta} \\ \frac{-z^{-1}Z_N(z)\theta}{(1+Z_D(z)\theta)^2} \\ \vdots \\ \frac{-z^{-n_f}Z_N(z)\theta}{(1+Z_D(z)\theta)^2} \end{pmatrix} \frac{1+Z_{D,H}(z)\theta}{1+Z_{N,H}(z)\theta} u(t) \qquad \text{(B.5)}$$

which is a rational function in θ. This rational function can be expressed as in (3.29) with $f = 3$ (see Figure B.1):

$$\underbrace{\begin{pmatrix} p_1 \\ p_2 \\ p_3 \end{pmatrix}}_{=p_F} = (I_3 \otimes \theta) \underbrace{\begin{pmatrix} q_1 \\ q_2 \\ q_3 \end{pmatrix}}_{=q_F}$$

Figure B.1: Representation of the vector $F_u(z, \theta)$ given in (B.5)

$$
\begin{pmatrix} q_1 \\ q_2 \\ q_3 \\ s_1 \\ \vdots \\ s_{n_b+1} \\ s_{n_b+2} \\ \vdots \\ s_{k_G} \end{pmatrix} = \underbrace{\begin{pmatrix} -Z_{N,H} & 0 & 0 & 1 \\ Z_\Delta & -Z_D & 0 & 1 \\ 0 & -Z_N & -Z_D & 0 \\ z^{-n_k}Z_\Delta & -z^{-n_k}Z_D & 0 & z^{-n_k} \\ \vdots & \vdots & \vdots & \vdots \\ z^{-n_k-n_b}Z_\Delta & -z^{-n_k-n_b}Z_D & 0 & z^{-n_k-n_b} \\ 0 & -z^{-1}Z_N & -z^{-1}Z_D & 0 \\ \vdots & \vdots & \vdots & \vdots \\ 0 & -z^{-n_f}Z_N & -z^{-n_f}Z_D & 0 \end{pmatrix}}_{M_F(z)} \begin{pmatrix} p_1 \\ p_2 \\ p_3 \\ u \end{pmatrix}
$$

with $Z_\Delta(z) = Z_{D,H}(z) - Z_{N,H}(z)$. When $H(z, \theta) = 1$, the above LFT can be simplified. The first row and the first column of M_F can indeed be removed and we have thus $f = 2$.

B.4 Useful lemma for the proof of Proposition 3.3

Lemma B.1. *Consider an Hermitian matrix $A = A^*$ of dimension $n \times n$ and a (complex) matrix B of dimension $n \times \tilde{n}$. Then, we have that*

$$A \geq 0 \Longrightarrow B^*AB \geq 0$$

Proof. $B^*AB \geq 0$ is equivalent to the fact that, for all complex vector x of dimension $\tilde{n}$,

$$x^*B^*ABx \geq 0$$

Denoting y the complex vector Bx of dimension n, the latter matrix inequality is equivalent to:

$$y^*Ay \geq 0$$

which always holds since $A \geq 0$. ∎

113

Appendices for Chapter 4

C.1 Derivation of the expression for $R^u(z, \theta_0)$ and $R^y(z, \theta_0)$

Let us first derive the expression for $R^u(z, \theta_0)$. For this purpose, let us pose $ref_{ext} = 0$ and $\bar{e} = 0$ in the equations (4.3), (4.8) and (4.9). This yields:

$$\bar{y} = \bar{G}(z, \theta_0)\bar{u} \tag{C.1}$$

$$\bar{u}(t) = \bar{m}_l \ r(t) + \bar{K}(z) \ (\bar{y}_{ref}(t) - \bar{y}(t)) \tag{C.2}$$

$$\bar{y}_{ref}(t) = \mathcal{A} \ (\bar{y}(t) - \bar{m}_l x(t)) \tag{C.3}$$

By inserting (C.2) into (C.1) and using the notation (4.14), we obtain successively:

$$\bar{y} = \bar{G}(z, \theta_0) \left(\bar{m}_l \ r(t) + \bar{K}(z) \ (\bar{y}_{ref}(t) - \bar{y}(t)) \right)$$

$$\bar{y} = \bar{S}(z, \theta_0)\bar{G}(z, \theta_0) \ \bar{m}_l \ r(t) + \bar{S}(z, \theta_0)\bar{G}(z, \theta_0)\bar{K}(z)\bar{y}_{ref}(t)$$

$$\bar{y} = \bar{m}_l \ T_{0,l}(z) \ r(t) + \bar{S}(z, \theta_0)\bar{G}(z, \theta_0)\bar{K}(z)\bar{y}_{ref}(t) \tag{C.4}$$

with $T_{0,l}(z) = G_l(z, \theta_{0,l})/(1 + K_l(z)G_l(z, \theta_{0,l}))$. The last equivalence is obtained by using the fact that $\bar{S}(z, \theta_0)\bar{G}(z, \theta_0)$ is a diagonal matrix.

By inserting (C.4) into (C.3) and by using the definition of $\bar{S}(z, \theta_0)$ in (4.7) for x, we obtain successively:

$$\bar{y}_{ref}(t) = \mathcal{A} \ \left(\bar{m}_l \ (T_{0,l}(z) - T_{init,l}(z)) \ r(t) + \bar{S}(z, \theta_0)\bar{G}(z, \theta_0)\bar{K}(z)\bar{y}_{ref}(t) \right)$$

$$\bar{y}_{ref}(t) = \left(I_{N_{mod}} - \mathcal{A}\bar{S}(z, \theta_0)\bar{G}(z, \theta_0)\bar{K}(z) \right)^{-1} \mathcal{A} \ \bar{m}_l \ (T_{0,l}(z) - T_{init,l}(z)) \ r(t) \tag{C.5}$$

Let us now insert (C.4) into (C.2) and use the fact that $I_{N_{mod}} - \bar{S}(z, \theta_0)\bar{G}(z, \theta_0)\bar{K}(z) = \bar{S}(z, \theta_0)$ due to the diagonal structure of the matrix. This successively yields:

$$\bar{u}(t) = \bar{m}_l \ r(t) + \bar{K}(z) \ \left(\bar{y}_{ref}(t) - \bar{m}_l \ T_{0,l}(z) \ r(t) - \bar{S}(z, \theta_0)\bar{G}(z, \theta_0)\bar{K}(z)\bar{y}_{ref}(t) \right)$$

$$\bar{u}(t) = \bar{m}_l \underbrace{(1 - K_l(z)T_{0,l}(z))}_{=S_{0,l}(z)} r(t) + \bar{K}(z)\bar{S}(z,\theta_0)\bar{y}_{ref}(t) \tag{C.6}$$

with $S_{0,l}(z) = 1/(1 + K_l(z)G_l(z,\theta_{0,l}))$. Finally, by inserting (C.5) into (C.6), we obtain:

$$\bar{u}(t) = \left(\bar{m}_l\, S_{0,l}(z)\ +\ \bar{K}(z)\bar{S}(z,\theta_0) \left(I_{N_{mod}} - \mathcal{A}\bar{S}(z,\theta_0)\bar{G}(z,\theta_0)\bar{K}(z)\right)^{-1} \mathcal{A}\,\bar{m}_l\ (T_{0,l}(z) - T_{init,l}(z)) \right) r(t) \tag{C.7}$$

which is the desired expression for $R^u(z,\theta_0)$. The expression for $R^y(z,\theta_0)$ follows by inserting (C.7) into (C.1).

C.2 Proof of Proposition 4.1

Let us consider the expression (4.19) for the individual costs $\mathcal{J}_i(\theta_0, \Phi_r)$ $(i = 1, \ldots, N_{mod})$ and introduce the following notations to distinguish them in the stealth (superscript S) and non-stealth case (superscript NS):

$$\mathcal{J}_i^S(\theta_0, \Phi_r) = \frac{1}{2\pi} \int_{-\pi}^{\pi} \left(1 + \beta|G_i(e^{j\omega},\theta_{0,i})|^2\right)\ |R_i^u(e^{j\omega},\theta_0)|^2 \Phi_r(\omega)\ d\omega \tag{C.8}$$

$$\mathcal{J}_i^{NS}(\theta_0, \Phi_r) = \frac{1}{2\pi} \int_{-\pi}^{\pi} \left(1 + \beta|G_i(e^{j\omega},\theta_{0,i})|^2\right)\ |R_i^{u,NS}(e^{j\omega},\theta_0)|^2 \Phi_r(\omega)\ d\omega \tag{C.9}$$

where R^u is given by (4.12) and $R^{u,NS}$ is given by (4.20). Let us now observe that, for $i \neq l$, we have that:

$$|R_i^u(e^{j\omega},\theta_0)|^2\Phi_r(\omega) = |\bar{N}_i(e^{j\omega},\theta_0)|^2|T_{0,l}(e^{j\omega}) - T_{init,l}(e^{j\omega})|^2\Phi_r(\omega)$$

$$|R_i^{u,NS}(e^{j\omega},\theta_0)|^2\Phi_r(\omega) = |\bar{N}_i(e^{j\omega},\theta_0)|^2|T_{0,l}(e^{j\omega})|^2\Phi_r(\omega)$$

Let us first consider the indexes $i \in \mathcal{P}_l$ and recall Assumption 4.2. In this case, if $T_{init,l}$ satisfies (4.22) for all frequencies ω where $\Phi_r(\omega) \neq 0$, we have for all these frequencies that:

$$|R_i^{u,NS}(e^{j\omega},\theta_0)|^2\Phi_r(\omega) > |R_i^u(e^{j\omega},\theta_0)|^2\Phi_r(\omega)$$

Consequently, for all $i \in \mathcal{P}_l$, we have that $\mathcal{J}_i^S(\theta_0, \Phi_r) < \mathcal{J}_i^{NS}(\theta_0, \Phi_r)$.

Finally, for the indexes $i \neq l$, $i \notin \mathcal{P}_l$, $\mathcal{J}_i^S(\theta_0, \Phi_r) = \mathcal{J}_i^{NS}(\theta_0, \Phi_r) = 0$ since $\bar{N}_i(z,\theta_0) = 0$ in this case.

C.3 Consistency and accuracy of (4.23)

C.3.1 Proof of Proposition 4.2

Let us first consider the stealth setting. As discussed in Chapter 2, we can prove the consistency of (4.23) by showing that $\theta_{0,l}$ is the unique minimum of the following asymptotic identification criterion:

$$\theta_l^* = \arg\min_\theta \bar{E}\epsilon^2(t,\theta_l) \tag{C.10}$$

The prediction error $\epsilon(t,\theta_l)$ in (4.23) can be rewritten as follows using (4.1) and (4.11):

$$\epsilon(t,\theta_l) = e_l(t) + \frac{\Delta G_l(z,\theta_l)}{H_l(z,\theta_l)}\left(R_l^u\ r(t) + R_{ext,l}^u\ ref_{ext}(t) + \sum_{i\in\mathcal{L}_l} S_{li}^u\ e_i(t)\right) \tag{C.11}$$

$$+ \left(\frac{\Delta H_l(z,\theta_l)}{H_l(z,\theta_l)} + \frac{\Delta G_l(z,\theta_l)}{H_l(z,\theta_l)}S_{ll}^u\right)e_l \tag{C.12}$$

where $\Delta G_l(z,\theta_l) = G_l(z,\theta_{0,l}) - G_l(z,\theta_l)$ and $\Delta H_l(z,\theta_l) = H_l(z,\theta_{0,l}) - H_l(z,\theta_l)$. Using now the fact that there is at least a delay in the product $K_l G_l$ (and thus in the product $\Delta G_l(z,\theta_l)S_{ll}^u$), that H_l is monic and that r, ref_{ext} and the white noises e_j ($j = 1,\ldots,N_{mod}$) are mutually independent, the power $\bar{E}\epsilon^2(t,\theta_l)$ of $\epsilon(t,\theta_l)$ is given by:

$$\bar{E}\epsilon^2(t,\theta_l) = \sigma_{e_l}^2 + \bar{E}s_r^2(t,\theta_l) + \bar{E}s_{ref_{ext}}^2(t,\theta_l) + \bar{E}s_{e_l}^2(t,\theta_l) + \sum_{i\in\mathcal{L}_l}\bar{E}s_{e_i}^2(t,\theta_l) \tag{C.13}$$

with $s_r = \frac{\Delta G_l(z,\theta_l)}{H_l(z,\theta_l)}R_l^u\ r$, $s_{ref_{ext}} = \frac{\Delta G_l(z,\theta_l)}{H_l(z,\theta_l)}\ R_{ext,l}^u\ ref_{ext}$, $s_{e_l} = \left(\frac{\Delta H_l(z,\theta_l)}{H_l(z,\theta_l)} + \frac{\Delta G_l(z,\theta_l)}{H_l(z,\theta_l)}S_{ll}^u\right)e_l$ and, for $i\in\mathcal{L}_l$, $s_{e_i} = \frac{\Delta G_l(z,\theta_l)}{H_l(z,\theta_l)}\ S_{li}^u\ e_i$.

Since $\bar{E}\epsilon^2(t,\theta_{0,l}) = \sigma_{e_l}^2$, we thus need to have $\bar{E}\epsilon^2(t,\theta_l^*) = \sigma_{e_l}^2$ for all minimizers θ_l^* of the asymptotic criterion (C.10). Since we assume that the model structure $\mathcal{M}$ is identifiable, the consistency will thus be proven if we show that $\bar{E}s_r^2(t,\theta_l) = \bar{E}s_{ref_{ext}}^2(t,\theta_l) = \bar{E}s_{e_j}^2(t,\theta_l) = 0$ ($j = l$ and $j\in\mathcal{L}_l$) implies $\Delta G_l(z,\theta_l) = \Delta H_l(z,\theta_l) = 0$.

Let us first consider the case where $\mathcal{L}_l$ is non-empty i.e. there is at least one path from a node $i \neq l$ to Node l. Due to the existence of this path, S_{li}^u is a nonzero transfer function (see Assumption 4.3). Consequently, $\bar{E}s_{e_i}^2(t,\theta_l) = 0$ implies $\Delta G_l(z,\theta_l) = 0$. Since $\Delta G_l(z,\theta_l) = 0$, we have that $\bar{E}s_{e_l}^2(t,\theta_l) = 0$ implies that $\Delta H_l(z,\theta_l) = 0$ and we have therefore proven the consistency of $\hat{\theta}_{N,l}$ for this case (independently of the value of r and ref_{ext}).

Let us now consider the case where $\mathcal{L}_l$ is empty (it is e.g. the case of Node 1 in the network of Figure 4.1). In that particular case, $y_{ref,l}$ must[1] be equal to ref_{ext}.

---

[1] If it was not the case, Node l could not track ref_{ext} while we have stated that the objective of the network configuration is that each node follows ref_{ext}.

Consequently, the data set $Z_l^N = \{y_l(t), \ u_l(t) \mid t = 1, \dots, N\}$ is generated by the closed-loop system described by (4.24)-(4.25) and the consistency property have to be evaluated on this loop. As shown in Section 2.3 (see in particular Assumption 2.3), the orders of excitation of r and/or ref_{ext} will need to be sufficient to yield a consistent $\hat{\theta}_{N,l}$.

Finally, let us note that the above reasoning remains exactly the same for the non-stealth setting i.e. when R_l^u is replaced by $R_l^{u,NS}$ in the expression of $s_r(t, \theta)$ in (C.13).

Remark C.1. The result given in this proposition is close to the result in Theorem 1 in [17]. The main differences are that we here consider the influence of ref_{ext} and that we also derive the consistency for the stealth setting.

C.3.2 Accuracy

Since $\epsilon(t, \theta_{0,l}) = e_l(t)$ and since $\hat{\theta}_{N,l}$ is a consistent estimate of $\theta_{0,l}$, $\hat{\theta}_{N,l}$ is asymptotically normally distributed around $\theta_{0,l}$ [1] and the inverse of its covariance matrix is given by:

$$P_{\theta_l}^{-1} = \frac{N}{\sigma_{e_l}^2} \bar{E} \psi(t, \theta_{0,l}) \psi^T(t, \theta_{0,l})$$

with $\psi(t, \theta_l) = \frac{-\partial \epsilon(t,\theta_l)}{\partial \theta_l}$ [1].

Let us first show that the above expression is equivalent to (4.26) in the stealth setting. It is easy to show (see e.g. [3]) that $\psi(t, \theta_{0,l}) = F_l(z, \theta_{0,l}) u_l(t) + L_l(z, \theta_{0,l}) e_l(t)$ with $F_l(\theta_l)$ as defined below (4.26) and with $L_l(\theta_l) = H_l^{-1}(\theta_l) \frac{\partial H_l(\theta_l)}{\partial \theta_l}$.

Using (4.11) and recalling that r and ref_{ext} and the white noises in $\bar{e}$ are all mutually independent, we obtain the expression (4.26) with [17]:

$$M_{\bar{e}} = \frac{N}{2\pi \sigma_{e_l}^2} \int_{-\pi}^{\pi} \mathcal{Z}_l(e^{j\omega}) diag(\sigma_{e_1}^2, \sigma_{e_2}^2, \dots, \sigma_{e_{N_{mod}}}^2) \mathcal{Z}_l^*(e^{j\omega}) d\omega$$

with $\sigma_{e_i}^2$ $(i = 1, \dots, N_{mod})$ the variance of e_i and with $\mathcal{Z}_l(z)$ a matrix of transfer functions of dimension $n_{\theta_l} \times N_{mod}$ whose l^{th} column is $L_l + F_l S_{ll}^u$ and whose k^{th}-column $(k \neq l)$ is equal to $F_l S_{lk}^u$ (S_{lk}^u is the entry $l \times k$ of S^u in (4.11)).

In the non-stealth setting, the above reasoning and the expression (4.26) remain valid, but we have to replace R_l^u by $R_l^{u,NS}$ (see (4.20)).

C.4 Proof of Proposition 4.3

Let us introduce the following notations to distinguish the covariance matrix $P_{\theta_l}(\theta_0, \Phi_r)$ in the stealth and non-stealth case and let us also consider the notations introduced in (C.8)-(C.9) to distinguish the individual costs in those two cases.

$$P_{\theta_l,S}^{-1}(\theta_0, \Phi_r^S) = M_{\bar{e}}(\theta_0) +$$
$$\frac{N}{2\pi\sigma_l^2} \int_{-\pi}^{\pi} F_l(e^{j\omega}, \theta_{0,l}) F_l^*(e^{j\omega}, \theta_{0,l}) \left(|R_l^u(e^{j\omega}, \theta_0)|^2 \Phi_r^S(\omega) + |R_{ext,l}^u(e^{j\omega}, \theta_0)|^2 \Phi_{ref_{ext}}(\omega) \right) \ d\omega$$

$$P_{\theta_l,NS}^{-1}(\theta_0, \Phi_r^{NS}) = M_{\bar{e}}(\theta_0) +$$
$$\frac{N}{2\pi\sigma_l^2} \int_{-\pi}^{\pi} F_l(e^{j\omega}, \theta_{0,l}) F_l^*(e^{j\omega}, \theta_{0,l}) \left(|R_l^{u,NS}(e^{j\omega}, \theta_0)|^2 \Phi_r^{NS}(\omega) + |R_{ext,l}^u(e^{j\omega}, \theta_0)|^2 \Phi_{ref_{ext}}(\omega) \right) \ d\omega$$

Using the optimal spectrum $\Phi_{r,opt}^{NS}$ in the non-stealth case, let us define the following spectrum:

$$\Phi_r^S(\omega) = \frac{|R_l^{u,NS}(e^{j\omega}, \theta_0)|^2}{|R_l^u(e^{j\omega}, \theta_0)|^2} \Phi_{r,opt}^{NS}(\omega) \tag{C.14}$$

Let us note that the ratio in the right hand side of (C.14) can neither be infinite nor zero due to Assumption 4.4 (in particular, this ratio is equal to one at the frequencies ω where $K_l(e^{j\omega})$ is infinite). Consequently, the spectrum $\Phi_r^S(\omega)$ is well defined at all frequencies ω and is equal to zero at the same frequencies ω as $\Phi_{r,opt}^{NS}(\omega)$ is equal to zero.

If an excitation signal r having that spectrum is used during an experiment where the stealth configuration is implemented, it is clear that the obtained covariance matrix $P_{\theta_l,S}(\theta_0, \Phi_r^S)$ will be equal to the one obtained in the non-stealth case with $\Phi_{r,opt}^{NS}$ (i.e. $P_{\theta_l,NS}(\theta_0, \Phi_{r,opt}^{NS})$). Consequently, an experiment with this spectrum Φ_r^S will satisfy the accuracy constraint (4.28). Due to (C.14), (C.8) and (C.9), we have also the following relation for the individual cost at Node l:

$$\mathcal{J}_l^S(\theta_0, \Phi_r^S) = \mathcal{J}_l^{NS}(\theta_0, \Phi_{r,opt}^{NS})$$

Moreover, for $i \neq l$, we have that:

$$|R_i^u(e^{j\omega}, \theta_0)|^2 \Phi_r^S(\omega) = |\bar{N}_i(e^{j\omega}, \theta_0)|^2 |T_{0,l}(e^{j\omega}) - T_{init,l}(e^{j\omega})|^2 \Phi_r^S(\omega)$$

$$|R_i^{u,NS}(e^{j\omega}, \theta_0)|^2 \Phi_{r,opt}^{NS}(\omega) = |\bar{N}_i(e^{j\omega}, \theta_0)|^2 |T_{0,l}(e^{j\omega})|^2 \frac{|R_l^u(e^{j\omega}, \theta_0)|^2}{|R_l^{u,NS}(e^{j\omega}, \theta_0)|^2} \Phi_r^S(\omega)$$

Consequently, due to Assumption 4.1, for $i \in \mathcal{P}_l$, we have that $\mathcal{J}_i^S(\theta_0, \Phi_r^S) < \mathcal{J}_i^{NS}(\theta_0, \Phi_{r,opt}^{NS})$ if $T_{init,l}$ satisfies (4.29) for all frequencies ω where $\Phi_r^S(\omega) \neq 0$ (and thus for all frequencies ω where $\Phi_{r,opt}^{NS}(\omega) \neq 0$). Moreover, for $i \neq l$ and $i \notin \mathcal{P}_l$, we have that $\mathcal{J}_i^S(\theta_0, \Phi_r^S) = \mathcal{J}_i^{NS}(\theta_0, \Phi_{r,opt}^{NS}) = 0$. Due to (4.17), we have thus shown that, in the stealth case, we can find a spectrum Φ_r^S leading to the same accuracy as with $\Phi_{r,opt}^{NS}$, but with a strictly smaller cost. The result of the proposition is therefore proven since, by definition, $\mathcal{J}^S(\theta_0, \Phi_r^S) \geq \mathcal{J}^S(\theta_0, \Phi_{r,opt}^S)$.

C.5   Computation of the quantities $\tilde{c}_i(\omega)$ and $\rho_i(\omega)$

This appendix shows how the quantities $\tilde{c}_i(\omega)$ and $\rho_i(\omega)$ (see (4.48)) can be computed for a given i and a given ω. For this purpose, let us first give an expression of $\tilde{T}_i(e^{j\omega}, \theta_i)$ as a function of θ_i using the following notation[2] for $G_i(e^{j\omega}, \theta_i) = \frac{Z_{1,i}(e^{j\omega})\theta_i}{1+Z_{2,i}(e^{j\omega})\theta_i}$. In the last expression, $Z_{1,i}(z)$ and $Z_{2,i}(z)$ are row vectors containing only delays or zeros (see [51]). This yields

$$\tilde{T}_i(e^{j\omega}, \theta_i) = \frac{-1 + Z_{N,i}(e^{j\omega})\theta_i}{1 + Z_{D,i}(e^{j\omega})\theta_i} \tag{C.15}$$

with $Z_{D,i} = Z_{2,i} + K_i Z_{1,i}$ and $Z_{N,i} = \frac{Z_{1,i}}{T_i(e^{j\omega}, \hat{\theta}_{init,i})} - Z_{D,i}$. Based on (C.15), the quantities $\tilde{c}_i(\omega)$ and $\rho_i(\omega)$ can be exactly computed using the LMI optimization problem given in the following proposition whose proof can be found in [17].

Proposition C.1. *Consider the notation* $\tilde{T}_i(e^{j\omega}, \theta_i) = \frac{-1 + Z_{N,i}(e^{j\omega})\theta_i}{1 + Z_{D,i}(e^{j\omega})\theta_i}$ *given in (C.15). The optimization problem (4.48) at a given ω and at a given i is equivalent to the following LMI optimization problem having as decision variables a positive real scalar $\mu_i(\omega)$, a complex scalar $\tilde{c}_i(\omega)$, a positive real scalar $\xi_i(\omega)$ and a skew-symmetric matrix $\mathcal{X}_i(\omega) \in \mathbf{R}^{(n_{\theta_i}+1) \times (n_{\theta_i}+1)}$ (n_{θ_i} is the dimension of θ_i):*

$$\min \ \mu_i(\omega) \quad subject \ to$$

$$\left(\begin{array}{c|c} -\mu_i(\omega) & \lambda_i(\omega) \\ \hline \lambda_i^*(\omega) & -A_i(\omega) - \xi_i(\omega)B_i + j\mathcal{X}_i(\omega) \end{array} \right) < 0 \tag{C.16}$$

with $j = \sqrt{-1}$, $\lambda_i(\omega) = \left(\ Z_{N,i} - Z_{D,i}\tilde{c}_i \ \middle| \ -1 - \tilde{c}_i \ \right)$ and

$$A_i(\omega) = \left(\begin{array}{cc} Z_{D,i}^* Z_{D,i} & Z_{D,i}^* \\ Z_{D,i} & 1 \end{array} \right) \quad B_i = \left(\begin{array}{cc} P_{init,i}^{-1} & -P_{init,i}^{-1}\hat{\theta}_{init,i} \\ -\hat{\theta}_{init,i}^T P_{init,i}^{-1} & \hat{\theta}_{init,i}^T P_{init,i}^{-1}\hat{\theta}_{init,i} - \chi \end{array} \right)$$

The above optimization problem is not explicitly function of $\rho_i(\omega)$. However, the optimal $\rho_i(\omega)$ can be obtained by taking the square root of the optimal $\mu_i(\omega)$. ∎

C.6   Proof of Proposition 4.5

The result of Proposition 4.5 will be proven if we can show that the LMI (4.52) implies:

$$\mathcal{F}^* \left(M_\Delta(e^{j\omega}), \Delta(e^{j\omega}) \right) \ \mathcal{F} \left(M_\Delta(e^{j\omega}), \Delta(e^{j\omega}) \right) < \tilde{\gamma}(\omega) \ \ \forall \Delta(e^{j\omega}) \in \boldsymbol{\Delta}(\omega) \tag{C.17}$$

---

[2]As shown in Appendix A, $G(z, \theta)$ is a rational function of θ for all classical model structures (see also Observation 3.1). Consequently, such notation is always possible.

To show this, let us expand the LFT $\mathcal{F}\left(M_{\Delta}(e^{j\omega}), \Delta(e^{j\omega})\right)$ into

$$\bar{p} = \Delta(e^{j\omega})\bar{q} \quad \text{and} \quad \begin{pmatrix} \bar{q} \\ \bar{s} \end{pmatrix} = M_{\Delta}(e^{j\omega}) \begin{pmatrix} \bar{p} \\ 1 \end{pmatrix} \qquad (C.18)$$

where $\bar{q}$, $\bar{p}$ and $\bar{s}$ are complex vectors and where $\bar{s} = \mathcal{F}\left(M_{\Delta}(e^{j\omega}), \Delta(e^{j\omega})\right)$. Let us now consider this LFT (C.18) for a given $\Delta(e^{j\omega}) \in \boldsymbol{\Delta}(\omega)$ and let us also consider the corresponding signals $\bar{p}$, $\bar{q}$ and $\bar{s}$. Let us then pre- and post-multiply the LMI constraint (4.52) with $(\bar{p}^*, 1)$ and $(\bar{p}^T, 1)^T$, respectively. Using (C.18), this yields:

$$\begin{pmatrix} \bar{q} \\ \bar{p} \end{pmatrix}^* \underbrace{\begin{pmatrix} T_{\omega}(R_{\omega} - C_{\omega}^* C_{\omega}) & T_{\omega} C_{\omega}^* \\ T_{\omega} C_{\omega} & -T_{\omega} \end{pmatrix}}_{=A} \begin{pmatrix} \bar{q} \\ \bar{p} \end{pmatrix} + \bar{s}^* \bar{s} < \tilde{\gamma}(\omega) \qquad (C.19)$$

Since $\bar{p} = \Delta(e^{j\omega})\bar{q}$, we can rewrite the first term of the left hand side of (C.19) as follows:

$$\begin{pmatrix} \bar{q} \\ \bar{p} \end{pmatrix}^* A \begin{pmatrix} \bar{q} \\ \bar{p} \end{pmatrix} = \bar{q}^* \begin{pmatrix} I_{N_{mod}} \\ \Delta(e^{j\omega}) \end{pmatrix}^* A \begin{pmatrix} I_{N_{mod}} \\ \Delta(e^{j\omega}) \end{pmatrix} \bar{q} \qquad (C.20)$$

The above reasoning can be done for any value of $\Delta(e^{j\omega}) \in \boldsymbol{\Delta}(\omega)$. In other words, for the matrix T_{ω} found by the optimization problem, (C.19) holds true for all $\Delta(e^{j\omega}) \in \boldsymbol{\Delta}(\omega)$. Let us also observe that, when T_{ω} is a strictly positive definite diagonal matrix, (C.20) is a positive quantity for all $\Delta(e^{j\omega}) \in \boldsymbol{\Delta}(\omega)$. Recalling that $\bar{s} = \mathcal{F}\left(M_{\Delta}(e^{j\omega}), \Delta(e^{j\omega})\right)$, we have therefore also that (C.17) holds, which is the desired result.

Appendix for Chapter 5

The results of Section 5.5 for the RLS algorithm have been obtained when the forgetting factor λ (see Section 5.3) is chosen equal to $1 - 10^{-6}$ which is the optimal value we have determined. To illustrate why this value is optimal, let us analyze the results for a smaller value of λ ($\lambda = 0.999$) and a larger one ($\lambda = 1 - 10^{-8}$). For this purpose, let us re-do the simulation presented in Section 5.5 with an RLS algorithm using these two new values and let us compare the obtained results with the results obtained in Section 5.5 with $\lambda = 1 - 10^{-6}$. Let us first do that based on the estimated resonance frequency $\hat{\omega}_{r,x}(t)$ (see Figure D.1). It is clear that with respect to the original result (red curve), the estimated resonace frequency $\hat{\omega}_{r,x}$ obtained with the smaller value of λ (blue curve) presents a larger variance and the estimated resonance frequency $\hat{\omega}_{r,x}$ obtained with the larger value of λ (yellow curve) presents a strong bias.

The fact that $\lambda = 1 - 10^{-6}$ is optimal is also confirmed when analysing the energies of the signals u_x and ϵ_x (see Table D.1).

The above simulations have been repeated for other rate of variations α_w in (5.15) and similar phenomena have been observed.

Table D.1: $\mathcal{E}(u_x, .)$ and $\mathcal{E}(\epsilon_x, .)$ obtained with the RLS algorithm for different values of λ

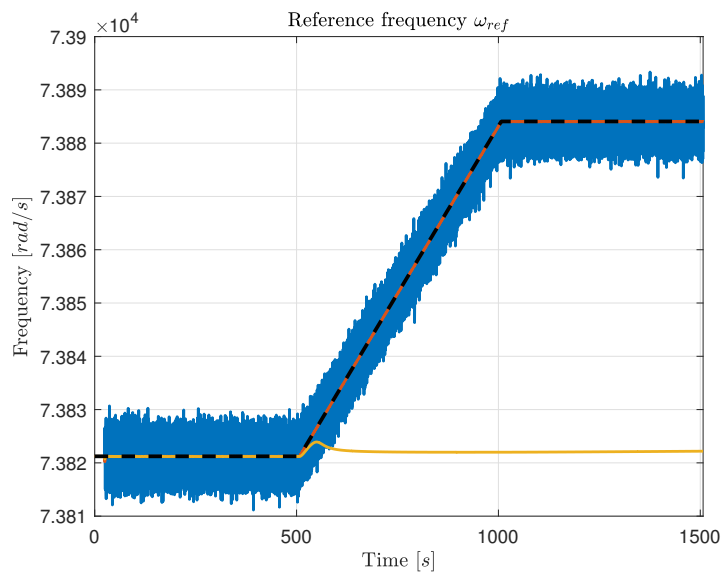|		$\mathcal{E}(u_x, .)$			$\mathcal{E}(\epsilon_x, .)$		
		Δt_1	Δt_2	Δt_3	Δt_1	Δt_2	Δt_3
	0.999	$9.91 \ 10^5$	10^6	10^6	51.1	53.1	53.2
λ	$1 - 10^{-6}$	$6.46 \ 10^5$	$6.48 \ 10^5$	$6.46 \ 10^5$	48.8	50.6	50.6
	$1 - 10^{-8}$	$6.47 \ 10^5$	$1.12 \ 10^9$	$3.19 \ 10^9$	48.7	$2.37 \ 10^3$	$7.1 \ 10^3$

Figure D.1: Resonance frequency estimated using the RLS algorithm with $\lambda = 1 - 10^{-6}$ (red line), with $\lambda = 0.999$ (blue line) and with $\lambda = 1 - 10^{-8}$ (yellow curve) compared to the true resonance frequency (black dashed line).

Résumée de la Thèse

E.1 Introduction

E.1.1 Identification des Systèmes

Les modèles dynamiques paramétriques nous permettent d'avoir une description mathématique d'un système dynamique. Sans eux, de nombreux domaines des sciences et de l'ingénierie, de la chimie, de la mécanique, de l'électronique, de la biologie et bien d'autres, n'existeraient pas. Sans eux, nous ne pouvons pas faire de prévisions sur l'évolution d'une épidémie, nous ne pouvons pas concevoir le système de contrôle d'un résonateur, surveiller la santé d'une éolienne afin de planifier la maintenance, et la liste peut se poursuivre indéfiniment.

Comment obtenir un modèle dynamique ? Nous pouvons construire un modèle pour un système dynamique en partant des principes fondamentaux, les lois de la physique déterminant son comportement. Nous appelons cette méthode la modélisation de la *boîte blanche* ou la modélisation des principes fondamentaux. Le modèle ainsi obtenu a une interprétation physique immédiate, mais il peut reposer sur des constantes ou des paramètres difficiles à déterminer.

Une méthode importante consiste à obtenir un modèle à partir d'observations, de données recueillies dans le système étudié, plutôt qu'à partir de lois physiques. Selon la définition de [1], c'est le sujet principal de l'Identification des Systèmes. Ces données sont collectées au cours d'une expérience, qui est réalisée en excitant le système avec un signal connu. Pendant que le système est excité, nous recueillons des mesures du signal d'entrée et du signal de sortie, corrompus par un bruit stochastique. Les étapes nécessaires pour obtenir un modèle en utilisant les techniques développées dans l'Identification des Systèmes sont les suivantes:

1. Sélection de la structure du modèle. Nous choisissons le type de modèle (linéaire, non linéaire, etc.) ainsi que sa complexité (par exemple l'ordre de la fonction de transfert) et nous définissons quels sont les paramètres scalaires $\theta \in \mathbf{R}^k$ que nous devrons déterminer, puis nous définissons un ensemble de modèles paramétriques.

Nous voulons généralement choisir une structure de modèle telle que le modèle à obtenir puisse décrire le *vrai système*, c'est-à-dire qu'il existe un vecteur de paramètres $\theta_0 \in \mathbf{R}^k$, appelé *vrai vecteur de paramètres*, tel que le modèle paramétrique décrit "exactement" les données observées. Ce choix dépend généralement du fait que l'on souhaite que les paramètres θ aient une signification physique ou non. Nous ne pouvons choisir la structure du modèle que pour ce qui concerne sa capacité à décrire les données observées, et nous appelons ce choix *modélisation de la boîte noire*. Une autre possibilité consiste à dériver le modèle à partir des principes fondamentaux et ensuite à déterminer les paramètres du modèle à partir des données; nous appelons cette méthode *modélisation de la boîte grise*, car elle se situe entre la modélisation de la boîte noire et celle de la boîte blanche.

2. Conception d'expériences. Décider de tous les détails de l'expérience n'est pas une simple étape formelle. En effet, de nombreux aspects comme le signal utilisé pour exciter le système et la quantité de données collectées ont un effet important sur la qualité du modèle final. En outre, lors de la conception de l'expérience, nous devons tenir compte de la configuration dans laquelle l'expérience sera réalisée.

3. Estimation des paramètres. A partir des données recueillies, nous devons alors obtenir une estimation $\hat{\theta} \in \mathbf{R}^k$ de θ_0. Ceci est fait en minimisant un certain critère qui vise à maximiser la capacité du modèle à expliquer les données. Un critère largement utilisé est le critère dit *Prediction Error* [1].

4. Validation du modèle. Une fois qu'on a obtenu le modèle, nous savons qu'il sera en mesure de reproduire les données utilisées pour l'identification. Cependant, cela ne nous assure pas que le modèle sera capable de prédire le comportement du système. Nous recueillons alors un autre ensemble de données du système et nous effectuons des tests sur le modèle pour vérifier s'il est capable de reproduire ce nouvel ensemble de données.

Cette thèse sera composée d'une partie théorique et d'une partie appliquée. Dans la partie théorique, nous apporterons de nouvelles contributions à la conception optimale d'une expérience d'identification. Dans la deuxième partie, nous montrerons que l'identification de systèmes peut être utilisée comme un outil efficace pour résoudre un problème qui se pose dans le cadre du projet Next4MEMS , le projet qui a contribué à financer cette thèse de doctorat.

E.1.2   Conception Optimale de l'Expérience d'Identification

État de l'art

La conception optimale de l'expérience d'identification consiste à concevoir de manière optimale le signal d'excitation d'une expérience d'identification pour accorder deux objectifs contradictoires:

- obtenir l'estimation la plus précise $\hat{\theta}$ de θ_0, c'est-à-dire obtenir une estimation $\hat{\theta}$ avec la matrice de covariance la plus petite possible P_θ

- le signal d'excitation perturbe le moins possible le système à identifier, c'est-à-dire que le coût de l'expérience est le plus faible possible.

Ces objectifs sont contradictoires car plus le spectre Φ du signal d'excitation est grand, plus P_θ est "petite", mais en même temps, plus le spectre est grand, plus le coût de l'expérience est élevé. Pour équilibrer ces objectifs contradictoires, on peut par exemple maximiser la précision de $\hat{\theta}$ en tenant compte d'une certaine limite au coût de l'expérience. C'est la formulation classique du problème de la conception optimale de l'expérience qui remonte aux années 70 (voir par exemple [2]). Plus récemment, une deuxième formulation (la formulation dite *least costly*) a été proposée, où l'objectif est de déterminer le spectre Φ du signal d'excitation de telle sorte que le coût de l'expérience soit minimisé tout en garantissant une précision donnée pour le modèle identifié [3]. En termes mathématiques, le problème de conception *least costly* d'expérience consiste à déterminer le spectre Φ du signal d'excitation qui minimise le coût $\mathcal{J}(\Phi)$ de l'expérience tout en garantissant que $P_\theta^{-1}(\Phi) \geq R_{adm}$ où R_{adm} est une matrice représentant la précision souhaitée et où le coût $\mathcal{J}(\Phi)$ est mesuré par une combinaison linéaire de la puissance de la perturbation produite par le signal d'excitation sur le signal d'entrée et de sortie du système à identifier [3, 4].

La formulation pour la conception *least costly* de l'expérience est plus proche des exigences en matière de contrôle robuste où la performance robuste d'un contrôleur conçu avec le modèle identifié peut être garantie si l'incertitude du modèle est inférieure à une limite donnée (ou, de manière équivalente, si la précision du modèle identifié est supérieure à une certaine limite). Cela a donné lieu à un certain nombre de contributions sur la *conception least costly d'expérience pour le contrôle robuste*. Dans [3], une méthodologie est développée pour concevoir le spectre d'excitation de telle manière que, avec le coût d'identification le plus faible, le modèle identifié soit garanti d'avoir une incertitude suffisamment faible pour permettre un design de contrôle robuste. Dans [3], un cadre de contrôle H_∞ est utilisé, mais d'autres cadres de contrôle peuvent également être considérés comme indiqué dans [4, 5]. Les résultats dans [3] et [4] sont basés sur les résultats techniques dans [6, 7, 8]. En effet, les articles [6, 7, 8] montrent qu'en utilisant des paramétrisations appropriées du spectre à déterminer Φ, tant $\mathcal{J}(\Phi)$ que $P_\theta^{-1}(\Phi)$ peuvent être exprimés sous forme de fonctions affines des coefficients du spectre (à déterminer). Deux paramétrisations de Φ sont en fait considérées dans [6, 7, 8] : l'une correspondant au spectre d'un signal d'excitation multisinusoïdal et l'autre correspondant au spectre d'un bruit blanc filtré où le filtre est limité pour avoir une réponse impulsionnelle finie. Sur la base de ces résultats techniques, il est clair que le problème de conception *least costly* introduit dans le paragraphe précédent se résume à un problème d'optimisation de LMI [1] [9]. Il est cependant important de noter que ce problème d'optimisation de LMI dépend du vecteur de paramètres vrais inconnus θ_0

---

[1]Linear Matrix Inequality.

puisque tant la matrice de covariance P_θ que le coût $\mathcal{J}$ de l'expérience ne dépendent pas seulement de Φ, mais aussi de θ_0 (nous utiliserons donc les notations $\mathcal{J}(\theta_0, \Phi)$ et $P_\theta(\theta_0, \Phi)$ dans la suite). Une approche classique (mais pas totalement satisfaisante) pour contourner ce problème dit de "*chicken-and-egg*" consiste à remplacer, dans le problème d'optimisation de LMI, l'inconnu θ_0 par une estimation initiale $\hat{\theta}_{init}$ (voir par exemple [8, 3]). L'une des contributions de cette thèse portera sur cette question du *chicken-and-egg*.

Les résultats dans [3] et [4] concernent des expériences visant à identifier des systèmes linéaires à entrée simple et sortie simple (SISO[2]) invariants dans le temps (LTI[3]) qui peuvent être décrits par des équations différentielles ordinaires et qui sont exploités soit en boucle ouverte soit en boucle fermée. Les résultats ont été étendus aux systèmes multivariables dans [10] et aux systèmes qui peuvent être décrits par des équations différentielles partielles dans [11, 12]. Les premières tentatives pour traiter la conception optimale de l'expérience pour les systèmes non linéaires se trouvent dans [13, 14, 15, 16]. Une première contribution à la conception optimale de l'expérience dans une autre configuration de fonctionnement que celle en boucle ouverte et en boucle fermée peut être trouvée dans [17] où une configuration de réseau est considérée. Une deuxième contribution de cette thèse sera d'étendre les résultats présentés dans cet article.

Contributions Théorique

Conception robuste de l'expérience Le problème de la conception *least-costly* d'expérience consiste à déterminer le spectre Φ du signal d'excitation qui minimise le coût $\mathcal{J}(\theta_0, \Phi)$ de l'expérience sous la contrainte que $P_\theta^{-1}(\theta_0, \Phi) \geq R_{adm}$. Comme mentionné dans la sous-section précédente, ce problème d'optimisation est un problème d'optimisation de LMI, ayant solution à condition que le véritable vecteur de paramètre θ_0 soit inconnu. Comme déjà mentionné, ce problème *chicken-and-egg* est généralement contourné en remplaçant θ_0 dans le problème d'optimisation par une estimation initiale $\hat{\theta}_{init}$ de θ_0 (voir par exemple [8, 3]). Toutefois, cette approche présente l'inconvénient que le spectre optimal $\Phi_{opt}^{\hat{\theta}_{init}}$ obtenu de cette manière n'est pas garanti de donner la précision souhaitée et que le coût de l'expérience $\mathcal{J}(\hat{\theta}_{init}, \Phi_{opt}^{\hat{\theta}_{init}})$ calculé avec $\hat{\theta}_{init}$ et $\Phi_{opt}^{\hat{\theta}_{init}}$ peut sous-estimer le coût réel de l'expérience $\mathcal{J}(\theta_0, \Phi_{opt}^{\hat{\theta}_{init}})$. Ces observations sont à l'origine du domaine de recherche sur le *robust design optimale d'expérience* (voir [20] pour une revue).

Dans le cadre de la conception robuste de l'expérience, différentes lignes de recherche ont été envisagées. Dans [21], un spectre qui donne une bonne précision pour un très large ensemble de systèmes (également d'ordres différents) est discuté. Cependant, dans la littérature technique, l'approche la plus largement utilisée est celle qui consiste à considérer un ensemble d'incertitudes U contenant le vrai vecteur inconnu de

---

[2]Single-input, single-output.

[3]Linear Time Invariant.

paramétres θ_0 (le design dit min-max [20, 22]). Le problème du design optimal de l'expérience peut alors être formulé comme déterminant le spectre Φ minimisant la valeur d'un scalaire γ sous les contraintes que le coût de l'expérience $\mathcal{J}(\theta, \Phi) \leq \gamma$ $\forall \theta \in U$ et que $P_\theta^{-1}(\theta, \Phi) \geq R_{adm}$ $\forall \theta \in U$. Si nous dénotons par γ_{opt} et Φ_{opt} la solution de ce problème d'optimisation, nous avons la garantie que $P_\theta^{-1}(\theta_0, \Phi_{opt}) \geq R_{adm}$ et que γ_{opt} est une limite supérieure pour le coût réel de l'expérience $\mathcal{J}(\theta_0, \Phi_{opt})$. Cependant, trouver une approche souple pour résoudre un problème de conception optimal d'expérience aussi robustifié reste une question de recherche ouverte. Bien que ce problème d'optimisation puisse être résolu avec exactitude dans des situations très particulières et simples (voir par exemple [20, 23]), l'approche générale, lorsqu'il s'agit de systèmes plus complexes, consiste à remplacer l'ensemble d'incertitude initial (contenant un nombre infini d'éléments) par un nombre n_g de points de grille de cet ensemble d'incertitude U (voir par exemple [8, 3, 20]). Par conséquent, la contrainte de coût et la contrainte de précision sur l'ensemble U dans le problème du design d'expérience optimale robuste sont remplacées chacune par des contraintes n_g (une pour chaque point de grille). Même s'il est évidemment préférable, du point de vue de la robustification, de remplacer θ_0 par un seul point de grille, c'est-à-dire $\hat{\theta}_{init}$, cet assouplissement du problème original de la conception optimale robuste de l'expérience ne peut pas donner les garanties liées au problème original.

Dans [26, 27, 28], des approches sont présentées pour attaquer uniquement la contrainte de coût robuste $\mathcal{J}(\theta, \Phi) \leq \gamma$ $\forall \theta \in U$ (c'est-à-dire que dans la contrainte de précision, θ_0 est remplacé par $\hat{\theta}_{init}$). Cependant, ces approches impliquent toutes une certaine approximation : une approximation du premier ordre dans [27], une approximation du second ordre dans [26] et une approximation basée sur la transformée *unscented* dans [28].

Dans cette thèse, notre contribution est de présenter une approche permettant d'aborder sans approximation le problème de la conception optimale robuste de l'expérience. À cette fin, nous observons que, à l'exception de sa dépendance au spectre à déterminer, la contrainte de coût et la contrainte de précision robustes sont similaires aux contraintes traitées dans l'analyse de robustesse. Sur la base de cette observation et du cadre de la séparation des graphes [29, 30, 31], nous dérivons des contraintes qui sont linéaires dans les variables de décision du problème de la conception optimale d'expérience et qui impliquent les contraintes de coût et de précision robustifiées originales. Comme nous le montrerons, l'approche proposée ne couvrira néanmoins pas toutes les situations possibles. Ces restrictions seront détaillées au Chapitre 3, ainsi que notre approche de conception robuste d'expérience.

Conception *Least Costly* de l'Expérience pour une Réseau de Systèmes Commandées Localement Jusqu'à récemment, l'identification des systèmes ne prenait en compte que les systèmes fonctionnant en boucle ouverte ou fermée. En raison de l'importance croissante du concept de réseau dans l'Automatique, nous avons cependant vu récemment des efforts importants pour développer des techniques d'identification

pour de systèmes à grande échelle ou interconnectés. Dans de nombreux articles, le problème est considéré comme un problème d'identification multivariable et les propriétés structurelles du système sont alors utilisées pour simplifier ce problème complexe (voir par exemple [32]). L'identifiabilité de la structure multivariable est étudiée dans un contexte Prediction Error dans [33] tandis que cette structure multivariable est exploitée dans d'autres articles pour réduire la variance d'un module donné dans le réseau (voir [34, 35, 36]). Dans d'autres contributions, les conditions sont dérivées pour l'estimation cohérente d'un module donné dans un réseau dynamique (voir par exemple [37, 38, 39]).

Si de nombreux problèmes différents ont ainsi été étudiés de manière approfondie dans le contexte des réseaux dynamiques, ce n'est pas le cas pour la conception optimale des expériences. Dans la littérature très limitée sur ce sujet particulier, la contribution [17] présente les premiers pas vers une conception optimale d'expérience dans un contexte de réseau dynamique. L'article [17] considère le cas d'un réseau constitué de systèmes contrôlés localement, c'est-à-dire de modules, dont l'interconnexion est réalisée en échangeant leur sortie mesurée entre des modules voisins (ce type de réseaux est habituel dans la littérature sur les systèmes multi-agents (voir par exemple [40, 41])). Pour ce type particulier de réseaux dynamiques, il est montré comment concevoir les signaux d'excitation, qui doivent être ajoutés à chaque module, afin d'identifier des modèles de ces différents modules qui soient suffisamment précis pour améliorer les performances du réseau par une reconception des contrôleurs locaux. La précision de chaque modèle peut être mesurée par l'inverse de la matrice de covariance du vecteur des paramètres identifié de chaque module. Dans [17], une expression pour l'inverse de cette matrice de covariance en fonction affine des spectres des signaux d'excitation est dérivée. Il est important de noter que l'inverse de la matrice de covariance d'un module donné l est évidemment une fonction du signal d'excitation appliqué à ce module particulier, mais aussi, bien que dans une moindre mesure, une fonction des signaux d'excitation appliqués à tous les modules k ayant un chemin vers l. Par conséquent, le signal d'excitation appliqué à un tel module k contribue à la précision du modèle de l. En d'autres termes, la propagation des signaux d'excitation due à l'interconnexion est une caractéristique positive lorsque l'on veut obtenir des estimations suffisamment précises de chaque module ayant la plus petite puissance d'excitation (voir également [42, 43, 44]).

Dans le Chapitre 4 de cette thèse, comme dans [17], nous examinerons le problème de la conception optimale d'expérience pour un réseau de systèmes contrôlés localement. Cependant, contrairement à [17], nous le ferons pour le cas où nous ne sommes intéressés que par l'identification précise d'un module spécifique l du réseau. Comme dans [17], pour maintenir les performances du réseau, cette identification sera effectuée dans la configuration originale du réseau via l'application d'un signal d'excitation au module l. Comme les autres modules n'ont pas à être identifiés, la propagation de ce signal d'excitation aux autres modules, en raison de l'interconnexion, est une caractéris-

tique négative qui doit être limitée autant que possible[4] À cette fin, nous étendons le cadre d'identification *least-costly* à ce problème particulier d'identification d'un réseau dynamique. En particulier, nous concevons le spectre du signal d'excitation appliqué à l de manière à ce que la précision du modèle identifié (mesurée par l'inverse de la matrice de covariance) soit supérieure à un seuil donné, tout en entraînant la plus faible perturbation sur le réseau. La perturbation (c'est-à-dire le coût de l'identification) sera mesurée par la somme des effets du signal d'excitation sur l'entrée et la sortie de chaque système du réseau.

Par rapport au framework *least-costly* introduit dans [3] pour une seule boucle fermée, le coût de l'expérience d'identification dans le contexte du réseau contient donc non seulement la perturbation induite par le signal d'excitation dans la boucle fermée où le système doit être identifié, mais aussi la perturbation induite dans d'autres boucles par ce signal d'excitation. Cette propagation de l'effet du signal d'excitation est due au fait que le signal de sortie de la boucle à identifier (qui est perturbée par le signal d'excitation) est transmis aux modules voisins. Dans cette thèse, afin de réduire cette propagation, nous proposons une approche où le signal transmis aux modules voisins n'est plus le signal de sortie réel, mais une version purifiée de ce signal de sortie où la contribution du signal d'excitation a été (partiellement) supprimée. Cette approche s'inspire du concept d'identification *stealth* introduit dans [45] pour une boucle fermée unique et que nous étendons ici au cas du réseau.

E.1.3 Suivi de la Fréquence de Résonance d'un Gyroscope MEMS

Dans la première partie de cette thèse, nous avons examiné l'identification des systèmes invariants dans le temps. Dans la deuxième partie, nous examinerons le cas d'un système variant dans le temps, c'est-à-dire un système dont les paramètres varient avec le temps. Dans ce cas également, l'identification des systèmes peut être un outil efficace pour dériver des modèles mathématiques précis basés sur des données d'entrée-sortie. En particulier, l'identification récursive [1] permet de déterminer, à chaque instant, une estimation du vecteur de paramètres variant dans le temps d'un système variant dans le temps.

Dans le Chapitre 5, nous utiliserons l'identification récursive pour aborder un problème survenu dans le cadre du projet Next4MEMS , le projet qui a financé ce doctorat. L'objectif du projet Next4MEMS est d'améliorer le système de contrôle des gyroscopes MEMS afin d'augmenter leur fiabilité. Dans un gyroscope MEMS, l'une des principales boucles de contrôle est celle qui se rapporte au système de masse drive [46]. Le système de masse drive est essentiellement une masse fixée à un cadre de référence par des micro-poutres de silicium et qui peut être actionnée par une force. La fonction de transfert entre cette force u_x et la position x de la masse drive est un système résonant du second ordre et l'objectif du système de contrôle de la masse drive est que x suive

---

[4]C'est particulièrement le cas lorsque l'expérience est réalisée dans un réseau où tous les modules doivent suivre une référence donnée. Dans ce cas, le signal d'excitation introduit une perturbation indésirable sur les performances de suivi.

un signal de référence sinusoïdal x_{ref}. En général, cet objectif de contrôle est atteint par deux boucles parallèles qui contrôlent respectivement l'amplitude et la phase de la représentation du phaseur du signal à contrôler x [46]. Cette approche par phase introduit des non-linéarités inutiles (par exemple, pour transformer le signal x en sa description de phase) et une autre approche de contrôle a été proposée dans le projet Next4MEMS . Dans cette configuration de commande alternative (et plus classique), la force u_x est calculée comme la sortie d'un contrôleur linéaire K_x qui prend comme entrée la différence entre le signal de référence sinusoïdal x_{ref} et le signal x, c'est-à-dire la position de la masse drive. Indépendamment de l'approche de contrôle, il est important de noter que, pour réduire la consommation d'énergie (c'est-à-dire pour imposer un petit signal d'actionnement u_x), la fréquence du signal de référence sinusoïdal x_{ref} doit être égale à la fréquence de résonance du système de masse drive.

Un gyroscope MEMS doit fonctionner dans une large gamme de températures ambiantes et il est bien connu [46] que la fréquence de résonance du système de masse drive change avec la température. Dans la configuration de commande classique (la configuration à phaseurs), ces variations étaient automatiquement prises en charge par la boucle de phase. Cependant, ce n'est plus le cas dans la nouvelle configuration de contrôle et une procédure doit être conçue afin d'adapter la fréquence du signal de référence x_{ref} de telle sorte que cette fréquence soit toujours égale (ou au moins proche) de la fréquence de résonance réelle du système. Au Chapitre 5, nous utilisons l'identification récursive pour suivre la dynamique du système de masse drive permettant ainsi d'adapter la fréquence du signal de référence x_{ref}. Nous montrons le potentiel de cette approche par des simulations et nous comparons l'approche récursive avec une autre approche possible pour aborder ce problème, l'approche de recherche des extremums, dit *Extremum Seeking*. Cette approche a en effet déjà été utilisée dans le cadre de l'approche par phaseurs pour adapter la référence de la boucle de phase afin de traiter plus efficacement l'effet des variations de température [47].

E.1.4 Contenu de la thèse

Dans le Chapitre 2, nous avons présenté plus en détail la méthode d'identification des erreurs de prédiction et la conception optimale des expériences d'identification.

Au Chapitre 3, nous avons présenté notre contribution sur la conception d'expériences optimales robustes. Ce chapitre est basé sur le document suivant :

> X. Bombois, F. Morelli, H. Hjalmarsson, L. Bako and K. Colin, "Robust optimal identification experiment design for multisine excitation", submitted to Automatica, September 2019

Au Chapitre 4, nous avons présenté notre extension du cadre *least costly* à la configuration du réseau. Ce chapitre s'appuie sur les documents suivants :

F. Morelli, X. Bombois, H. Hjalmarsson, L. Bako and K. Colin, "Optimal experiment design for the identification of one module in the interconnection of locally controlled systems", European Control Conference, Naples, 2019

F. Morelli, X. Bombois, H. Hjalmarsson, L. Bako and K. Colin, "Least costly identification experiment for the identification of one module in a dynamic network", submitted to Automatica, November 2019

Enfin, au Chapitre 5, nous avons abordé le problème du suivi de la fréquence de résonance du système de masse drive d'un gyroscope inertiel.

E.2 Conception Optimale Robuste de l'Expérience d'Identification avec une Excitation Multisinusoïdal

E.2.1 Identification en boucle ouvert dans une structure du modèle de type BJ

On considère des systèmes linéaires temps-invariantes avec une entrée $u(t)$ et une sortie $y(t)$ (SISO). On peut décrire ce système SISO par l'équation suivante:

$$\mathcal{S}: \quad y(t) = G_0(z)u(t) + \underbrace{H_0(z)e(t)}_{=v(t)} \tag{E.1}$$

où $v(t) = H_0(z)e(t)$ est la perturbation agissant dans le système. Dans (E.1), $e(t)$ est un bruit blanc ayant variance σ_e^2 et $G_0(z)$ et $H_0(z)$ sont des fonctions de transfert stables. De plus, on présume que $H_0(z)$ soit aussi inversement stable et monique. L'Identification des Systèmes nous permet d'obtenir un modèle pour ce ceci-dit *système-réel* (*true system*) à partir des données d'entrée et sortie.

Dans cette thèse, nous considérions l'identification du système (E.1) dans le cadre *Prediction Error* [1] (erreur de prédiction). Dans ce cadre, nous avons besoin de définir la structure du modèle, dans laquelle les modèles de $G_0(z)$ et $H_0(z)$ seront identifiés. Une structure du modèle $\mathcal{M}$ est un ensemble de fonctions de transfert d'ordre fixé, paramétrées par un vecteur des paramètres θ: $\mathcal{M} = \{G(z, \theta), H(z, \theta) \mid \theta \in \mathbf{R}^k\}$. Dans cette thèse, on présume que la structure du modèle $\mathcal{M}$ ait été choisie tel qu'elle soit suffisamment riche pour contenir le système réel $\mathcal{S} = \{G_0(z) \ H_0(z)\}$ (structure du modèle d'ordre plein ou *full-order model structure*) et qu'elle soit identifiable: $\mathcal{M}$ est tel qu'il exists un ceci-dit vecteur des paramètres réels $\theta_0 \in \mathbf{R}^k$ tel que $G_0(z) = G(z, \theta_0)$ et $H_0(z) = H(z, \theta_0)$ et que ce vecteur des paramètres θ_0 soit unique.

Nous identifierons le système réel (E.1) dans une structure du modèle (d'ordre plein) du type BJ:

$$\mathcal{M} = \{G(z, \theta) = G(z, \rho), \ H(z, \theta) = H(z, \zeta) \mid \theta = (\rho^T, \zeta^T)^T \in \mathbf{R}^k\} \tag{E.2}$$

$$G(z, \theta) = \frac{z^{-n_k} \left(b_0 + b_1 z^{-1} + \cdots + b_{n_b} z^{-n_b} \right)}{1 + f_1 z^{-1} + \cdots + f_{n_f} z^{-n_f}}$$

$$H(z, \theta) = \frac{1 + c_1 z^{-1} + \cdots + c_{n_c} z^{-n_c}}{1 + d_1 z^{-1} + \cdots + d_{n_d} z^{-n_d}}$$

avec $\theta = (\rho^T, \zeta^T)^T \in \mathbf{R}^k$ avec $\rho = (b_0, \ldots, b_{n_b}, f_1, \ldots, f_{n_f})^T$ et $\zeta = (c_1, \ldots, c_{n_c}, d_1, \ldots, d_{n_d})^T$. Nous indiquerons par k_G (resp. k_H) la dimension de ρ (resp. ζ) et nous avons donc $k_G = n_b + n_f + 1$, $k_H = n_c + n_d$ et $k = k_G + k_H$. L'utilisateur peut choisir librement les ordres n_b, n_f, n_c et n_d et aussi le retard n_k.

Si nous appliquons à (E.1) la séquence $\{u(t) \mid t = 1, \ldots, N\}$ ayant spectre Φ_u et nous collectons la sortie correspondante $\{y(t) \mid t = 1, \ldots, N\}$, nous pouvons obtenir une estimation $\hat{\theta}_N = (\hat{\rho}_N^T, \hat{\zeta}_N^T)^T$ de $\theta_0 = (\rho_0^T, \zeta_0^T)^T$ en utilisant le critère dit *Prediction Error*:

$$\hat{\theta}_N = \arg \min_{\theta} \frac{1}{N} \sum_{t=1}^{N} \epsilon^2(t, \theta) \tag{E.3}$$

où $\epsilon(t, \theta)$ est le ceci-dit erreur de prédiction:

$$\epsilon(t, \theta) = H^{-1}(z, \theta) \left(y(t) - G(z, \theta) u(t) \right) \tag{E.4}$$

Si u est *informative* par rapport à la structure du modèle choisi, [48], cette estimation $\hat{\theta}_N$ est distribuée (asymptotiquement) normalement autour de θ_0, avec matrice de covariance $P_\theta(\theta_0, \Phi_u)$. Dans le cas d'une identification en boucle ouvert dans une structure du modèle du type BJ, P_θ est soumise à une structure diagonale à blocs [8, 50]:

$$P_\theta = \begin{pmatrix} P_\rho & \mathbf{0} \\ \mathbf{0} & P_\zeta \end{pmatrix} \tag{E.5}$$

et l'inverse des blocs diagonaux est donnée par:

$$P_\rho^{-1}(\theta_0, \Phi_u) = \frac{N}{\sigma_e^2} \frac{1}{2\pi} \int_{-\pi}^{\pi} F_{u,\rho}(e^{j\omega}, \theta_0) F_{u,\rho}^*(e^{j\omega}, \theta_0) \Phi_u(\omega) \, d\omega \tag{E.6}$$

$$P_\zeta^{-1}(\theta_0) = N \frac{1}{2\pi} \int_{-\pi}^{\pi} F_{e,\zeta}(e^{j\omega}, \theta_0) F_{e,\zeta}^*(e^{j\omega}, \theta_0) \, d\omega \tag{E.7}$$

avec

$$F_{u,\rho}(z, \theta) = H^{-1}(z, \zeta) \frac{\partial G(z, \rho)}{\partial \rho} \quad \text{et} \quad F_{e,\zeta}(z, \theta) = H^{-1}(z, \zeta) \frac{\partial H(z, \zeta)}{\partial \zeta} \tag{E.8}$$

Notez que les notations $P_\rho(\theta_0, \Phi_u)$ et $P_\zeta(\theta_0)$ sont utilisées pour souligner que la matrice de covariance de $\hat{\rho}_N^T$ est une fonction de θ_0 et Φ_u et que cela de $\hat{\zeta}_N^T$ est une fonction de θ_0 seul. Nous utiliserons aussi la notation $P_\theta(\theta_0, \Phi_u)$ pour la matrice de covariance entière (E.5).

Dans la suite, on suppose qu'une première expérience d'identification ait livré une estimation initiale $\hat{\theta}_{init} = (\hat{\rho}_{init}^T, \hat{\zeta}_{init}^T)^T$ avec matrice de covariance $P_{\theta,init}$. Par conséquence, l'ellipsoïde U_{init} suivante est une région de confiance au $\eta\%$ pour le vrai vecteur inconnu des paramètres θ_0:

$$U_{init} = \left\{ \theta \mid (\theta - \hat{\theta}_{init})^T P_{\theta,init}^{-1}(\theta - \hat{\theta}_{init}) \leq \chi \right\} \tag{E.9}$$

avec χ tel que $Pr(\chi^2(k) \leq \chi) = \eta$ (e.g. 95 %). L'ellipsoïde U_{init} peut être utilisée comment une description de l'incertitude de l'estimation initiale $\hat{\theta}_{init}$ et, à partir de maintenant, nous présumons que θ_0 appartienne en effet à l'ellipsoïde U_{init}, construite à partir de l'estimation initiale $\hat{\theta}_{init}$ et sa matrice de covariance $P_{\theta,init}$.

Nous présumerons que la precision $P_{\rho,init}^{-1}$ de $\hat{\rho}_{init}$ ne soit pas suffisante pour l'objectif du modèle identifié ($P_{\rho,init} = (I_{k_G} \; \mathbf{0})P_{\theta,init}(I_{k_G} \; \mathbf{0})^T$). Nous jugerons suffisamment précise une estimation de ρ_0 quand l'inverse de sa matrice de covariance satisfait $P_\rho^{-1} \geq R_{adm,\rho}$ pour une matrice définie positive $R_{adm,\rho} \in \mathbf{R}^{k_G \times k_G}$ donnée.

Afin d'obtenir une telle estimation suffisamment précise, nous nécessitons de réaliser une deuxième expérience qui livre une nouvelle estimation $\hat{\theta}_N = (\hat{\rho}_N^T, \hat{\zeta}_N^T)^T$ de θ_0 ayante matrice de covariance P_θ. On peut donc combiner l'information sur θ_0 contenue dans les estimations $\hat{\theta}_N$ et $\hat{\theta}_{init}$, en utilisant l'estimateur suivant:

$$\hat{\theta}_{final} = (P_\theta^{-1} + P_{\theta,init}^{-1})^{-1} \left(P_\theta^{-1}\hat{\theta}_N + P_{\theta,init}^{-1}\hat{\theta}_{init} \right)$$

laquelle matrice de covariance est donnée par $(P_\theta^{-1} + P_{\theta,init}^{-1})^{-1}$ [1, page 464]. L'estimation $\hat{\theta}_{final}$ peut être fractionnée dans $\hat{\theta}_{final} = (\hat{\rho}_{final}^T, \hat{\zeta}_{final}^T)^T$ et l'inverse de la matrice de covariance $P_{\rho,final}$ de $\hat{\rho}_{final}$ a donc l'expression suivante:

$$P_{\rho,final}^{-1} = P_\rho^{-1}(\theta_0, \Phi_u) + P_{\rho,init}^{-1}$$

avec Φ_u le spectre du signal d'entrée utilisé pendant la deuxième expérience. Par conséquent, il faut que le spectre de l'entrée Φ_u soit conçu afin de garantir que $P_{\rho,final}^{-1} = P_\rho^{-1}(\theta_0, \Phi_u) + P_{\rho,init}^{-1} \geq R_{adm,\rho}$.

Dans la suite, ça sera important de faire l'observation suivante et la supposition suivante:

Observation E.1. *Dans la structure du modèle BJ (E.2), $G(z, \theta)$ et $H(z, \theta)$ sont des fonctions rationnelles du vecteur des paramètres θ. Par conséquence, il est possible de les exprimer dans la façon suivante:*

$$G(z, \theta) = \frac{Z_N(z)\theta}{1 + Z_D(z)\theta} \tag{E.10}$$

$$H(z, \theta) = \frac{1 + Z_{N,H}(z)\theta}{1 + Z_{D,H}(z)\theta} \tag{E.11}$$

où $Z_N(z)$, $Z_D(z)$, $Z_{N,H}(z)$ et $Z_{D,H}(z)$ sont des vecteurs ligne de fonctions de transfert. ∎

Supposition E.1. L'incertitude U_{init} définie dans (E.9) est suffisamment petite pour garantir que, comment $G(z, \theta_0)$ et $H^{-1}(z, \theta_0)$, $G(z, \theta)$ et $H^{-1}(z, \theta)$ soient des fonctions de transfert stables pour tous les $\theta \in U_{init}$. En raison de (E.8), cela implique aussi que $F_{u,\rho}(z, \theta)$ est un vecteur de fonctions de transfert stables pour tous les $\theta \in U_{init}$. ∎

E.2.2 Robust optimal experiment design

Le spectre Φ_u de la susmentionnée deuxième expérience sera celui-là qu'il aboutit au moindre cout d'identification $\mathcal{J}(\theta_0, \Phi_u)$, en garançant au même temps que $P_\rho^{-1}(\theta_0, \Phi_u) + P_{\rho,init}^{-1} \geq R_{adm}$. La définition du cout dépends de la configuration dans laquelle on effectue l'expérience. Nous supposons que N a été préalablement fixé and nous définissons le cout comme la perturbation induite par le signal d'excitation u. Pour un système comme (E.1), la perturbation induite par u peut être mesurée par une combinaison linéaire de la puissance du signal d'entrée et de la puissance de $\breve{y}(t) = G(z, \theta_0)u(t)$:

$$\mathcal{J}(\theta_0, \Phi_u) = \frac{1}{2\pi} \int_{-\pi}^{\pi} \left(1 + \beta \left| G(e^{j\omega}, \theta_0) \right|^2 \right) \Phi_u(\omega) \, d\omega \tag{E.12}$$

où β est un facteur de pondération choisi par l'utilisateur .Comme tous les autres problèmes de conception optimale de l'expérience, le susmentionné problème d'optimisation malheureusement dépend du vecteur inconnu des paramètres réels via $\mathcal{J}(\theta_0, \Phi_u)$ et $P_\rho^{-1}(\theta_0, \Phi_u)$. Comme mentionné dans l'introduction, l'approche classique de traiter avec ce problème du type ceci-dit *chicken-and-egg* est de remplacer le vrai vecteur de paramètres inconnu θ_0 avec son estimation initiale $\hat{\theta}_{init}$. Cela conduit au problème d'optimisation suivant:

$$\min_{\Phi_u^{\hat{\theta}_{init}}} \mathcal{J}(\hat{\theta}_{init}, \Phi_u^{\hat{\theta}_{init}}) \tag{E.13}$$

$$\text{tel que } P_\rho^{-1}(\hat{\theta}_{init}, \Phi_u^{\hat{\theta}_{init}}) + P_{\rho,init}^{-1} \geq R_{adm,\rho} \tag{E.14}$$

Cette approche a deux inconvénients principaux. Si on dénote par $\Phi_{u,opt}^{\hat{\theta}_{init}}$ la solution de (E.13)-(E.14), le cout réel $\mathcal{J}(\theta_0, \Phi_{u,opt}^{\hat{\theta}_{init}})$ de l'identification peut être sous-estimé par $\mathcal{J}(\hat{\theta}_{init}, \Phi_{u,opt}^{\hat{\theta}_{init}})$. En autre, $\Phi_{u,opt}^{\hat{\theta}_{init}}$ peut amener à une matrice de covariance $P_\rho^{-1}(\theta_0, \Phi_{u,opt}^{\hat{\theta}_{init}})$ pour laquelle $P_\rho^{-1}(\theta_0, \Phi_{u,opt}^{\hat{\theta}_{init}}) + P_{\rho,init}^{-1} \geq R_{adm}$ n'est pas respecté.

L'approche robuste pour la conception optimale de l'expérience a été introduit afin d'accroître les garanties de la conception de l'expérience, en tenant en compte non seulement de l'estimation initiale $\hat{\theta}_{init}$ de θ_0, mais aussi de l'incertitude U_{init} [20, 22].

Le problème de la conception optimale robuste de l'expérience est défini comment:

$$\min_{\Phi_u, \; \gamma} \gamma \tag{E.15}$$

$$\text{tel que } \mathcal{J}(\theta, \Phi_u) \leq \gamma \quad \forall \theta \in U_{init} \tag{E.16}$$

$$\text{et } P_\rho^{-1}(\theta, \Phi_u) + P_{\rho,init}^{-1} \geq R_{adm,\rho} \quad \forall \theta \in U_{init} \tag{E.17}$$

Si on dénote par $\Phi_{u,opt}^{orig}$ et γ_{opt}^{orig} la solution de ce problème d'optimisation, on a que $\gamma_{opt}^{orig} = \sup_{\theta \in U_{init}} \mathcal{J}(\theta, \Phi_{u,opt}^{orig})$. En outre, le spectre $\Phi_{u,opt}^{orig}$ est, par construction, le spectre menant au moindre valeur de $\sup_{\theta \in U_{init}} \mathcal{J}(\theta, \Phi_u)$, en garançant au même temps la contrainte faite robuste de précision (E.17). Puisque nous présumons que $\theta_0 \in U_{init}$, cette formulation robuste assure que:

- le cout a-priori inconnu $\mathcal{J}(\theta_0, \Phi_{u,opt}^{orig})$ soit plus faible que γ_{opt}^{orig}

- $P_\rho(\theta_0, \Phi_{u,opt}^{orig})$ aie la garantie de satisfaire $P_\rho^{-1}(\theta_0, \Phi_{u,opt}^{orig}) + P_{\rho,init}^{-1} \geq R_{adm,\rho}$.

Notez que ces avantages propres de l'approche robuste ont une contrepartie. Puisque $\Phi_{u,opt}^{orig}$ doit satisfaire (E.16) et (E.17) pour tous les $\theta \in U_{init}$ et non seulement pour $\hat{\theta}_{init}$, le spectre $\Phi_{u,opt}^{orig}$ sera plus *grand* que $\Phi_{u,opt}^{\hat{\theta}_{init}}$ (i.e., la solution de (E.13)-(E.14)) et, par conséquent, nous aurons que $\mathcal{J}(\theta_0, \Phi_{u,opt}^{orig}) > \mathcal{J}(\theta_0, \Phi_{u,opt}^{\hat{\theta}_{init}})$ dans la majorité des cas.

Comme déjà mentionné précédemment dans la Section E.1, le problème d'optimisation (E.15)-(E.17) a été abordé par l'utilisation d'un approche de type gridding jusqu'à maintenant (voir e.g. [8, 3, 20]). Cette approche amène à un problème d'optimisation laquelle solution $\gamma_{g,opt}$ est une borne inférieure de la solution γ_{opt}^{orig} de (E.15)-(E.17). Pour la même raison, cette approche de type gridding ne peut pas assurer les garanties liées au problème original (E.15)-(E.17). La contribution principale de cette partie de la thèse est la dérivation d'un problème d'optimisation convexe ayant les même garanties du problème original (E.15)-(E.17). À ces fins nous utiliserons les outils de l'analyse de robustesse.

Le problème original de conception optimale robuste de l'expérience (E.15)-(E.17) peut être détendue en un problème d'optimisation convexe si (E.16) et (E.17) peuvent être transformés en deux contraintes linéaires dans les variables de décision Φ_u et γ.

Dans la suite, nous montrerons que nous ne pouvons pas trouver des contraintes linéaires tractables qu'ils soient équivalentes à (E.16) et (E.17), mais nous pouvons en trouver un qu'il implique (E.16) et un autre qu'il implique (E.17). Cela comporte un certain conservatisme. Cependant, si nous résolvons le problème d'optimisation avec ces contraintes alternatives et si on dénote sa solution par γ_{opt} et $\Phi_{u,opt}$, nous avons toujours la garantie que:

1. $P_\rho^{-1}(\theta, \Phi_{u,opt}) + P_{\rho,init}^{-1} \geq R_{adm,\rho} \quad \forall \; \theta \in U_{init}$ et donc $P_\rho^{-1}(\theta_0, \Phi_{u,opt}) + P_{\rho,init}^{-1} \geq R_{adm,\rho}$

2. $\mathcal{J}(\theta_0, \Phi_{u,opt}) \leq \sup_{\theta \in U_{init}} \mathcal{J}(\theta, \Phi_{u,opt}) \leq \gamma_{opt}.$

En autre, nous avons aussi que γ_{opt} est une borne supérieure de γ_{opt}^{orig}, la solution du problème d'optimisation original (E.15)-(E.17).

Nous dériverons ces contraintes tractables alternatives dans le cas où le spectre Φ_u possède une paramétrisation qu'il correspond au spectre d'un signal d'excitation multi-sinusoïdal, ayant fréquences fixées ω_m $(m = 1, \ldots, L)$ mais avec amplitudes arbitraires

$$\Phi_u(\omega) = \pi \sum_{m=1}^{L} c_m \ (\delta(\omega - \omega_m) + \delta(\omega + \omega_m)) \tag{E.18}$$

où $c_m \geq 0$ $(m = 1, \ldots, L)$ sont les coefficients du spectre qu'il faut déterminer par le problème d'optimisation et les L fréquences ω_m $(m = 1, \ldots, L)$ sont choisies afin de couvrir l'intervalle $[0, \ \pi]$. Pour des c_m $(m = 1, \ldots, L)$ donnés, (E.18) peut être réalisé par un signal multisinusoïdal $u(t) = \sum_{m=1}^{L} \sqrt{2c_m} \ sin(\omega_m t + \psi_m)$ avec déphasages ψ_m $(m = 1, \ldots, L)$ arbitraires. En utilisant la particulière parametrisation de Φ_u, la contrainte (E.16) peut être réécrite dans la façon suivante:

$$\sum_{m=1}^{L} c_m \left(1 + \beta \ |G(e^{j\omega_m}, \theta)|^2 \right) \leq \gamma \ \ \forall \ \theta \in U_{init} \tag{E.19}$$

En rassemblant les termes $G(e^{j\omega_m}, \theta)$ $(m = 1, \ldots, L)$ dans $\mathcal{G}(\theta) = (G(e^{j\omega_1}, \theta), G(e^{j\omega_2}, \theta), \ldots, G(e^{j\omega_L}, \theta))^T$, on peut réécrire (E.19) comme:

$$\left(\sum_{m=1}^{L} c_m\right) \ + \ \beta \ \mathcal{G}^*(\theta) \ \bar{C} \ \mathcal{G}(\theta) \leq \gamma \ \ \forall \ \theta \in U_{init} \tag{E.20}$$

avec $\bar{C} = diag(c_1, c_2, \ldots, c_L)$. En utilisant (E.6) et (E.18), on peut aussi réécrire le terme $P_\rho^{-1}(\theta, \Phi_u)$ dans (E.17) dans la façon suivante:

$$P_\rho^{-1}(\theta, \Phi_u) = \frac{N}{2 \ \sigma_e^2} \sum_{m=1}^{L} c_m \left(F_{u,\rho}(e^{j\omega_m}, \theta)F_{u,\rho}^*(e^{j\omega_m}, \theta) + F_{u,\rho}(e^{-j\omega_m}, \theta)F_{u,\rho}^*(e^{-j\omega_m}, \theta)\right)$$

Si on dénote par $F_{u,\rho,i}(z, \theta)$ le $i^{\text{ème}}$ élément du vecteur $F_{u,\rho}(z, \theta)$ et on rassemble les termes $F_{u,\rho,i}(e^{j\omega_m}, \theta)$ $(m = 1, \ldots, L)$ dans des vecteurs complexes $\mathcal{F}_i(\theta)$ $(i = 1, \ldots, k_G)$, de dimension $L \times 1$, définis comme:

$$\mathcal{F}_i(\theta) = (F_{u,\rho,i}(e^{j\omega_1}, \theta), F_{u,\rho,i}(e^{j\omega_2}, \theta), \ldots, F_{u,\rho,i}(e^{j\omega_L}, \theta))^T \tag{E.21}$$

on peut réécrire $P_\rho^{-1}(\theta, \Phi_u)$ comme:

$$P_\rho^{-1}(\theta, \Phi_u) = \frac{N}{2 \ \sigma_e^2} \sum_{i=1}^{k_G} \sum_{j=1}^{k_G} (m_i \otimes \mathcal{F}_i(\theta))^* \bar{C}(m_j \otimes \mathcal{F}_j(\theta)) + (m_i \otimes \mathcal{F}_j(\theta))^* \bar{C}(m_j \otimes \mathcal{F}_i(\theta))$$

$$\tag{E.22}$$

où m_i $(i = 1, \ldots, k_G)$ est un vecteur unitaire de dimension $1 \times k_G$ lesquelles éléments sont tous égales à zero sauf le $i^{éme}$, qu'il est égal à 1.

Remarque. La particulière structure (E.22) sera déterminante pour développer un assouplissement convexe pour la contrainte robuste de précision (E.17). Puisque l'inverse $P_\zeta^{-1}(\theta_0)$ de la matrice de covariance de $\hat\zeta_N$ (voir (E.7)) ne peut pas être réécrite dans une structure similaire, on ne peut pas utiliser les mêmes outils de l'analyse de robustesse pour robustifier une contrainte de précision basée sur cette partie de la matrice de covariance.

E.2.3 Attaquer la contrainte robuste sur le cout en utilisant les outils de l'analyse de robustesse

Nous commencerons par la dérivation d'une alternative tractable pour (E.19)-(E.20). Les contraintes (E.19)-(E.20) sont en effet équivalentes à (E.16) quand pour Φ_u on utilise la paramétrisation (E.18). Un point important vers l'élaboration de cet résultat est la réécriture de $\mathcal{G}(\theta)$ dans le cadre LFT (Linear Fractional Transformation) [52].

Linear Fractional Transformation

Observons d'abord que, du fait de l'Observation E.1, $\breve{y}(t) = G(z,\theta)u(t)$ peut s'écrire comme la LFT suivante dans θ, incluant le signal scalaire interne $q(t)$ et le vecteur interne de signaux $p(t)$:

$$p(t) = \theta \ q(t) \ \ \text{et} \ \ \begin{pmatrix} q(t) \\ \breve{y}(t) \end{pmatrix} = \underbrace{\begin{pmatrix} -Z_D(z) & 1 \\ Z_N(z) & 0 \end{pmatrix}}_{M_G(z)} \begin{pmatrix} p(t) \\ u(t) \end{pmatrix} \tag{E.23}$$

Rappelons maintenant que la transformée de Fourier $\breve{y}(e^{j\omega})$ de $\breve{y}(t) = G(z,\theta)u(t)$ est égale à $G(e^{j\omega}, \theta)$ quand $u(t)$ est égal à un signal impulsionnel $\delta(t)$ (i.e. $u(e^{j\omega}) = 1$). Par conséquent, la réponse en fréquence $G(e^{j\omega}, \theta)$ de $G(z,\theta)$ à une fréquence donnée ω peut également être déduite en résolvant pour $\breve{y}(e^{j\omega})$ le système d'équations suivant:

$$p(e^{j\omega}) = \theta \ q(e^{j\omega}) \ \ \text{et} \ \ \begin{pmatrix} q(e^{j\omega}) \\ \breve{y}(e^{j\omega}) \end{pmatrix} = M_G(e^{j\omega}) \begin{pmatrix} p(e^{j\omega}) \\ 1 \end{pmatrix} \tag{E.24}$$

Notez que, dans ce système d'équations, toutes les transformations de Fourier sont bien définies pour tous les $\theta \in U_{init}$ en raison de la Supposition E.1.

Selon le même raisonnement, le vecteur $\mathcal{G}(\theta)$, qui contiens la réponse en fréquence de $G(z,\theta)$ aux fréquences présentes dans le spectre (E.18), peut être déterminé en

résolvant pour $\bar{y}$ le système d'équations (E.25) obtenu utilisant (E.24):

$$\bar{p} = (I_L \otimes \theta) \ \bar{q} \qquad \text{et}$$
$$\left(\begin{array}{c} \bar{q} \\ \bar{y} \end{array} \right) = \underbrace{\left(\begin{array}{cc} \bar{M}_{11,\mathcal{G}} & \bar{M}_{12,\mathcal{G}} \\ \bar{M}_{21,\mathcal{G}} & \bar{M}_{22,\mathcal{G}} \end{array} \right)}_{\bar{M}_{\mathcal{G}}} \left(\begin{array}{c} \bar{p} \\ 1 \end{array} \right) \qquad \text{(E.25)}$$

avec $\bar{p} = (p^T(e^{j\omega_1}), \ldots, p^T(e^{j\omega_L}))^T$, $\bar{q} = (q(e^{j\omega_1}), \ldots, q(e^{j\omega_L}))^T$ et

$$\bar{M}_{11,\mathcal{G}} = -bdiag(Z_D(e^{j\omega_1}), \ldots, Z_D(e^{j\omega_L}))$$
$$\bar{M}_{12,\mathcal{G}} = (1, \ldots, 1)^T$$
$$\bar{M}_{21,\mathcal{G}} = bdiag(Z_N(e^{j\omega_1}), \ldots, Z_N(e^{j\omega_L}))$$
$$\bar{M}_{22,\mathcal{G}} = \mathbf{0}$$

Set des multipliers lié à la région d'incertitude U_{init}

Puisque nous considérons ici (E.20), le vecteur des paramètres θ dans la LFT pour $\mathcal{G}(\theta)$ est limité à être dans le set d'incertitude U_{init} (voir (E.9)). Dans notre approche, une composante fondamentale pour trouver une alternative tractable pour (E.20) est d'associer un ceci-dit set des multipliers au set U_{init}. En quelques mots, le set des multipliers $\mathcal{A}_n$ que nous considérons ici est une paramétrisation affine explicite des contraintes quadratiques satisfaites par les graphes des signaux q_n et p_n quand $p_n(t) = (I_n \otimes \theta)q_n(t)$ avec $\theta \in U_{init}$ (n est un entier arbitraire tel que $n \geq 1$) [29, 30, 31].

Definition E.1. *Considérez le set U_{init} défini dans (E.9) satisfaisant la Supposition E.1. Considérez aussi un entier $n \geq 1$. Nous définissons le set des multipliers $\mathcal{A}_n$ comment un set de matrices Hermitiennes A_n (de dimension $n(k+1) \times n(k+1)$) paramétrées affinement et qu'elles ont la propriété suivante:*

$$\left(\begin{array}{c} I_n \\ I_n \otimes \theta \end{array} \right)^T A_n \left(\begin{array}{c} I_n \\ I_n \otimes \theta \end{array} \right) \geq 0 \quad \forall \theta \in U_{init} \qquad \text{(E.26)}$$

En d'autres termes, $A_n \in \mathcal{A}_n \Longrightarrow$ (E.26).

Il est important de souligner que plus la paramétrisation de l'ensemble des multiplicateurs est étendue, plus le conservatisme évoqué dans la section E.2.2 sera faible [29, 30, 31]. Une paramétrisation extensive de l'ensemble des multiplicateurs correspondant à U_{init} est donnée dans la thèse dans la Proposition 3.1.

Contrainte sur le cout faite robuste

À partir des sets des multipliers $\mathcal{A}_n$ quand $n = L$ et de la représentation LFT (E.25) de $\mathcal{G}(\theta)$, maintenant nous avons tout le nécessaire afin de dériver une contrainte tractable alternative pour (E.20).

Proposition E.1. *Considérez un set initial d'incertitude U_{init} (vois (E.9)) satisfaisant la Supposition E.1 et la contrainte robuste sur le cout (E.20) obtenue quand le spectre Φ_u est paramétré comme dans (E.18). Considérez la représentation LFT (E.25) pour $\mathcal{G}(\theta)$ aussi bien que le set des multipliers $\mathcal{A}_L$ associé avec U_{init} (voir la Définition E.1 et la Proposition 3.1 avec $n = L$). Or, la contrainte (E.20) est réspectée pour un γ donné si on peut trouver une matrice $A_L \in \mathcal{A}_L$ tel que*

$$\mathcal{V}^* \, A_L \, \mathcal{V} + \mathcal{L}^* \, \bar{C} \, \mathcal{L} \leq \begin{pmatrix} \boldsymbol{0} & \boldsymbol{0} \\ \boldsymbol{0} & \frac{\gamma - \left(\sum_{m=1}^{L} c_m\right)}{\beta} \end{pmatrix} \tag{E.27}$$

où $\mathcal{L} = \begin{pmatrix} \bar{M}_{21,\mathcal{G}} & \bar{M}_{22,\mathcal{G}} \end{pmatrix}$ et

$$\mathcal{V} = \begin{pmatrix} \bar{M}_{11,\mathcal{G}} & \bar{M}_{12,\mathcal{G}} \\ I_{kL} & \boldsymbol{0} \end{pmatrix}$$

On observe que l'inégalité de la matrice (E.27) est linéaire en γ, A_L et dans les coefficients c_m ($m = 1, \ldots, L$) présentes dans $\bar{C}$.

Démonstration. Voir le Chapitre 3. ∎

Comme déjà mentionné, dans la Proposition E.1, quand nous parlons de trouver une matrice $A_L \in \mathcal{A}_L$, nous voulons dire plus précisement trouver les paramètres libres dans la structure affine de la matrice A_L (i.e. A_0, $\tilde{A}$, $\tilde{B}$, $\hat{v}_{lr}$ et $\tilde{v}_{lr}$ ($l = 1, \ldots, L$ et $r = 1, \ldots, L$)).

E.2.4   Attaquer la contrainte robuste sur la précision

Nous dérivons ici l'alternative tractable pour la contrainte de précision (E.17), quand la paramétrisation (E.18) est utilisée pour Φ_u. À cette fin, nour prénonos inspiration par ce que nous avons fait pour la contrainte robuste sur le cout. Dans ce cas, $P_\rho^{-1}(\theta, \Phi_u)$ a l'expression donnée dans (E.22) et nous procéderons d'abord à réécrire $\mathcal{F}_i$, dans (E.22), dans le cadre LFT.

Nous observons d'abord que $F_{u,\rho}(z, \theta)$ (voir (E.8)) est une fonction rationnelle de θ en raison de l'Observation E.1. En conséquence, nous pouvons trouver des signaux p_F et q_F tels que $s(t) = F_{u,\rho}(z, \theta)u(t)$ puisse être exprimé comme:

$$p_F = (I_f \otimes \theta) \, q_F \qquad \text{et}$$
$$\begin{pmatrix} q_F \\ s \end{pmatrix} = \underbrace{\begin{pmatrix} M_{11,F} & M_{12,F} \\ M_{21,F} & M_{22,F} \end{pmatrix}}_{M_F(z)} \begin{pmatrix} p_F \\ u \end{pmatrix} \tag{E.28}$$

où $f = 3$ pour une structure de modèle du type BJ (voir L'Annexe B.3). Notez que $f = 2$ dans le cas où $H(z, \theta) = 1$ (structure du modèle de type OE).

En utilisant un raisonnement similaire à celui utilisé dans la Section E.2.3, nous pouvons dériver par (E.28) une expression LFT pour $\bar{s}_i = \mathcal{F}_i(\theta)$ $(i = 1, \ldots, k_G)$ défini dans (E.21). De plus, si nous dénotons $\bar{s} = (\bar{s}_1^T, \bar{s}_2^T, \ldots, \bar{s}_{k_G}^T)^T$:

$$\bar{p}_F = (I_{fL} \otimes \theta) \ \bar{q}_F \qquad \text{et}$$
$$\left(\begin{array}{c} \bar{q}_F \\ \bar{s} \end{array} \right) = \underbrace{\left(\begin{array}{cc} \bar{M}_{11,F} & \bar{M}_{12,F} \\ \bar{M}_{21,F} & \bar{M}_{22,F} \end{array} \right)}_{\bar{M}_F(z)} \left(\begin{array}{c} \bar{p}_F \\ 1 \end{array} \right) \tag{E.29}$$

$$\bar{M}_{11,F} = bdiag(M_{11,F}(e^{j\omega_1}), \ldots, M_{11,F}(e^{j\omega_L}))$$
$$\bar{M}_{12,F} = (M_{12,F}(e^{j\omega_1}), \ldots, M_{12,F}(e^{j\omega_L}))^T$$
$$\bar{M}_{21,F} = (\mathcal{H}_1^T, \ldots, \mathcal{H}_{k_G}^T)^T \quad \bar{M}_{22,F} = (\mathcal{K}_1^T, \ldots, \mathcal{K}_{k_G}^T)^T$$
$$\mathcal{H}_i = bdiag(M_{21,F}^{i:}(e^{j\omega_1}), \ldots, M_{21,F}^{i:}(e^{j\omega_L})) \ \ (i = 1, \ldots, k_G)$$
$$\mathcal{K}_i = (M_{22,F}^i(e^{j\omega_1}), \ldots, M_{22,F}^i(e^{j\omega_L}))^T \ \ (i = 1, \ldots, k_G)$$

où $M_{21,F}^{i:}$ (resp. $M_{22,F}^i$) dénote la ligne $i^{ème}$ de $M_{21,F}$ (resp. l'élément $i^{émé}$ de $M_{22,F}$). Notez que, dans cet système d'équations, tous les éléments sont bien définis pour tous les $\theta \in U_{init}$ grâce à la Supposition E.1.

Nous avons donc le résultat suivant qu'il donne une contrainte tractable alternative pour la contrainte de précision faite robuste (E.17).

Proposition E.2. *Considérez un set initial d'incertitude U_{init} (vois (E.9)) satisfaisant la Supposition E.1 et la contrainte robuste de précision (E.17) obtenue quand le spectre Φ_u est paramétré comme dans (E.18) et où, pour cette raison, $P_\rho^{-1}(\theta, \Phi_u)$ a 'expression donnée dans (E.22). Considérez la LFT (E.29) dans $I_{fL} \otimes \theta$ qui est la représentation LFT pour $\bar{s} = (\mathcal{F}_1(\theta)^T, \mathcal{F}_2(\theta)^T, \ldots, \mathcal{F}_{k_G}(\theta)^T)^T$ et considérez le set des multipliers $\mathcal{A}_{k_G fL}$ associé avec U_{init} (voir la Définition E.1 et la Proposition 3.1 avec $n = k_G fL$). Or, la contrainte (E.17) est réspectée pour un $R_{adm,\rho}$ donné et un $P_{\rho,init}$ donné si on peut trouver une matrice $A_{k_G fL} \in \mathcal{A}_{k_G fL}$ tel que*[5]

$$\frac{N}{2 \sigma_e^2} \sum_{i=1}^{k_G} \sum_{j=1}^{k_G} \left((m_i \otimes \mathcal{X}_i)^* \bar{C}(m_j \otimes \mathcal{X}_j) + (m_i \otimes \mathcal{X}_j)^* \bar{C}(m_j \otimes \mathcal{X}_i) \right) + \ldots$$
$$\ldots + \left((P_{\rho,init}^{-1} - R_{adm,\rho}) \otimes \left(\begin{array}{cc} \mathbf{0} & \mathbf{0} \\ \mathbf{0} & 1 \end{array} \right) \right) - \mathcal{M}^* A_{k_G fL} \mathcal{M} \geq 0 \tag{E.30}$$

où $\mathcal{X}_i = \left(\begin{array}{cc} \mathcal{H}_i & \mathcal{K}_i \end{array} \right)$ $(i = 1, \ldots, k_G)$ et

$$\mathcal{M} = \left(\begin{array}{c} I_{k_G} \otimes \left(\begin{array}{cc} \bar{M}_{11,F} & \bar{M}_{12,F} \end{array} \right) \\ I_{k_G} \otimes \left(\begin{array}{cc} I_{kfL} & \mathbf{0} \end{array} \right) \end{array} \right)$$

---

[5]La matrice faite des zéros et uns dans la deuxiéme ligne de (E.30) a dimension $(fLk+1) \times (fLk+1)$.

On observe que l'inégalité de la matrice (E.30) est linéaire en $A_{k_G f L}$ et dans les coefficients c_m ($m = 1, \ldots, L$) présentes dans $\bar{C}$.

Démonstration. Voir le Chapitre 3. ∎

E.2.5 Formulation convexe du problème de la conception optimale de l'expérience

À partir des Propositions E.1 et E.2, nous pouvons maintenant dériver une formulation convexe pour le problème de conception optimale de l'expérience (E.15)-(E.17). Nous rappelons d'abord les différentes composantes nécessaires pour définir pleinement cet problème d'optimisation convexe. Nous supposons qu'une identification initiale aie livré une estimation initiale $\hat{\theta}_{init}$ du vrai vecteur de paramètres θ_0 avec matrice de covariance $P_{\theta,init}$. Pour une valeur du niveau de confiance η choisie par l'utilisateur, nous pouvons donc définir la valeur de χ qui définit le set d'incertitude U_{init}. Comme utilisateurs, nous pouvons aussi choisir la matrice R_{adm} qui décrit la précision souhaitée, le scalaire β définissant le cout (E.12) de l'expérience et les fréquences ω_m ($m = 1, \ldots, L$) qu'ils seront considérées dans la paramétrisation (E.18) du spectre Φ_u à déterminer. Une fois que les fréquences ω_m ($m = 1, \ldots, L$) ont été choisies, le spectre Φ_u est entièrement défini par les coefficients c_m ($m = 1, \ldots, L$). En utilisant ces ingrédients, nous pouvons maintenant résoudre le problème d'optimisation de LMI suivant [9] qu'il est une formulation convexe pour le problème de la conception optimale robuste d'expérience (E.15)-(E.17):

Formulation LMI *Considérez la paramétrisation (E.18) pour le spectre Φ_u à concevoir. Le problème d'optimisation de LMI a comme variables de décision un scalaire $\gamma > 0$, les coefficients $c_m \geq 0$ ($m = 1, \ldots, L$), une matrice $A_L \in \mathcal{A}_L$ et une matrice $A_{k_G f L} \in \mathcal{A}_{k_G f L}$ (voir la Définition E.1) et il consiste dans la détermination de la valeur la plus petite de γ pour laquelle les contraintes LMI (E.27) et (E.30) sont respectées.*

Comme déjà surligné dans la Section E.2.2, si nous dénotons la solution du problème d'optimisation LMI susmentionné par γ_{opt} et $\Phi_{u,opt}$, γ_{opt} est une borne supérieure pour la solution γ_{opt}^{orig} du problème d'optimisation fait robuste original (E.15)-(E.17) i.e. la moindre valeur du cout qu'il est requis pour garantir la contrainte fait robuste pour la précision (E.17). De plus, γ_{opt} ets un borne supérieure pour $\sup_{\theta \in U_{init}} \mathcal{J}(\theta, \Phi_{u,opt})$ et, puisque nous supposons que $\theta_0 \in U_{init}$, nous avons les garanties suivantes:

1. $P_\rho^{-1}(\theta_0, \Phi_{u,opt}) + P_{\rho,init}^{-1} \geq R_{adm,\rho}$

2. $\mathcal{J}(\theta_0, \Phi_{u,opt}) \leq \gamma_{opt}$.

E.2.6 Résumé

Dans le Chapitre correspondant à cette Section, nous avons présenté un assouplissement convexe qui permet de faire robuste le problème de la conception optimale *least costly* d'expérience, en utilisant un set initial d'incertitude pour le vrai vecteur inconnu de paramètres θ_0. Cette robustification[6] est obtenue en utilisant les outils de l'analyse de robustesse, tout en limitant notre attention à un signal d'excitation multisinusoïdal. Cette approche est capable d'assurer que la nouvelle expérience conduira à une estimation ayant la précision souhaitée. En outre, en utilisant notre approche, la solution du problème d'optimisation donne un cout optimal, qu'il est assuré d'être une borne supérieure du cout de l'expérience réelle.

E.3 Expérience *least costly* pour l'identification d'un module dans un réseau dynamique.

E.3.1 Description de la configuration du réseau

Nous considérons un réseau composé de N_{mod} systèmes SISO $\mathcal{S}_i$ $(i = 1, \ldots, N_{mod})$ fonctionnant en boucle fermée avec un contrôleur décentralisé SISO K_i $(i = 1, \ldots, N_{mod})$:

$$\mathcal{S}_i : \ y_i(t) = G_{0,i}(z)u_i(t) + v_i(t) \tag{E.31}$$

$$u_i(t) = K_i(z)(y_{ref,i}(t) - y_i(t)) \tag{E.32}$$

où le signal u_i est l'entrée appliquée au système $\mathcal{S}_i$ et y_i est la sortie mesurée. Cette sortie est constituée d'une contribution de l'entrée u_i et d'un terme de perturbation $v_i(t) = H_{0,i}(z)e_i(t)$ qui représente à la fois les bruits de processus et de mesure. Les différents systèmes $\mathcal{S}_i$ $(i = 1, \ldots, N_{mod})$ sont donc décrits par deux fonctions de transfert stables $G_{0,i}(z)$ et $H_{0,i}(z)$, cette dernière étant également à phase minimale et monique. Pour la suite, il sera important de supposer que ces fonctions de transfert sont paramétrées par un vrai vecteur de paramètres inconnu $\theta_{0,i} \in \mathbf{R}^{n_{\theta_i}}$ dans une structure de modèle connue: $G_{0,i}(z) = G_i(z, \theta_{0,i})$ et $H_{0,i}(z) = H_i(z, \theta_{0,i})$. Pour chaque i $(i = 1, \ldots, N_{mod})$, le signal e_i $(i = 1, \ldots, N_{mod})$ définissant v_i est un signal de bruit blanc de variance moyenne zéro $\sigma_{e_i}^2$ et ces signaux de bruit blanc e_i sont, pour des raisons de simplicité, supposés être mutuellement indépendants. Le signal de référence $y_{ref,i}$ sera calculé sur la base des sorties mesurées des modules voisins (voir plus loin). Nous pouvons réécrire les équations ci-dessus comme suit:

$$\bar{y}(t) = \bar{G}(z, \theta_0)\bar{u}(t) + \bar{H}(z, \theta_0)\bar{e}(t) \tag{E.33}$$

$$\bar{u}(t) = \bar{K}(z)(\bar{y}_{ref}(t) - \bar{y}(t)) \tag{E.34}$$

où $\bar{y} = (y_1, \ldots, y_{N_{mod}})^T$ et $\bar{u}$, $\bar{e}$, $\bar{y}_{ref}$ sont définis de manière similaire et où $\theta_0 = (\theta_{0,1}^T, \ldots, \theta_{0,N_{mod}}^T)^T \in \mathbf{R}^{n_\theta}$ concatène les vrais vecteurs de paramètres $\theta_{0,i}$ $(i = 1, \ldots, N_{mod})$. Dans ces équations, nous utilisons également la notation $\bar{G} = diag(G_1, \ldots, G_{N_{mod}})$ ($\bar{H}$

---

[6]Façon de faire robuste.

et $\bar{K}$ sont définis de manière similaire).

Les systèmes en boucle fermée décrits dans (E.33)-(E.34) sont interconnectés par l'équation suivante:

$$\bar{y}_{ref}(t) = \mathcal{A} \ \bar{y}(t) \ + \ \mathcal{B} \ ref_{ext}(t) \tag{E.35}$$

où la matrice $\mathcal{A}$ et le vecteur $\mathcal{B}$ représentent le flux d'informations dans le réseau et ref_{ext} est un signal de référence externe (scalaire) qui doit être suivi par toutes les sorties y_i et qui n'est généralement disponible qu'à un seul noeud du réseau. Ce type d'interconnexions est typique des systèmes de contrôle de formation ou des systèmes multi-agents (voir par exemple [40, 41]).

Pour illustrer (E.35), considérons le réseau représenté dans la Figure E.1. Dans ce réseau, nous avons des systèmes/modules $N_{mod} = 6$, tous de la forme (E.31) et tous exploités comme dans (E.32) avec un contrôleur décentralisé K_i (voir la Figure E.2). L'objectif de ce réseau est que les sorties y_i de tous les modules suivent la référence externe ref_{ext} même si cette référence n'est disponible qu'au nœud 1. À cette fin, un certain nombre de nœuds sont autorisés à échanger des informations (c'est-à-dire leur sortie mesurée) avec d'autres nœuds voisins.
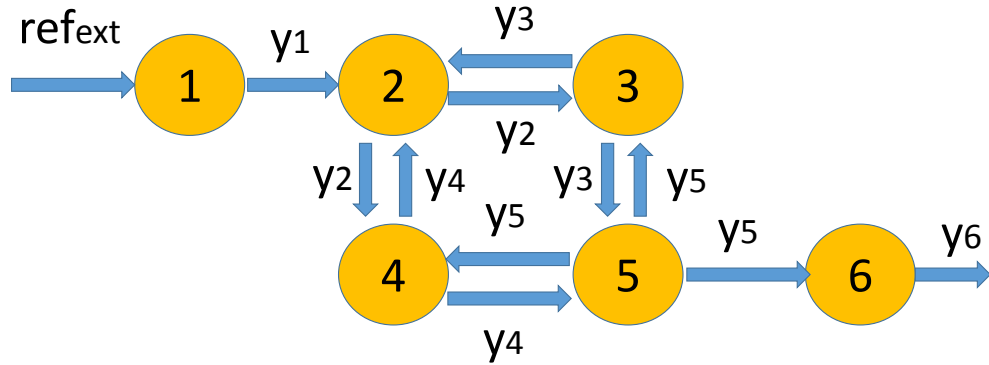
Figure E.1: Exemple de représentation par graphe du réseau, chaque cercle représente un nœud i et les flèches représentent les connexions de communications entre les nœuds.

Le signal de référence $y_{ref,i}$ du nœud i sera calculé comme une combinaison linéaire des informations reçues au nœud i. Pour le nœud 5, $y_{ref,5}$ sera donc une combinaison linéaire de y_3 et y_4. Plus précisément, pour toutes les sorties y_i afin de pouvoir suivre
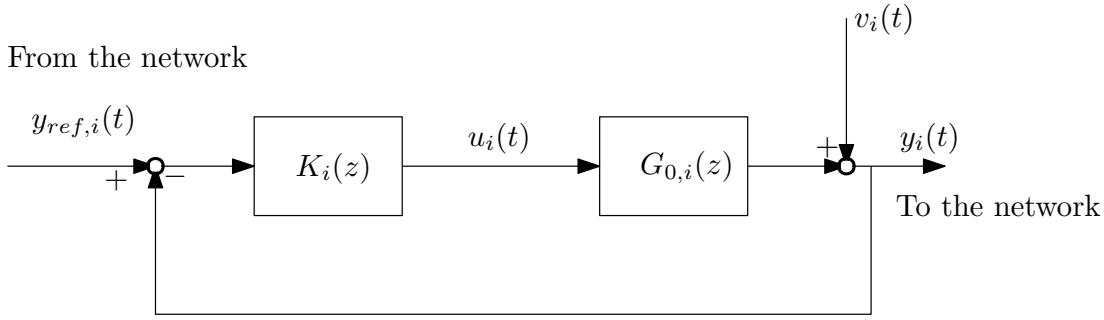
Figure E.2: Représentation d'un module/nœud simple i.

la référence externe ref_{ext}, $\mathcal{A}$ et $\mathcal{B}$ in (E.35) sont généralement choisis comme [40, 41]:

$$
\mathcal{A} = \left(\begin{array}{cccccc} 0 & 0 & 0 & 0 & 0 & 0 \\ 1/3 & 0 & 1/3 & 1/3 & 0 & 0 \\ 0 & 0.5 & 0 & 0 & 0.5 & 0 \\ 0 & 0.5 & 0 & 0 & 0.5 & 0 \\ 0 & 0 & 0.5 & 0.5 & 0 & 0 \\ 0 & 0 & 0 & 0 & 1 & 0 \end{array} \right) \qquad \mathcal{B} = \left(\begin{array}{c} 1 \\ 0 \\ 0 \\ 0 \\ 0 \\ 0 \end{array} \right).
$$

La matrice $\mathcal{A}$ est appelée la matrice de adjacence normalisée dans la littérature [40]. Si les différentes boucles $[K_i \ G_i]$ sont conçues pour rendre l'erreur de suivi $y_{ref,i} - y_i$ aussi faible que possible, il peut être prouvé qu'une telle interconnexion permet un bon suivi de ref_{ext} à tous les nœuds [41, 40]. Une matrice de contiguïté normalisée peut être définie pour tout flux d'informations à l'aide des règles suivantes. La ligne i de $\mathcal{A}$ est égale à zéro si aucune sortie n'est envoyée au nœud i. Si y_i est envoyé au nœud j, l'entrée (j, i) de $\mathcal{A}$ sera non nulle. Enfin, toutes les entrées non nulles d'une ligne sont égales et s'additionnent pour donner un.

Nous devons également introduire la notion de *chemin (dirigé)* entre deux nœuds. Il existe un chemin du nœud i au nœud j si $\mathcal{A}_{ji} \neq 0$ ou nous pouvons trouver un ensemble de nœuds intermédiaires ζ décrits par les index $\{n_1, \ldots, n_\zeta\}$ such that $\mathcal{A}_{n_1 i} \neq 0$, $\mathcal{A}_{n_2 n_1} \neq 0$, $\ldots$, $\mathcal{A}_{j n_\zeta} \neq 0$. En utilisant cette notion de chemin, Définition E.2 introduit deux ensembles d'index pour chaque noeud du réseau:

Definition E.2. *Considérons un nœud arbitraire d'un réseau contenant N_{mod} nœuds, disons le nœud j ($j = 1, \ldots, N_{mod}$). Pour ce nœud, nous définissons l'ensemble $\mathcal{P}_j$ comme un ensemble des indexes des nœuds. Un certain index $i \neq j$ appartient à $\mathcal{P}_j$ s'il existe un chemin du nœud j au nœud i. De même, pour le même nœud j, nous définissons également l'ensemble $\mathcal{L}_j$. Un certain index $i \neq j$ appartient à $\mathcal{L}_j$ s'il existe un chemin du nœud i au nœud j.*

Par exemple, $\mathcal{P}_5 = \{2, 3, 4, 6\}$ et $\mathcal{L}_5 = \{1, 2, 3, 4\}$ pour le réseau de la Figure E.1. Pour la suite, il est important de noter les faits suivants. Si un signal externe (par exemple, la perturbation v_i ou un signal d'excitation r) est ajouté au nœud j, ce signal externe

influencera également tous les nœuds i avec $i \in \mathcal{P}_j$. Inversement, le nœud j sera influencé par tous les signaux externes ajoutés dans les nœuds i avec $i \in \mathcal{L}_j$.

Dans la suite, nous supposerons qu'une procédure d'identification *prediction error* a fourni des estimations initiales $\theta_{init,i}$ de $\theta_{0,i}$ ($i = 1, \ldots, N_{mod}$) et que, par conséquent, toutes ces estimations sont (asymptotiquement) normalement réparties autour de $\theta_{0,i}$ avec une matrice de covariance $P_{init,i}$ [1, 17]. Ces estimations initiales peuvent par exemple être obtenues en utilisant une expérience en boucle ouverte sur chaque système $\mathcal{S}_i$ déconnecté du réseau ou via la procédure d'identification présentée dans [17] (l'expérience est ensuite réalisée dans la configuration du réseau). On peut alors dire que le vecteur concaténé $\theta_{init} = (\theta_{init,1}^T, \ldots, \theta_{init,N_{mod}}^T)^T$ est normalement distribué autour de $\theta_0 = (\theta_{0,1}^T, \ldots, \theta_{0,N_{mod}}^T)^T$ avec une matrice de covariance $P_{init} = bdiag(P_{init,1}, \ldots, P_{init,N_{mod}})$. Sur la base de cette propriété statistique, l'ellipsoïde suivant U_{init} est une région de confiance $\eta\%$ pour le vecteur paramètre inconnu θ_0 :

$$U_{init} := \left\{ \theta \in \mathbf{R}^{n_\theta} \mid (\theta - \theta_{init})^T P_{init}^{-1} (\theta - \theta_{init}) < \chi_\eta \right\} \tag{E.36}$$

où $\theta = (\theta_1^T, \ldots, \theta_{N_{mod}}^T)^T$ et $Pr(\chi^2(n_\theta) < \chi_\eta) = \eta$. Cet ellipsoïde U_{init} peut être considéré comme un set d'incertitude pour le vrai vecteur de paramètres inconnu θ_0. A partir de maintenant, nous supposerons donc que $\theta_0 \in U_{init}$.

Dans la suite, nous supposerons que la précision du modèle obtenue après cette première expérience est satisfaisante pour tous, sauf un nœud, disons le nœud l ($l = 1, \ldots, N_{mod}$). Nous devrons donc réaliser une nouvelle expérience d'identification pour obtenir une meilleure estimation du vecteur de paramètres $\theta_{0,l}$ décrivant ce nœud. Cette expérience est décrite dans la sous-section suivante.

E.3.2 Identification d'un module dans le réseau et cout de l'expérience

cout de l'expérience dans les configurations stealth et non-stealth

Nous souhaitons donc obtenir une meilleure estimation du vecteur de paramètres $\theta_{0,l}$ décrivant le nœud l. Conformément à la philosophie *least costly* cette estimation sera obtenue en réalisant une expérience d'identification dans la configuration originale du réseau tout en limitant autant que possible les perturbations induites par cette expérience sur le fonctionnement normal du réseau. L'expérience est réalisée dans la configuration originale du réseau puisque nous souhaitons maintenir les performances de suivi pendant l'expérience d'identification, c'est-à-dire maintenir les fonctions de transfert entre ref_{ext} et les sorties y_i ($i = 1, \ldots, N_{mod}$) et les fonctions de transfert entre ref_{ext} et les sorties u_i ($i = 1, \ldots, N_{mod}$).

Pendant l'expérience d'identification, nous utilisons un signal d'excitation $r(t)$ du spectre Φ_r et nous appliquons une séquence $\{r(t) \mid t = 1, \ldots, N\}$ de ce signal à la sortie du contrôleur K_l (voir Figure E.3). Cela permet de collecter l'ensemble des
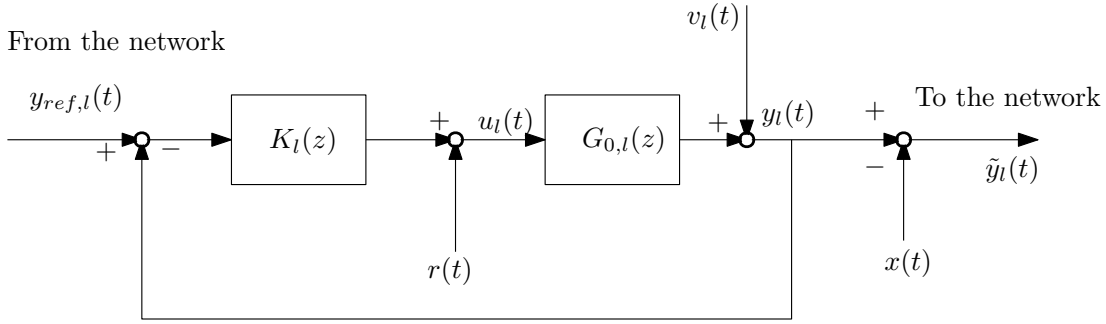
From the network

Figure E.3: Nœud à identifier (c'est-à-dire Nœud l) pendant l'expérience d'identification. Dans la configuration stealth, $x(t)$ est donné par (E.37). Dans la configuration non-stealth, $x(t) = 0$.

données $Z_l^N = \{y_l(t), u_l(t) \mid t = 1, \ldots, N\}$ qui seront utilisées pour l'identification (voir la Section E.3.2). Dans la Figure E.3, on observe également le signal $x(t)$. Ici, nous allons considérer deux choix pour $x(t)$ correspondant à deux configurations/réglages: la configuration stealth et la configuration non-stealth. Dans la configuration non stealth, le signal $x(t)$ sera choisi égal à zéro. Ce choix correspond au réglage classique pour une expérience d'identification dans un contexte de boucle fermée/réseau (voir par exemple [17]). Dans le cadre stealth, $x(t)$ sera choisi comme l'estimation suivante de la contribution de r en y_l:

$$x(t) = \underbrace{\frac{G_l(z, \theta_{init,l})}{1 + K_l(z)G_l(z, \theta_{init,l})}}_{=T_{init,l(z)}} r(t) \quad (t = 1, \ldots, N) \tag{E.37}$$

où $\theta_{init,l}$ est le sous-vecteur de θ_{init} qui correspond à $\mathcal{S}_l$. Notez que (E.37) peut être calculé facilement puisque r et $T_{init,l}(z)$ sont connus.

Comme montré dans la Figure E.3, le signal $x(t)$ est soustrait de la sortie mesurée $y_l(t)$ pour donner $\tilde{y}_l(t) = y_l(t) - x(t)$ qui sera le signal qui sera transmis pour calculer $\bar{y}_{ref}$. Par conséquent, pendant l'expérience d'identification, les équations (E.34)-(E.35) deviennent:

$$\bar{u}(t) = \bar{m}_l \, r(t) + \bar{K}(z) \, (\bar{y}_{ref}(t) - \bar{y}(t)) \tag{E.38}$$
$$\bar{y}_{ref}(t) = \mathcal{A} \, (\bar{y}(t) - \bar{m}_l x(t)) + \mathcal{B} \, ref_{ext}(t) \tag{E.39}$$

où $\bar{m}_i \, (i = 1, \ldots, N_{mod})$ désigne un vecteur d'unité (colonne) de dimension N_{mod} pour lequel l'entrée i-iéme est égale à 1 et les autres entrées sont égales à zéro.

Nous montrerons, dans la suite, l'avantage du cadre stealth afin de réduire le coût de l'expérience d'identification. Pour cela, nous devons définir ce dernier. Considérons d'abord le cadre stealth. Dans ce cas, le vecteur de sortie $\bar{y}$ et le vecteur d'entrée $\bar{u}$

dans la configuration du réseau (E.33)-(E.38)-(E.39) peuvent être réécrits comme suit en fonction des signaux externes r, ref_{ext} et $\bar{e}$:

$$\bar{y}(t) = R^y(z, \theta_0) \; r(t) + R^y_{ext}(z, \theta_0) \; ref_{ext}(t) + S^y(z, \theta_0) \; \bar{e}(t) \tag{E.40}$$

$$\bar{u}(t) = R^u(z, \theta_0) \; r(t) + R^u_{ext}(z, \theta_0) \; ref_{ext}(t) + S^u(z, \theta_0) \; \bar{e}(t) \tag{E.41}$$

pour certains vecteurs de fonctions de transfert R^y_{ext}, R^u_{ext}, certaines matrices de fonctions de transfert S^y, S^u et

$$R^u(z, \theta_0) = \bar{m}_l \; S_{0,l}(z) + \bar{\mathcal{N}}(z, \theta_0) \; (T_{0,l}(z) - T_{init,l}(z)) \tag{E.42}$$

$$R^y(z, \theta_0) = \bar{G}(z, \theta_0) \; R^u(z, \theta_0) \tag{E.43}$$

où $S_{0,l}(z) = 1/(1 + K_l(z)G_l(z, \theta_{0,l}))$ et $T_{0,l}(z) = G_l(z, \theta_{0,l})/(1 + K_l(z)G_l(z, \theta_{0,l}))$ sont des fonctions de transfert scalaires et $\bar{\mathcal{N}}(z, \theta_0)$ est un vecteur de fonctions de transfert:

$$\bar{\mathcal{N}}(z, \theta_0) = \bar{K}(z)\bar{S}(z, \theta_0) \left(I_{N_{mod}} - \mathcal{A}\bar{S}(z, \theta_0)\bar{G}(z, \theta_0)\bar{K}(z) \right)^{-1} \mathcal{A} \; \bar{m}_l$$
$$\bar{S}(z, \theta_0) = \left(I_{N_{mod}} + \bar{G}(z, \theta_0)\bar{K}(z) \right)^{-1} \tag{E.44}$$

Pour la suite, il est important de noter que $T_{init,l}(z)$ (voir (E.37)) est le modèle initial de $T_{0,l}(z)$ qui correspond au paramètre $\theta_{init,l}$. Par conséquent, dans (E.42), $T_{0,l}(z) - T_{init,l}(z)$ est l'erreur de modélisation de ce modèle initial $T_{init,l}(z)$.

Par rapport aux opérations normales (E.33)-(E.34)-(E.35), $\bar{y}$ et $\bar{u}$ sont donc perturbés pendant l'expérience d'identification par $R^y(z)r(t)$ et $R^u(z)r(t)$, respectivement. Par conséquent, il est logique de définir le coût de l'expérience d'identification comme la fonction suivante du spectre Φ_r du signal d'excitation r:

$$\mathcal{J}(\Phi_r, \theta_0) = \frac{1}{2\pi} \int_{-\pi}^{\pi} \left(\left(R^y(e^{j\omega}, \theta_0) \right)^* R^y(e^{j\omega}, \theta_0) + \; \beta \; \left(R^u(e^{j\omega}, \theta_0) \right)^* R^u(e^{j\omega}, \theta_0) \right) \; \Phi_r(\omega) \; d\omega$$
$$\mathcal{J}(\Phi_r, \theta_0) = \frac{1}{2\pi} \int_{-\pi}^{\pi} \mathcal{R}^*(e^{j\omega}, \theta_0)\mathcal{R}(e^{j\omega}, \theta_0) \; \Phi_r(\omega) \; d\omega \tag{E.45}$$

où $\beta > 0$ est un facteur de pondération choisi par l'utilisateur et $\mathcal{R}(z, \theta_0)$ est le vecteur suivant des fonctions de transfert de dimension $2N_{mod}$:

$$\mathcal{R}(z, \theta_0) = \begin{pmatrix} R^y(z, \theta_0) \\ \sqrt{\beta} \; R^u(z, \theta_0) \end{pmatrix} \tag{E.46}$$

Dans le cadre non stealth, le coût $\mathcal{J}(\Phi_r, \theta_0)$ d'une expérience d'identification peut être défini de manière très similaire. Cependant, les expressions pour R^y et R^u qui sont utilisées dans (E.45) ont une expression différente:

$$R^{u,NS}(z, \theta_0) = \bar{m}_l \; S_{0,l}(z) + \bar{\mathcal{N}}(z, \theta_0) \; T_{0,l}(z) \tag{E.47}$$

$$R^{y,NS}(z, \theta_0) = \bar{G}(z, \theta_0) \; R^{u,NS}(z, \theta_0) \tag{E.48}$$

En comparant (E.47) et (E.42), on observe que l'erreur de modélisation $T_{0,l}(z) - T_{init,l}(z)$ est remplacée par $T_{0,l}(z)$ dans l'expression de $R^{u,NS}$.

Le rôle de la compensation stealth $x(t)$ est de réduire autant que possible la propagation de l'influence de l'excitation r (appliquée dans le nœud l) vers les nœuds $i \in \mathcal{P}_l$. Avant d'expliquer cela plus en détail, faisons les suppositions suivantes sur le nœud l et le réseau considéré:

Supposition E.2. Considérons l'ensemble $\mathcal{P}_l$ (voir Définition E.2) correspondant au nœud à identifier l. Nous supposons que $\mathcal{P}_l$ est un ensemble non vide.

Supposition E.3. Considérons l'ensemble $\mathcal{P}_l$ (voir Définition E.2) correspondant au nœud à identifier l et le vecteur de fonctions de transfert $\mathcal{N}(z, \theta_0)$ (voir (E.44)). Nous supposerons que, pour tous les $i \in \mathcal{P}_l$, l'entrée i^{th} $\mathcal{N}_i(z, \theta_0)$ de $\mathcal{N}(z, \theta_0)$ est telle que $\mathcal{N}_i(e^{j\omega}, \theta_0) \neq 0$ pour (presque) toutes les fréquences.

Si $\mathcal{P}_l$ était vide, il n'y aurait bien sûr pas besoin du cadre steatlh puisque le signal r ne serait pas propagé aux autres nœuds. La Supposition E.3 sera en fait toujours valable, sauf dans les cas pathologiques que nous voulons ici exclure formellement.

Nous pouvons maintenant expliquer le rôle de la compensation stealth dans la réduction de la propagation de l'influence de l'excitation r vers les nœuds $i \in \mathcal{P}_l$. Considérons d'abord le cas idéal, c'est-à-dire lorsque $T_{init,l} = T_{0,l}$. Ce choix ne change pas la situation dans le cadre non stealth, c'est-à-dire que $R_i^{u,NS}$ et $R_i^{y,NS}$, le i-ième terme dans $R^{u,NS}$ et $R^{y,NS}$ respectivement, restent les mêmes fonctions de transfert non nulles pour tous les $i \in \mathcal{P}_l$ (elles ne sont pas fonction de $T_{init,l}$). Cependant, dans le cadre stealth, pour tous les $i \neq l$, les fonctions de transfert R_i^u et R_i^y, le i-ième terme dans R^u et R^y respectivement, sont identiques à zéro lorsque $T_{init,l} = T_{0,l}$. Par conséquent, dans ce cas idéal, l'effet de l'excitation $r(t)$ ne se fera sentir que dans le module à identifier.

En pratique, $T_{init,l}$ sera bien sûr toujours différent de $T_{0,l}$, mais la configuration stealth restera bénéfique si $T_{init,l}$ satisfait à une certaine contrainte de précision, donnée dans la Proposition 4.1 de la thèse, qui s'appliquera dans la grande majorité des cas.

Identification of d'un module

Dans la Section E.3.1, nous avons supposé que nous avions obtenu une estimation initiale $\theta_{init} = (\theta_{init,1}^T, \ldots, \theta_{init,N_{mod}}^T)^T$ du vrai vecteur de paramètres $\theta_0 = (\theta_{0,1}^T, \ldots, \theta_{0,N_{mod}}^T)^T$. Comme déjà mentionné à la fin de la Section E.3.1, nous supposerons que nous voulons augmenter la précision de l'estimation[7] $\theta_{init,l}$ du vrai vecteur de paramètres $\theta_{0,l}$ correspondant au Noeud l. La précision de $\theta_{init,l}$ peut être mesurée avec $P_{init,l}^{-1}$, où $P_{init,l}$ est la matrice de covariance de $\theta_{init,l}$. La précision de $\theta_{init,l}$ peut être améliorée en la combinant avec une nouvelle estimation de $\theta_{0,l}$ obtenue en utilisant un ensemble de données $Z_l^N = \{y_l(t), u_l(t) | t = 1, \ldots, N\}$ recueillies comme indiqué dans la Figure E.3

---

[7]Cette estimation $\theta_{init,l}$ est également celle avec laquelle la fonction de transfert $T_{init,l}$, utilisée pour la compensation stealth, est construite.

dans le cadre stealth ou non-stealth.

Nous considérons à cet effet une structure de modèle d'ordre complet $\mathcal{M} = \{G_l(z, \theta_l), H_l(z, \theta_l) \mid \theta_l \in \mathbf{R}^{n_{\theta_l}}\}$ pour $\mathcal{S}_l$. Nous supposons que $\mathcal{M}$ est globalement identifiable à $\theta_{0,l}$, c'est-à-dire que $\theta_l = \theta_{0,l}$ est le seul vecteur de paramètres pour lequel $G_l(z, \theta_l)$ et $H_l(z, \theta_l)$ correspondent à $\mathcal{S}_l$. En d'autres termes, $\mathcal{M}$ satisfait la Supposition E.1 pour le système $\mathcal{S}_l$. Nous supposerons également que le signal d'excitation $r(t)$ (voir la Figure E.3) et le vecteur de bruits blancs $\bar{e}$ (voir (E.33)) ne sont pas corrélés et que $ref_{ext}(t)$ est un signal stationnaire non corrélé avec $r(t)$ et $\bar{e}(t)$. Ensuite, en utilisant la structure du modèle $\mathcal{M}$ et l'ensemble de données $Z_l^N = \{y_l(t), u_l(t) | t = 1, \ldots, N\}$, une estimation $\hat{\theta}_{N,l}$ de $\theta_{0,l}$ peut être obtenue via l'identification *Prediction Error* [1]:

$$
\begin{aligned}
\hat{\theta}_{N,l} &= \arg\min_{\theta_l} \frac{1}{N} \sum_{t=1}^{N} \epsilon^2(t, \theta_l) \quad \text{with:} \\
\epsilon(t, \theta_l) &= H_l^{-1}(z, \theta_l) \left(y_l(t) - G_l(z, \theta_l) u_l(t)\right)
\end{aligned} \tag{E.49}
$$

Comme nous l'avons montré dans la Proposition 4.2 de la thèse, l'estimation (E.49) est une estimation cohérente de $\theta_{0,l}$ dans des conditions souples sur le signal d'excitation $r(t)$.

Nous supposerons dorénavant que l'estimation $\hat{\theta}_{N,l}$ est cohérente. L'estimation $\hat{\theta}_{N,l}$ est alors aussi (asymptotiquement) normalement distribuée autour de $\theta_{0,l}$ avec une matrice de covariance P_{θ_l} qui peut être estimée à partir des données et dont l'inverse a l'expression suivante:

$$
P_{\theta_l}^{-1}(\Phi_r, \theta_0) = M_{\bar{e}}(\theta_0) +
$$
$$
\frac{N}{2\pi\sigma_l^2} \int_{-\pi}^{\pi} F_l(e^{j\omega}, \theta_{0,l}) F_l^*(e^{j\omega}, \theta_{0,l}) \left(|R_l^u(e^{j\omega}, \theta_0)|^2 \Phi_r(\omega) + |R_{ext,l}^u(e^{j\omega}, \theta_0)|^2 \Phi_{ref_{ext}}(\omega)\right) \, d\omega
$$
$$
\tag{E.50}
$$

avec R_l^u et $R_{ext,l}^u$ l'entrée l^{th} de R^u et de R_{ext}^u, respectivement, et avec $\Phi_{ref_{ext}}$ le spectre de puissance de ref_{ext}, $F_l(z, \theta_l) = H_l^{-1}(z, \theta_l) \frac{\partial G_l(z, \theta_l)}{\partial \theta_l}$ et $M_{\bar{e}}(\theta_0)$ la contribution de $\bar{e}$ à la précision de l'estimation. On observe que $P_{\theta_l}^{-1}(\Phi_r, \theta_0)$ est une fonction affine du spectre de puissance Φ_r, du signal d'excitation r, et du spectre de puissance $\Phi_{ref_{ext}}$, de la référence externe ref_{ext}, (et une fonction plus complexe de θ_0). L'équation (E.50) se rapporte à la configuration stealth. Dans la configuration non stealth, nous pouvons utiliser la même expression pour $P_{\theta_l}(\Phi_r, \theta_0)$, mais nous devons remplacer R_l^u par $R_l^{u,NS}$ (voir (E.47)).

Comme nous l'avons fait dans le chapitre E.2, nous pouvons combiner les informations sur $\theta_{0,l}$ contenues dans les estimations $\hat{\theta}_{N,l}$ et $\theta_{init,l}$ en utilisant l'estimateur

suivant $\hat{\theta}_{final,l} = (P_{\theta_l}^{-1} + P_{init,l}^{-1})^{-1} \left(P_{\theta_l}^{-1}\hat{\theta}_{N,l} + P_{init,l}^{-1}\theta_{init,l} \right)$ dont la matrice de covariance est donnée par $(P_{\theta_l}^{-1} + P_{init,l}^{-1})^{-1}$ [1, page 464].

La précision de l'estimation $\hat{\theta}_{final,l}$ peut donc être mesurée avec $P_{\theta_l}^{-1}(\Phi_r,\theta_0)+P_{init,l}^{-1}$. Comme pour la Section E.2, nous supposerons alors que cette précision sera jugée satisfaisante si la contrainte de précision suivante $P_{\theta_l}^{-1}(\Phi_r,\theta_0)+P_{init,l}^{-1} > R_{adm}$ est satisfaite. La matrice R_{adm} est une matrice donnée strictement positive et symétrique qui reflète la précision souhaitée [49, 53].

E.3.3 Problème de la conception optimale de l'expérience

Conformément à la philosophie *least costly*, nous concevrons le spectre Φ_r du signal d'excitation r de l'expérience d'identification de telle sorte que la contrainte de précision $P_{\theta_l}^{-1}(\Phi_r,\theta_0)+P_{init,l}^{-1} > R_{adm}$ soit satisfaite au moindre coût $\mathcal{J}(\Phi_r,\theta_0)$ (voir (E.45)). Ce problème d'optimisation peut donc être formulé comme suit:

$$\min_{\Phi_r} \mathcal{J}(\Phi_r,\theta_0) \tag{E.51}$$

$$\text{tel que} \quad P_{\theta_l}^{-1}(\Phi_r,\theta_0) + P_{init,l}^{-1} \geq R_{adm} \tag{E.52}$$

Ce problème d'optimisation peut être considéré à la fois dans le cadre stealth et dans le cadre non-stealth en utilisant les expressions respectives pour $\mathcal{J}(\Phi_r,\theta_0)$ et pour $P_{\theta_l}^{-1}(\Phi_r,\theta_0)$ dans les deux cas. Cependant, la configuration stealth est, dans la plupart des cases, avantageuse afin d'obtenir la précision requise pour $\mathcal{S}_l$ au moindre cout, comme nous l'avons montré dans la Proposition 4.3 de la thèse.

On observe que, comme des nombreux problèmes de conception optimale de l'expérience, ce problème d'optimisation dépend du vecteur inconnu $\theta_0 = (\theta_{0,1}^T, \ldots, \theta_{0,N_{mod}}^T)^T$. Puisque θ_0 est inconnu, le problème d'optimisation (E.51)-(E.52) ne peut pas être abordé en tant que tel. Comme déjà mentionné à la Section E.2, une approche couramment utilisée pour contourner ce problème consiste à remplacer θ_0 par une estimation initiale. Si nous utilisons l'estimation initiale θ_{init} à cette fin (voir la Section E.3.1), cela donnerait lieu à un problème d'optimisation consistant à minimiser $\mathcal{J}(\Phi_r,\theta_{init})$ sous la contrainte $P_{\theta_l}^{-1}(\Phi_r,\theta_{init})+P_{init,l}^{-1} \geq R_{adm}$. Outre les défauts typiques de cette approche (voir la Section E.2), cette approche classique présente, dans la configuration stealth, un inconvénient encore plus important. Rappelons en effet que $T_{init,l}$ in (E.37) est également calculé sur la base de θ_{init}. Ce dernier a pour conséquence que R_i^u et R_i^y seront considérés comme identiques à zéro pour tous les $i \neq l$. En d'autres termes, la propagation du signal $r(t)$ vers les nœuds i avec $i \in \mathcal{P}_l$ ne sera pas prise en compte dans le problème de la conception optimale de l'expérience si nous remplaçons θ_0 par θ_{init}. Nous allons donc plutôt envisager la formulation suivante, dans laquelle la contrainte de coût a été robustfiée en utilisant la région d'incertitude initiale U_{init} (voir (E.36)):

$$\min_{\Phi_r,\gamma} \gamma \tag{E.53}$$

$$\text{tel que} \quad \mathcal{J}(\Phi_r,\theta) \leq \gamma \quad \forall \theta \in U_{init} \tag{E.54}$$

$$\text{et} \quad P_{\theta_l}^{-1}(\Phi_r,\theta_{init}) + P_{init,l}^{-1} \geq R_{adm} \tag{E.55}$$

Ce problème d'optimisation peut être pris en compte à la fois dans le cadre stealth et dans le cadre non-stealth en utilisant les expressions respectives pour $\mathcal{J}(\Phi_r,\theta)$ et pour $P_{\theta_l}^{-1}(\Phi_r,\theta_{init})$ dans les deux cas.

Contrairement au cas où θ_0 est remplacé par θ_{init}, la formulation ci-dessus prendra également en compte la propagation du signal d'excitation dans le cadre stealth. Dans ce cadre, on observera également une *robustification* de la compensation stealth. En effet, la formulation robustifiée favorisera les spectres Φ_r donnant, pour tous les $\theta \in U_{init}$, des petites perturbations $R_i^u(z,\theta)r(t)$ et $R_i^y(z,\theta)r(t)$ pour $i = l$ et pour $i \in \mathcal{P}_l$ (voir (E.41)-(E.40)). Pour les nœuds $i \in \mathcal{P}_l$, cela signifie par exemple que la puissance du signal suivant doit être rendue faible pour tous les $\theta \in U_{init}$:

$$R_i^u(z,\theta)r(t) = \bar{\mathcal{N}}_i(z,\theta)\left(\frac{G_l(z,\theta)}{1 + K_l(z)G_l(z,\theta)} - T_{init,l}(z)\right)r(t)$$

Par conséquent, le problème de la conception optimale robuste de l'expérience favorisera généralement et entre autres considérations les spectres $\Phi_r(\omega)$ avec plus de contributions dans les gammes de fréquences où la compensation stealth sera plus efficace en raison d'une petite incertitude de $T_{init,l}(z)$ (ce qui *fait robuste* la configuration stealth). Notez que, par souci de simplicité, nous n'avons pas robustifié la contrainte de précision (E.55).

Dans les deux configurations, stealth et non-stealth, le problème de la conception optimale robuste de l'expérience (E.53)-(E.55), a également les propriétés suivantes (voir aussi la Section E.2). Si nous désignons par $\Phi_{r,opt}$ et γ_{opt} la solution de ce problème d'optimisation, nous avons que $\gamma_{opt} = \sup_{\theta \in U_{init}} \mathcal{J}(\Phi_{r,opt},\theta)$. Comme nous supposons que $\theta_0 \in U_{init}$, cette formulation robustifiée garantit que le coût a-priori inconnu $\mathcal{J}(\Phi_{r,opt},\theta_0)$ est inférieur à γ_{opt}. Cela n'aurait pas été le cas si, au lieu de la contrainte robustifiée (E.54), nous avions utilisé la contrainte non robustifiée $\mathcal{J}(\Phi_r,\theta_{init}) \leq \gamma$.

Comme le problème d'optimisation (E.53)-(E.55) peut être considéré pour les configurations stealth et non stealth, la solution du problème d'optimisation dans les deux cas peut être comparée pour vérifier si la configuration stealth entraîne effectivement un coût moindre. Il convient de noter que ce sera généralement le cas puisque, comme expliqué ci-dessus, la formulation robuste impliquera une robustification de la compensation stealth.

E.3.4   Attaquer la contrainte robuste sur le cout dans une façon convexe

Puisque (E.55) est affine dans la variable de décision Φ_r, le problème d'optimisation (E.53)-(E.55) sera convexe si (E.54) peut être transformé en une contrainte linéaire dans les variables de décision Φ_r et γ.

Afin de dériver une contrainte tractable impliquant (E.54), nous devons tenir compte du fait que nous sommes dans le contexte d'un réseau et donc que le vecteur θ peut être de grande dimension. Par conséquent, l'utilisation des résultats de la Section E.2 pour dériver cette contrainte tractable peut conduire à un problème trop complexe du point de vue du calcul. Par conséquent, au lieu de travailler directement sur le vecteur incertain θ comme dans la Section E.2, il est préférable d'envisager l'approche dite hiérarchique. L'approche hiérarchique a en effet été introduite dans [54] pour analyser la robustesse des systèmes à grande échelle (interconnectés). Par conséquent, notre objectif ici sera de déterminer une contrainte tractable impliquant (E.54) et qui peut être utilisée dans le cadre de l'approche hiérarchique.

Pour dériver une telle contrainte linéaire tractable impliquant (E.54), nous supposerons, comme à la Section E.2, que le signal d'excitation à concevoir r est un signal multisinusoïdal, c'est-à-dire $r(t) = \sum_{m=1}^{L} A_m \sin(\omega_m t)$ où les fréquences ω_m $(m = 1, \ldots, L)$ sont fixées par l'utilisateur (comme par exemple une grille fine de la gamme de fréquences $[0. \ \pi]$) et où les amplitudes A_m $(m = 1, \ldots, L)$ seront déterminées de façon optimale. Une telle paramétrisation du signal d'excitation correspond au spectre suivant:

$$\Phi_r(\omega) = \pi \sum_{m=1}^{L} c_m \ \left(\delta(\omega - \omega_m) + \delta(\omega + \omega_m)\right) \geq 0 \ \forall \omega \qquad (E.56)$$

où $c_m = \frac{A_m^2}{2}$ $(m = 1, \ldots, L)$ seront les variables de décision du problème d'optimisation. La positivité de $\Phi_r(\omega)$ pour tous les ω peut être imposée par les contraintes $c_m \geq 0$ $(m = 1, \ldots, L)$ sur ces variables de décision.

En utilisant (E.56) et (E.45), la contrainte de coût robuste (E.54) peut être réécrite comme suit:

$$\sum_{m=1}^{L} c_m \ \left(\mathcal{R}^*(e^{j\omega_m}, \theta)\mathcal{R}(e^{j\omega_m}, \theta)\right) \leq \gamma \qquad \forall \theta \in U_{init} \qquad (E.57)$$

Dans le Chapitre 4 de la thèse, nous avons montré que l'approche hiérarchique peut être utilisée pour déduire, pour chaque ω, une limite supérieure précise $\alpha(\omega)$ pour

$$\mathcal{J}_{wc}(\omega) = \sup_{\theta \in U_{init}} \ \left(\mathcal{R}^*(e^{j\omega}, \theta)\mathcal{R}(e^{j\omega}, \theta)\right) \qquad (E.58)$$

i.e. $\mathcal{J}_{wc}(\omega) \leq \alpha(\omega)$. Cette borne supérieure calculable $\alpha(\omega)$ pour $\mathcal{J}_{wc}(\omega)$ est importante car elle est un ingrédient nécessaire pour dériver une contrainte linéaire tractable

impliquant la contrainte de coût robuste (E.57) comme le montre la proposition suivante.

Proposition E.3. *Considérons la contrainte de coût robuste* (E.57) *correspondant à un spectre du type* (E.56)*. Ensuite, la contrainte* (E.57) *est vérifiée pour un γ donné si l'inégalité suivante linéaire dans les variables de décision c_m ($m = 1, \ldots, L$) est vérifiée:*

$$\sum_{m=1}^{L} c_m \ \alpha(\omega_m) \leq \gamma \tag{E.59}$$

où $\alpha(\omega)$ ($m = 1, ..., L$) est une borne supérieure pour $\mathcal{J}_{wc}(\omega)$ (voir (E.58)*)*

Démonstration. Voir le Chapitre 4. ∎

Observons que (E.59) est une contrainte d'inégalité linéaire dans les coefficients c_m ($m = 1, \ldots, L$). De plus, puisque Φ_r est affine dans c_m ($m = 1, \ldots, L$), la contrainte de précision (E.55) est également linéaire dans ces coefficients. Par conséquent, le problème d'optimisation LMI suivant est une formulation convexe pour le problème de la conception optimale robuste de l'expérience original (E.53)-(E.55).

Formulation LMI. *Considérez la paramétrisation* (E.56) *pour le spectre à concevoir Φ_r. Pour cette paramétrisation, le problème d'optimisation de LMI a comme variables de décision un scalaire $\gamma > 0$ et des coefficients $c_m \geq 0$ ($m = 1, \ldots, L$) et consiste à déterminer la plus petite valeur de γ pour laquelle la contrainte LMI* (E.55) *et la contrainte* (E.59) *sont respectées pour quelques $c_m \geq 0$ ($m = 1, \ldots, L$).*

Désignons par $c_{m,opt}$ ($m = 1, \ldots, L$) et par γ_{opt} la solution de ce problème d'optimisation de LMI et désignons également par $\Phi_{r,opt}$ le spectre correspondant aux coefficients $c_{m,opt}$. Ensuite, grâce à la Proposition E.3, nous avons que γ_{opt} est une borne supérieure de $\sup_{\theta \in U_{init}} \mathcal{J}(\Phi_{r,opt}, \theta)$ et donc de $\mathcal{J}(\Phi_{r,opt}, \theta_0)$. De plus, par construction, le spectre $\Phi_{r,opt}$ est aussi celui qui donne la plus petite valeur de (la borne supérieure de) $\sup_{\theta \in U_{init}} \mathcal{J}(\Phi_{r,opt}, \theta)$ pour lequel la contrainte de précision (E.55) est satisfaite.

Remarque E.1. L'approche que nous proposons dans cette Section pour robustifier la contrainte de coût n'est pas basée sur aucune approximation. Elle s'accompagne toutefois d'une dose de conservatisme. Il y a deux sources de conservatisme lorsque nous remplaçons la contrainte initiale (E.57) par la contrainte (E.59). La première source consiste à aller de (E.57) à $\sum_{m=1}^{L} c_m \mathcal{J}_{wc}(\omega_m) \leq \gamma$ et la seconde à aller de $\sum_{m=1}^{L} c_m \mathcal{J}_{wc}(\omega_m) \leq \gamma$ à (E.59). Expliquons plus en détail ces sources de conservatisme. Dans la première source de conservatisme, nous considérons le problème d'optimisation (E.58) conduisant à $\mathcal{J}_{wc}(\omega_m)$ indépendamment à chaque ω_m ($m = 1, \ldots, L$). Par conséquent, le paramètre θ auquel le supremum $\mathcal{J}_{wc}(\omega_m)$ est obtenu peut être différent à chaque fréquence ω_m (contrairement à la contrainte initiale (E.57)).

Dans la deuxième source de conservatisme, nous remplaçons la quantité $\mathcal{J}_{wc}(\omega_m)$ par une borne supérieure calculable $\alpha(\omega_m)$ par l'approche hiérarchique.

E.3.5 Résumé

Dans le Chapitre 4 de la thèse, nous étendons le cadre de la conception *least costly* de l'expérience d'identification au cas de l'identification d'un module dans un réseau de systèmes contrôlés localement. Le coût de l'expérience d'identification (qui est minimisé sous une certaine contrainte de précision) est ici défini comme une fonction des perturbations induites par le signal d'excitation sur les signaux d'entrée et de sortie de chaque module. La propagation de l'influence du signal d'excitation est encore réduite par une extension du paradigme de l'identification stealth. Notez que les résultats présentés ici peuvent facilement être étendus aux situations de réseau où le coût de l'expérience n'est pas lié à la perturbation induite par le signal d'excitation sur la sortie de chaque module, mais est plutôt lié à la perturbation induite par le signal d'excitation sur les différences entre les sorties des modules voisins. Cette situation peut se produire lorsque les différents agents du réseau doivent rester autant que possible dans une configuration de formation donnée [56].

E.4 Suivi de la fréquence de résonance d'un gyroscope MEMS

E.4.1 Le gyroscope

Description du résonateur

Un résonateur est un système dynamique qui peut être décrit par une fonction de transfert de second ordre avec des pôles complexes:

$$\tilde{G}(s) = \frac{k}{\frac{s^2}{\omega_{n,x}^2} + \frac{2\xi}{\omega_{n,x}}s + 1} \tag{E.60}$$

où s est la variable de la transformée de Laplace, $\xi < 1/\sqrt{2}$ est le rapport d'amortissement, $\omega_{n,x}$ la fréquence naturelle et k le gain statique. La fréquence de résonance de $\tilde{G}$ est définie comme la fréquence ω pour laquelle le gain $|\tilde{G}(j\omega)|$ est le plus important. Pour (E.60), cette fréquence de résonance $\omega_{r,x}$ est donnée par $\omega_{r,x} = \omega_{n,x}\sqrt{1 - 2\xi^2}$.

La dynamique du système de masse drive (5.1) varie avec la température. Plus précisément, nous supposons que le seul paramètre qui change avec la température soit la fréquence naturelle $\omega_{n,x}$ (k et ξ restent constants), qui comporte une variation de la fréquence de résonance $\omega_{r,x}$.

Nous analyserons maintenant le système de masse drive, considéré dans le projet Next4MEMS , à la température nominale de $T_{nom} = 30$ dégrées. À cette température nominale, le système de masse drive est décrit par (5.1) avec $k = 6.12\ 10^{-6}$, $\xi = 9.4$

10^{-6} et $\omega_{n,x} = 73821.22474\ rad/s$. Ces paramètres correspondent à une fréquence de résonance nominale $\omega_{r,x}^{nom} = 73821.22473\ rad/s$.

Puisque le gyroscope considéré est opéré avec une carte électronique, nous préférons ici une représentation en temps-discret du système. À la température nominale, nous avons la description suivante en temps-discret[8] pour la fonction de transfert entre u_x et x, quand le temps d'échantillonnage T_s est egal à $1.6\ 10^{-5}\ s$.

$$G_x(z) = \frac{b_{0,0}z^{-1} + b_{0,1}z^{-2}}{1 + f_{0,1}z^{-1} + f_{0,2}z^{-2}} \tag{E.61}$$

avec

$$\begin{pmatrix} b_{0,0} \\ b_{0,1} \\ f_{0,1} \\ f_{0,2} \end{pmatrix} = \begin{pmatrix} 4.562\ 10^{-6} \\ -1.216\ 10^{-5} \\ -0.7597 \\ 1 \end{pmatrix}$$

La description du système de masse drive peut être complété avec le bruit de processus et de mesure $v_x(t)$ agissant sur la sortie $x(t)$:

$$x(t) = \underbrace{G_x(z)u_x(t)}_{\breve{x}(t)} + \underbrace{H_x(t)e_x(t)}_{v_x(t)} \tag{E.62}$$

où e_x est un bruit blanc Gaussien ayant variance $\sigma_e^2 = 7.2\ 10^{-7}$ et H_x est la fonction de transfert en temps-discret d'ordre 5 suivante:

$$H_x(z) = \frac{1 + \sum_{i=1}^{5} c_{0,i}z^{-i}}{1 + \sum_{i=1}^{5} d_{0,i}z^{-i}} \tag{E.63}$$

avec

$$\begin{pmatrix} c_{0,1} \\ c_{0,2} \\ c_{0,3} \\ c_{0,4} \\ c_{0,5} \end{pmatrix} = \begin{pmatrix} 1.265 \\ -0.08948 \\ -1.339 \\ -0.7302 \\ -0.02449 \end{pmatrix} \quad , \quad \begin{pmatrix} d_{0,1} \\ d_{0,2} \\ d_{0,3} \\ d_{0,4} \\ d_{0,5} \end{pmatrix} = \begin{pmatrix} 0.2669 \\ -0.6584 \\ -0.8586 \\ +0.262 \\ -0.0002082 \end{pmatrix}$$

Dans les Figures E.4 et E.5 nous avons montré le gain de G_x et H_x. Nous pouvons remarquer dans les Figures E.4a et E.5a que le pic de résonance est assez net, comme prévu en raison de la faible valeur de ξ. De plus, H_x présente un gain important aux basses fréquences, comme on peut le voir dans la Figure E.4b, et un pic à une fréquence supérieure à $\omega_{r,x}$ (voir la Figure E.5b).

Performances nominales

Les résonateurs sont souvent utilisés de telle manière que leur sortie x suit un signal sinusoïdal à la fréquence de résonance du résonateur. Cette dernière est imposée pour

---

[8]Le modèle du système présenté ici provient de l'identification effectuée dans le cadre du projet Next4MEMS . Le zéro supplémentaire n'influence pas la dynamique principale.
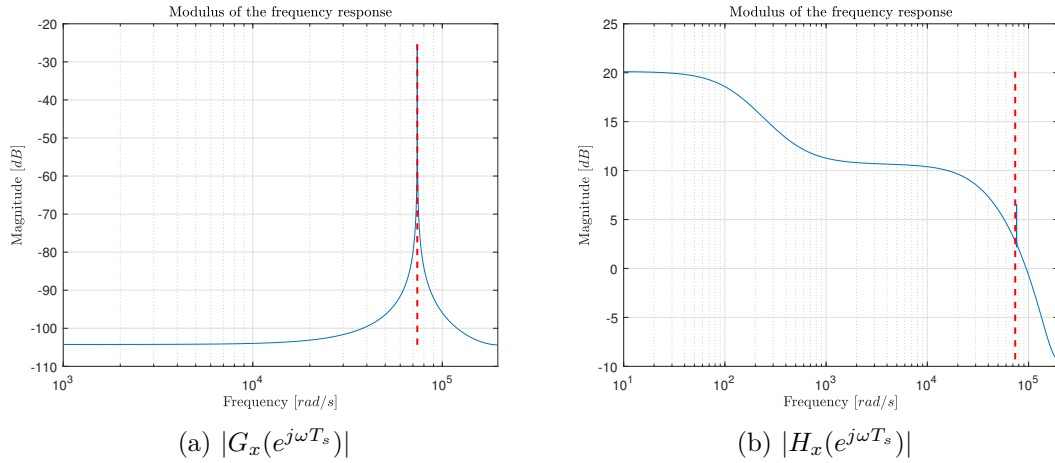
(a) $|G_x(e^{j\omega T_s})|$

(b) $|H_x(e^{j\omega T_s})|$

Figure E.4: Modulus des réponses en fréquence de G_x (ligne bleu dans le tracé (a)) et de H_x (ligne bleu dans le tracé (b)). La ligne tireté verticale est placée dans les deux tracées à $\omega = \omega_{r,x}^{nom}$
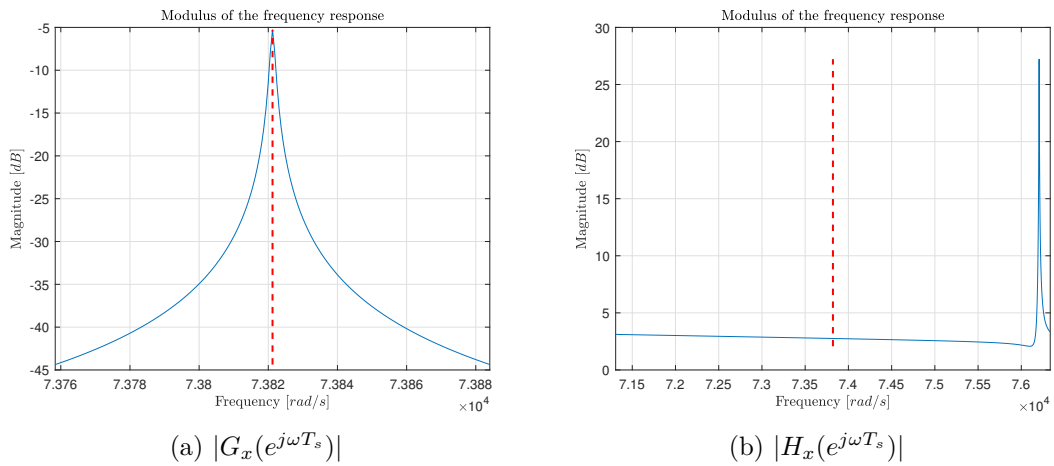

(a) $|G_x(e^{j\omega T_s})|$

(b) $|H_x(e^{j\omega T_s})|$

Figure E.5: Zoom de la Figure E.4 autour de $\omega = \omega_{r,x}^{nom}$.

garantir que ces oscillations sont obtenues avec le plus petit signal d'entrée possible u_x. Dans cette Section, nous supposerons que ces oscillations seront obtenues dans une configuration en boucle fermée (voir la Figure E.6):

$$\begin{cases} x(t) = G_x(z)u_x(t) + v_x(t) \\ u_x(t) = K_x(z)\epsilon_x(t) \\ \epsilon_x(t) = x_{ref}(t) - x(t) \end{cases} \tag{E.64}$$

Où le signal de référence $x_{ref}(t)$ est choisi comme

$$x_{ref}(t) = A_x \sin\left(\omega_{ref} t\right) \tag{E.65}$$

avec A_x l'amplitude souhaitée de l'oscillation ($A_x = 0,1$ dans notre cas) et ω_{ref} la fréquence souhaitée de l'oscillation qui devra être choisie égale à la fréquence de résonance de G_x. Le contrôleur K_x sera conçu tel que le suivi de x_{ref} soit aussi précis que possible, tout en limitant l'action de contrôle u_x. Un autre objectif de K_x sera de rejeter le bruit v_x autant que possible. Cependant, cet objectif ne pourra être atteint que pour la composante de v_x autour de la fréquence de résonance puisque le procédé G_x n'a un gain significatif qu'autour de cette fréquence de résonance (voir la Figure E.5).
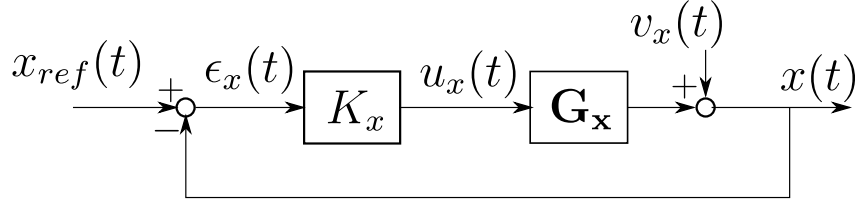
Figure E.6: Schéma de la stratégie de commande pour le système de masse drive.

Dans ce document, K_x sera conçu sur la base du système (E.62), c'est-à-dire le résonateur à la température nominale (avec une fréquence de résonance $\omega_{r,x}^{nom}$). Comme indiqué dans [58], cela donne:

$$K_x(z) = \frac{1.65 - 1.249z^{-1} - 1.659z^{-2} + 2.519z^{-3} - 1.659z^{-4} - 1.251z^{-5} + 1.649z^{-6}}{1 - 1.973z^{-1} + 3.452z^{-2} - 2.979z^{-3} + 2.186z^{-4} - 0.7527z^{-5} + 0.1971z^{-6}} \tag{E.66}$$

Analysons la performance nominale de ce contrôleur K_x, c'est-à-dire sa performance lorsque G_x est donné par (E.62) et lorsque $x_{ref}(t) = A_x \sin(\omega_{r,x}^{nom} t T_s)$. À cette fin, considérons les deux fonctions de transfert en boucle fermée suivantes:

$$S(z) = \frac{1}{1 + G_x(z)K_x(z)} \quad , \quad F(z) = \frac{K_x(z)}{1 + G_x(z)K_x(z)} \tag{E.67}$$

Dont les gains sont représentés dans la Figure E.7. Rappelons que pour la boucle (E.64) l'erreur de poursuite ϵ_x et le contrôle u_x peuvent être exprimés comme:

$$\epsilon_x(t) = S(z)x_{ref}(t) - S(z)v_x(t) \quad \text{and} \quad u_x(t) = F(z)x_{ref}(t) - F(z)v_x(t)$$

159

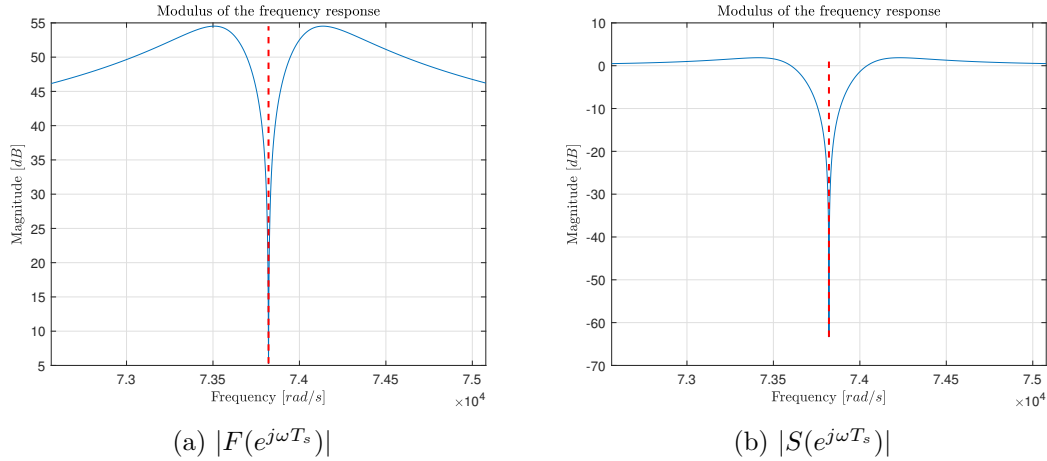(a) $|F(e^{j\omega T_s})|$ (b) $|S(e^{j\omega T_s})|$

Figure E.7: Modulus des réponses en fréquence de $F(z)$ (ligne bleu dans le tracé (a)) et de $S(z)$ (ligne bleu dans le tracé (b)). La ligne tireté verticale est placée dans les deux tracées à $\omega = \omega_{r,x}^{nom}$.

On observe que la fonction de sensibilité S a un gain très faible ($-63dB$) à $\omega = \omega_{r,x}^{nom}$. Cela permet un suivi précis de x_{ref} et le rejet de la composante du bruit v_x autour de la fréquence de résonance. On observe également que la fonction de transfert F (qui est la fonction de transfert entre x_{ref} et u_x et aussi la fonction de transfert entre v_x et u_x) a un minimum local à $\omega = \omega_{r,x}^{nom}$ ($|F| = 5dB$). Par conséquent, le suivi de x_{ref} et le rejet de la composante du bruit v_x autour de la fréquence de résonance seront réalisés avec des faibles efforts de contrôle. Comme mentionné ci-dessus, le rejet de v_x sera très partiel. Évaluons l'influence de la contribution de v_x sur l'erreur de suivi ϵ_x. A cet effet, observons que la contribution de x_{ref} dans ϵ_x est une sinusoïde d'amplitude $A_x|S(e^{j\omega_{r,x}^{nom}T_s})| = A_x/1415 = 7\ 10^{-5}$. De plus, observons que $||H_xS||_2 = 1,69$. Par conséquent, cette contribution est un bruit gaussien de déviation standard $||H_xS||_2\sigma_e = 0.0014$. Cette contribution sera donc la partie dominante de ϵ_x. En ce qui concerne u_x, on observe que $||H_xF||_2 = 65,7$. Par conséquent, u_x est constitué d'une partie sinusoïdale d'amplitude $A_x|F(e^{j\omega_{r,x}^{nom}T_s})| = 1.78A_x = 0.178$ et d'une contribution de bruit ayante déviation standard $||H_xF||_2\sigma_e = 0.055$.

Dependance par la température du résonateur et performance de la stratégie de commande quand $T \neq T_{nom}$

Lorsque la température change, la fréquence de résonance $\omega_{r,x}$ de (E.60) change. Nous supposerons que, dans la plage de température $\Xi = [T_{min} = -10\ ^oC \quad T_{max} = 70\ ^oC]$, la fréquence de résonance $\omega_{r,x}(T)$ variera comme indiqué dans la Figure E.8. Comme le montre cette figure, $\omega_{r,x}$ varie linéairement entre $\Omega = [\omega_{min} \quad \omega_{max}]$ avec $\omega_{min} = \omega_{r,x}^{nom} - 20\pi$ et $\omega_{max} = \omega_{r,x}^{nom} + 20\pi$.

D'après le raisonnement ci-dessus, lorsque la température est différente de T_{nom}, la fonction de transfert du résonateur sera différente de celle représentée dans la Fig-
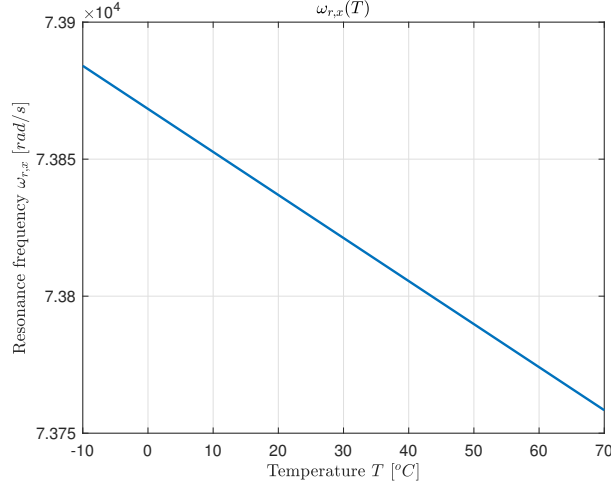
Figure E.8: Relation entre la fréquence de résonance $\omega_{r,x}$ et la température T.

ure E.4. En supposant que l'amortissement ξ est indépendant de la température, la fonction de transfert du résonateur lorsque la température est constante et égale à T est donnée par $\tilde{\mathbf{G}}(s, \omega_{r,x}(T))$ avec:

$$\tilde{\mathbf{G}}\big(s, \omega_{r,x}(T)\big) = \frac{k}{\frac{\omega_{r,x}^2(T)}{1-\xi^2} + \frac{\omega_{r,x}(T)\xi}{\sqrt{1-\xi^2}}s + s^2} \tag{E.68}$$

La version en temps discret de (E.68) est donnée par:

$$\mathbf{G_x}(z, \omega_{r,x}) = \frac{b_{0,0}(\omega_{r,x})z^{-1} + b_{0,1}(\omega_{r,x})z^{-2}}{1 + f_{0,1}(\omega_{r,x})z^{-1} + f_{0,2}(\omega_{r,x})z^{-2}} \tag{E.69}$$

où la valeur des coefficients dépend de la fréquence de résonance réelle. Le gain $|\mathbf{G_x}(e^{j\omega T_s}, \omega_{r,x})|$ de $\mathbf{G_x}(z, \omega_{r,x})$ est représenté dans la Figure E.9 pour différentes valeurs de $\omega_{r,x}$ dans l'intervalle Ω.

Voyons maintenant comment nous pouvons générer des oscillations à la fréquence de résonance $\omega_{r,x}(T)$ pour le résonateur lorsqu'il fonctionne à une température T différente de T_{nom}. Cela se fera en utilisant la configuration en boucle fermée présentée précédemment avec le contrôleur K_x conçu avec la dynamique du résonateur à $T = T_{nom}$, mais avec une référence sinusoïdale x_{ref} dont la fréquence ω_{ref} est égale[9] à $\omega_{r,x}(T)$. Pour analyser les performances de cette configuration particulière pour différentes valeurs de la température T (et donc différentes valeurs de $\omega_{r,x}(T)$), nous pouvons définir:

$$S_{\omega_{r,x}}(z) = \frac{1}{1 + \mathbf{G_x}(z, \omega_{r,x})K_x(z)} \quad , \quad F_{\omega_{r,x}}(z) = \frac{K_x(z)}{1 + \mathbf{G_x}(z, \omega_{r,x})K_x(z)} \tag{E.70}$$

dont les gains sont représentés dans la Figure E.10 pour différentes valeurs de $\omega_{r,x} \in \Omega$.

---

[9]Généralement, $\omega_{r,x}(T)$ est inconnu et ω_{ref} sera choisi comme estimation de cette résonance (voir les Sections E.4.2 et E.4.3).
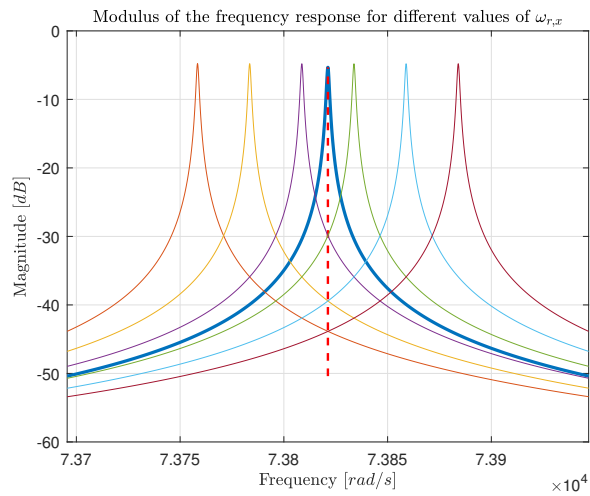
Figure E.9: $|\mathbf{G_x}(e^{j\omega T_s}, \omega_{r,x})|$ pour des différentes valeurs de $\omega_{r,x} \in \Omega$. La ligne bleue épaisse représente cet module pour $\omega_{r,x} = \omega_{r,x}^{nom}$. La ligne tiretée verticale rouge est placée à $\omega = \omega_{r,x}^{nom}$.
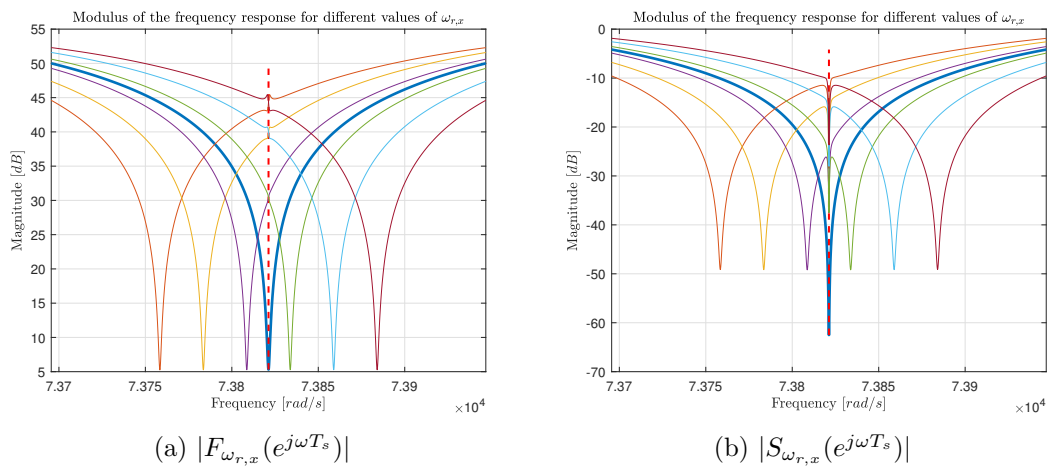

(a) $|F_{\omega_{r,x}}(e^{j\omega T_s})|$

(b) $|S_{\omega_{r,x}}(e^{j\omega T_s})|$

Figure E.10: Modulus des réponses en fréquence des deux fonctions de transfert dans (E.70), pour des différents valeurs de $\omega_{r,x} \in \Omega$. La ligne bleue épaisse dans les deux tracées représente le module pour $\omega_{r,x} = \omega_{r,x}^{nom}$. La ligne tiretée verticale rouge est placée dans les deux tracées à $\omega = \omega_{r,x}^{nom}$.

Puisque la référence sera sinusoïdale à une fréquence égale à $\omega_{r,x}$, analysons le gain de $S_{\omega_{r,x}}$ et de $F_{\omega_{r,x}}$ à $\omega_{r,x}$. Nous observons que $|F_{\omega_{r,x}}(e^{j\omega_{r,x}T_s})| = 5 \ dB$ pour tous les $\omega_{r,x} \in \Omega$. Le gain $|S_{\omega_{r,x}}(e^{j\omega_{r,x}T_s})|$ de $S_{\omega_{r,x}}$ à $\omega_{r,x}$ est égal à $-50 \ dB$ pour $\omega_{r,x} \neq \omega_{r,x}^{nom}$ ce qui est un peu plus grand que le $63 \ dB$ original. De plus, $||H_x F_{\omega_{r,x}}||_2$ et $|||H_x S_{\omega_{r,x}}||_2$ restent respectivement égaux à 65.7 et 1.69. Par conséquent, la configuration choisie semble acceptable pour toutes les températures comprises dans Ξ, du moins tant que la température est supposée constante et égale à une valeur comprise dans Ξ.

Performance de la stratégie de commande quand la température change

Supposons donc que la température $T(t)$ varie avec le temps à l'intérieur de Ξ. Nous supposerons que la fréquence de résonance correspondant à cette variation de température sera donnée par $\omega_{r,x}(T(t))$. Nous supposerons également que le contenu fréquentiel du bruit v_x est indépendant de la température. Sur la base de ces hypothèses, lorsque, en raison de la variation $T(t)$, la fréquence de résonance varie comme $\omega_{r,x}(t) = \omega_{r,x}(T(t))$, le système d'entrée-sortie (E.62) devient l'opérateur LPV suivant:

$$\begin{cases} \mathbf{G_x}(\omega_{r,x}(t)) \ : \ \breve{x}(t) = b_{0,0}(\omega_{r,x}(t))u_x(t-1) + b_{0,1}(\omega_{r,x}(t))u_x(t-2) + \dots \\ \qquad\qquad\qquad \cdots - f_{0,1}(\omega_{r,x}(t))\breve{x}(t-1) + f_{0,2}(\omega_{r,x}(t))\breve{x}(t-2) \\ x(t) = \breve{x}(t) + v_x(t) \end{cases} \tag{E.71}$$

Notez que $\mathbf{G_x}(\omega_{r,x}(t)) = \mathbf{G_x}(z, \omega_{r,x})$ lorsque $\omega_{r,x}(t) = \omega_{r,x} \ \forall t$.

Comme présenté précédemment, l'opérateur LPV (E.71) sera contrôlé avec le contrôleur K_x indiqué dans (E.66). (voir la Figure E.11) et avec une référence sinusoïdale qui suit au plus près la fréquence de résonance. Pour ce faire, nous choisirons une référence de la forme:

$$x_{ref}(t) = A_x \sin\left(\sum_{\tau=1}^{t} \omega_{ref}(\tau)T_s\right) \tag{E.72}$$

avec $\omega_{ref}(t) = \omega_{r,x}(t)$ (voir la Figure E.11).
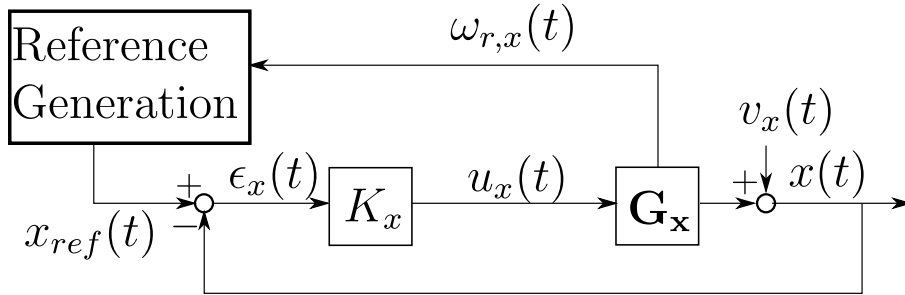

Figure E.11: Commande du système de masse drive pour une fréquence de résonance $\omega_{r,x}(t)$ temps variant. Dans cette figure, $\mathbf{G_x}$ est l'opérateur LPV (E.71).

Nous simulerons la boucle représentée dans la Figure E.11 dans le cas où $\omega_{r,x}(t)$ varie[10] de sa valeur nominale $\omega_{r,x}^{nom}$ à soit ω_{max} ou ω_{min} en 500 s. Cela donne le signal $\omega_{r,x}$ suivant[11]:

$$\omega_{r,x}(t) = \begin{cases} \omega_{r,x}^{nom} & tT_s \leq 507 \\ \omega_{r,x}^{nom} + \alpha_\omega(tT_s - 507) & 507 < tT_s \leq 1007 \\ \omega_{r,x}^{nom} + 500\alpha_\omega & 1007 < tT_s \leq 1507 \end{cases} \qquad \text{(E.73)}$$

Si nous choisissons $\alpha_\omega = 0,1257$, nous obtenons la variation représentée dans la partie gauche de la Figure E.12 et si nous choisissons $\alpha_\omega = -0,1257$, nous obtenons la variation représentée dans la partie droite de la Figure E.12.
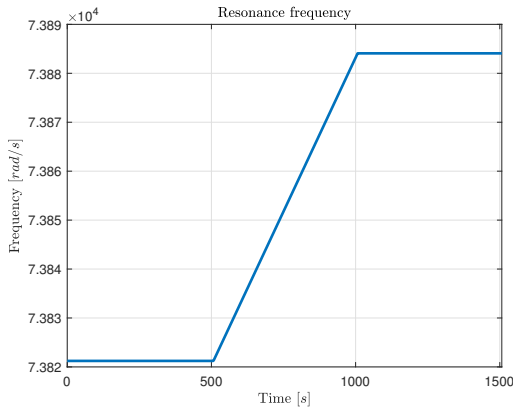
(a) $\alpha_\omega = 0.1257$.
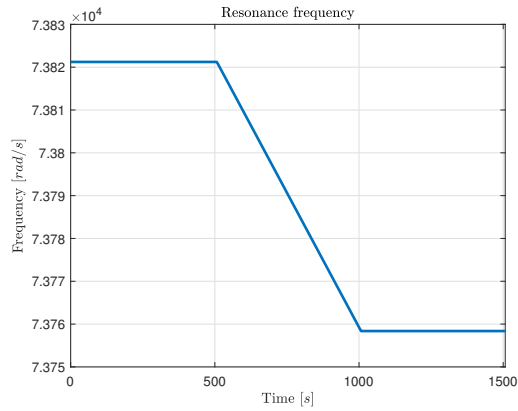
(b) $\alpha_\omega = -0.1257$.

Figure E.12: Variation de la fréquence de résonance $\omega_{r,x}(t)$ comme donné par (E.73) avec $\alpha_\omega = 0.1257$ (tracé (a)) et avec $\alpha_\omega = -0.1257$ (tracé (b)).

Lors de la simulation de la boucle fermée dans la Figure E.11 avec un opérateur LPV $\mathbf{G_x}$ (E.71) avec une variable de scheduling donnée par (E.73) avec $\alpha_\omega = \pm 0.1257$, on obtient les signaux ϵ_x et u_x donnés en rouge dans les Figures E.13 et E.14, respectivement. Notez que les 507 premières secondes des Figures E.13 et E.14 sont obtenues dans le réglage nominal (c'est-à-dire $\omega_{r,x}(t) = \omega_{r,x}^{nom}$ et $\omega_{ref}(t) = \omega_{r,x}^{nom}$). Il ressort donc clairement des Figures E.13 et E.14 que la configuration proposée dans la Figure E.11 pour traiter la fréquence de résonance variable donne des résultats acceptables, puisque nous ne pouvons observer aucune différence nette entre les premières 507 secondes et le reste des simulations.

Il est également important de noter que le choix de $\omega_{ref}(t) = \omega_{r,x}(t)$ dans (E.72) est crucial pour obtenir ces résultats. En effet, si nous choisissons $\omega_{ref}(t) = \omega_{r,x}^{nom}$

---

[10]Nous supposerons que c'est le taux de variation le plus élevé qui sera rencontré dans la pratique.

[11] Dans cette simulation, pendant les premières 7 secondes, l'amplitude A_x de x_{ref} est augmentée progressivement de 0 à 0.1. Cela pour limiter le comportement transitoire [58].

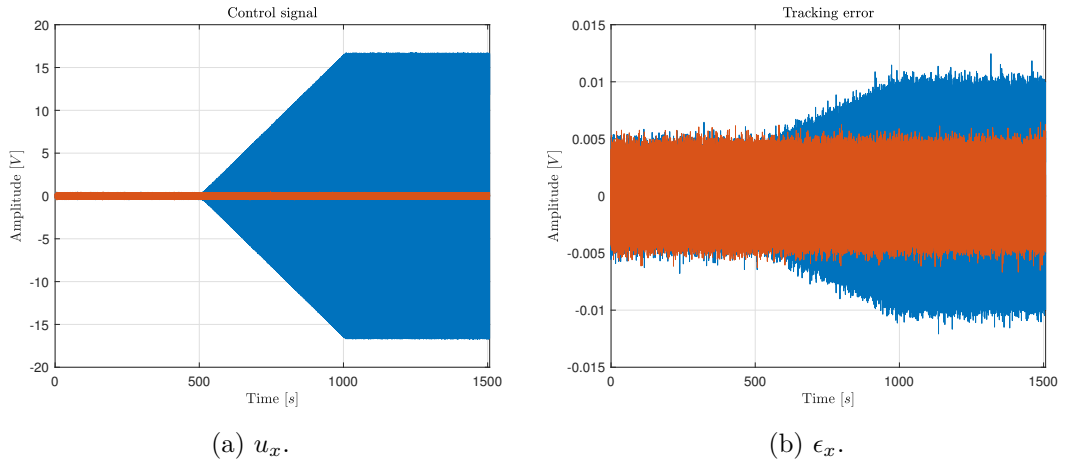(a) u_x.

(b) ϵ_x.

Figure E.13: Résultats de la simulation décrite dans la Section E.4.1 avec $\alpha_\omega = 0.1257$. La courbe rouge corresponde au cas où x_{ref} est donne par (E.72) avec $\omega_{ref}(t) = \omega_{r,x}(t)$ et la courbe bleue corresponde au cas où x_{ref} est donné par (E.72) avec $\omega_{ref}(t) = \omega_{r,x}^{nom}$.
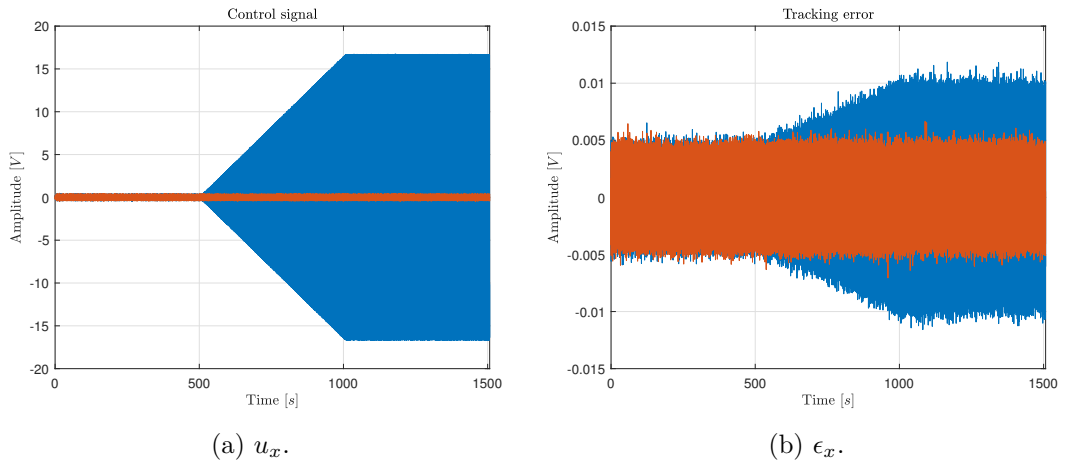

(a) u_x.

(b) ϵ_x.

Figure E.14: Résultats de la simulation décrite dans la Section E.4.1 avec $\alpha_\omega = -0.1257$. La courbe rouge corresponde au cas où x_{ref} est donne par (E.72) avec $\omega_{ref}(t) = \omega_{r,x}(t)$ et la courbe bleue corresponde au cas où x_{ref} est donné par (E.72) avec $\omega_{ref}(t) = \omega_{r,x}^{nom}$.

$\forall t$ in (E.72) (c'est-à-dire $x_{ref} = A_x \sin(\omega_{r,x}^{nom} t)$), le signal ϵ_x et u_x serait donné par la courbe bleue dans les Figures E.13 et E.14. Il est clair que la performance de contrôle est fortement altérée à partir de 507 seconds, c'est-à-dire le moment où $\omega_{r,x}(t) \neq \omega_{r,x}^{nom}$.

Pour référence, analysons plus en détail les courbes rouges des Figures E.13 et E.14. À cette fin, calculons l'énergie de $\epsilon_x(t)$ et de $u_x(t)$ dans trois intervalles de temps, c'est-à-dire $\Delta t_1 = \{t \mid 7 < tT_s \leq 507\}$ (cas nominal), $\Delta t_2 = \{t \mid 507 < tT_s \leq 1007\}$ (fréquence de résonance variable) et $\Delta t_3 = \{t \mid 1007 < tT_s \leq 1507\}$ ($\omega_{r,x} = \omega_{max}$ ou $= \omega_{min}$). L'énergie d'un signal $\psi(t)$ dans un intervalle Δt est définie comme suit:

$$\mathcal{E}(\psi, \Delta t) = \sum_{t \in \Delta t} |\psi(t)|^2 \tag{E.74}$$

Les résultats sont donnés dans le Tableau E.1. Dans ce tableau, on observe que l'énergie de u_x est la même dans les trois intervalles. L'énergie de ϵ_x est légèrement plus grande dans Δt_2 et Δt_3 que dans le cas nominal Δt_1. Cette différence peut s'expliquer par l'observation de la Figure E.10b: la performance de suivi d'une sinusoïde à $\omega_{r,x}$ est (légèrement) plus faible lorsque $\omega_{r,x} \neq \omega_{r,x}^{nom}$.

Table E.1: $\mathcal{E}(u_x,.)$ et $\mathcal{E}(\epsilon_x,.)$ pour les deux simulations avec $\omega_{ref}(t) = \omega_{r,x}(t)$

		$\mathcal{E}(u_x,.)$			$\mathcal{E}(\epsilon_x,.)$		
		Δt_1	Δt_2	Δt_3	Δt_1	Δt_2	Δt_3
α_ω	0.1257	$6.4\ 10^5$	$6.4\ 10^5$	$6.4\ 10^5$	48.7	50.5	50.6
	-0.1257	$6.4\ 10^5$	$6.4\ 10^5$	$6.4\ 10^5$	48.7	50.6	50.6

Résumons maintenant les résultats obtenus jusqu'à présent. La configuration de contrôle proposée (voir la Figure E.11), composée du contrôleur nominal K_x et d'un signal de référence (E.72) avec $\omega_{ref}(t) = \omega_{r,x}(t)$, donne des résultats satisfaisants tant pour une fréquence de résonance constante $\omega_{r,x}$ que pour une fréquence de résonance variable (la Figure E.12 est supposé représenter le taux de variation de $\omega_{r,x}$ le plus élevé que l'on puisse rencontrer en pratique).

E.4.2 Identification récursive

L'identification récursive est une technique d'identification qui nous permet d'estimer l'évolution des paramètres d'un système variant dans le temps, comme celui donné dans (E.71); avec un certain abus de langage, nous appellerons cette estimation des paramètres un modèle variant dans le temps de (E.71). Nous utiliserons ici cette technique pour obtenir un modèle variant dans le temps $\hat{G}(t)$ du vrai système LPV (E.71) et, à partir de ce modèle variant dans le temps $\hat{G}(t)$, nous pourrons dériver une estimation $\hat{\omega}_{r,x}(t)$ de la fréquence de résonance $\omega_{r,x}(t)$, qui est la variable de scheduling du système LPV (E.71). À chaque instant t, cette estimation $\hat{\omega}_{r,x}(t)$ sera donnée par la
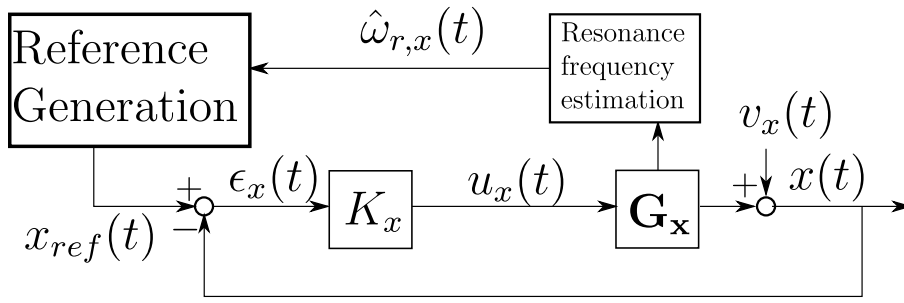
Figure E.15: Commande du système de masse drive avec la fréquence de résonance estimée $\hat{\omega}_{r,x}$.

fréquence de résonance de la fonction de transfert qui peut être obtenue si nous "gelons" les coefficients de l'opérateur variant dans le temps $\hat{G}(t)$ à leur valeur à l'instant t.

Cette estimation $\hat{\omega}_{r,x}(t)$ peut ensuite être utilisée dans la configuration de contrôle de la Figure E.15 pour générer x_{ref}. Comme mentionné à la Section E.1, nous devrons exciter le système avec un signal externe $r(t)$ pour pouvoir dériver le modèle $\hat{G}(t)$ de (E.71). Ce signal externe sera ajouté à la sortie du contrôleur K_x:

$$u_x(t) = K_x(z)\left(x_{ref}(t) - x(t)\right) + r(t) \tag{E.75}$$

où $r(t)$ est choisi égal à un signal RBS d'amplitude 0.01. La Figure E.15 est donc modifié dans la Figure E.16.
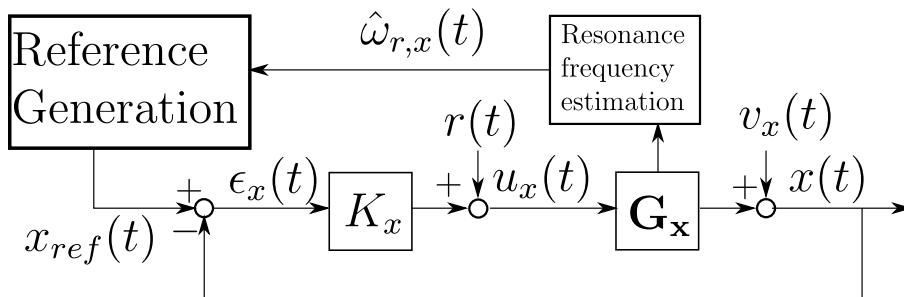

Figure E.16: Commande du système de masse drive avec la fréquence de résonance estimée $\hat{\omega}_{r,x}$ avec le signal d'excitation rajouté pour l'identification.

Le système (E.71) est un système Box-Jenkins. L'identification récursive des systèmes Box-Jenkins peut être lourde en pratique. Par conséquent, nous allons plutôt identifier un modèle ARX pour le système (E.71). En d'autres termes, nous supposerons que (E.71) peut être décrit une précision suffisante par la relation entrée-sortie suivante:

$$x(t) = \varphi(t)^T \theta_0(t) + e(t), \quad \varphi(t) = \begin{pmatrix} -x(t-1) \\ \vdots \\ -x(t-n_a) \\ u_x(t-n_k) \\ \vdots \\ u_x(t-n_k-n_b) \end{pmatrix} \tag{E.76}$$

où $e(t)$ est un signal de bruit blanc et $\theta_0(t)$ est un paramètre variable dans le temps que nous estimerons à chaque instant t. Il est bien connu que, dans le cas des systèmes LTI, tout système Box-Jenkins peut être représenté avec précision par un système ARX d'ordre élevé. Ici, en utilisant une approche *trial-and-error*, nous avons observé que, si nous choisissons $n_a = 9$, $n_b = 4$ et $n_k = 1$, (E.76) permet de représenter suffisamment (E.71).

Nous souhaitons donc déterminer, par identification récursive, une estimation de $\theta_0(t)$ à partir des données $u_x(t)$ et $x(t)$ collectées dans la boucle représentée dans la Figure E.16. L'algorithme d'identification récursive pour l'identification *prediciton error* des systèmes du type (E.76) est également appelé "Recursive Least Squares (RLS)" dans la littérature [1]. Le RLS détermine l'estimation $\hat{\theta}(t)$ de $\theta_0(t)$ sur la base de l'estimation $\hat{\theta}(t-1)$ au moment $t-1$ comme suit:

$$\hat{\theta}(t) = \hat{\theta}(t-1) + R^{-1}(t)\varphi(t)(x(t) - \varphi^T(t)\hat{\theta}(t-1)) \tag{E.77}$$

$$R(t) = \lambda R(t-1) + \varphi(t)\varphi^T(t) \tag{E.78}$$

Nous observons que, pour obtenir $\hat{\theta}(t)$ à partir de $\hat{\theta}(t-1)$, nous n'avons besoin que du régresseur φ au temps t et de la sortie x au temps t. Outre les valeurs d'initialisation $\hat{\theta}(0)$ et $R(0)$, le seul autre coefficient que l'utilisateur doit choisir dans (E.77)-(E.78) est le *forgetting factor* λ $(0 < \lambda < 1)$. Pour obtenir un compromis satisfaisant entre biais et variance, λ doit être choisi sur la base du taux de variation *supposé* de $\theta_0(t)$, c'est-à-dire que plus $\theta_0(t)$ varie rapidement, plus λ doit être choisi petit. Ici, en utilisant une approche *trial-and-error* avec variation de la fréquence de résonance comme dans (E.73) avec différents α_ω, nous avons déterminé que $\lambda = 1 - 10^{-6}$ est une valeur raisonnable. En outre, l'algorithme (E.77)-(E.78) sera initialisé[12] avec

$$\hat{\theta}(0) = (-1.06, 0.92, -0.45, 0.22, -0.42, 0.14,\ 0.13, -4.5\ 10^{-5}, -1.5\ 10^{-4}, \ldots$$

$$\ldots, -4.5\ 10^{-5}, 4.7\ 10^{-5}, 5\ 10^{-5}, 7.4\ 10^{-6}, -5.2\ 10^{-6})$$

et $R(0) = I_{n_a+n_b}\ 10^2$ (voir [59, pp. 299-302] pour plus des détails concertants cet choix). Il est à noter que l'algorithme (E.77)-(E.78) nécessite une inversion de matrice

---

[12]La valeur suivante pour $\hat{\theta}(0)$ provient d'une précédente expérience d'identification pour (E.76) avec $\omega_{r,x}(t) = \omega_{r,x}^{nom}$. Son but est simplement d'éviter d'initialiser $\hat{\theta}(0)$ avec un vecteur de zéros afin d'éviter de longs comportements transitoires, comme le suggère [59, pp. 299-302].

à chaque itération. Cependant, comme montré dans [1], cet algorithme peut également être mis en œuvre dans une version où aucune inversion de matrice n'est impliquée.

Montrons maintenant comment nous pouvons dériver $\hat{\omega}_{r,x}(t)$ de $\hat{\theta}(t)$. Si nous gelons la valeur de $\hat{\theta}(t)$ à sa valeur au temps t, la fonction de transfert correspondant à $\hat{\theta}(t)$ est donnée par (voir (E.76)):

$$\hat{G} = \frac{z^{-1}\left(b_0 + \sum_{l=1}^{4} b_l z^{-l}\right)}{1 + \sum_{l=1}^{9} a_l z^{-l}} \tag{E.79}$$

Contrairement à (E.61), cette fonction de transfert sera caractérisée par 9 pôles. Toutefois, l'un de ces pôles sera (relativement) proche du pôle p_{nom} de (E.61). Par conséquent, le pôle p^*de $\hat{G}$ proche de p_{nom} peut être déterminé en utilisant un schéma de Newton-Raphson, voir [60], initialisé à p_{nom}. À partir de ce pôle p^*, on peut alors utiliser l'expression suivante pour déterminer (approximativement) la fréquence de résonance[13] $\hat{\omega}_{r,x}$ de $\hat{G}$:

$$\hat{\omega}_{r,x}(t) = \frac{1}{T_s}\arg(p^*(t)) \tag{E.80}$$

La procédure ci-dessus est répétée à chaque instant, ce qui donne l'estimation $\hat{\omega}_{r,x}(t)$ de $\omega_{r,x}(t)$ en (E.71). La configuration de contrôle avec l'estimation RLS de la fréquence de résonance est résumée dans la Figure E.17 où x_{ref} est donné par (E.72) avec $\omega_{ref}(t) = \hat{\omega}_{r,x}(t)$.
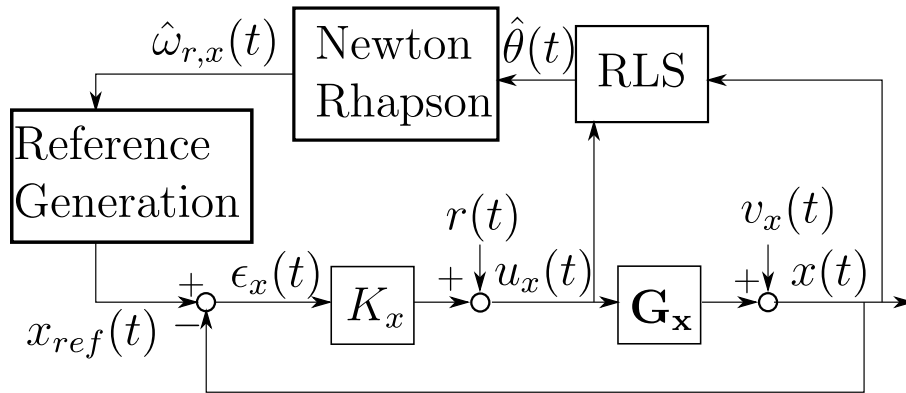

Figure E.17: Commande du système de masse drive avec la fréquence de résonance estimée $\hat{\omega}_{r,x}$ obtenue avec l'algorithme Recursive Least Squares.

E.4.3 Extremum Seeking

La méthode *Extremum Seeking* a été introduite en 1922 en tant que schéma de contrôle adaptatif, [57]. Il vise à adapter l'entrée d'une procédé afin de minimiser les

---

[13]Cette approximation est très précise lorsque l'amortissement est très faible comme dans le cas considéré dans ce document.

valeurs de sa sortie. Au lieu de l'utiliser comme schéma de contrôle adaptatif, nous l'utilisons ici pour estimer $\omega_{r,x}$, en profitant du fait que nous savons que l'amplitude de u_x est minimale lorsque $\omega_{ref} = \omega_{r,x}$. Avant de présenter son utilisation pour notre problème, nous présentons brièvement ses aspects généraux pour un système de temps continu *non linéaire*, qui est le cadre général de la méthode ES.

Aspects générales

Considérons une dynamique d'un procédé, avec une entrée w et une sortie q, décrite comme suit:

$$\begin{cases} \dot{\zeta}(\tilde{t}) = f(\zeta, w, \tilde{t}) \\ q_p(\tilde{t}) = h(\zeta, \tilde{t}) \\ q(\tilde{t}) = q_p(\tilde{t}) + v(\tilde{t}) \end{cases} \tag{E.81}$$

où ζ la variable d'état et v le bruit de mesure. En outre, les fonctions f et h sont supposées être différentiables dans leurs arguments. Lorsque nous appliquons une entrée constante $w(\tilde{t}) = w_c$ au temps $\tilde{t}_0$ nous supposons que $\exists g : \mathcal{R} \to \mathbf{R}$ une fonction trois fois différentiable, tel que: $\lim_{\tilde{t} \to \infty} q_p(\tilde{t}) = g(w_c)$. Donc, $\exists \tau$ tel que $|q_p(\tilde{t}) - g(w_c)| < c$ $\forall \tilde{t} > \tau + \tilde{t}_0$ avec $c = g(w_c)/20$; nous appellerons τ le temps caractéristique du procédé. En outre, nous appellerons alors g la caractéristique stationnaire du procédé et nous utiliserons la notation $q_p = g(w)$ pour $\lim_{\tilde{t} \to \infty} q_p(\tilde{t}) = g(w_c)$. De plus, nous supposons qu'il existe un minimum (local) (w^*, q_p^*) de g: $\frac{dg}{dw}(w^*) = 0$ et $\frac{d^2g}{dw^2}(w^*) > 0$. La stratégie "Extremum Seeking" vise à adapter w afin d'atteindre (w^*, q_p^*). Intuitivement, cette stratégie analyse la relation stationnaire g comme une méthode de descente de gradient, afin d'atteindre (w^*, q_p^*). Dans la Figure E.18 est représentée la stratégie "Extremum Seeking".
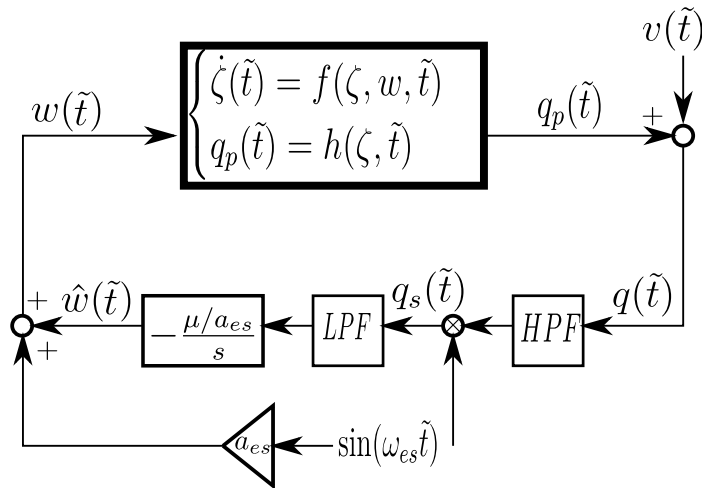

Figure E.18: Schéma de la stratégie Extremum Seeking.

Le signal de perturbation $\sin(\omega_{es}\tilde{t})$ est utilisé pour moduler la sortie du procédé $q(\tilde{t})$. Les filtres HPF et LPF sont des filtres passe-haut et passe-bas, respectivement, ayant des fréquences de coupure ω_h et ω_l. La sortie modulée passe à travers l'intégrateur avec un gain $-\frac{\mu}{a_{es}}$ afin de calculer le signal d'entrée adapté $\hat{w}(\tilde{t})$. Le paramètre μ est généralement interprété comme le *taux d'apprentissage* du schéma et régule la dynamique de $\hat{w}(\tilde{t})$. Ensuite, le signal d'entrée du procédé est calculé comme:

$$w(\tilde{t}) = \hat{w}(\tilde{t}) + a_{es}\sin(\omega_{es}\tilde{t}) \tag{E.82}$$

La convergence de w et q vers un voisinage de (w^*, q_p^*) a été prouvée dans la littérature [57] sous certaines conditions sur le bruit $v(\tilde{t})$ et avec un choix approprié des paramètres impliqués dans la stratégie Extremum Seeking. Plus précisément: (i) $\frac{1}{\tau} \gg \omega_{es}$ c'est-à-dire que la réponse transitoire du procédé doit être rapide par rapport à l'excitation injectée par la stratégie ES. (ii) $\mu \ll \omega_{es}$ c'est-à-dire que la dynamique du terme adapté $\hat{w}(\tilde{t})$ doit être lente par rapport à l'excitation injectée. (iii) $\omega_l \ll \omega_{es}$, $\omega_h \ll \omega_{es}$ c'est-à-dire que l'excitation injectée doit être bien à l'intérieur de la bande passante du filtre HP et bien à l'extérieur de la bande passante du filtre LP.

Application à l'estimation de la fréquence de résonance d'un résonateur

Considérons d'abord le cas où la température est constante, c'est-à-dire quand le résonateur est donné par $\mathbf{G_x}(z, \omega_{r,x})$ avec $\omega_{r,x} = \omega_{r,x}(T)$ (voir la Section E.4.1). Dans ce cas, la fonction de transfert $F_{\omega_{r,x}}(z) = \frac{K_x(z)}{1 + K_x(z)\mathbf{G_x}(z, \omega_{r,x})}$, de la référence externe $x_{ref}(t)$ au signal d'entrée $u_x(t)$, est telle que son gain a un minimum local à $\omega = \omega_{r,x}$. Si l'on considère un signal de référence $x_{ref} = A_x\sin(\omega_{ref}t)$ avec une ω_{ref} constante, le signal d'entrée $u_x(t)$ sera juste donné par $A_u\sin(\omega_{ref}t + \phi_u)$, où $A_u = A_x|F_{\omega_{r,x}}(e^{j\omega_{ref}T_s})|$ et $\phi_u = \arg(F_{\omega_{r,x}}(e^{j\omega_{ref}T_s}))$. Nous pouvons donc considérer $A_x|F_{\omega_{r,x}}(e^{j\omega_{ref}T_s})|$ comme une caractéristique stationnaire entre la fréquence ω_{ref} de x_{ref} et l'amplitude A_u du signal de commande u_x. Par conséquent, si nous sommes en mesure de récupérer l'amplitude A_u de u_x (en utilisant par exemple la démodulation synchrone [58]), nous pouvons utiliser la stratégie Extremum Seeking afin de déterminer la fréquence ω_{ref} de la référence x_{ref} qui donnera le plus petit A_u.

L'ES est implémenté comme dans la Figure E.18 avec l'excitation $a_{es}\sin(\omega_{es}t)$ et les filtres HF et LP. L'entrée $q(t)$ de la stratégie est ici l'amplitude du signal de contrôle $u_x(t)$ (obtenu par démodulation synchrone) tandis que la sortie $w(t)$ de la cadre rouge sera ici dénotée par $\omega_{ref}(t)$. Cet signal $\omega_{ref}(t)$ est donné par:

$$\omega_{ref}(t) = \hat{\omega}_{r,x}(t) + a_{es}\sin(\omega_{es}tT_s) \tag{E.83}$$

où $a_{es}\sin(\omega_{es}tT_s)$ est le petit signal de perturbation introduit par la stratégie extremum seeking et $\hat{\omega}_{r,x}(t)$ est la sortie du bloc intégrateur ($\hat{\omega}_{r,x}(t)$ peut être consideré une estimation de la fréquence de résonance). Cet signal $\omega_{ref}(t)$ est donc utilisé pour générer le signal de référence x_{ref} en utilisant (5.14). Cela donne la configuration de contrôle
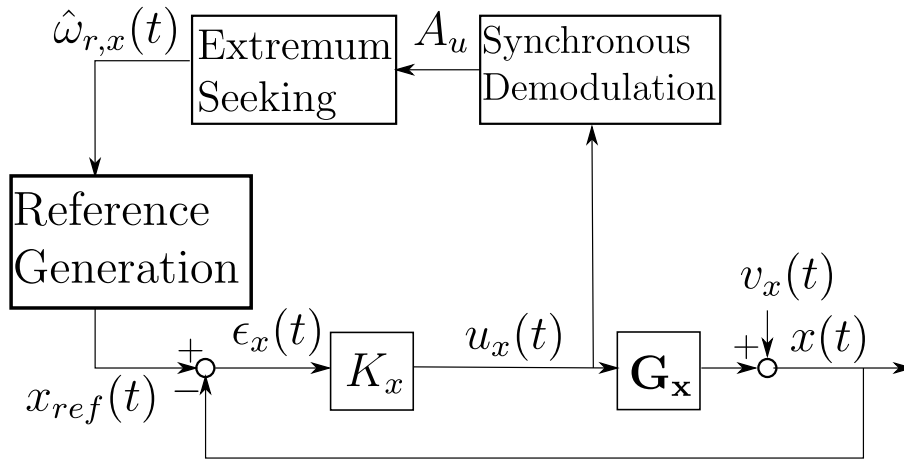
Figure E.19: Commande du système de masse drive avec la fréquence de résonance estimée $\hat{\omega}_{r,x}$ obtenue avec la stratégie Extremum Seeking.

de la Figure E.19.

Le raisonnement ci-dessus se rapporte au cas où $\omega_{r,x}$ reste constant. Cependant, si le taux de variation de $\omega_{r,x}(t)$ est lent par rapport au taux d'apprentissage de l'algorithme ES (qui est gouverné par le paramètre μ), le schéma ci-dessus peut également être utilisé pour obtenir une estimation $\hat{\omega}_{ref}(t) = \hat{\omega}_{r,x}(t)$ d'une fréquence de résonance variable dans le temps $\omega_{r,x}(t)$.

Réglage des paramètres

Nous illustrons ici comment régler le schéma Extremum Seeking utilisé dans la Figure E.19. Pour régler le schéma, nous devons connaître τ, le temps après lequel nous pouvons considérer que la dynamique transitoire du procédé s'est éteinte. Une fois que nous connaissons ce paramètre, nous pouvons choisir ω_{es} selon les conditions indiquées dans la Section E.4.3 et ensuite régler tous les autres paramètres. Ce qui est généralement fait pour estimer τ consiste alors à observer la réponse du système à une entrée du type échelon. Pour le schéma utilisé dans la Figure E.19, τ est le temps après lequel l'amplitude de u_x se règle sur une valeur fixe, en réponse à une variation du type échelon dans ω_{ref}. Nous considérons que le système est comme dans (E.64), avec K_x, donné dans (E.66) et $x_{ref}(t)$ comme dans (E.72). Comme premier test, nous avons considéré $\omega_{r,x} = \omega_{r,x}^{nom}$ et effectué un premier test de simulation de 4 s de fonctionnement où ω_{ref} était comme:

$$\omega_{ref}(t) = \begin{cases} \omega_{r,x}^{nom} & tT_s < 3 \ s \\ \omega_{r,x}^{nom} + \Delta_\omega & tT_s \geq 3 \ s \end{cases} \tag{E.84}$$

où $\Delta_\omega = \pi \ rad/s$. Ce choix a été fait pour étudier la réponse de A_u à un signal d'entrée du type échelon. Dans la Figure E.20 on peut remarquer que A_u présente un petit dépassement avant de se stabiliser à une valeur fixe avec un peu de bruit. Nous avons

alors $\tau = 0.2$ et, par conséquent, nous choisissons une fréquence ω_{es} pour le signal de perturbation égale à 0.5 rad/s et un gain $\mu = 0.1\omega_{es}$. Ensuite, nous choisissons les fréquences de coupure $\omega_h = 0.1\omega_{es}$ et $\omega_l = 0.1\omega_{es}$, des filtres HP et LP respectivement. Enfin, il ne reste plus qu'à régler l'amplitude a_{es} du signal de perturbation injecté par la stratégie ES. Il est à noter que a_{es} n'apparaît pas dans les conditions permettant d'assurer la convergence du schéma et peut donc être choisi librement. Puisque $\mu \ll \omega_{es}$, nous pouvons considérer que $\hat{\omega}_{r,x}(t)$ soit constant pendant une période du signal de perturbation $a_{es}\sin(\omega_{es}tT_s)$. Par conséquent, en utilisant (E.83), le signal $\omega_{ref}(t)$ aura de valeurs dans l'intervalle $[\hat{\omega}_{r,x} - a_{es} \ \hat{\omega}_{r,x} + a_{es}]$. Le signal de référence sera généré comme (E.72) avec cet $\omega_{ref}(t)$, donc c'est important que la caractéristique stationnaire $A_x|F_{\omega_{r,x}}(e^{j\omega T_s})|$ reste presque constante pour toutes ω dans cet intervalle $[\hat{\omega}_{r,x} - a_{es} \ \hat{\omega}_{r,x} + a_{es}]$. En utilisant Figure E.10a, nous choisissons $a_{es} = 0.06$.

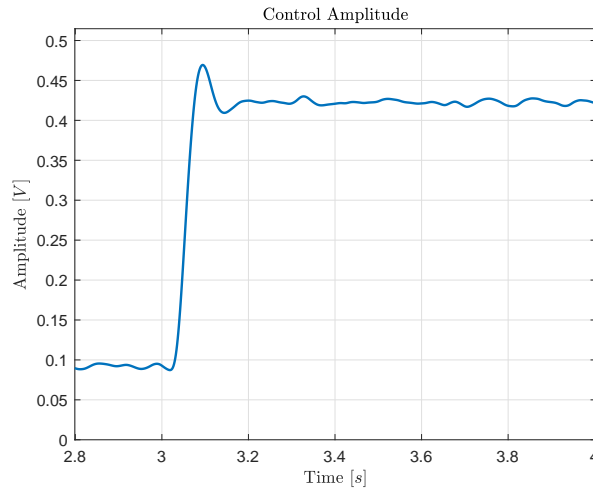Figure E.20: Amplitude A_u correspondant au test décrit dans la Section E.4.3.

E.4.4 Comparaison de l'algorithme RLS et de l'algorithme ES

Nous allons maintenant effectuer des simulations similaires à celles de la Section E.4.1. En effet, nous allons simuler la boucle fermée composée de K_x et du système LPV (E.71) avec la variable de scheduling $\omega_{r,x}(t)$ donnée par (E.73) ($\alpha_\omega = 0.1257$). La seule différence est que le signal de référence (E.72) ne sera plus construit avec la valeur exacte de $\omega_{r,x}(t)$, mais avec l'estimation de ce signal obtenue soit avec l'algorithme RLS de la Section E.4.2 soit avec l'algorithme ES de la Section E.4.3. Commençons par le cas où l'algorithme RLS est utilisé pour estimer $\omega_{r,x}$. Les signaux ϵ_x et u_x sont représentés en rouge dans la Figure E.21. En comparant ces signaux avec ceux obtenus dans la Figure E.13, nous ne constatons aucune différence. Cela est également confirmé par les énergies calculées dans le Tableau E.2.
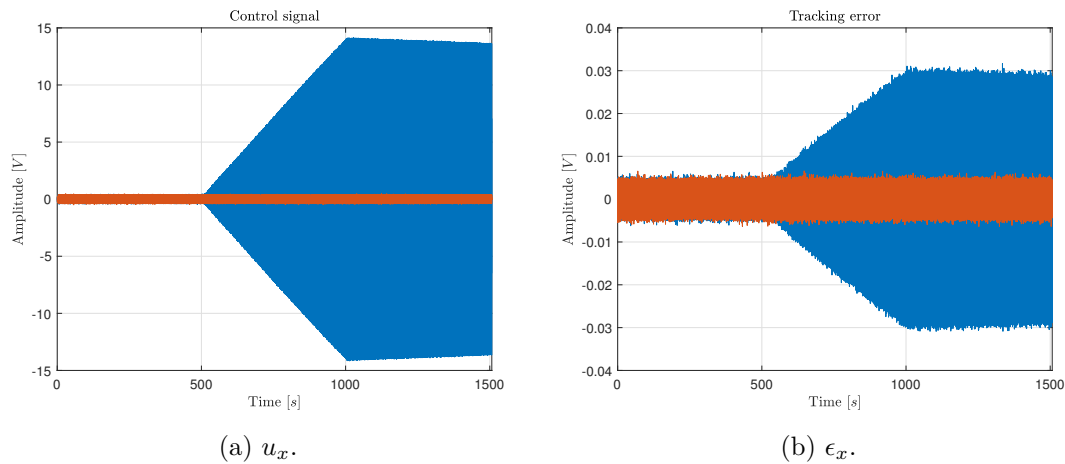
(a) u_x.   (b) ϵ_x.

Figure E.21: Résultats des simulations décrites dans la Section E.4.4. La courbe rouge corresponde à l'algorithme RLS et la courbe bleue corresponde à l'algorithme ES avec le réglage donné dans la Section E.4.3.

Table E.2: $\mathcal{E}(u_x, .)$ et $\mathcal{E}(\epsilon_x, .)$ obtenus pour les simulations décrites dans la Section E.4.4 avec la méthode RLS et avec la méthode ES (réglage de la Section E.4.3).

		$\mathcal{E}(u_x, .)$			$\mathcal{E}(\epsilon_x, .)$		
		Δt_1	Δt_2	Δt_3	Δt_1	Δt_2	Δt_3
Method	RLS	$6.46\ 10^5$	$6.48\ 10^5$	$6.46\ 10^5$	48.8	50.6	50.6
	ES	$6.45\ 10^5$	$1.05\ 10^9$	$2.93\ 10^9$	48.8	$3.7\ 10^3$	$1.05\ 10^4$

En effet, même si un signal d'excitation a été ajouté à la boucle et que la fréquence de résonance est maintenant estimée, ces énergies ne sont que légèrement supérieures à celle obtenue dans le cas idéal considéré dans la Section E.4.1. (voir le Tableau E.1). On ne peut pas en dire autant lorsque $\omega_{r,x}(t)$ est estimé à l'aide de l'algorithme ES (voir la courbe bleue dans la Figure E.21 et le Tableau E.2). En fait, l'algorithme ES n'est pas capable de suivre le taux de variation élevé de $\omega_{r,x}(t)$ comme le montre la Figure E.22, où l'on voit que $\hat{\omega}_{r,x}(t)$ est une mauvaise estimation de $\omega_{r,x}(t)$. En revanche, l'algorithme RLS donne une estimation de $\hat{\omega}_{r,x}(t)$ qui suit presque parfaitement $\omega_{r,x}(t)$.

Dans le Chapitre 5 nous avons comparé le RLS avec un autre réglage du ES. Cet réglage présent une bonne capacité de suivi, au prix de la perte de toute garantie de stabilité et/ou de convergence, car il ne respecte pas les critères classiques.

E.4.5   Résumé

Dans cette Section, deux solutions principales pour suivre la fréquence de résonance d'un résonateur ont été étudiées. La technique Extremum Seeking présente une certaine capacité de suivi tant que la dynamique de $\omega_{r,x}$ est très lente, mais elle échoue dans le
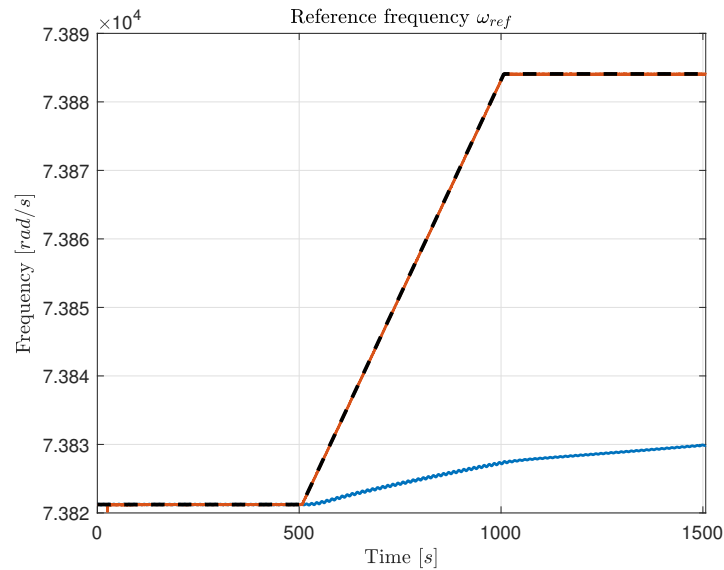
Figure E.22: Fréquence de résonance estimée avec la méthode RLS (ligne rouge) et avec la méthode ES utilisant le réglage de la Section E.4.3 (ligne bleue) comparées à la vraie fréquence de résonance (ligne tiretée noire).

test présenté ici. D'autre part, elle n'est pas facile à régler et les hypothèses qui doivent être respectées pour assurer la convergence ne nous permettent même pas d'avoir une idée de la mesure dans laquelle nous pouvons améliorer le jeu des paramétrés. La technique RLS est une technique facile à régler, puisqu'il suffit de changer le *forgetting factor*, qui est muni d'une interprétation plus solide. Il est donc facile de comprendre l'effet des différents *forgetting factors* et donc d'améliorer le réglage. De plus, elle présente une bonne capacité de suivi également pour des changements rapides de $\omega_{r,x}$, représentant alors le meilleur choix entre les deux méthodes présentées ici.

E.5 Conclusion

E.5.1 Resumé

Dans le Chapitre 2 de la thèse, nous avons présenté les aspects généraux de l'identification *Prediction Error* et de la conception optimale des expériences. Ces concepts ont servi de base aux discussions des Chapitres 3 et 4 de la thèse, où nous avons présenté nos contributions en matière de conception d'expériences robustes et dans le cadre *least costly* pour les réseaux.

Conception robuste de l'expérience

Nous avons limité notre attention à un système SISO G_0 fonctionnant en boucle ouverte qui peut être décrit par des modèles sans termes communs entre le processus et le modèle de bruit, c'est-à-dire Box-Jenkins et Output Error. Pour un tel système, nous avons considéré que nous disposions déjà d'un modèle paramétrique initial provenant d'une précédente expérience d'identification. Avec les paramètres identifiés, nous disposons également d'une zone de confiance pour ces paramètres, qui est malheureusement trop "large" pour l'application prévue. Nous considérons alors le problème de la conception optimale de l'expérience qui conduit à un modèle identifié avec un niveau de précision prescrit avec le coût d'expérience le plus petit possible. Nous avons notamment limité notre attention à une expérience réalisée en excitant le système avec un signal d'excitation multisinusoïdal. De plus, nous nous sommes concentrés uniquement sur la précision du modèle du procédé.

Nous avons abordé le problème *chicken-and-egg* de notre problème de conception optimale de l'expérience dans le cadre de la conception robuste de l'expérience, qui, d'autre part, conduit à un problème d'optimisation dont les contraintes ne sont pas tractables en tant que telles. Des efforts ont été faits dans la littérature pour rendre ces contraintes tractables, mais les solutions proposées n'assurent pas pleinement les garanties associées aux contraintes initiales. Notre contribution au Chapitre 3 (ici Section E.2) a été de développer des contraintes alternatives tractables aux contraintes originales. Lorsqu'elles sont utilisées à la place des contraintes originales, elles garantissent que la solution obtenue aura les garanties souhaitées associées aux contraintes originales. Ces contraintes alternatives sont développées en s'inspirant à certaines méthodes de la théorie du contrôle robuste. Afin de développer ces contraintes, nous avons exploité la structure du modèle afin de réécrire les contraintes sous une forme cohérente avec le contrôle robuste, la forme LFT. Successivement, nous avons introduit ce qu'on appelle un set de multipliers pour un ensemble d'incertitudes provenant d'une expérience d'identification précédente. En utilisant ces deux ingrédients, les multipliers et la forme LFT des contraintes, nous avons proposé des contraintes alternatives tractables pour le problème original de conception robuste de l'expérience. Elles nous assurent que le spectre optimal ainsi obtenu sera tel que le coût de l'expérience sera inférieur à celui de l'expérience optimale et que l'estimation à obtenir aura la précision souhaitée.

Conception optimale de l'expérience pour les réseaux

Dans le Chapitre 4 (ici Section E.3), nous avons étendu le cadre de la conception *least costly* de l'expérience à l'identification d'un module dans l'interconnexion de systèmes contrôlés localement. Nous avons défini le coût de l'expérience comme une mesure de la perturbation induite par l'expérience sur l'ensemble du réseau, et nous avons proposé l'utilisation de la configuration stealth afin de réduire la propagation des effets de l'expérience aux autres modules. Au Chapitre 4 de la thèse, nous avons fourni les conditions permettant d'obtenir une estimation consistante pour le module à identifier. Ces conditions concernent à la fois les cas où la configuration stealth est

utilisée ou non. En outre, nous avons également fourni les conditions que le modèle initial, utilisé dans la configuration stealth, devrait avoir afin d'assurer que la propagation est réduite. De plus, pour le problème de la conception *least costly* d'expérience, nous avons donné les conditions qui nous permettent de savoir s'il est plus avantageux ou non de considérer le problème dans la configuration stealth.

Lors de la formulation du problème de la conception *least-costly* de l'expérience, l'utilisation d'une estimation initiale pour contourner le problème *chicken-and-egg* présente un inconvénient important lors de l'utilisation de la configuration stealth: nous négligeons la propagation à travers les autres modules. Nous devons donc robustifier la contrainte de coût. Cela a également pour effet de *robustifier* la configuration stealth, puisque le problème d'optimisation obtenu favoriserait généralement les spectres ayant des contributions importantes dans la gamme de fréquences où la compensation stealth est plus efficace, en raison d'une petite incertitude du modèle utilisé pour la configuration stealth. La contrainte de coût robustifiée n'est pas tractable en tant que telle, mais nous pouvons utiliser les outils du Chapitre 3 (ici Section E.2) pour résoudre ce problème. Cependant, cela impliquerait un temps de calcul élevé en raison de la dimension du réseau. Ainsi, dans le Chapitre 4 (ici Section E.3) nous avons également proposé une approche de robustification qui implique un certain conservatisme, mais qui nous permet de résoudre le problème efficacement. Enfin, les illustrations numériques montrent l'avantage de la configuration stealth pour ce qui concerne la propagation de la perturbation à travers le réseau.

Suivi de la fréquence de résonance

Dans le Chapitre 5 (ici Section E.4), nous avons abordé le problème du suivi de la fréquence de résonance du système de masse drive d'un gyroscope MEMS. Ce travail a débuté dans le cadre du projet Next4MEMS , où le gyroscope MEMS présente une fréquence de résonance qui change en fonction des variations de température. Nous avons montré, par des simulations, que le suivi de la fréquence de résonance afin de faire osciller le résonateur à sa fréquence de résonance permet d'avoir de bonnes performances malgré les changements de température. Nous avons ensuite présenté deux méthodes pour suivre la fréquence de résonance: l'identification récursive et l' *Extremum Seeking*. La première est bien connue dans la littérature et facile à mettre en œuvre et à régler. La seconde a déjà été utilisée dans la littérature, mais son réglage n'est pas trivial. Pour les deux méthodes, nous avons proposé une mise en œuvre efficace adaptée à la stratégie de contrôle utilisée dans le projet Next4MEMS . Enfin, nous avons comparé les deux méthodes au moyen de simulations où nous avons observé que l'identification récursive surpasse l'*Extremum Seeking*. Nous avons également observé que certains réglages de l'*Extremum Seeking* présentent une bonne capacité de suivi, au prix de la perte de toute garantie de stabilité et/ou de convergence, car ils ne respectent pas les critères classiques indiqués dans la section E.4.3. Par conséquent, l'identification récursive semble être une meilleure solution pour le suivi de la fréquence de résonance, en raison de sa facilité de réglage et de sa capacité de suivi.

E.5.2 Suggestions pour extensions futures

Conception robuste de l'expérience

Les résultats que nous avons présentés au Chapitre 3 (ici Section E.2) nous permettent d'obtenir une solution au problème de la conception robuste d'expériences, qui assure en fait la contrainte d'origine. Cependant, pour la robustification de la contrainte de précision, nous pouvons développer une alternative tractable uniquement pour la partie de la matrice de covariance P_θ donnée par le spectre du signal d'excitation Φ_u. Dans les structures de modèle telles que ARX et ARMAX, où le modèle du procédé et le modèle de bruit ont des termes en commun, le bruit contribue également à l'identification du modèle du procédé. Un premier axe de recherche important consiste à étendre les résultats du Chapitre 3 (ici Section E.2) également à la contribution du bruit en P_θ. Ce résultat permettra ensuite l'extension aux expériences réalisées en boucle fermée, où le bruit joue toujours un rôle dans l'identification du modèle du procédé.

À l'avenir, nous chercherons à savoir si le problème de la conception *least-costly* des expériences peut également être robustifié lorsque le spectre d'excitation à déterminer est celui d'un bruit blanc filtré. Nous étudierons également comment ces résultats présentés peuvent être étendus pour aborder la robustification de contraintes de précision plus complexes (telles que celles présentées dans [3]).

Conception optimale de l'expérience pour les réseaux

Comme nous l'avons déjà mentionné au Chapitre 4 (ici Section E.3), l'utilisation des outils que nous avons développés au Chapitre 3 (ici Section E.2) pour obtenir une formulation tractable de la contrainte de coût conduirait à des temps de calcul excessivement élevés dans un contexte de réseau. C'est pourquoi nous avons utilisé une approche différente pour la robustification du coût, dont le conservatisme plus élevé était contrebalancé par son temps de calcul bien plus faible. Malheureusement, nous n'avons pas de résultats similaires pour la robustification de la contrainte de précision. Cela implique que l'utilisateur doit se fier à une approche par grille, qui ne garantit pas complètement que la contrainte de précision sera respectée dans la pratique. L'utilisateur peut également se fier à nos résultats présentés au Chapitre 3 (ici Section E.2), ces qui nécessitent éventuellement un long temps de calcul dans un contexte de réseau. Il est alors intéressant d'aborder la contrainte de précision d'une manière similaire à ce que nous avons fait dans le Chapitre 3 (ici Section E.2) pour le coût, afin de développer une contrainte alternative qui assure la contrainte de précision robuste au prix d'un plus grand conservatisme, mais avec une complexité numérique moindre.

Un autre axe de recherche important consisterait à étendre l'approche de robustification du Chapitre 4 (ici Section E.3) également à un autre type de signal d'excitation largement utilisé: le bruit blanc filtré. À cette fin, la robustification du problème des OED devrait être réalisée à l'aide d'outils similaires à ceux utilisés dans le Chapitre 4 (ici

Section E.3), afin de résoudre efficacement le problème malgré la dimension éventuellement élevée du réseau, tout en admettant un certain conservatisme.

Enfin, dans cette thèse, nous avons limité notre attention à un réseau constitué par l'interconnexion de systèmes contrôlés localement. Il est évident que ce n'est pas le seul type de réseau existant. Juste pour donner une idée de la diversité des configurations de réseau, il existe de nombreux types de configuration de réseau uniquement pour une tâche de contrôle de formation, voir [62] pour un aperçu. Par conséquent, une autre ligne de recherche serait l'extension des résultats du Chapitre 4 (ici Section E.3) également à d'autres types de réseau.

Suivi de la fréquence de résonance

L'étude présentée au Chapitre 5 (ici Section E.4) a été réalisée au moyen de simulations. La première extension consiste évidemment à tester ces deux algorithmes sur le gyroscope MEMS du projet Next4MEMS . Cela implique de réaliser des tests dans une chambre qui nous permet d'imposer un certain profil de température, et donc de fréquence de résonance. Les premiers tests pour le Extremum Seeking ont déjà été effectués à température ambiante et ont montré une réponse légèrement plus rapide que ce que nous avons observé dans la Section E.4.4, mais de nombreux réglages qui étaient stables dans les simulations se sont révélés instables lorsqu'ils ont été mis en œuvre sur le gyroscope réel.

Le résonateur MEMS du Chapitre 5 (ici Section E.4) est un système LPV, dont la variable de *scheduling* est la fréquence de résonance. Cette fréquence varie avec la température suivant une relation connue. Dans le projet Next4MEMS , la stratégie de contrôle du résonateur vient d'être modifiée pour utiliser un contrôleur LPV, ayant comme variable de *scheduling* la fréquence de résonance. Par conséquent, la discussion que nous avons faite dans le Chapitre 5 (ici Section E.4) devrait être étendue au cas où l'estimation de la fréquence de résonance est utilisée non seulement pour générer le signal de référence, mais aussi comme variable de *scheduling* pour le contrôleur. Dans cette ligne, nous pouvons utiliser les résultats présentés dans [53] pour évaluer si la fréquence de résonance estimée donne des performances satisfaisantes lorsqu'elle est utilisée dans le contrôleur LPV.

Outre ces extensions, une autre consisterait à inclure dans la comparaison également d'autres techniques telles que le filtrage de Kalman et le filtrage *notch* adaptatif.

AUTORISATION DE SOUTENANCE

Vu les dispositions de l'arrêté du 25 mai 2016,

Vu la demande du directeur de thèse

Monsieur X. BOMBOIS

et les rapports de

M. C. ROJAS
Professeur Associé - KTH Royal Institute of Technology
Division of Decision and Control Systems - Malvinas Väg 10 - 100 44 Stockholm - Suède

et de

M. G. MERCERE
Maître de Conférences HDR - ENSIP - Université de Poitiers - LIAS - Bât. B25
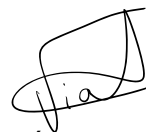2 rue Pierre Brousse - TSA 41105 - 86073 Poitiers cedex 9

Monsieur MORELLI Federico

est autorisé à soutenir une thèse pour l'obtention du grade de **DOCTEUR**

Ecole doctorale ELECTRONIQUE, ELECTROTECHNIQUE, AUTOMATIQUE

Fait à Ecully, le 5 janvier 2021

P/Le directeur de l'E.C.L.
Le directeur des Etudes

Grégory VIAL